STRESSES IN THE ADHESIVE LAYER OF BONDED MID-PANEL JOINTS CONNECTING SANDWICH PANELS

A. Salahuddin

A THESIS

IN THE

FACULTY OF ENGINEERING

Presented in partial fulfilment of the requirements for the

Degree of DOCTOR OF ENGINEERING

at

Sir George Williams University

Montreal, Canada

September, 1971

STRESSES IN THE ADHESIVE LAYER OF BONDED MID-PANEL JOINTS CONNECTING SANDWICH PANELS

ABSTRACT

In this investigation, theoretical and experimental study of adhesive-bonded connections has been carried out.

To begin with, a brief and up-to-date survey of the available literature on connections has been presented. Use has been made of the theory of elasticity to develop mathematical expressions for the shear stress, τ and the normal stress, σ in the adhesive layer of the bonded joint. In this analysis, two approaches with different sets of assumptions were used: (a) small deflection theory and (b) large deflection theory.

To verify these results experimentally, several adhesive-bonded connections were fabricated and tested under various loading conditions. The photoelastic method of analysis was used to analyse the experimental data. Experimental and theoretical results compare favorably.

In addition to the bonded connections, nailed and adhesive-nailed connections were also tested, and their photoelastic data recorded. Stress results for these were also plotted.

The experimental data was processed from about 600 colored photographs of fringe patterns.

ACKNOWLEDGEMENTS

The author wishes to express his deep sense of indebtedness to Dr. P. P. Fazio, Associate Professor, for originating this research, and for his guidance, advice, interest and encouragement throughout the course of this investigation.

The writer also wishes to thank Professor Cedric Marsh, and Dr. S. Palusamy for reviewing the manuscript.

The support of the Aluminum Company of Canada and of the National Research Council (Grant No. A-4770) for sponsoring and financing this project is gratefully acknowledged.

Thanks are also due to the technical staff in the Machine Shop and in the Structures Laboratory, for their assistance in the experimental part of this investigation.

TABLE OF CONTENTS

PAGE

LIST OF TABLES

LIST OF FIGURES

NOTATIONS

SYMBOL	DEFINITIONS
A_f	Cross-sectional area of one face, in^2
A_s	Cross-sectional area of one-half of edge member, in^2
a,b	Lengths as shown, in
D	Flexural rigidity of a plate
D_{f_1}	Flexural rigidity for the thinner section of the plate, lbs in
D_{f_2}	Flexural rigidity for the thicker section of the plate, lbs in
E	Young's modulus of elasticity for facings, psi
E_s	Young's modulus of elasticity for the edge-member, psi
f	Thickness of aluminum sheet, in
G_c	Adhesive shear modulus, psi
M_f	Negative moment developed at the fixed edges of the plate, lbs in
P	Concentrated load, lbs
s	Subscript denoting edge member
T_f	Axial force in aluminum facing, lbs
t_s	Thickness of one-half the edge member
Y_1, Y_2	Deflections of plate, in
β	Normal component of T_f for a unit deflection of specimen at its centre, psi

SYMBOL	DEFINITIONS
γ	Shearing strain
ξf	Thickness of cover plate, in.
σ	Normal stress in adhesive, psi.
τ	Shear stress in adhesive, psi.
μ	Axial strain
ν	Poisson's ratio for facings
ψ	Thickness of adhesive layer, in.
ω	Width of specimen, in.

PREFACE

The existing building methods in the construction industry cannot meet adequately the demand of building space foreseen for the future. It is vital that prefabrication techniques be used in order to satisfy the ever-increasing residential and industrial space requirements.[19,52]

Because of its many advantages over the conventional materials of construction, sandwich construction is finding wide application in the prefabrication industry.

Extensive bibliographies, outlining the present and future possibilities of using the principles of sandwich construction in designing various structural elements, have appeared, confirming the wide spread interest this construction material is gaining.

To exploit sandwich construction in the building industry, however, it is necessary (i) to develop effective and economic means of connections (ii) to formulate design criteria for the basic sandwich components and (iii) to understand the behaviour of sandwich panel assemblies.

This project has been limited to the study of mid-panel connections and in particular, bonded connections.

CHAPTER I

INTRODUCTION

Connections are an integral part of panelized building construction. They can be of innumerable configurations, depending on the particular requirements of a connection design. For joining sandwich panels a commonly used connection is the one that employs a double-tapered key in the core to transfer transverse shear across the panels. And in order to transmit the axial forces in the facings, cover plates are bonded to the facings of the sandwich panels using adhesives.

As is well-known from the fundamentals of the theory of elasticity that external forces acting on any homogeneous body seldom produce a uniform state of stress; but when two or more materials are joined together as in an adhesive-bonded joint, the state of uniform stress distribution is virtually non-existent. The difference of physical properties at either side of the joint between the adhesive and the adherend will produce a varying intensity of stress, hence will introduce some degree of stress concentration in the adhesive layer.

The significance of such stress concentrations has been neglected by many investigators in the past which led to many erroneous conclusions and some confusion. It has been customary to express the strength of an adhesive-

bonded joint as an average failure stress, i.e., the failure load divided by the area of the overlap.

However, during the last decade some investigators found out that the stresses developed in the adhesive layer are not uniform, and the stress concentrations are a function of the shape and size of the test specimens so that the more highly stressed areas break first and give rise to stress waves which travel from the higher-stressed zones to the lower-stressed zones in the adhesive layer.

An accurate knowledge of the stress distribution in an adhesive is, therefore, indispensable for the prediction of their strength; it also gives a better insight into the behaviour of the adhesive under all external forces and loading conditions. The investigation in this study is mainly confined to stress distribution below the elastic limit. The stress distribution above it is not included here,which is not a serious limitation because the adhesives are mostly brittle, breaking with little or no creep.

The two fundamental works in this study appear by Reissner and Volkersen[80,96]. Both of these authors have assumed that stresses in a lap joint are constant across the thickness of the adhesive layer and come to the conclusion that with flexible adhesive layers, the highest shear stress develops at the edges of the overlap. The adhesive layer, however, has a definite thickness and ends in free adhesive-to-air surfaces at each end of the overlap. On such free

boundaries the conditions of equilibrium limit the internal stresses to simple tangential tension or compression without any shear. A longitudinal shear component may exist only at places where the boundary forms an oblique angle to this direction. Thus, the assumption of constant shear across the adhesive is not permissible.

Besides having the theoretical expressions for determining the shear and normal stresses in the adhesive, it is necessary to get some insight into the behaviour of the joint in experimental set up. The obvious check on the theoretical strength of a joint is its test to destruction, but this gives no specific cause of rupture or any indication of how to improve its strength. The necessary information can only be obtained by the knowledge of stress distribution throughout the joint. It can be acquired experimentally by measuring the stresses actually developing in the models similar to real joints and similarly loaded.

In the following Chapters, expressions for τ (the shear stress) and σ (the normal stress) are developed for an adhesive in a double-tapered, adhesive bonded mid-panel joint between two sandwich panels. Both small and large theories of deflection are employed in the mathematical investigation. The results obtained theoretically are verified experimentally by testing joint specimens with different loading conditions.

CHAPTER II

GENERAL SURVEY OF RECENT DEVELOPMENTS IN THE DESIGN AND ANALYSIS OF CONNECTIONS

To become familiar with the present state of knowledge on connections, it was deemed necessary to carry out an extensive literature survey in this field. The main topics of investigation were:

a) Riveted and bolted connections

b) Welds and welding processes

c) Adhesion and adhesive joints

The subject matter of a selected number of research papers (see "Selected Bibliography") is presented below.

2.1 RIVETED AND BOLTED CONNECTIONS

2.1.1 High Strength Fasteners

Douty and McGuire[21] analyzed the relationship between the performance and the design of the more common types of high-strength bolted moment connections. Although it was undertaken for the specific purpose of studying their use in plastically designed structures, many of the findings pertain to elastic behaviour as well. This work was extended by Chesson, Faustino and Munse[16] who investigated the strength and behaviour characteristics of single high strength bolts subjected to various combinations of tension and shear. These results were then related to the strength and behaviour

of rivets under similar loading conditions. Kinney[51] discusses briefly his experience with high-strength bolts in the Mackinac Bridge. The procedure for bolting and inspection as developed on the project, is outlined. Ball and Higgins[7] carried this work further by describing the installation and tightening of high-strength bolts so as to produce the minimum bolt tension required by specifications. The behaviour of A440 steel joints connected by A490 (high strength) bolts is studied by Sterling and Fisher[88]. They emphasize this selection by arguing that the recent development of the ASTM A490 high-strength bolt was necessitated by the increased use of high-strength steels. Fasteners of higher strength than the A325 bolt had to be developed so that the connections could have reasonable proportions. Prynne[77] describes a comprehensive research project carried out to investigate the fundamental problems associated with friction grip joints using high tensile bolts. The effectiveness of a number of bolt-tightening techniques is assessed and the results of carefully controlled tests on simple bolted joints are presented.

2.1.2 Analysis of Riveted and Bolted Joints

Fisher and Rumpf[27] have developed a general theoretical solution for the load partition in double-lap plate splices which is applicable to the load region between major joint slip and ultimate load. The solution is based on the observed behaviour of plates with holes and of high-strength

bolts in bearing and shear; it is verified by experimental results. Lewitt, Chesson and Munse[13] have extended the above work by discussing the behaviour of bolted structural connections under repeated loadings. They also report the results for recent fatigue tests on joints assembled without hardened washers. The test results indicate that hardened washers generally have no significant effect on the fatigue strength of a bolted shear type connection when properly assembled.

A comprehensive investigation of 24S-T riveted tension joints has been carried out by Fefferman and Langhaar[26]. They tested 55 different joints each having two specimens made up by connecting 24S-T sheets with protruding-head rivets. With the aid of a general empirical "stress-concentration" factor, the data are well-correlated with a modified form of the elementary theory of tension joints. The modification lies in the assumption that rivets of unequal diameter in a joint carry equal bearing stresses, rather than equal shearing stresses when the ultimate load is approached. The authors have also developed mathematical expressions to optimize multiple row joints. Monroe[69] goes a step further and outlines a semi-graphical analysis applicable to all riveted and bolted joints eccentrically loaded but not stressed beyond the elastic limit. By using his method, it is possible to calculate stress on each rivet or bolt by plotting one point on a scale drawing of the joint and multiplying the distance from this point to each rivet or bolt

by a constant factor. The application of this method is simple and brief. Another significant contribution is made by Chesson and Munse[13] who performed experiments on various truss-type tensile connections, made up of plates and rolled shapes, to provide information on their general behaviour and ultimate strength. The variables of the test program included specimen configuration, method of hole preparation, and type and size of fasteners. The comparative behaviour of typical specimens is presented. A comparison of predicted and actual efficiencies is made and recommendations are given for the design of truss-type members. Munse and Chesson[70] elaborate on the various aspects of the net section design for riveted and bolted joints. It is well-known that structural tension connections have long been designed on the basis of the theoretical net section and an allowable working or design stress. However, as the authors argue, research has shown that the effective net section of such connections is a function also of (a) the geometry of the member and connection, (b) the manners in which the stress is transferred through the connection and (c) the method of fabrication. Recommendations are made, in the above reference, for empirical design rules for tension connections that will result in a more realistic section, a more consistent factor of safety based on ultimate strength, and often a savings in material. In another study on the strength of rivets and bolts in tension, Munse, Petersen and Chesson[71] have considered such factors as the flexibility of the connected

members, the magnitude of the initial clamping force in the members, the number of lines of fasteners, and the grip of the fasteners. Hansen[35] studied the aspect of fatigue of joints of high strength steels. He has presented a condensed summary of a program of fatigue testing, in direct tension, of joints connecting various structural steel sections such as channels, angles, etc. His study revealed that clamping force was the most important variable governing the fatigue of the joints tested.

Hewitt[38] has written on various joint designs, joint efficiencies, types of rivets and special treatments for joints. This work is followed by that of Beedle and Christopher[8] who in their report have compiled and discussed some important studies of rigid moment connections in building frames. They have analysed three types of connecting media: welding, riveting and bolting. Primary attention is focused on the moment and deformation capacities of these joints. It is assumed in the above report that connection is able to undergo inelastic strain resulting in joint rotation many times that associated with initial yielding, while providing a predictable resisting moment. The most important result of these tests is the fact that for all properly designed, detailed and bolted moment connections the plastic moment of the adjoining members was developed and large plastic rotation capacities were observed.

2.1.3 Additional Aspects of Riveted and Bolted Joints

Misalignment in bolted joints was studied by Vasarhelyi and Chang[95]. From a series of tests carried out on misaligned bolted joint specimens, they concluded that misalignment, even in a rather severe arrangement, does not seem to have a significant effect on the ultimate load carrying capacity of the bolted joint, but might somewhat reduce its efficiency.

Jones[47] offers evidence that in riveted joints of usual structural proportions, subjected to substantially static loads, the joint strength will not be reduced if the ratio of rivet bearing stress to axial or shearing stress is increased above that sanctioned by most specifications.

Vasarhelyi,et al[94] have discussed the effects of fabrication techniques on the efficiency of bolted joints, especially such factors as punching of the holes, misalignments, and the paint on the faying surfaces. Tests on joints with drilled and with misaligned punched holes showed that the method of punching of holes does effect significantly the efficiency of the joint, whereas, the misalignment and the paint do not.

Winter[97] summarizes the results from 574 tests on bolted connections in light-gage steel considering many pertinent variables such as bolt diameter, sheet thickness, mechanical properties of sheet and bolt steels, edge dis-

tance, etc. The following criteria are established for predicting failure loads which are in satisfactory agreement with test results:

i) Longitudinal shearing of the sheet along two practically parallel planes whose distance equals the bolt diameter,

ii) Shearing-tearing along two distinctly inclined planes with considerable "piling-up" of the material in front of the bolt,

iii) Transverse tension-tearing across the sheet,

iv) Shearing of bolt, with more or less pronounced preceding elongation of the hole.

A realistic evaluation of the factor of safety of a bolted bracket has been made by Shaffer[85] by analysing a bolted bracket when it was subjected to pure bending moment of sufficient intensity to induce first an elastic, then an elastic-plastic, and finally a fully plastic stress distribution within the supporting set of bolts. It is shown that when the bracket is held in place by three equally spaced bolts, it can resist at least 28 percent more load than a conventional elastic analysis of the problem indicates.

Yienger and Walker[99] have tabulated equations for bolt-point-reactions along three mutually perpendicular axes.

These equations apply to forces at the mounting points for a package with a rectangular attachment pattern for either externally applied loads or loads produced by inertia due to acceleration of the base structure.

2.2 WELDS AND WELDING PROCESSES

2.2.1 Design of Welding Joints

Koopman[56] presents a design of joints to be fusion welded by any of the arc or gas processes. His design would apply to either manual or machine welding. A specialized aspect of a theoretically sound design is discussed by McCampbell, Cook, Nordholt and Merrick[65]. They have described an automatic control system which senses direct weld properties entirely from the arc side and makes the necessary compensation to travel speed or to weld current as required to achieve consistent weldments. The paper covers only research done with aluminum, but the techniques are equally applicable to other materials.

2.2.2 Welding Methods....A General Review

There are very few engineering products manufactured today which do not make use of one or more of the established methods of metal jointing. A commonly used method is explosive welding. Addison, Fog, Betz and Hussey[2] have discussed its application to aluminum alloys. According to them, the process offers promise for supplementing and, in certain instances, replacing conventional fusion welding

processes. This process, therefore, is receiving considerable attention from several researchers like Bahraini and Crossland[4] who have performed a number of experiments on the explosive cladding of mild steel with stainless steel, 70/30 brass, and high conductivity copper. They have also determined the mechanical strength of the welded joints by shear, tension and bend tests. The authors conclude that explosively cladded material has some advantages over conventionally pressure cladded material due to higher strength of the welded interface.

Hewitt[37, 39, 40, 41,42] has conducted a survey of the established processes for the jointing of metals. He describes the automatic and semi-automatic processes, e.g., soldering, brazing, electrical resistance methods, high frequency induction methods and fusion welding. The fusion welding process is treated extensively by him to suit requirements of welding various metals using several different weld metals. Other topics include arc welding, atomic hydrogen welding, the Weibel process, the thermit process, projection welding and flash welding. Long and Cremer[61] have expostulated that high temperature corrosion-resistant brazing seems destined to play an important role in the fabrication of structures meeting the exacting demands of advanced missile and space vehicle designers. This process, introduced recently, gives promise of producing complex but light weight structures that are both strong and reliable at the temperatures encountered in hypervelocity flight. Adams[1] has deduced certain

engineering relationships through the use of mathematical approximations which determine the centre line cooling rate and peak temperature distribution in fusion welding. The most significant feature of the simplified equations is the clarity with which effects of changes in any welding, thermal or geometric variables, can be predicted.

Another important welding technique, gas metal arc welding, is presented by Lohr and Watkins[59]. They have quoted a specific example of a low-alloy steel pipe and describe how the welding is accomplished in all positions with the short-circuiting arc process wherein 97% of the electrode is deposited in the joint and savings up to 40% are realized over conventional manual-arc welding. Kaehler, Bank and Trabold[50] have described one of the most advanced techniques of welding: arc image welding--a process in which weldments can be produced by focusing the image of a carbon arc or any other high temperature source on the components to be welded together. The authors have speculated that when fully developed this technique can be effectively used for repairing damage to spacecraft which may occur due to meteorites during rendezvous operations. The high temperature source in this case would be the sun's energy.

Bratkovich, Roth and Purdy[9] have developed techniques to reduce cost, decrease weight, increase reliability and solve complicated design problems in electron beam welding. The paper presents the applications and design considerations for

electron beam welding of critical aircraft engine parts such as highly loaded power train and accessory gears. The main advantage of this process is its capability of fusion welding with minimum distortion. Meier[67] attributes the wide acceptability of this process to the following three major advantages:

a) Low-total energy input to the workpiece for a given job.

b) Precise controllability of the process, and

c) Very high purity welding environment.

All three factors are associated with the operating characteristics of the equipment and the phenomena governing the weld formation.

The formation of weld seams in electron beam welding has been discussed by Lockshin and Puzrin[39] briefly.

2.2.3 Ultrasonic Welding

Jones and Meyer[49] have discussed the applications of ultrasonic welding to structural aluminum alloys. The process deals with joining metals and metal alloys without the aid of solders, fluxes or filler metals and usually without externally-applied heat. The metals to be joined are clamped at low static pressure between welding tips or sonotrodes, and the ultrasonic energy is introduced for a brief interval.

A strong metallurgical bond is produced without the significant external deformation that characterizes pressure welding and without the cast-metal zones associated with resistance welding. The paper outlines a program undertaken to explore the ultrasonic weldability of aircraft structural aluminum alloys and to investigate the effect of resistance heating as an auxiliary to such vibratory welding. Phenomenological consideration in ultrasonic welding are presented by Jones, Maropis, Thomas and Bancroft[48]. The paper describes investigation resulted in special instrumentation and techniques for observing phenomena and interpreting factors relevant to the ultrasonic welding process. It included preliminary study of certain ultrasonic weld phenomena and considered the influence of material properties on weldability. A comprehensive study is made of

i) The stress distribution in the weld zone,

ii) The vibratory energy delivered to the weld zone,

iii) The energy transmitted through weld zone,

iv) The temperatures developed in the weld zone,

v) The material properties and their relationship to ultrasonic weldability, and

vi) Of the interface disturbance and metallurgy.

2.2.4 Laser Welding

A great deal of interest has been shown in the development and application of high energy intensity heating techniques in the fields of material processing and fabrication. One of these, laser beam fusion welding, represents one of the earliest proposed uses of laser device. A laser welding machine has the potential capability for extremely high energy, precise energy control and exact welding spot location. Since the advent of the higher energy lasers, laser welding development has advanced from micro applications to the more common macro joining problems.

Five excellent papers have been reviewed on laser. The first of the series by Earvolino and Kennedy [42] describes an investigation of a high energy output laser device for use as an industrial tool for the fusion welding of current structural alloys. The primary objective of this work was to demonstrate that a high energy, pulsed laser has the capability of producing reliable and consistent weld joints in selected materials typical of aerospace structural applications. The evaluation is based mainly on the results obtained through study of each of the following areas:

i) Laser welding techniques and procedures.

ii) Mechanical properties of weld joints at various temperatures.

iii) Mechanism of laser bonding.

iv) Metallurgical effects on base material and equipment versatility.

The following topics are presented in detail in the discussion of this work:

a) Equipment,procedure.

b) Welding parameters,

c) Mechanical testing, and

d) Metallographic examination.

Included in the presentation are a comparison of laser welding with electron beam welding and a general discussion of high energy fusion welding process. Anderson and Jackson[3] elaborate on the theory and application of pulsed laser welding and have concluded after sufficient experimental evidence, that wire-to-wire and sheet-to-sheet welds involving a variety of materials are successfully achieved using this process. They have also discussed its basic advantages and limitations in the light of the latest experimental data. Laser performance in microwelding has been evaluated by Schmidt, Ham and Hoshi[83] who have established conditions for obtaining satisfactory welds in 0.005 and 0.010 in. thick type 302 stainless steel as well as 0.005, 0.010 and 0.015 in. thick nickel-steel. A disadvantage of laser welding, pointed out by the authors, is vaporization of the metal in excessive temperatures.

They recommend that for laser welding, the laser pulse, the thermal and set up conditions must be such that melting and only little or no vaporization occurs. To apply the laser beam to microwelding, many factors must be considered such as mode of operation, type of laser material, capacity of unit, characteristics of laser pulse, energy intensity, thermal properties of material, etc. Miller and Ninnikhoven[68] state that any joint can be laser welded if it can be fusion welded by any other process. According to them, the materials which can be joined by laser welding are about the same as those joined by the electron-beam process. The only major difference is the joining of dissimilar alloys, where the electron beam is excellent, but the laser is even better since it does not need the protection against atmospheric contamination that the electron beam process requires. A further application of laser beam fusion welding is discussed by Fairbanks and Adams[24] who conclude that a capability to withstand very high instantaneous temperatures without expulsion associated with high thermal diffusivities makes metals such as copper, gold and aluminum ideally suited to laser welding.

2.2.5 Special Topics in Welding

The various welding methods have been discussed,to a large extent, in the preceding paragraphs. In this section, a few special topics related to welding are included. Heuschkel[36] has presented an extensive coverage to "Composition Controlled, High-Strength, Ductile, Tough, Steel Weld Metals". He

argues that the newly available high-strength welding steels provide no advance in structural usefulness until they are accompanied by a suitable welding system. Advanced arc-welding electrodes, and close process control, are required for these steels. Laboratory studies have led to a technical solution of this problem. This solution involves selective additions of metallic elements to pure iron to secure the required alloy balance. Simultaneously, the elements which reduce ductility and notch-toughness in as-deposited weld metals were removed. Deliberately added components of the welding electrode surfaces were found to be one source of such offending elements.

Experimentally derived bi-axial stress-strain data have been presented on weld metal of five high strength-density ratio alloys by Baird[5]. The test result conclusively debunk the often stated general rule that all welds are weaker than base metal because cast structures are inherently weaker than wrought structures. In three test materials, after heat treatment, welds were shown to possess stress-strain characteristics identical to base metal. In one test material they were shown to possess slightly reduced biaxial yield stress values due to imperfect heat treat response, and in yet another they were shown to possess totally unacceptable biaxial strength properties due to inherent metallurgical deficiencies.

Joining new high-strength aluminum alloy X7005 has been discussed by Dudas[22]. X7005 is one of the most versa-

tile of the new heat-treatable aluminum-zinc-magnesium alloys, because it can be easily welded, brazed and soldered. It is well suited for applications in sheet, plate, extrusions and tubing where high strength is needed and solution heat treatment after joining is undesired. The paper discussed the joining characteristics and properties of joints in this promising aluminum alloy.

The fracture characteristics of aluminum alloy welds have been evaluated from the results of tear and notch-tensile tests by Nelson, Kaufman and Holt[73]. The tear resistance and notch toughness of welds are generally greater than those of cold-worked or heat-treated base metal, and approach those of annealed base metal. Subsequent thermal treatment of heat-treatable filler metals may appreciably change the fracture characteristics.

Brungraber and Clark[10] have discussed the strength of welded aluminum columns. As is known, welding heat-treated or cold-worked aluminum alloys causes partial annealing of the material in the vicinity of the welds so that the strength of the material near the welds is lower than the strength of the material in the rest of the structure. An experimental and analytical investigation was conducted to determine the effect of the varying mechanical properties on column strength. The strength of aluminum columns with longitudinal welds can be computed by means of the same techniques used in determining the effect of residual stresses on column

strength. Columns with transverse or other localized welds can be analyzed as stepped columns. Working along the same lines, but on a broader level, Goodwin[34] has carried out an investigation on the effects of variations in twelve parameters on the static and fatigue strength of spot-and seam-welded aluminum alloy joints. This study was undertaken in response to the demands of aircraft structural engineers and 10,000 aluminum alloy joint specimens were tested. The program related the strengths of resistance welded joints to those of riveted joints.

Hydraulic and weight features of welded spiral cases of draft tubes are discussed by Sutherland[89] . An illustrative example of comparative head loss of welded and riveted plate-steel spiral cases shows that a substantial monetary value may accrue by the use of a welded case.

2.2.6 Residual Stresses Due to Welding

Residual stresses and distortions due to welding are important factors to be considered. Masubuchi[54] has developed an analytical method for studying these residual stresses and distortions. The analysis is based on an analogy between the theory of residual stresses in mechanics of a deformable body and the theory of vortex motion in fluid dyanmics. The fundamental principles of the theory and a summary of the results obtained in its experimental verification are described in this paper. The following are investigated:

i) Transverse shrinkage and residual stresses in a butt joint.

ii) Distortion of a structure caused by angular change occurring in a butt joint.

iii) Distortion of a structure caused by angular changes occurring in a fillet joint.

iv) Longitudinal distortion of a welded beam.

A few brief but important comments on pre-heating, residual stresses and stress relieving in welded joints have been made by Spraragen[87].

2.3 ADHESION AND ADHESIVE JOINTS

2.3.1 General

Although most of the metals may be more or less satisfactorily joined by welding, brazing, soldering or riveting, there are many instances in which it may be possible and convenient to overcome some of the difficulties and disadvantages of these methods by glueing with a plastic adhesive.

Plastic bonding materials received considerable attention in many countries during World War II, and have been applied with various degrees of success to the production of metal to metal and metal to wood, glass and thermo-setting plastic joints. Some of the advantages which may be gained by the use of this type of bonding process compared to

other metal jointing techniques are:

i) Joints of clean and pleasing appearance may be obtained which are often stronger than those produced by riveting or spot welding;

ii) Freedom from the distortion and other heating effects which occur during brazing and welding;

iii) The bonding material forms an electrically insulating film between the metal surfaces, thus avoiding the corrosion which may occur in metal to metal joints made by other processes. (This problem may be especially serious in the jointing of dissimilar metals).

A survey of plastic structural sandwich construction has been presented by Baldanza[6] containing technical information and references that should give the designer and materials engineer a better understanding of the potential usage of these techniques. The information is applicable to the design and fabrication of structural sandwich components for tank-automotive usage or similar applications. Included are technical data and references relating to specifications, various types of sandwich facings and core components, adhesives, sealants, fasteners, ballistics, and

nuclear radiation protections. The state-of-the-art search concludes that sufficient advantages of sandwich construction exist to warrant further investigation of practical applications. Hewitt[37] has given a detailed description of plastic bonding. Some recent European developments in the structural-adhesive field are outlined in Catchpole's article[12] which gives information on recent design, production, and service experience of bonded structures in Europe, including the limited number of space applications, as well as hovercraft and other miscellaneous uses. While the main European contribution to the subject lies in this extensive experience, there have also been interesting developments in both adhesive and core materials, notably adhesives applicable to supersonic airliner service and aluminum core materials with high temperature strength and high resistance to bond splitting for use in nonperforated sandwich.

Metallizing history, joint design, joint materials, methods of wetting, methods of increasing braze strength and other pertinent topics have been reviewed by Van Houten[93] in his literature survey of "The bonding of cermets to metals". In his paper he reasons that brazing cermets to metals is complicated by the great differences in thermal coefficients of expansion and by the difficulty in finding braze metals which will wet cermet surfaces. The need for brazes which are strong at high temperature further increases the problem of differential expansion. Slaughter, Patriarca and Manly[86] have outlined the techniques and procedures utilized to bond

cermet-valve components successfully to metals for high-temperature fluid service. The cermets studies contained varying percentages of titanium carbide, tungsten carbide, tungsten-titanium complex carbide and niobium-tantalum-titanium complex carbide. The binder materials were primarily nickel and cobalt. The results of wetting tests on these cermets with different brazing alloys are presented, as are photomicrographs of many of the most promising cermet-to-metal joints. Dean[17] gives a brief account of water-proof adhesives for cellulose mostly from chemical point of view. He also conducts a survey of commercial waterproof adhesives for plywood.

Humke[44] has written a selection guide for sandwich panel adhesives. In wetting behaviour and bond reliability, they have kept pace as sandwich construction has advanced to prove itself under widely different environments of heat, cold, impact loads, fatigue and corrosion. But the wide choice has complicated the job of selecting the adhesive for a specific application.

2.3.2 Properties and Tests of Adhesive Bonded Joints

Numerous articles have appeared on the properties and tests of adhesive-bonded joints. The first in the series is a comprehensive study of micromechanical properties of adhesive-bonded joints by Hughes[43]. The basic purpose of the test program described in this report was to demonstrate the feasibility and utility of making microstrain measurements to establish the

mechanical properties of adhesives in metal-metal bonds. Loading modes were tension, compression and shear as a function of joint thickness and test temperature for selected adhesive systems. A high sensitivity capacitance-type extensometer was used to measure deformations. It was shown that this micro-strain method is fully capable of establishing the mechanical properties of adhesive materials in metal-metal joints. While the principal experimental variables of glue-line thickness, test temperature and composition were investigated, it was also shown that the properties of the epoxy adhesives are influenced by stress level, pre-strain, loading rate, time at load, time between successive loads and strain rate.

Delollis, Rucker and Wier[18] have carried out a study of the comparative strengths of some adhesive-adherend systems. The adhesives were polyvinyl acetate, cellulose nitrate, resorcinol resin, casein, gum arabic, natural rubber, and neoprene. The adherends were stainless steel, aluminum alloy, paper phenolic laminate, glass, birchwood, and hard rubber. The properties studied were double lap shear, tensile, long-time loading shear, and impact strengths. Test results were tabulated for various adhesive-adherend systems for comparison and various conclusions drawn from them.

An article appears on the fracture toughness of adhesive joints by Ripling, Mostovy and Patrick[81] in which specimen designs and a testing method have been developed for investigating the fracture toughness of adhesive joints. The technique makes control of strain rate feasible for both

homogeneous and hetrogeneous systems.

Lunsford[63] has developed a theoretical analysis for designs of metal-to-metal joints to replace empirical analysis which he believes to be costly and time-consuming because it involves the testing of components to prove the design. In his paper, theoretical analysis, considering completely elastic elements, has been derived for three types of basic joints: type 1, joints in which all the load is transferred to the skins through the bond line; type 2, joints in which the facing is loaded partly in bearing and partly by shear transfer through the bond line; type 3, joints in which the load is transferred to the edge member through a row of fasteners and to the face by shear transferred through the bond line. Test specimens representing type 1 and 2 joints were designed, fabricated and tested. The results of the tests correlate well with the predicted values. An idealized specimen simulating the torque loading of a thin walled tube with a large diameter was developed as a means of establishing a true stress-strain curve and thus the modulus of rigidity and shear strength of the adhesive.

The effect of joint design and dimensions on adhesives is studied by Bryant and Dukes[11]. They performed experiments on

i) Circular butt joints in simple shear,

ii) Circular butts in torsion, and

iii) Tubular butts in torsion to measure their shear strengths, using steel adherends and rubbery adhesives cured at room temperature.

Tests revealed that variation of adherend dimensions did not affect the failing stress. The authors have concluded that torsional testing gives the best estimate of fundamental shear strength. They have also made several recommendations on the optimum-strength design of adhesive joints. Segerlind[84] has presented a short mathematical treatment on the determination of shear stresses in bonded joints.

2.3.3 Conclusions

The above literature survey has revealed the numerous means by which structural members can be connected. The requirements listed above for most of these connection methods, however, are not altogether satisfactory in joining sandwich panels in the construction industry.

Bolted and riveted connections are not suitable because of their

i) High cost of production,

ii) Heat conductivity, and

iii) Exposed heads and nuts.

Ordinary welding techniques such as soldering, brazing, fusion welding, resistance welding, flux soldering develop high temperatures and cannot be used for sandwich panels having non-metallic cores. In addition, these methods are not adequate for welding thin metallic sheets especially under field conditions. Special techniques such as laser, ultrasonic and arc-image welding would be ideally suited for thin metallic sheets. However, they are not yet developed to the stage where they can be used economically in the field.

It would seem that adhesives and nails may be used to provide more effective means of connecting sandwich panels. A series of examples of these types of connections is given in Appendix I.

The following Chapters present a theoretical and experimental study of adhesive connections and an experimental study only of nailed connections only.

CHAPTER III

ADHESIVE BONDED JOINTS

3.1 TYPES AND TYPICAL STRESS ANALYSIS OF AN EDGE MEMBER ATTACHMENT

A brief description of three different types of adhesive joints follows.

3.1.1 Butt Joints and Joints Subjected to Peeling

In butt joints (Fig. 1a), the surface area of the adhesive is determined by the cross-section of the adherends. Since the synthetic resin bonding agents so far developed have only a small tensile strength in comparison with that of the usual structural metals, the joint forms the weakest link and determines the breaking strength of the whole system. Consequently, the tensile strength of the metals is far from being utilized, so that the butt joint cannot be regarded as an efficient type.

This evaluation of the butt joint is confirmed when it is realized that the normal forces are also non-uniformly distributed because of the difference in the elastic moduli of metal and adhesives. As a consequence, local stress concentrations occur which can be several times that of the mean stress computed from the tensile load divided by the cross-section. A uniform stress distribution could only occur if the metal and adhesive experienced the same lateral

contraction which means that both materials would have to have the same value of m/E (m=Poisson's ratio).

Particularly unfavourable circumstances occur when thin sheets are subjected to peeling (Fig. 1b), where progressive failure occurs along a line because of the increased stress in a smaller area.

3.1.2 Simple and Double Lap Joints

In these types of joints, shear forces are set up in the plane of the joints (Fig. 1c and 1d). Such joints are far better suited to the characteristics of adhesives, since the possibility here exists of making the joint surfaces big enough for the shear strength of the joint to be of the same order of magnitude as the ultimate strength of the adherends. In this way, an optimum utilization both of the adherend and of the adhesive is attained. It must, however, be noted that, as a consequence of the differential strains between the metal and the adhesive, the stress distribution will be non-uniform even in joints subjected to pure shearing forces, and stress maxima, which are far greater than the mean stress, will be present at the ends of the overlap. This is particularly so for relatively rigid adhesives such as thermosetting synthetic resins with a high E value, while in extensible adhesives, for example those of a rubbery basis, the stress concentrations are reduced so that a more uniform distribution is attained over the whole joint surface. The disadvantages, however, of the deformable adhesives are the smaller breaking strengths and the liability to creep, particularly at elevated tempera-

tures. In the simple lap joint shown in Fig. 1c, there is superimposed on this stress distribution an additional effect produced by the couple which is a consequence of the eccentric loading and as a result, there are force components perpendicular to the plane of the joint. On account of its symmetrical structure, the double lap joint shown in Fig. 1d is free from this additional stress system caused by bending moments and thus has advantages over the simple lap joint.

3.1.3 Tapered Joints

In considering tapered joints (Fig. 1e), it must be borne in mind on the one hand, that the area of the joint surface, as in the butt joint, is limited and because of machining difficulties cannot be indefinitely increased. On the other hand, the gradual reduction in the cross-section of the metal reduces the differential strain between metal and adhesive below that of the usual lap joint, so that the stress concentrations at the ends of the joint are reduced. From this point of view, the tapered joint represents a very good solution from a structural point of view. To be sure, scarfed joints have the disadvantage of requiring more machining, and are hardly feasible with thin sheets. The various kinds of stressing and the stress distributions resulting must, of course, be carefully considered in analysing the breaking strength, since their effect cannot be evaluated in terms of a uniform mean stress but by the maximum stress occurring. Deformations both in the adhesive and in the adjacent metal parts are on the one hand, affected by the material constants concerned - modulus of

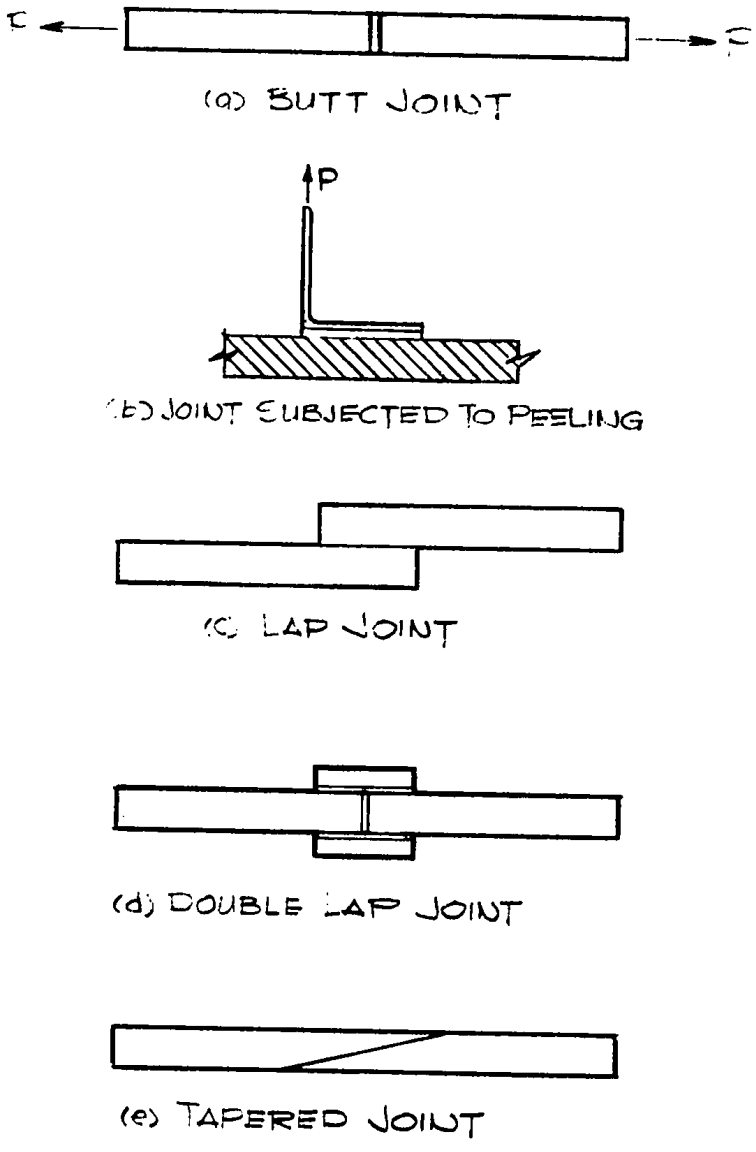

FIG. 1 VARIOUS TYPES OF ADHESIVE-BONDED JOINTS

elasticity, shear modulus, Poisson's ratio - and on the other hand, by the geometrical shape and the dimensions. Universally valid values for the breaking strength of a given adhesive cannot therefore be given, due to the influence of the above-mentioned factors.

3.2 TYPICAL STRESS ANALYSIS OF AN ADHESIVE JOINT

Presented in this section is a brief analytical study of the structural behaviour of a sandwich panel joining an edge solid member. Based on the following assumptions, a theoretical expression for τ (the shear stress in the adhesive) is developed which when maximized predicts the maximum axial load that can be transferred to the edge member through the facings of the sandwich. This study provides a good insight into the behaviour of the adhesive for further analysis in subsequent chapters.

3.2.1 Basic Assumptions

An example of the theoretical analysis of a bonded joint is given in this section. The joint considered (Fig. 2) connects a sandwich panel to an edge member. Analytical expressions for the stress distribution in the joint neglecting thermal stresses have been derived to define the stresses. The derivations of these expressions are based on the principles of elasticity, and the following assumptions: (a) plane sections will remain plane, (b) the proportional limit is not exceeded, (c) the adhesive is a Hookian solid, (d) the normal stress

system across any section of the skin or core is uniform, (e) shear deformations in the skin and core are negligible, (f) the joint is free of significant bending stresses, and (g) the manufacturing process of the panel is controlled to such an extent that the various physical dimensions and mechanical properties of the skins, cores and adhesives are uniform and predictable.

The most questionable assumption in these derivations is that the adhesive is a Hookian solid and not a Newtonian fluid. The basic difference is that a Hookian solid has no time dependency, whereas the force resisted by a Newtonian fluid is completely time-dependent. No material can be classified as completely Hookian or Newtonian in character, although many adhesives will be more nearly Hookian and so classified.

3.2.2 General Solution

The joint configuration to be analyzed is illustrated by the bonded honeycomb sandwich specimen, shown in Fig. 2 that provides metal-to-metal joints free of bending and peeling stresses.

The symmetrical specimen is divided into two equal portions to simplify the development of the analytical expression. (See Fig. 2(b)). The load T_f carried by each facing is equal to the load T_s carried by one-half of the edge member. A_s is the cross-sectional area of one half of the edge member while ω is the width of the same.

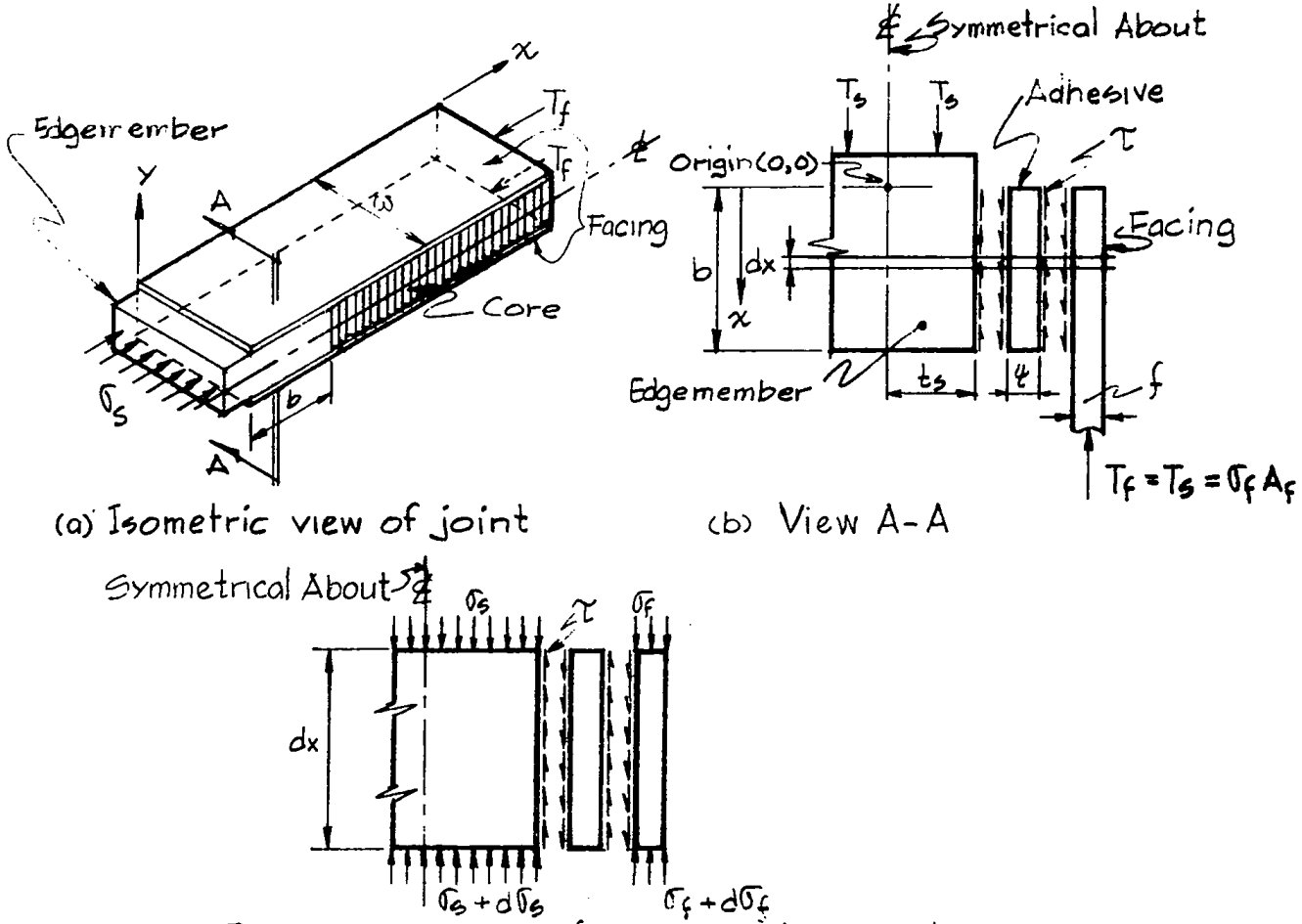

FIG. 2 DETAILS OF A BONDED JOINT

From the free body diagram shown in Fig. 2(c), the equilibrium conditions yield the following:

$$-A_s d\sigma_s = \tau\omega dx = +A_f d\sigma_f \quad (1)$$

The shear strain is

$$\gamma = \mu_f/\psi - \mu_s/\psi \quad (2)$$

The increment of shear strain is

$$d\gamma = 1/\psi[(\sigma_f/E) - (\sigma_s/E_s)]dx \quad (3)$$

The increment of shear stress is

$$d\tau = G_c/\psi[(\sigma_f/E) - (\sigma_s/E_s)]dx \quad (4)$$

Differentiating again gives

$$\frac{\delta^2\tau}{\delta x^2} = G_c/\psi[(1/E)(d\sigma_f/dx) - (1/E_s)(d\sigma_s/dx)] \quad (5)$$

Substituting from eq. (1) produces the following

$$\frac{\delta^2\tau}{\delta x^2} = (G_c/\psi)[(\omega\tau/A_s E_s) + (\omega\tau/A_f E)] \quad (6)$$

This results in the differential equation

$$\frac{\delta^2\tau}{\delta x^2} - G_c\omega/\psi[(1/A_s E_s) + (1/A_f E)]\tau = 0 \quad (7)$$

which takes the form

$$\frac{\delta^2\tau}{\delta x^2} - K^2\tau = 0$$

where

$$K = \left[(G_c \omega / \psi) \left(\frac{1}{A_s E_s} + \frac{1}{A_f E} \right) \right]^{1/2} \qquad (8)$$

The general solution for this equation is

$$\tau_x = A \sinh Kx + B \cosh Kx \qquad (9)$$

It can be seen from Fig. 2(c) that the joint is representative of double lap shear joints in which all the load is transferred to the facings through the bond line. The boundary conditions at $x = 0$ are

$$\sigma_f = 0 \quad \text{and} \quad \sigma_s A_s = T_s$$

At $x = b$, the boundary conditions are

$$\sigma_f A_f = T_f \quad \text{and} \quad \sigma_s = 0$$

Differentiating Eq. (9) gives

$$\frac{\delta \tau}{\delta x} = AK \cosh Kx + BK \sinh Kx \qquad (10)$$

At $x = 0$, Eqs. (4) and (10) yield

$$AK = -G_c \sigma_s / \psi E_s$$

and

$$A = -(1/K)(G_c \sigma_s / \psi E_s)$$

Substituting A in Eq. (10) at $x = L$ results in the following:

$$\frac{\delta \tau}{\delta x} = -(G_c \sigma_s / \psi E_s (\cosh KL) + \sinh KL = G_c \sigma_f / \psi E$$

Then $B = G_b/\psi[(\sigma_s/E_s)\ \cosh KL + \sigma_f/E]/K \sinh KL$

Substituting A and B in Eq. (9) yields

$$\tau = G_c T_f/K\psi[-(1/E_s A_s)\ \sinh KX + (1/E_s A_s)\ \coth KL \cosh KX + (1/EA_f)(\cosh KX/\sinh KL)] \quad (11)$$

This expression relates the adhesive shear stress at any point along the joint as a function of the load, adhesive shear modulus, adherend modulus, and thickness. To determine the maximum load that can be applied to this type of joint, τ_{max} must be located with respect to x. Calculating the maximum value of τ, τ_{max} occurs at x = b(at the bonded edge). Then

$$\frac{T_f}{\omega} = N_f = \tau_{max} \frac{(K\psi E_s t_s)}{G_c} \left[\frac{\sinh KL}{(E_s t_s/E_\omega f)\ \cosh KL + 1}\right] \quad (12)$$

where K is modified by substituting ω = 1 in. into Eq. (8),

$$K = \left[-\frac{G_c}{\psi}\left(\frac{1}{t_s E_s} + \frac{1}{fE}\right)\right]^{1/2}$$

Since the analytical expressions were derived from one-half of the joint specimen, the load obtained from Eq. (12) must be doubled to obtain the total that can be applied to the specimen.

CHAPTER IV

THEORETICAL ANALYSIS OF ADHESIVE BONDED MID-PANEL JOINTS CONNECTING SANDWICH PANELS SMALL DEFLECTION THEORY:COMPRESSION SIDE OF SPECIMENS

The type of joint selected for the theoretical analysis is as shown in Fig. 3. In accordance with the assumptions generally made in sandwich construction, the bending moment is taken by the facings and the shear is transferred across the core through the tapered shear key. Normal stresses in the facings of one panel are transmitted to the respective facings of the second panel through the adhesive layer.

4.1 ASSUMPTIONS

(i) The stress in the adhesive is assumed to have only two non-vanishing components, the normal stress σ and the shear stress τ, which vary negligibly across the small thickness of the bond.

(ii) The aluminum sheets are assumed fixed at the positions where the loads P are applied, thus introducing fixing end moments in the facings at the load locations. It should be noted that at these points, the loads cause upward bulging in the facing thus justifying the assumption.

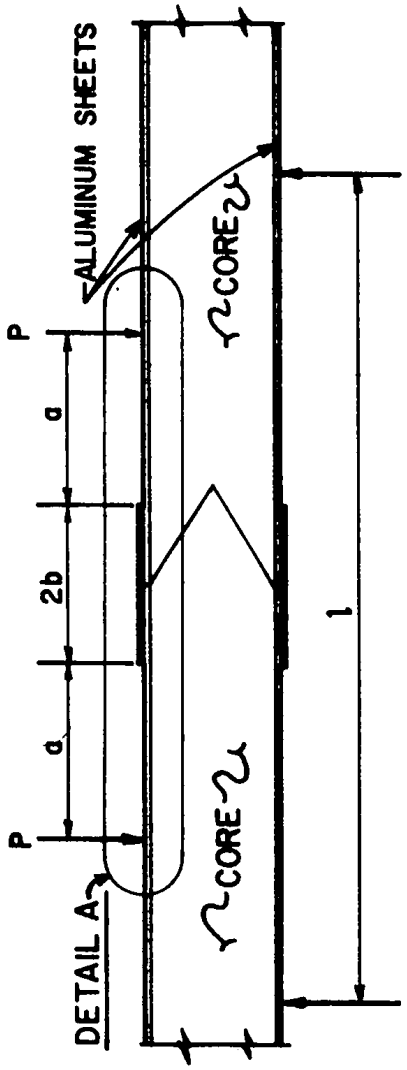

FIG. 3 ADHESIVE BONDED TAPERED JOINT

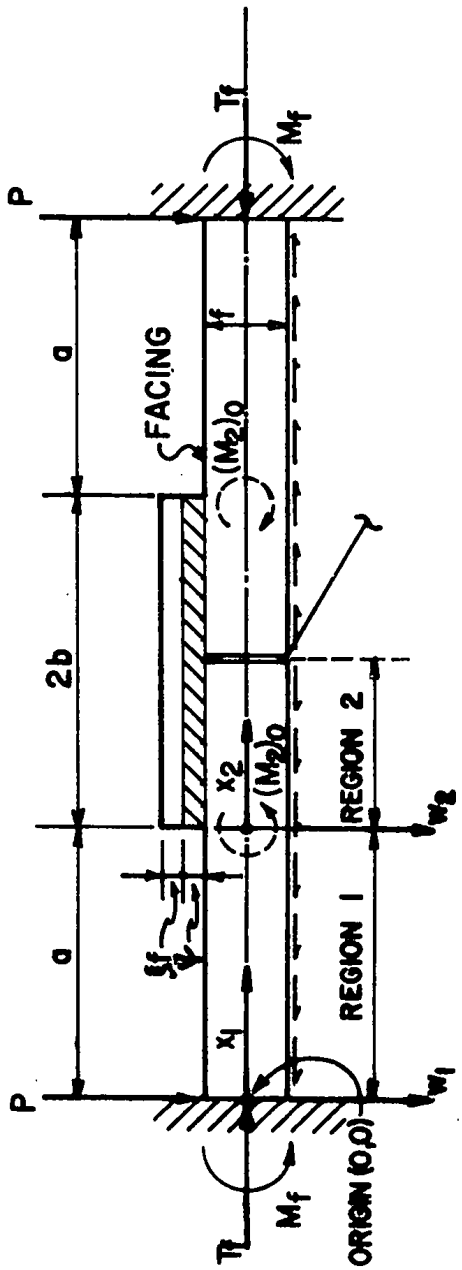

FIG. 4 DETAIL A

(iii) The bending effect on the facings due to the shear stress τ between aluminum sheets and core is neglected.

(iv) Deflections are assumed to be small, hence small deflection theory is used.

(v) As shown in Fig. 4, we are considering two rectangular sheets of the same material of unit width and of lengths $2(a + b)$, and $2b$. The faces of the longer and shorter sheets of thickness f and ξf respectively, $(0 < \xi \leq 1)$, are cemented by an adhesive layer of thickness ψ, where ψ is small compared to f. The force T_f induced in the faces due to bending of the sandwich beam is considered per unit width. The stiffened structure is considered as a homogeneous thin plate with finite discontinuities in its thickness and in its neutral plane. Bending of the neutral plane occurs under the applied loads; hence, a bending moment and compressive force acts on the longer sheet at the bond edges.

The basic equations necessary for the solution of the problem are formulated within the framework of classical plate theory together with a system of sufficient boundary conditions.

4.2 STRESS RESULTANTS AT THE BOND EDGES

The composite plate shown in Fig. 4 will be considered as a homogeneous cylindrically-bent plate with a discontinuous thickness and neutral plane. For this calculation, since the thickness ψ of the adhesive layer is relatively small compared to the thickness f of the facings, the effect of adhesive thickness will be initially neglected. The loading T_f and M_f at the edges of the plate, will produce a stress couple resultant $(M_2)_o$ acting on the facings at the bond edges. $(M_2)_o$ can be expressed in terms of the forces (T_f, M_f) and the physical dimensions of the plate, as shown below:

$$\frac{d^2\omega}{dx^2} = -\frac{M}{D} \qquad (1)$$

which is the general expression relating curvature and bending moment, where

D, the flexural rigidity of the plate, is given by

$$D = \frac{E_f \cdot f^3}{12(1-\nu^2)}$$

where

E_f is Young's Modulus for facings,

and ν is Poisson's ratio for facings.

The deformation of the structure may be conveniently studied by separating it into regions 1 and 2 with

coordinates (x_1,ω_1) and (x_2,ω_2) respectively, where both coordinate systems are fixed, as shown in Fig. 2. Then the bending moments acting at generic sections of regions 1 and 2 are given by

$$M_1 = M_f - T_f\omega_1 \qquad 0 \leq x_1 \leq a \tag{3}$$

$$M_2 = M_f + T_f(\frac{\xi f}{2} - \omega_2) \quad 0 \leq x_2 \leq b \tag{4}$$

where M_f is the moment in the facings at the concentrated loads P. In Eq. (4), the adhesive thickness ψ is neglected and the neutral axis of the facing is assumed to shift upward by half the thickness of the cover plate $\frac{\xi f}{2}$ at the beginning of region 2. It should be noted that the length of region 2 (4 to 8 in) is so large, relative to the facing thickness (.030"), that the assumption made regarding the upward shifting of the neutral axis is not unrealistic.

Substituting Eqs. (3) and (4) into Eq. (1), respectively, and introducing the factor $(1+\xi)^3$ to account for the variable thickness, the following equations are obtained

$$\frac{d^2\omega_1}{dx_1^2} - \frac{T_f}{D}\omega_1 = -\frac{M_f}{D} \qquad 0 \leq x_1 \leq a \tag{5}$$

$$\frac{d^2\omega_2}{dx^2_2} - \frac{T_f\omega_2}{(1+\xi)^3 D} = \frac{-1}{(1+\xi)^3 D}\{M_f + \frac{T_f\xi f}{2}\} \quad 0 \leq x_2 \leq b \tag{6}$$

Eqs. (5) and (6) have general solutions

$$\omega_1 = A \sinh\{(\frac{T_f}{D})^{\frac{1}{2}}x_1\} + B \cosh\{(\frac{T_f}{D})^{\frac{1}{2}}x_1\} + \frac{M_f}{T_f} \tag{7}$$

$$\omega_2 = C \sinh\left\{\left(\frac{T_f}{(1+\xi)^3 D}\right)^{\frac{1}{2}}\right\}x_2 + D \cosh\left\{\left(\frac{T_f}{(1+\xi)^3 D}\right)^{\frac{1}{2}}\right\}x_2 +$$

$$+ \frac{M_f}{T_f} + \frac{\xi f}{2} \qquad (8)$$

The intermediate steps have been omitted for brevity. The constants of integration A,B,C,D and M_f are determined from the following five conditions:

$$\text{at} \qquad x_1 = 0, \quad \omega_1 = 0, \quad \frac{d\omega_1}{dx_1} = 0$$

$$\text{at} \qquad x_1 = a, \quad x_2 = 0, \quad \omega_1 = \omega_2, \frac{d\omega_1}{dx_1} = \frac{d\omega_2}{dx_2} \qquad (9)$$

$$\text{at} \qquad x_2 = b, \quad \frac{d\omega_2}{dx_2} = 0$$

After the constants in Eqs. (7) and (8) have been determined by use of Eq. (9), the bending moment at the bond edges is given by

$$(M_2)_o = (M_1)_{x_1=a} = - D\left\{\frac{d^2\omega_1}{dx_1^2}\right\}_{x_1=a}$$

$$(M_2)_o =$$

$$\frac{\frac{-\xi f T_f}{2} \sinh\left\{\left(\frac{T_f}{(1+\xi)^3 D}\right)^{\frac{1}{2}} b\right\} \cosh\left\{\left(\frac{T_f}{D}\right)^{\frac{1}{2}} a\right\}}{(1+\xi)^{\frac{3}{2}}\left\{\sinh\left(\frac{T_f}{D}\right)^{\frac{1}{2}} a\right\}\left\{\cosh b\left(\frac{T_f}{(1+\xi)^3 D}\right)^{\frac{1}{2}}\right\} + \cosh\left\{a\left(\frac{T_f}{D}\right)^{\frac{1}{2}}\right\}\sinh\left\{b\left(\frac{T_f}{(1+\xi)^3 D}\right)^{\frac{1}{2}}\right\}}$$

(10a)

Eq. (10) applies to the moment $(M_2)_o$ in the connected facings on the compression side of the sandwich beam. For the tension side, the following equation applies.

$$(M_2)_o = \frac{+\xi f T_f}{2} \frac{\sinh\{(\frac{T_f}{(1+\xi)^3 D})^{\frac{1}{2}} b\}\cosh\{(\frac{T_f}{D})^{\frac{1}{2}} a\}}{(1+\xi)^{\frac{3}{2}}\sinh\{(\frac{T_f}{D})^{\frac{1}{2}} a\}\cosh\{(\frac{T_f}{(1+\xi)^3 D})^{\frac{1}{2}} b\}+\cosh\{(\frac{T_f}{D})^{\frac{1}{2}} a\}\sinh\{(\frac{T_f}{(1+\xi)^3 D})^{\frac{1}{2}} b\}} \qquad (10b)$$

4.3 EQUATIONS FOR STRESSES σ AND τ IN THE ADHESIVE LAYER

We now consider the bonded region. The ends of the lower sheet, Fig. 5 are acted upon by a compressive force resultant T_f and by a bending moment resultant $(M_2)_o$ given by Eq. (10). Because the bond is considered in its undeformed state, symmetry requires the shear to vanish at the ends. The x-axis has its origin, as shown in Fig. 5. Equations which must be satisfied by each of the bonded sheets and by the adhesive will now be formulated.

According to the theory of cylindrically-bent plates, an element of the upper sheet will be acted upon by T_u and Q_u, the axial and shear force resultants and by M_u, a bending moment resultant, as shown in Fig. 6(a). Counter-clockwise moments and downward forces are taken positive. Since the forces and the moments are in equilibrium with the adhesive stresses σ and τ, the following equations hold

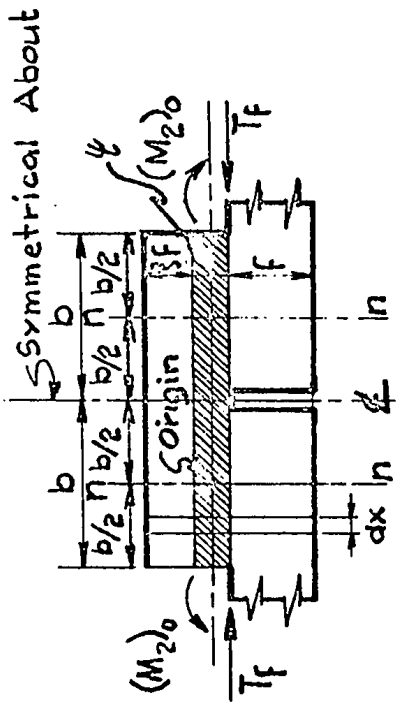

FIG. 5 BONDED REGION SHOWING APPLIED LOADS

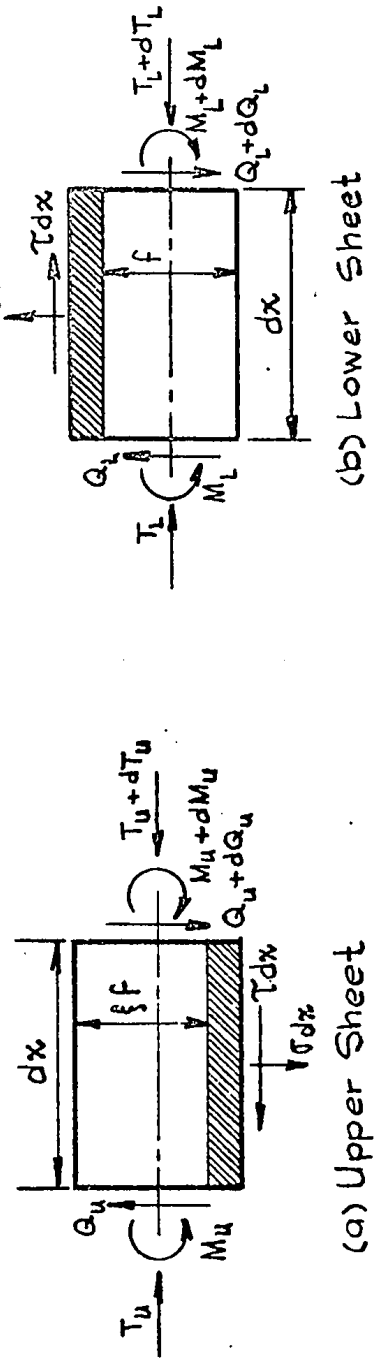

FIG. 6 STRESSES ON AN ELEMENT OF BONDED REGION

$$\frac{dM_u}{dx} + Q_u + \frac{\tau \xi f}{2} = 0$$

$$\frac{dQ_u}{dx} + \sigma = 0 \qquad (11)$$

$$\frac{dT_u}{dx} + \tau = 0$$

Similarly, if an element of the lower sheet (Fig. 6(b) is considered, then for equilibrium, the following equations must be satisfied.

$$\frac{dM_L}{dx} + Q_L + \frac{\tau f}{2} = 0$$

$$\frac{dQ_L}{dx} - \sigma = 0 \qquad (12)$$

$$\frac{dT_L}{dx} - \tau = 0$$

If the positive transverse deflections of the neutral planes of the upper and lower sheets are denoted by ω_u and ω_L respectively, then from the Bernoulli's law

$$\frac{d^2\omega_u}{dx^2} = -\frac{M_u}{\xi^3 D}$$

$$\frac{d^2\omega_L}{dx^2} = -\frac{M_L}{D} \qquad (13)$$

If u_U and u_L are the longitudinal displacements of the lowermost and the uppermost fibres of the upper and lower sheets respectively, then

$$\frac{du_U}{dx} = \frac{1}{E}\{\frac{T_u}{\xi f} + \frac{6M_u}{\xi^2 f^2}\}$$
$$\frac{du_L}{dx} = \frac{1}{E}\{\frac{T_L}{f} - \frac{6M_L}{f^2}\} \qquad (14)$$

Finally, from the stress-strain relations for the adhesive, we have

$$\frac{\tau}{G_c} = \frac{u_L - u_U}{\psi} \qquad (15)$$

$$\frac{\sigma}{E_c} = \frac{\omega_L - \omega_U}{\psi} \qquad (16)$$

where E_c and G_c are the Young's and the shear moduli respectively for the adhesive and ψ is the thickness of the adhesive.

Equations for the determination of the adhesive stresses σ and τ can now be formulated. Differentiating Eq. (15) and substituting Eq. (14) gives

$$\frac{d\tau}{dx} = \frac{G_c}{\psi E f}\{(T_L - \frac{6M_L}{f}) - \frac{1}{\xi}(T_u + \frac{6M_u}{f})\} \qquad (17)$$

Differentiating Eq. (17) twice and substituting Eqs. (11) and (12) yields

$$\frac{d^3\tau}{dx^3} = \frac{G_c}{Ef\psi}\{\frac{4(1+\xi)}{\xi}\frac{d\tau}{dx} + \frac{6\sigma}{f}\frac{(1-\xi^2)}{\xi^2}\} \qquad (18)$$

In a similar manner, differentiating Eq. (16) and substituting Eq. (13), we obtain

$$\frac{d^2\sigma}{dx^2} = \frac{E_c}{\psi D}(\frac{M_u}{\xi^3} - M_L) \qquad (19)$$

Differentiating Eqs. (19) twice and substituting Eqs. (11) and (12) gives

$$\frac{d^4\sigma}{dx^4} = -\frac{E_c}{\psi D}\{\frac{\sigma(1+\xi^3)}{\xi^3} + \frac{f}{2\xi^2}(\xi^2 - 1)\frac{d\tau}{dx}\} \qquad (20)$$

Equations (18) and (20) form a pair of simultaneous, ordinary differential equations with constant coefficients for determination of the stress distribution in the adhesive. Moreover, seven conditions are necessary with which to evaluate the seven arbitrary constants involved in the solution of Equations (18) and (20). The following physical conditions hold at the bond edges. (Refer to left-hand side of Fig. 5).

$$\left.\begin{aligned} M_u = Q_u = T_u = 0 \\ M_L = (M_2)_o;\ T_L = T_f\ ;\ Q_L = 0 \end{aligned}\right\} \text{ at } x = \pm\frac{b}{2} \qquad (21)$$

Equivalently, the substitution of Eqs. (21) into Eqs. (17) and (19) yields

$$\left.\begin{aligned} \frac{d\tau}{dx} &= \frac{G_c}{E\psi f}\left(T_f - \frac{6(M_2)_o}{f}\right) \quad \text{at } x = +\frac{b}{2} \\ \frac{d\tau}{dx} &= -\frac{G_c}{\psi E f}\left(T_f - \frac{6(M_2)_o}{f}\right) \quad \text{at } x = -\frac{b}{2} \end{aligned}\right\} \tag{22}$$

$$\frac{d^2\sigma}{dx^2} = \frac{-E_c}{\psi D}(M_2)_o \qquad \text{at } x = \pm\frac{b}{2} \tag{23}$$

To Equations (22) and (23), the following equilibrium and symmetry conditions are added, assuming $\xi = 1$, that is when both plates are of equal thickness.

$$\int_{-\frac{b}{2}}^{0} \tau \, dx = \frac{T_f}{2} \tag{24}$$

$$\int_{-\frac{b}{2}}^{+\frac{b}{2}} \sigma \, dx = 0; \quad \sigma\left(\frac{b}{2}\right) = \sigma\left(-\frac{b}{2}\right) \tag{25}$$

4.3.1 Solution of the Differential Equations (18) and (20)

The solution of Eqs. (18) and (20) for the adhesive stresses subject to Equations (22) to (25) will now be considered. For the special case of $\xi = 1$, that is, when both sheets are of equal thickness, Eqs. (18) and (20) reduce to

$$\frac{d^3\tau}{dx^3} = \frac{8G_c}{E\psi f}\frac{d\tau}{dx} \tag{26}$$

$$\frac{d^4\sigma}{dx^4} = -\frac{2E_c}{\psi D}\sigma \qquad (27)$$

which are independent of each other.

The solution of Eqs. (26) with boundary conditions specified by Eqs. (22) and (24) is

$$\tau = \frac{3T_f+6\frac{(M_2)_o}{f}}{4b} + \frac{\frac{\sqrt{2}}{4}\left(\frac{G_c}{E\psi f}\right)^{\frac{1}{2}}\left(T_f-\frac{6(M_2)_o}{f}\right)\cosh\ 2\sqrt{2}\left(\frac{G_c}{E\psi f}\right)^{\frac{1}{2}}x\}}{\sinh\{2\sqrt{2}\left(\frac{G_c}{E\ f}\right)^{\frac{1}{2}}\frac{b}{2}\}} \qquad (28)$$

The solution of Eq. (27) under the conditions given by Eqs. (23) and (25) is

$$\begin{aligned}\sigma = & -2\left(\frac{E_c}{2\psi D}\right)^{\frac{1}{2}}(M_2)_o\left[\sin\{\left(\frac{E_c}{2\psi D}\right)^{\frac{1}{2}}b\} + \sinh\{\left(\frac{E_c}{2\psi D}\right)^{\frac{1}{4}}b\}\right]^{-1} X \\ & X\left[\cos\{\left(\frac{E_c}{2\psi D}\right)^{\frac{1}{4}}\frac{b}{2}\}\sinh\left(\frac{E_c}{2\psi D}\right)^{\frac{1}{4}}\frac{b}{2}\} - \sin\{\left(\frac{E_c}{2\psi D}\right)^{\frac{1}{4}}\frac{b}{2}\}\cos\{\left(\frac{E_c}{2\psi D}\right)^{\frac{1}{4}}\frac{b}{2}\}\right. \\ & \cos\{\left(\frac{E_c}{2\psi D}\right)^{\frac{1}{4}}x\}\cosh\{\left(\frac{E_c}{2\psi D}\right)^{\frac{1}{4}}x\} + \cos\{\left(\frac{E_c}{2\psi D}\right)^{\frac{1}{4}}\frac{b}{2}\}\sinh\{\left(\frac{E_c}{2\psi D}\right)^{\frac{1}{4}}\frac{b}{2}\} + \\ & \left. + \sin\{\left(\frac{E_c}{2\psi D}\right)^{\frac{1}{4}}\frac{b}{2}\}\cosh\{\left(\frac{E_c}{2\psi D}\right)^{\frac{1}{4}}\frac{b}{2}\}\sin\{\left(\frac{E_c}{2\psi D}\right)^{\frac{1}{4}}x\}\sinh\{\left(\frac{E_c}{2\psi D}\right)^{\frac{1}{4}}x\}\right]\end{aligned} \qquad (29)$$

The maximum values of τ and σ occur at the boundaries and are given by the following expressions:

$$\tau_{max} = \frac{3T_f + 6\frac{(M_2)_o}{f}}{4b} + \frac{\sqrt{2}}{4}\left(\frac{G_c}{E\psi f}\right)^{\frac{1}{2}}\left(T_f - 6\frac{(M_2)_o}{f}\right)\coth\left\{2\sqrt{2}\left(\frac{G_c}{E\psi f}\right)^{\frac{1}{2}}\frac{b}{2}\right\}$$

$$\sigma_{max} = \frac{-\left(\frac{E_c}{2\psi D}\right)^{\frac{1}{2}}(M_2)_o\left\{\left[\sinh\left\{\left(\frac{E_c}{2\psi D}\right)^{\frac{1}{4}}b\right\}\right] - \sin\left[\left\{\left(\frac{E_c}{2\psi D}\right)^{\frac{1}{4}}b\right\}\right]\right\}}{\left[\sinh\left\{\left(\frac{E_c}{2\psi D}\right)^{\frac{1}{4}}b\right\} + \sin\left\{\left(\frac{E_c}{2\psi D}\right)^{\frac{1}{4}}b\right\}\right]} \qquad (30)$$

4.4 ILLUSTRATIVE EXAMPLE

Calculations of the stresses in the adhesive are made for actual values of the parameters in a stiffened plate. Specimens of joints used for experimental verification of theoretical results were fabricated using the same values of parameters for comparison. For the designation of specimens, their types, mode of testing, etc., refer to Chapter VII. For the plates, the values chosen are $E_{Al} = 10.25 \times 10^6$ psi; $\nu = 0.33$; $a = 2.0$ in.; $b = 4.0$ in.; $f = 0.030$ in.; $\psi = 0.0128$ in. (Fig. 3). For the bond, the material constants are $E_c = 516 \times 10^3$ psi and $G_c = 184 \times 10^3$ psi, which are representative values for Waldex W-105 adhesive.

In Fig. 7, the stress variation of τ (Eq. 28) in the adhesive is plotted for the case $\xi = 1.0$ for 500, 750 and 1,000 lbs of applied load 2P on specimens (Fig. 3). These loads are converted into their corresponding T_fs and M_fs using the flexural properties of sandwich beams. Fig. 8 illustrates the nature of σ variation (Eq. 29) for $\xi = 1.0$ and is seen

to decay quite rapidly away from the edge. In Fig. (9), the maximum values of τ_{max} and σ_{max} of the adhesive stresses are plotted as a function of bond length for the case $\xi = 1$, using different cover plate lengths and calculating τ_{max} and σ_{max} at the bonded edges in each case separately.

4.5 CONCLUSIONS

The graphs in Fig. 7 and 8 reveal that the yielding of the adhesive will occur at the bond edges where the maximum stresses occur. Although σ_{max} is less than τ_{max}, σ_{max} is the stress which produces yielding because Waldex W-105, has a yield stress of approximatly 2485 psi in shear as compared to 1250 psi in tension. Furthermore, it is seen from Fig. 9 that the maximum stress is independent of bond length except when the bond length is very small. Hence, the bond will yield by tearing off at its edges. This tear travels in towards the centre of the bond and will probably stop when the remaining overlap becomes small.

Another theoretical study similar to the one outlined in this Chapter, but with a different set of assumptions is presented in Chapters V and VI.

These theoretical results are compared with their experimental counterparts collected from tests performed on the joint specimens in the structures laboratory (Chapter VII).

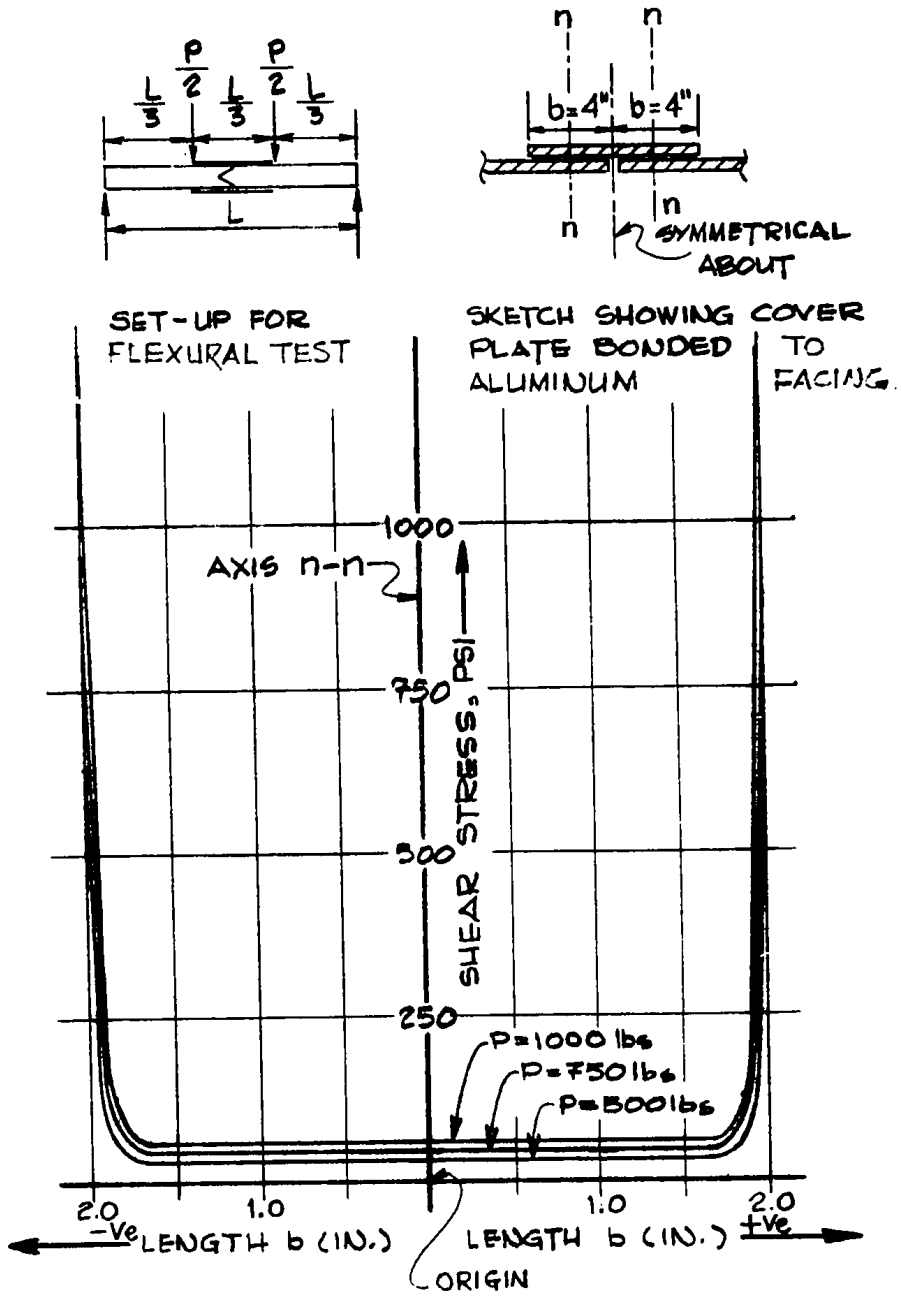

FIG. 7 THEORETICAL DISTRIBUTION OF SHEAR STRESS IN ADHESIVE ON THE COMPRESSION SIDE OF SPECIMEN A_1 IN FLEXURAL TESTING (SMALL DEFLECTION THEORY).

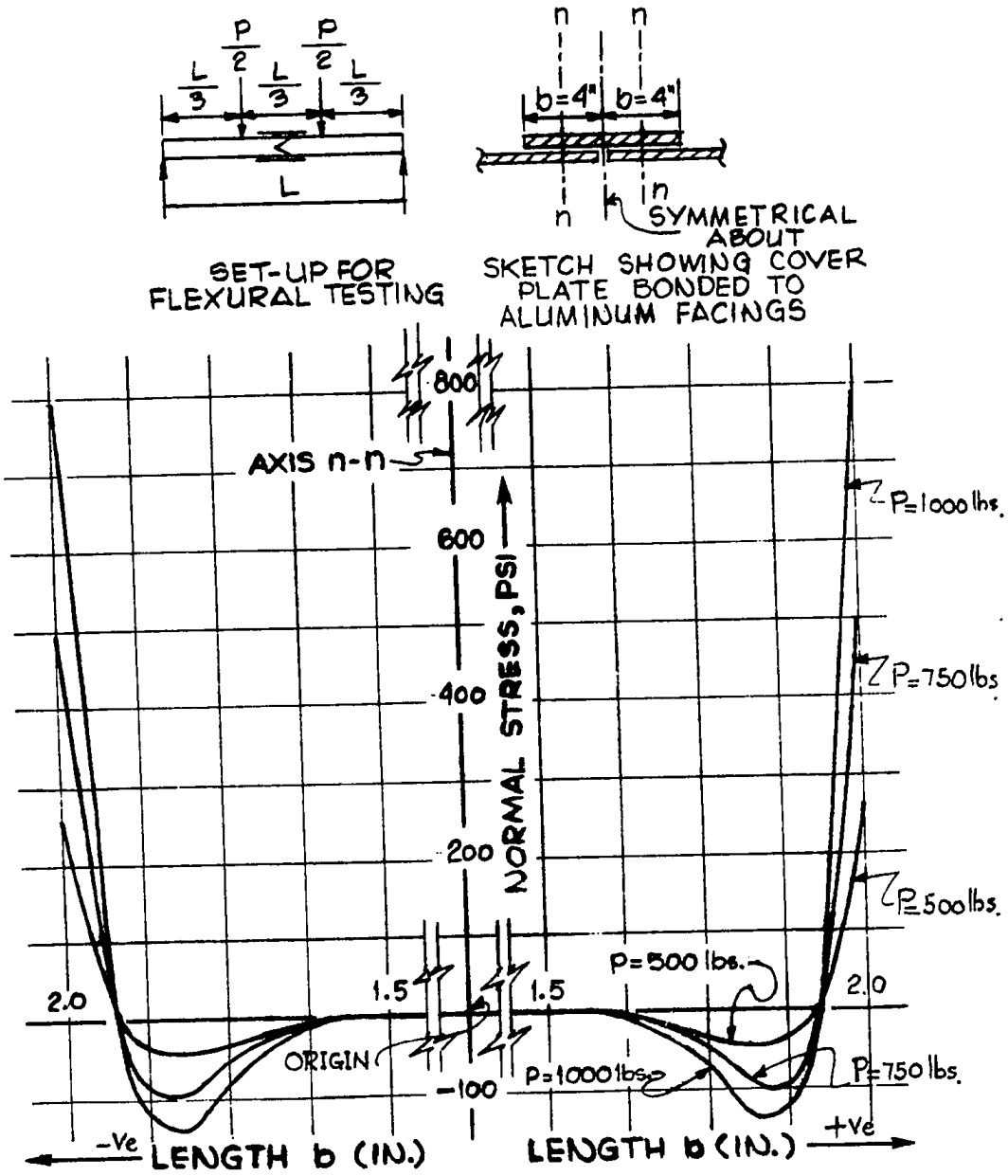

FIG. 8 THEORETICAL DISTRIBUTION OF NORMAL STRESS IN ADHESIVE ON THE COMPRESSION SIDE OF SPECIMEN A1 IN FLEXURAL TESTING (SMALL DEFLECTION THEORY)

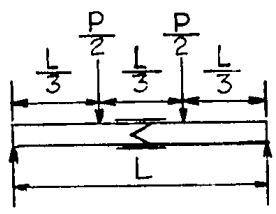

SET-UP FOR
FLEXURAL TESTING

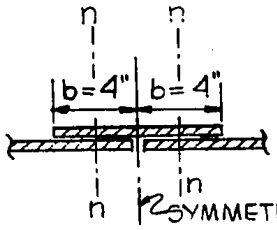

SKETCH SHOWING COVER PLATE
BONDED TO ALUMINUM FACINGS

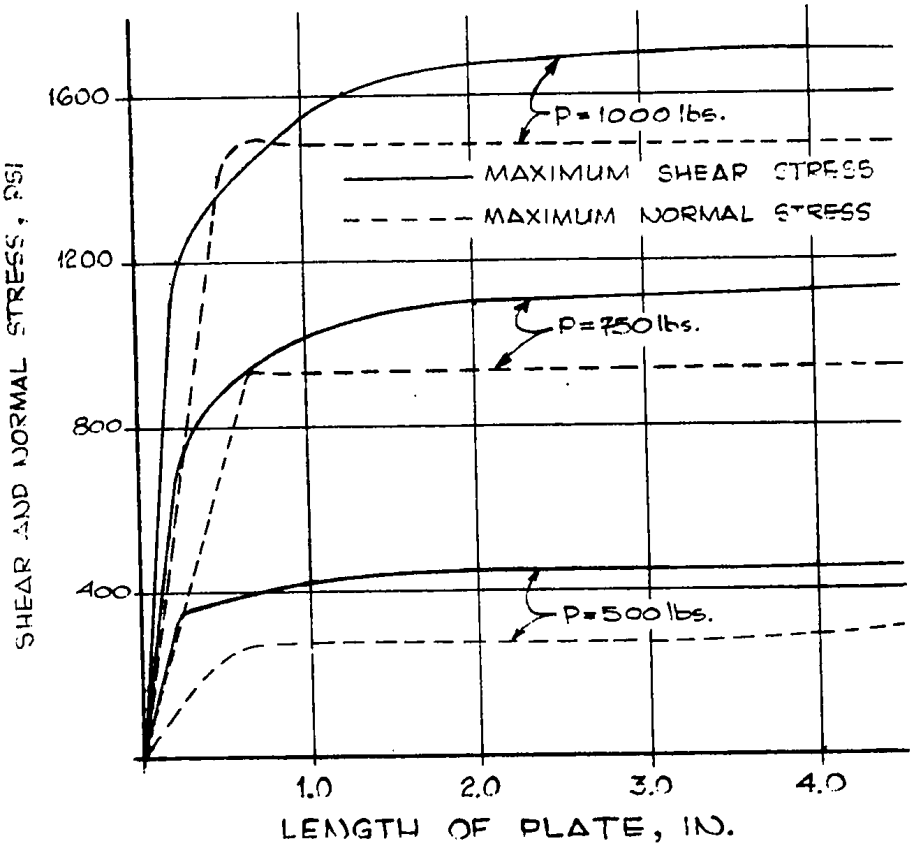

FIG. 9 MAXIMUM SHEAR AND NORMAL STRESSES IN THE ADHESIVE AS FUNCTIONS OF BOND LENGTH ON THE COMPRESSION SIDE OF SPECIMEN A, IN FLEXURAL TESTING (SMALL DEFLECTION THEORY).

CHAPTER V

THEORETICAL ANALYSIS OF ADHESIVE-BONDED MID-PANEL JOINTS CONNECTING SANDWICH PANELS

LARGE DEFLECTION THEORY : COMPRESSION SIDE OF SPECIMENS

The joint to be analyzed is the same as used in Chapter IV. This type of joint, as shown in Fig. 3, is primarily dependent on adhesives for its strength. The most critical area from the strength point of view, is the adhesive between the cover plate and the aluminum facings. This connection is to be used in joining sandwich panels in which all bending moment is taken by the aluminum facings and the shear by the core.

As shown in Fig. 10, we are considering two rectangular sheets of the same material of unit width and of lengths $(2a + b)$ and b. The faces of the longer and shorter sheets of thickness f and ξf respectively, $(0 < \xi < 1)$, are cemented by an adhesive layer of thickness ψ, where ψ is small compared to f. The force T_f induced in the faces due to bending of the sandwich beam is considered per unit width. The stiffened structure is considered as a homogeneous thin plate with finite discontinuities in its thickness and in its neutral plane. Bending of the neutral plane will occur under the applied loads; hence, a bending moment,and a compressive force acts on the longer sheet at the bond edges.

5.1 BASIC ASSUMPTIONS

The basic assumptions in this investigation are the following:

(i) The stress in the adhesive is assumed to have only two non-vanishing components, the normal stress σ and the shear stress τ, which vary negligibly across the small thickness of the bond.

(ii) The bending effect cn the facings due to the shear stress τ between aluminum sheets and core is neglected.

(iii) In this analysis β-vertical component of the axial force (T_f) induced in the facings of the sandwich beam has also been included. This component is a function of the deflections of the facing and because of its small magnitude was neglected in the analysis in Chapter IV.

5.2 STRESS RESULTANTS AT THE BOND EDGES

Because of the variable thickness of the structure shown in Fig. 10, bending will occur under the loading T_f and M_f, and will produce a stress couple resultant $(M_2)_o$ acting on the facings at the bond edges. To determine this bending moment, the structure will be considered as a homogeneous cylindrically bent plate with a discontinuous thickness and neutral plane. For this calculation, since

$\psi << f$, the effect of adhesive will be neglected.

We know that

$$\frac{d^2y}{dx^2} = -\frac{M}{D} \qquad (1)$$

which is the general expression relating curvature and bending moment, where D, the flexural rigidity of the plate, is given by

$$D = \frac{E_f \cdot f^3}{12(1 - \nu^2)}$$

In this analysis two values of D, i.e., D_{f_1} and D_{f_2} have been used corresponding to Section I and Section II, of the composite plate, respectively (Fig. 10).

E_f is Young's modulus for facings, and ν is Poisson's ratio for facings.

The deformation of the structure may be conveniently studied by separating it into Sections I and II, with coordinates (x,y_1) and (x,y_2), respectively, where both coordinate systems are as shown in Fig. 10. The bending moments acting at the general sections m-m and n-n of Sections I and II, respectively, are given by :

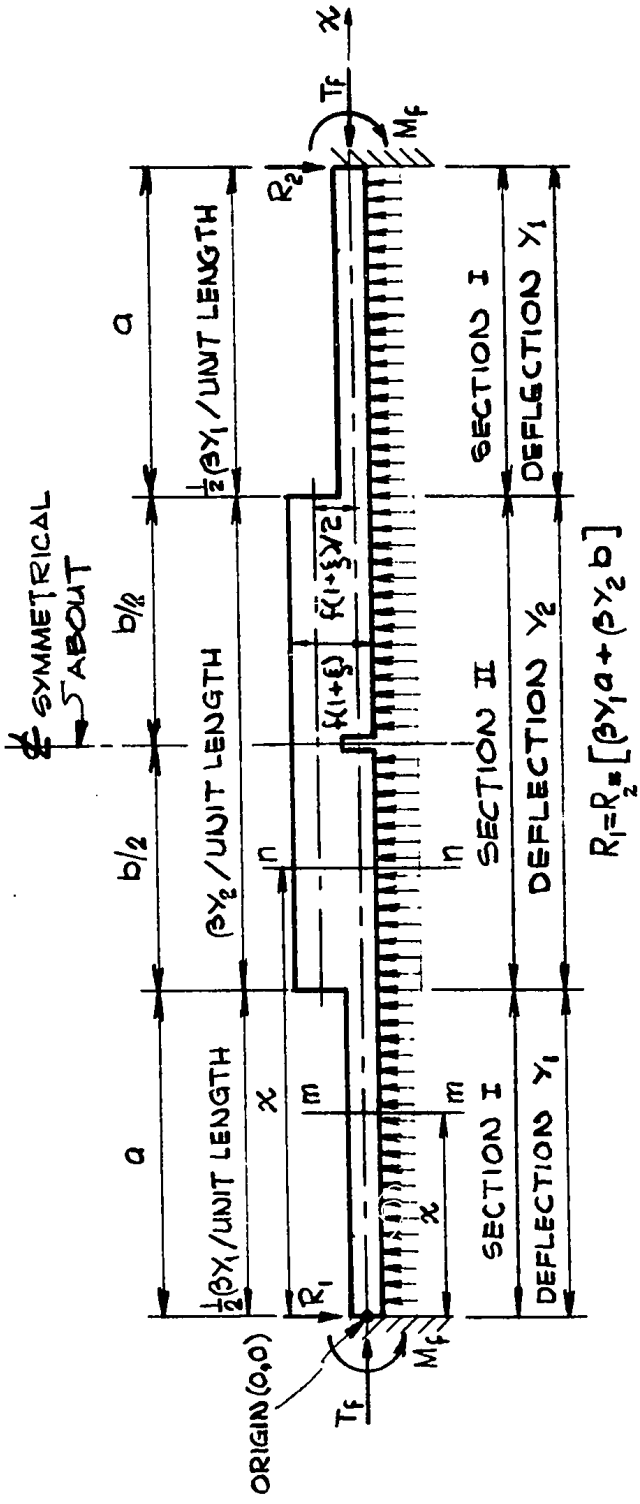

FIG. 10 ALUMINUM FACING AND COVER PLATE SHOWN AS A COMPOSITE PLATE WITH FINITE DISCONTINUITIES IN ITS THICKNESS (Thickness of adhesive being neglected).

$$M_1 = M_f + \left[\frac{\beta y_1 a}{2} + \frac{\beta y_2 b}{2}\right] x + \left[-T_f\right] y_1 - \frac{\beta y_1 x^2}{4} \quad \ldots\ldots\ldots\ldots\ldots\ldots o \leq x \leq a \qquad (2)$$

$$M_2 = M_f + \left[\frac{\beta y_1 a}{2} + \frac{\beta y_2 b}{2}\right] x - T_f\left[y_2 + \frac{f}{2} + \frac{\xi f}{2}\right] - \frac{\beta y_1 a}{2}\left[\frac{a}{2} + x - a\right] - \frac{\beta y_2}{2}\left[x^2 - 2ax + a^2\right] \ldots\ldots a \leq x \leq b \qquad (3)$$

The substitution of equations (2) and (3) into Eq. (1) yields:

$$\frac{d^2 y_1}{dx^2} = -\frac{M_f}{D_{f_1}} - \frac{\beta ax}{2D_{f_1}} y_1 - \frac{\beta bx}{2D_{f_1}} y_2 + \frac{T_f}{D_{f_1}} y_1 + \frac{\beta x^2}{4D_{f_1}} y_1 \qquad (4)$$

$$\frac{d^2 y_2}{dx^2} = -\frac{M_f}{D_{f_2}} - \frac{\beta ax}{2D_{f_2}} y_1 - \frac{\beta bx}{2D_{f_2}} y_2 + \frac{T_f}{D_{f_2}} y_2 + \frac{T_f . f}{2D_{f_2}} + \frac{T_f \xi f}{2D_{f_2}} + \frac{\beta ax}{2D_{f_2}} y_1 - \frac{\beta a^2}{4D_{f_2}} y_1 + \frac{\beta x^2}{2D_{f_2}} y_2$$

$$- \frac{\beta ax}{D_{f_2}} y_2 + \frac{\beta a^2}{2D_{f_2}} y_2 \qquad (5)$$

Now using operator D for $\frac{d}{dx}$ and assembling terms of y_1 and y_2 on the L.H.S., and the rest on the R.H.S., the following is obtained:

$$y_1\left[D^2 + \frac{\beta ax}{2D_{f_1}} - \frac{\beta x^2}{4D_{f_1}} - \frac{T_f}{D_{f_1}}\right] + y_2\left[\frac{\beta bx}{2D_{f_1}}\right] = \left[-\frac{M_f}{D_{f_1}}\right] \ldots\ldots\ldots o \leq x \leq a \qquad (6)$$

$$y_1\left[\frac{\beta a^2}{4D_{f_2}}\right] + y_2\left[\frac{\beta bx}{2D_{f_2}} - \frac{T_f}{D_{f_2}} - \frac{\beta x^2}{2D_{f_2}} + \frac{\beta ax}{D_{f_2}} - \frac{\beta a^2}{2D_{f_2}} + D^2\right] = \left[-\frac{M_f}{D_{f_2}} + \frac{T_f . f}{2D_{f_2}} + \frac{T_f . \xi f}{2D_{f_2}}\right] \qquad (7)$$

solving equations (6) and (7) for y_1 and y_2 by determinants, the following is obtained:

$$y_1 = \frac{\begin{vmatrix} \left[-\frac{M_f}{D_{f_1}}\right] & \left[\frac{\beta bx}{2D_{f_1}}\right] \\ \left[-\frac{M_f}{D_{f_2}} + \frac{T_f \cdot f}{2D_{f_2}} + \frac{T_f \cdot \xi f}{2D_{f_2}}\right] & \left[\frac{\beta bx}{2D_{f_2}} - \frac{T_f}{D_{f_2}} - \frac{\beta x^2}{2D_{f_2}} + \frac{\beta ax}{D_{f_2}} - \frac{\beta a^2}{2D_{f_2}} + D^2\right] \end{vmatrix}}{\begin{vmatrix} \left[D^2 + \frac{\beta ax}{2D_{f_1}} - \frac{\beta x^2}{4D_{f_1}} - \frac{T_f}{D_{f_1}}\right] & \left[\frac{\beta bx}{2D_{f_1}}\right] \\ \left[\frac{\beta a^2}{4D_{f_2}}\right] & \left[\frac{\beta bx}{2D_{f_2}} - \frac{T_f}{D_{f_2}} - \frac{\beta x^2}{2D_{f_2}} + \frac{\beta ax}{D_{f_2}} - \frac{\beta a^2}{2D_{f_2}} + D^2\right] \end{vmatrix}} \tag{8}$$

$$- \frac{M_f \beta bx}{2D_{f_1}D_{f_2}} + \frac{M_f T_f}{D_{f_1}D_{f_2}} + \frac{M_f \beta x^2}{2D_{f_1}D_{f_2}} - \frac{M_f \beta ax}{D_{f_1}D_{f_2}} + \frac{M_f \beta a^2}{2D_{f_1}D_{f_2}} - D^2\left(\frac{M_f}{D_{f_1}}\right) + \frac{M_f \beta bx}{2D_{f_1}D_{f_2}} - \frac{T_f \cdot f \beta bx}{4D_{f_1}D_{f_2}} - \frac{\beta b T_f \cdot \xi fx}{4D_{f_1}D_{f_2}}$$

$$y_1 = \frac{}{\left[\frac{D^2\beta bx}{2D_{f_2}} - \frac{D^2 T_f}{D_{f_2}} - \frac{D^2\beta x^2}{2D_{f_2}} + \frac{D^2\beta ax}{D_{f_2}} - \frac{D^2\beta a^2}{2D_{f_2}} + D^4 + \frac{\beta^2 abx^2}{4D_{f_1}D_{f_2}} - \frac{T_f \beta ax}{2D_{f_1}D_{f_2}} - \frac{\beta^2 ax^3}{4D_{f_1}D_{f_2}}\right.} \tag{9}$$

$$+ \frac{\beta^2 a^2 x^2}{2D_{f_1}D_{f_2}} - \frac{\beta^2 a^3 x}{4D_{f_1}D_{f_2}} + \frac{\beta ax D^2}{2D_{f_1}} - \frac{\beta^2 bx^3}{8D_{f_1}D_{f_2}} + \frac{\beta T_f x^2}{4D_{f_1}D_{f_2}} + \frac{\beta^2 x^4}{8D_{f_1}D_{f_2}} - \frac{\beta^2 ax^3}{4D_{f_1}D_{f_2}} + \frac{\beta^2 a^2 x^2}{8D_{f_1}D_{f_2}} - \frac{\beta x^2 D^2}{4D_{f_1}}$$

$$\left. - \frac{T_f \beta bx}{2D_{f_1}D_{f_2}} + \frac{T_f^2}{D_{f_1}D_{f_2}} + \frac{T_f \beta x^2}{2D_{f_1}D_{f_2}} - \frac{T_f \beta ax}{D_{f_1}D_{f_2}} + \frac{T_f \beta a^2}{2D_{f_1}D_{f_2}} - \frac{T_f D^2}{D_{f_1}} - \frac{\beta^2 a^2 bx}{8D_{f_1}D_{f_2}}\right]$$

$$\frac{d^2y_1}{dx^2}\left[\frac{\beta b}{2D_{f_2}}\right]x - \left[\frac{T_f}{D_{f_2}}\right]\frac{d^2y_1}{dx^2} - \left[\frac{\beta}{2D_{f_2}}\right]x^2\frac{d^2y_1}{dx^2} + \left[\frac{\beta a}{D_{f_2}}\right]x\frac{d^2y_1}{dx^2} - \left[\frac{\beta a^2}{2D_{f_2}}\right]\frac{d^2y_1}{dx^2} + \frac{d^4y_1}{dx^4} + \left[\frac{\beta^2 ab}{4D_{f_1}D_{f_2}}\right]x^2y_1 - \left[\frac{T_f\beta a}{2D_{f_1}D_{f_2}}\right]xy_1$$

$$- \left[\frac{\beta^2 a}{4D_{f_1}D_{f_2}}\right]x^3y_1 + \left[\frac{\beta^2 a^2}{2D_{f_1}D_{f_2}}\right]x^2y_1 - \left[\frac{\beta^2 a^3}{4D_{f_1}D_{f_2}}\right]xy_1 + \left[\frac{\beta a}{2D_{f_1}}\right]x\frac{d^2y_1}{dx^2} - \left[\frac{\beta^2 b}{8D_{f_1}D_{f_2}}\right]x^3y_1 + \left[\frac{\beta T_f}{4D_{f_1}D_{f_2}}\right]x^2y_1 + \left[\frac{\beta^2}{8D_{f_1}D_{f_2}}\right]x^4y_1$$

$$- \left[\frac{\beta^2 a}{4D_{f_1}D_{f_2}}\right]x^3y_1 + \left[\frac{\beta^2 a^2}{8D_{f_1}D_{f_2}}\right]x^2y_1 - \left[\frac{\beta}{4D_{f_1}}\right]x^2\frac{d^2y_1}{dx^2} - \left[\frac{T_f\beta b}{2D_{f_1}D_{f_2}}\right]xy_1 + \left[\frac{T_f^2}{D_{f_1}D_{f_2}}\right]y_1 + \left[\frac{T_f\beta}{2D_{f_1}D_{f_2}}\right]x^2y_1 - \left[\frac{T_f\beta a}{D_{f_1}D_{f_2}}\right]xy_1 + \left[\frac{T_f\beta a^2}{2D_{f_1}D_{f_2}}\right]y_1$$

$$- \left[\frac{T_f}{D_{f_1}}\right]\frac{d^2y_1}{dx^2} - \left[\frac{\beta^2 a^2 b}{8D_{f_1}D_{f_2}}\right]_1 + \left[\frac{M_f\beta b}{2D_{f_1}D_{f_2}}\right]x - \left[\frac{M_f T_f}{D_{f_1}D_{f_2}}\right] - \left[\frac{M_f\beta}{2D_{f_1}D_{f_2}}\right]x^2 + \left[\frac{M_f\beta a}{D_{f_1}D_{f_2}}\right]x - \left[\frac{M_f\beta a^2}{2D_{f_1}D_{f_2}}\right] + D^2\left(\frac{M_f^0}{D_{f_1}}\right)$$

$$- \left[\frac{M_f\beta b}{2D_{f_1}D_{f_2}}\right]x + \left[\frac{T_f \cdot f\beta b}{4D_{f_1}D_{f_2}}\right]x + \left[\frac{\beta b T_f \cdot \xi f}{4D_{f_1}D_{f_2}}\right]x = o \qquad (10)$$

$$\frac{d^4y_1}{dx^4} + \frac{d^2y_1}{dx^2}\left[-\frac{T_f}{D_{f_2}} - \frac{\beta a^2}{2D_{f_2}} - \frac{T_f}{D_{f_1}}\right] + \frac{d^2y_1}{dx^2}\left[-\frac{\beta}{2D_{f_2}} - \frac{3}{4D_{f_1}}\right]x^2 + \frac{d^2y_1}{dx^2}\left[\frac{\beta b}{2D_{f_2}} + \frac{\beta a}{D_{f_1}} + \frac{\beta a}{D_{f_2}}\right]x + y_1\left[\frac{\beta^2}{8D_{f_1}D_{f_2}}\right]x^4$$

$$+ y_1\left[-\frac{\beta^2 a}{4D_{f_1}D_{f_2}} - \frac{\beta^2 b}{8D_{f_1}D_{f_2}} - \frac{\beta^2 a}{4D_{f_1}D_{f_2}}\right]x^3 + y_1\left[\frac{\beta^2 ab}{4D_{f_1}D_{f_2}} + \frac{\beta^2 a^2}{2D_{f_1}D_{f_2}} + \frac{\beta T_f}{4D_{f_1}D_{f_2}} + \frac{\beta^2 a^2}{8D_{f_1}D_{f_2}} + \frac{T_f\beta}{2D_{f_1}D_{f_2}}\right]x^2$$

$$+ y_1\left[-\frac{T_f\beta a}{2D_{f_1}D_{f_2}} - \frac{\beta^2 a^3}{4D_{f_1}D_{f_2}} - \frac{T_f\beta b}{2D_{f_1}D_{f_2}} - \frac{T_f\beta a}{D_{f_1}D_{f_2}} - \frac{\beta^2 a^2 b}{8D_{f_1}D_{f_2}}\right]x + y_1\left[\frac{T_f^2}{D_{f_1}D_{f_2}} + \frac{T_f\beta a^2}{2D_{f_1}D_{f_2}}\right] - \left[\frac{M_f\beta}{2D_{f_1}D_{f_2}}\right]x^2$$

$$+ \left[\frac{M_f\beta a}{D_{f_1}D_{f_2}} + \frac{T_f \cdot f\beta b}{D_{f_1}D_{f_2}} - \frac{\beta b T_f \cdot \xi f}{D_{f_1}D_{f_2}}\right]x - \left[\frac{M_f T_f}{D_{f_1}D_{f_2}} - \frac{M_f\beta a^2}{2D_{f_1}D_{f_2}}\right] = o \qquad (11)$$

Now substituting coefficients k_1 , k_2 , k_3 ,.....in equation (11), we get:

$$\frac{d^4y_1}{dx^4} + k_1\frac{d^2y_1}{dx^2} + k_2x^2\frac{d^2y_1}{dx^2} + k_3x\frac{d^2y_1}{dx^2} + k_4x^4y_1 + k_5x^3y_1 + k_6x^2y_1 + k_7xy_1 + k_8y_1 + k_9x^2 + k_{10}x + k_{11} = 0 \qquad (12)$$

where :

$$k_1 = -\left[\frac{T_f}{D_{f_2}} + \frac{\beta a^2}{2D_{f_2}} + \frac{T_f}{D_{f_1}}\right] \quad \text{.....(a)}$$

$$k_2 = -\left[\frac{\beta}{2D_{f_2}} + \frac{\beta}{4D_{f_1}}\right] \quad \text{.....(b)}$$

$$k_3 = \left[\frac{\beta a}{2D_{f_1}} + \frac{\beta a}{D_{f_2}} + \frac{\beta b}{2D_{f_2}}\right] \quad \text{.....(c)}$$

$$k_4 = \left[\frac{\beta^2}{8D_{f_1}D_{f_2}}\right] \quad \text{.....(d)}$$

$$k_5 = -\left[\frac{\beta^2 a}{2D_{f_1}D_{f_2}} + \frac{\beta^2 b}{8D_{f_1}D_{f_2}}\right] \quad \text{.....(e)}$$

$$k_6 = \left[\frac{3\beta T_f}{4D_{f_1}D_{f_2}} + \frac{5\beta^2 a^2}{8D_{f_1}D_{f_2}} + \frac{\beta^2 ab}{4D_{f_1}D_{f_2}}\right] \quad \text{.....(f)}$$

$$k_7 = -\left[\frac{3T_f\beta a}{2D_{f_1}D_{f_2}} + \frac{T_f\beta b}{2D_{f_1}D_{f_2}} + \frac{\beta^2 a^3}{4D_{f_1}D_{f_2}} + \frac{\beta^2 a^2 b}{8D_{f_1}D_{f_2}}\right] \quad \text{.....(g)}$$

$$k_8 = \left[\frac{T_f^2}{D_{f_1}D_{f_2}} + \frac{T_f\beta a^2}{2D_{f_1}D_{f_2}}\right] \quad \text{.....(h)}$$

$$k_9 = -\left[\frac{M_f\beta}{2D_{f_1}D_{f_2}}\right] \quad \text{.....(i)}$$

$$k_{10} = \left[\frac{M_f\beta a}{D_{f_1}D_{f_2}} + \frac{T_f\beta b.f}{4D_{f_1}D_{f_2}} - \frac{T_f\beta b\xi f}{4D_{f_1}D_{f_2}}\right] \quad \text{.....(j)}$$

$$k_{11} = -\left[\frac{M_f T_f}{D_{f_1}D_{f_2}} + \frac{M_f\beta a^2}{2D_{f_1}D_{f_2}}\right] \quad \text{.....(k)}$$

(13)

Similarly:

$$y_2 = \frac{\begin{vmatrix} \left[D^2 + \frac{\beta a x}{2D_{f_1}} - \frac{\beta x^2}{4D_{f_1}} - \frac{T_f}{D_{f_1}}\right] & \left[-\frac{M_f}{D_{f_1}}\right] \\ \left[\frac{\beta a^2}{4D_{f_2}}\right] & \left[-\frac{M_f}{D_{f_2}} + \frac{T_f \cdot f}{2D_{f_2}} + \frac{T_f \cdot \xi f}{2D_{f_2}}\right] \end{vmatrix}}{\begin{vmatrix} \left[D^2 + \frac{\beta a x}{2D_{f_1}} - \frac{\beta x^2}{4D_{f_1}} - \frac{T_f}{D_{f_1}}\right] & \left[\frac{\beta b x}{2D_{f_1}}\right] \\ \left[\frac{\beta a^2}{4D_{f_2}}\right] & \left[\frac{\beta b x}{2D_{f_2}} - \frac{T_f}{D_{f_2}} - \frac{\beta x^2}{2D_{f_2}} + \frac{\beta a x}{D_{f_2}} - \frac{\beta a^2}{2D_{f_2}} + D^2\right] \end{vmatrix}} \tag{14}$$

$$= \frac{\left[-D^2\frac{M_f}{D_{f_2}} + D^2\frac{T_f \cdot f}{2D_{f_2}} + D^2\frac{T_f \cdot \xi f}{2D_{f_2}} - \frac{M_f \beta a x}{2D_{f_1}D_{f_2}} + \frac{T_f \cdot f \beta a x}{4D_{f_1}D_{f_2}} + \frac{T_f \cdot \xi f \beta a x}{4D_{f_1}D_{f_2}} + \frac{M_f \beta x^2}{4D_{f_1}D_{f_2}} - \frac{T_f \cdot f \beta x^2}{8D_{f_1}D_{f_2}} - \frac{T_f \cdot \xi f \beta x^2}{8D_{f_1}D_{f_2}} + \frac{T_f M_f}{D_{f_1}D_{f_2}} - \frac{T_f^2 \cdot f}{2D_{f_1}D_{f_2}} - \frac{T_f^2 \cdot \xi f}{2D_{f_1}D_{f_2}} + \frac{M_f \beta a^2}{4D_{f_1}D_{f_2}}\right]}{\left[\frac{D^2 \beta b x}{2D_{f_2}} - D^2\frac{T_f}{D_{f_2}} - D^2\frac{\beta x^2}{2D_{f_2}} + \frac{D^2 \beta a x}{D_{f_2}} - \frac{D^2 \beta a^2}{2D_{f_2}} + D^4 + \frac{\beta^2 a b x^2}{4D_{f_1}D_{f_2}} - \frac{T_f \beta a x}{2D_{f_1}D_{f_2}} - \frac{\beta^2 a x^3}{4D_{f_1}D_{f_2}} + \frac{\beta^2 a^2 x^2}{2D_{f_1}D_{f_2}} - \frac{\beta^2 a^3 x}{4D_{f_1}D_{f_2}} + D^2\frac{\beta a x}{2D_{f_1}} - \frac{\beta^2 b x^3}{8D_{f_1}D_{f_2}} + \frac{\beta T_f x^2}{4D_{f_1}D_{f_2}} + \frac{\beta^2 x^4}{8D_{f_1}D_{f_2}} - \frac{\beta^2 a x^3}{4D_{f_1}D_{f_2}} + \frac{\beta^2 a^2 x^2}{8D_{f_1}D_{f_2}} - D^2\frac{\beta x^2}{4D_{f_1}} - \frac{T_f \beta b x}{2D_{f_1}D_{f_2}} + \frac{T_f^2}{D_{f_1}D_{f_2}} + \frac{T_f \beta x^2}{2D_{f_1}D_{f_2}} - \frac{T_f \beta a x}{D_{f_1}D_{f_2}} + \frac{T_f \beta a^2}{2D_{f_1}D_{f_2}} - \frac{T_f D^2}{D_{f_1}} - \frac{\beta^2 a^2 b x}{8D_{f_1}D_{f_2}}\right]} \tag{15}$$

$$\frac{d^2y_2}{dx^2}\left[\frac{\beta b}{2D_{f_2}}\right]x-\left[\frac{T_f}{D_{f_2}}\right]\frac{d^2y_2}{dx^2}-\left[\frac{\beta}{2D_{f_2}}\right]x^2\frac{d^2y_2}{dx^2}+\left[\frac{\beta a}{D_{f_2}}\right]x\frac{d^2y_2}{dx^2}-\left[\frac{\beta a^2}{2D_{f_2}}\right]\frac{d^2y_2}{dx^2}+\frac{d^4y_2}{dx^4}+\left[\frac{\beta^2 ab}{4D_{f_1}D_{f_2}}\right]x^2y_2-\left[\frac{T_f\beta a}{2D_{f_1}D_{f_2}}\right]xy_2$$

$$-\left[\frac{\beta^2 a}{4D_{f_1}D_{f_2}}\right]x^3y_2+\left[\frac{\beta^2a^2}{2D_{f_1}D_{f_2}}\right]x^2y_2-\left[\frac{\beta^2a^3}{4D_{f_1}D_{f_2}}\right]xy_2+\left[\frac{\beta a}{2D_{f_1}}\right]x\frac{d^2y_2}{dx^2}-\left[\frac{\beta^2 b}{8D_{f_1}D_{f_2}}\right]x^3y_2+\left[\frac{\beta T_f}{4D_{f_1}D_{f_2}}\right]x^2y_2+\left[\frac{\beta^2}{8D_{f_1}D_{f_2}}\right]x^4y_2$$

$$-\left[\frac{\beta^2 a}{4D_{f_1}D_{f_2}}\right]x^3y_2+\left[\frac{\beta^2a^2}{8D_{f_1}D_{f_2}}\right]x^2y_2-\left[\frac{\beta}{4D_{f_1}}\right]x^2\frac{d^2y_2}{dx^2}-\left[\frac{T_f 3b}{2D_{f_1}D_{f_2}}\right]xy_2+\left[\frac{T_f^2}{D_{f_1}D_{f_2}}\right]y_2+\left[\frac{T_f\beta}{2D_{f_1}D_{f_2}}\right]x^2y_2-\left[\frac{T_f\beta a}{D_{f_1}D_{f_2}}\right]xy_2$$

$$+\left[\frac{T_f\beta a^2}{2D_{f_1}D_{f_2}}\right]y_2-\left[\frac{T_f}{D_{f_1}}\right]\frac{d^2y_2}{dx^2}-\left[\frac{\beta^2a^2b}{8D_{f_1}D_{f_2}}\right]xy_2+\left[\frac{M_f\beta a}{2D_{f_1}D_{f_2}}\right]x-\left[\frac{T_f.f\beta a}{4D_{f_1}D_{f_2}}\right]x-\left[\frac{T_f.\xi f\beta a}{4D_{f_1}D_{f_2}}\right]x-\left[\frac{M_f\beta}{4D_{f_1}D_{f_2}}\right]x^2$$

$$+\left[\frac{T_f.f\beta}{8D_{f_1}D_{f_2}}\right]x^2+\left[\frac{T_f.\xi f\beta}{8D_{f_1}D_{f_2}}\right]x^2-\left[\frac{T_fM_f}{D_{f_1}D_{f_2}}\right]+\left[\frac{T_f^2.f}{2D_{f_1}D_{f_2}}\right]+\left[\frac{T_f^2.\xi f}{2D_{f_1}D_{f_2}}\right]-\left[\frac{M_f\beta a^2}{2D_{f_1}D_{f_2}}\right]=0 \qquad (16)$$

$$\frac{d^4y_2}{dx^4}+\frac{d^2y_2}{dx^2}\left[-\frac{T_f}{D_{f_2}}-\frac{\beta a^2}{2D_{f_2}}-\frac{T_f}{D_{f_1}}\right]+\frac{d^2y_2}{dx^2}\left[-\frac{\beta}{2D_{f_2}}-\frac{\beta}{4D_{f_1}}\right]x^2+\frac{d^2y_2}{dx^2}\left[\frac{\beta b}{2D_{f_2}}+\frac{\beta a}{2D_{f_1}}+\frac{\beta a}{D_{f_2}}\right]x+y_2\left[\frac{\beta^2}{8D_{f_1}D_{f_2}}\right]x^4$$

$$+y_2\left[-\frac{\beta^2 a}{4D_{f_1}D_{f_2}}-\frac{\beta^2 b}{8D_{f_1}D_{f_2}}-\frac{\beta^2 a}{4D_{f_1}D_{f_2}}\right]x^3+y_2\left[\frac{\beta^2 ab}{4D_{f_1}D_{f_2}}+\frac{\beta^2a^2}{2D_{f_1}D_{f_2}}+\frac{\beta T_f}{4D_{f_1}D_{f_2}}+\frac{\beta^2a^2}{8D_{f_1}D_{f_2}}+\frac{T_f\beta}{2D_{f_1}D_{f_2}}\right]x^2$$

$$+y_2\left[-\frac{T_f\beta a}{2D_{f_1}D_{f_2}}-\frac{\beta^2a^3}{2D_{f_1}D_{f_2}}-\frac{T_f\beta b}{2D_{f_1}D_{f_2}}-\frac{T_f\beta a}{D_{f_1}D_{f_2}}-\frac{\beta^2a^2b}{8D_{f_1}D_{f_2}}\right]x+y_2\left[\frac{T_f^2}{D_{f_1}D_{f_2}}+\frac{T_f\beta a^2}{2D_{f_1}D_{f_2}}\right]+\left[-\frac{M_f\beta}{4D_{f_1}D_{f_2}}+\frac{T_f.f\beta}{8D_{f_1}D_{f_2}}+\frac{T_f.\xi f\beta}{8D_{f_1}D_{f_2}}\right]x^2$$

$$+\left[\frac{M_f\beta a}{2D_{f_1}D_{f_2}}-\frac{T_f.f\beta a}{4D_{f_1}D_{f_2}}-\frac{T_f.\xi f\beta a}{4D_{f_1}D_{f_2}}\right]x+\left[\frac{T_f^2.f}{2D_{f_1}D_{f_2}}-\frac{T_fM_f}{D_{f_1}D_{f_2}}+\frac{T_f^2.\xi f}{2D_{f_1}D_{f_2}}-\frac{M_f\beta a^2}{2D_{f_1}D_{f_2}}\right]=0 \qquad (17)$$

Now substituting coefficients k'_1 , k'_2 , k'_3 , in equation (17) we get:

$$\frac{d^4y_2}{dx^4} + k'_1\frac{d^2y_2}{dx^2} + k'_2x^2\frac{d^2y_2}{dx^2} + k'_3x\frac{d^2y_2}{dx^2} + k'_4x^4y_2 + k'_5x^3y_2 + k'_6x^2y_2 + k'_7xy_2 + k'_8y_2 + k'_9x^2 + k'_{10}x + k'_{11} = 0 \qquad (18)$$

where the corresponding coefficients are:

$$\left.\begin{aligned}
k'_1 &= -\left[\frac{T_f}{D_{f_2}} + \frac{\beta a^2}{2D_{f_2}} + \frac{T_f}{D_{f_1}}\right] \quad \text{.....(a)}\\
k'_2 &= -\left[\frac{\beta}{2D_{f_2}} + \frac{\beta}{4D_{f_1}}\right] \quad \text{.....(b)}\\
k'_3 &= \left[\frac{\beta a}{2D_{f_1}} + \frac{\beta a}{D_{f_2}} + \frac{\beta b}{2D_{f_2}}\right] \quad \text{.....(c)}\\
k'_4 &= \left[\frac{\beta^2}{8D_{f_1}D_{f_2}}\right] \quad \text{.....(d)}\\
k'_5 &= -\left[\frac{\beta^2 a}{2D_{f_1}D_{f_2}} + \frac{\beta^2 b}{8D_{f_1}D_{f_2}}\right] \quad \text{.....(e)}\\
k'_6 &= \left[\frac{3\beta T_f}{4D_{f_1}D_{f_2}} + \frac{5\beta^2a^2}{8D_{f_1}D_{f_2}} + \frac{\beta^2 ab}{4D_{f_1}D_{f_2}}\right] \quad \text{.....(f)}\\
k'_7 &= -\left[\frac{3T_f\beta a}{2D_{f_1}D_{f_2}} + \frac{T_f\beta b}{2D_{f_1}D_{f_2}} + \frac{\beta^2a^3}{2D_{f_1}D_{f_2}} + \frac{\beta^2a^2b}{8D_{f_1}D_{f_2}}\right] \quad \text{.....(g)}\\
k'_8 &= \left[\frac{T_f^2}{D_{f_1}D_{f_2}} + \frac{T_f\beta a^2}{2D_{f_1}D_{f_2}}\right] \quad \text{.....(h)}\\
k'_9 &= \left[-\frac{M_f\beta}{4D_{f_1}D_{f_2}} + \frac{T_f.f\beta}{8D_{f_1}D_{f_2}} + \frac{T_f.\xi f\beta}{8D_{f_1}D_{f_2}}\right] \quad \text{.....(i)}\\
k'_{10} &= \left[\frac{M_f\beta a}{2D_{f_1}D_{f_2}} - \frac{T_f\beta af}{4D_{f_1}D_{f_2}} - \frac{T_f.\xi f\beta a}{4D_{f_1}D_{f_2}}\right] \quad \text{.....(j)}\\
k'_{11} &= \left[\frac{T_f^2.f}{2D_{f_1}D_{f_2}} - \frac{T_fM_f}{D_{f_1}D_{f_2}} + \frac{T_f^2.\xi f}{2D_{f_1}D_{f_2}} - \frac{M_f\beta a^2}{2D_{f_1}D_{f_2}}\right] \quad \text{.....(k)}
\end{aligned}\right\} \qquad (19)$$

Equations (12) and (18) form the basic set of methematical expressions for solving the deflections y_1 and y_2 .

5.2.1 Solution of the Differential Equations for Deflections y_1 and y_2 :

As is obvious, Eqs. (12) and (18) are linear, non-homogeneous differential equations with variable coefficients. The integration of the two equations will be obtained by assuming y to be an unknown function expandable into an infinite series (converging for all values of x) i.e. : $y(x) = A_0 + A_1x + A_2x^2 + A_3x^3 \ldots + A_nx^n + \ldots$ where the A_n are undetermined coefficients.

Equation for the Deflection y_1 :

$$\frac{d^4y_1}{dx^4} + k_1\frac{d^2y_1}{dx^2} + k_2x^2\frac{d^2y_1}{dx^2} + k_3x\frac{d^2y_1}{dx^2} + k_4x^4y_1 + k_5x^3y_1 + k_6x^2y_1 + k_7xy_1 + k_8x^2 + k_9x + k_{10} = 0 \quad \ldots(12)$$

Assumed solution $$y_1(x) = A_0 + A_1x + A_2x^2 + A_3x^3 + \ldots\ldots\ldots + A_nx^n + \quad (20)$$

The derivatives of y_1 obtained by differentiating equation (20) term by term, are (assuming that the new series are also convergent for all values of x)

$$y_1'(x) = A_1 + 2A_2x^2 + 3A_3x^2 + \ldots\ldots\ldots + nA_nx^{n-1} + \ldots\ldots\ldots$$

$$y_1''(x) = 4A_2x + 6A_3x + \ldots\ldots\ldots + n(n-1)A_nx^{n-2} + \ldots\ldots\ldots$$

$$\vdots$$

etc.

The values of these derivatives when substituted in Eq. (12) must satisfy it. However, in order to form the recurrence equation, it was necessary to select the assumed solution and its successive derivatives as follows:

$$y_1(x) = A_{n-4}x^{n-4} + A_{n-3}x^{n-3} + A_{n-2}x^{n-2} + A_{n-1}x^{n-1} + A_nx^n \ldots\ldots(a)$$

$$y_1'(x) = (n-3)A_{n-3}x^{n-4} + (n-2)A_{n-2}x^{n-3} + (n-1)A_{n-1}x^{n-2} + nA_nx^{n-1} \ldots(b)$$

$$y_1''(x) = (n-2)(n-3)A_{n-2}x^{n-4} + (n-1)(n-2)A_{n-1}x^{n-3} + n(n-1)A_nx^{n-2} \ldots(c) \quad (21)$$

$$y_1'''(x) = (n-1)(n-2)(n-3)A_{n-1}x^{n-4} + n(n-1)(n-2)A_nx^{n-3} \ldots\ldots\ldots(d)$$

$$y_1^{iv}(x) = n(n-1)(n-2)(n-3)A_nx^{n-4} \ldots\ldots\ldots(e)$$

Substituting equations (21) in Eq. (12) gives the following :

$$\left[n(n-1)(n-2)(n-3)A_n x^{n-4}\right] + \left[(k_1 + k_2x^2 + k_3x)\left\{(n-2)(n-3)A_{n-2}x^{n-4} + (n-1)(n-2)A_{n-1}x^{n-3} + n(n-1)A_n x^{n-2}\right\}\right]$$
$$+\left[(k_4x^4 + k_5x^3 + k_6x^2 + k_7x + k_8)(A_{n-4}x^{n-4} + A_{n-3}x^{n-3} + A_{n-2}x^{n-2} + A_{n-1}x^{n-1} + A_n x^n)\right] + k_9x^2 + k_{10}x + k_{11} = o \qquad (21A)$$

$$n(n-1)(n-2)(n-3)A_n x^{n-4} + k_1(n-2)(n-3)A_{n-2}x^{n-4} + k_1(n-1)(n-2)A_{n-1}x^{n-3} + k_1(n)(n-1)A_n x^{n-2} + k_2(n-2)(n-3)A_{n-2}x^{n-2}$$
$$+ k_2(n-1)(n-2)A_{n-1}x^{n-1} + k_2 n(n-1)A_n x^n + k_3(n-2)(n-3)A_{n-2}x^{n-3} + k_3(n-1)(n-2)A_{n-1}x^{n-2} + k_3(n)(n-1)A_n x^{n-1}$$
$$+ k_4A_{n-4}x^n + k_4A_{n-3}x^{n+1} + k_4A_{n-2}x^{n+2} + k_4A_{n-1}x^{n+3} + k_4A_n x^{n+4} + k_5A_{n-4}x^{n-1} + k_5A_{n-3}x^n$$
$$+ k_5A_{n-2}x^{n+1} + k_5A_{n-1}x^{n+2} + k_5A_n x^{n+3} + k_6A_{n-4}x^{n-2} + k_6A_{n-3}x^{n-1} + k_6A_{n-2}x^n + k_6A_{n-1}x^{n+1}$$
$$+ k_6A_n x^{n+2} + k_7A_{n-4}x^{n-3} + k_7A_{n-3}x^{n-2} + k_7A_{n-2}x^{n-1} + k_7A_{n-1}x^n + k_7A_n x^{n+1} + k_8A_{n-4}x^{n-4} + k_8A_{n-3}x^{n-3}$$
$$+ k_8A_{n-2}x^{n-2} + k_8A_{n-1}x^{n-1} + k_8A_n x^n + k_9x^2 + k_{10}x + k_{11} = o \qquad (22)$$

If the trial function of equation (21) is to be an integral of equation (12), then equation (22) must be satisfied for all values of x and hence the coefficients of each power of x must vanish identically. Therefore, equating coefficient of x^{n-4} of Eq. (22) :

(1) $$n(n-1)(n-2)(n-3)A_n + k_1(n-2)(n-3)A_{n-2} + k_8A_{n-4} = o.$$

$$A_n = -\left[\frac{k_1A_{n-2}}{n(n-1)} + \frac{k_8A_{n-4}}{n(n-1)(n-2)(n-3)}\right] \ldots \text{for } n \geq 4 \ldots\ldots\ldots (a)$$

(2) equating coefficients of x^n

$$k_2(n)(n-1)A_n + k_4A_{n-4} + k_5A_{n-3} + k_6A_{n-2} + k_7A_{n-1} + k_8A_n = o.$$

$$A_n = -\left[\frac{k_4}{k_2(n)(n-1)-k_8}A_{n-4} + \frac{k_5}{k_2(n)(n-1)-k_8}A_{n-3} + \frac{k_6}{k_2(n)(n-1)-k_8}A_{n-2} + \frac{k_7}{k_2(n)(n-1)-k_8}A_{n-1}\right] \quad \text{....for } n \geq 4 \text{...(b)}$$

(3) Equating coefficients of x^{n+1}

$$k_4 A_{n-3} + k_5 A_{n-2} + k_6 A_{n-1} + k_7 A_n = o.$$

$$A_n = -\left[\frac{k_4}{k_7}A_{n-3} + \frac{k_5}{k_7}A_{n-2} + \frac{k_6}{k_7}A_{n-1}\right] \quad \text{....for } n \geq 3 \text{.....(c)}$$

(4) Equating coefficients of x^{n+2}

$$k_4 A_{n-2} + k_5 A_{n-1} + k_6 A_n = o.$$

$$A_n = -\left[\frac{k_4}{k_6}A_{n-2} + \frac{k_5}{k_6}A_{n-1}\right] \quad \text{....for } n \geq 2 \text{.....(d)}$$

(5) Equating coefficients of x^{n+3}

$$k_4 A_{n-1} + k_5 A_n = o.$$

$$A_n = -\left[\frac{k_4}{k_5}A_{n-1}\right] \quad \text{.....for } n \geq 1 \text{.....(e)}$$

(23)

Making use of the expressions of (a), (b).....(e) of Equation (23), the following composite values of the coefficients A_1 , A_2 .....are obtained.

$$A_1 = -\frac{k_4}{k_5}A_0 \quad \text{.....(i)}$$

$$A_2 = -\frac{k_4}{k_5}A_1 - \frac{k_4}{k_6}A_0 - \frac{k_5}{k_6}A_1$$

$$= -\left[\frac{k_4}{k_6}\right]A_0 - \left[\frac{k_4}{k_5} + \frac{k_5}{k_6}\right]A_1 \quad \text{.....(ii)}$$

$$A_3 = -\frac{k_4}{k_5}A_2 - \frac{k_4}{k_6}A_1 - \frac{k_5}{k_6}A_2 - \frac{k_4}{k_7}A_0 - \frac{k_5}{k_7}A_1 - \frac{k_6}{k_7}A_2$$

$$= -\left[\frac{k_4}{k_7}\right]A_0 - \left[\frac{k_4}{k_6} + \frac{k_5}{k_7}\right]A_1 - \left[\frac{k_4}{k_5} + \frac{k_5}{k_6} + \frac{k_6}{k_7}\right]A_2 \quad \text{.....(iii)}$$

$$A_4 = -\left(\frac{k_4}{12k_2 - k_8}\right)A_0 - \left(\frac{k_5}{12k_2 - k_8}\right)A_1 - \left(\frac{k_6}{12k_2 - k_8}\right)A_2 - \left(\frac{k_7}{12k_2 - k_8}\right)A_3 - \left(\frac{k_4}{k_5}\right)A_2 - \left(\frac{k_4}{k_5}\right)A_1 - \left(\frac{k_5}{k_6}\right)A_2 - \left(\frac{k_4}{k_7}\right)A_0 - \left(\frac{k_5}{k_7}\right)A_1 - \left(\frac{k_6}{k_7}\right)A_2$$

$$= -\left[\frac{k_4}{12k_2 - k_8} + \frac{k_4}{k_7}\right]A_0 - \left[\frac{k_5}{12k_2 - k_8} + \frac{k_4}{k_6} + \frac{k_5}{k_7}\right]A_1 - \left[\frac{k_6}{12k_2 - k_8} + \frac{k_4}{k_5} + \frac{k_5}{k_6} + \frac{k_6}{k_7}\right]A_2 - \left[\frac{k_7}{12k_2 - k_8}\right]A_3 \quad \text{.....(iv)}$$

or

$$\left.\begin{aligned} A_1 &= m_1 A_0 \quad \text{.....(i)} \\ A_2 &= n_1 A_0 + n_2 A_1 \quad \text{.....(ii)} \\ A_3 &= p_1 A_0 + p_2 A_1 + p_3 A_2 \quad \text{.....(iii)} \\ A_4 &= q_1 A_0 + q_2 A_1 + q_3 A_2 + q_4 A_3 \quad \text{.....(iv)} \end{aligned}\right\} \quad (24)$$

where, neglecting the terms of small value :

$$\left.\begin{aligned} m_1 &= -\left[-\frac{k_4}{k_5}\right] \quad \text{.....(a)} \\ n_1 &= -\left[-\frac{k_4}{k_6}\right]; \quad n_2 = -\left[\frac{k_4}{k_5}+\frac{k_5}{k_6}\right] \quad \text{.....(b)} \\ p_1 &= -\left[-\frac{k_4}{k_7}\right]; \quad p_2 = -\left[\frac{k_4}{k_6}+\frac{k_5}{k_7}\right]; \quad p_3 = -\left[\frac{k_4}{k_5}+\frac{k_5}{k_6}+\frac{k_6}{k_7}\right] \quad \text{.....(c)} \\ q_1 &= -\left[\frac{k_4}{12k_2-k_8}\right]; \quad q_2 = -\left[\frac{k_5}{12k_2-k_8}\right]; \quad q_3 = -\left[\frac{k_6}{12k_2-k_8}\right]; \quad q_4 = -\left[\frac{k_7}{12k_2-k_8}\right] \quad \text{.....(d)} \end{aligned}\right\} \quad (25)$$

$$y_1(x) = A_0 + A_1x + A_2x^2 + A_3x^3 + A_4x^4 \quad \text{.....}$$

$$= A_0 + m_1A_0x + (n_1A_0 + n_2A_1)x^2 + (p_1A_0 + p_2A_1 + p_3A_2)x^3 + (q_1A_0 + q_2A_1 + q_3A_2 + q_4A_3)x^4 \text{.....}$$

$$y_1(x) = A_0\left[1 + m_1x + n_1x^2 + p_1x^3 + q_1x^4\right] + A_1\left[n_2x^2 + p_2x^3 + q_2x^4\right] + A_2\left[p_3x^3 + q_3x^4\right] + \left[q_4x^4\right]A_3 + \quad (26)$$

where A_0 , A_1 , A_2 and A_3 are the constants of integration.

Equation For The Deflection y_2 :

The linear, non-homogeneous differential equation for deflection y_2 is:

$$\frac{d^4y_2}{dx^4} + k_1'\frac{d^2y}{dx^2}^2 + k_2'x^2\frac{d^2y}{dx^2}^2 + k_3'x\frac{d^2y}{dx^2}^2 + k_4'x^4y_2 + k_5'x^3y_2 + k_6'x^2y_2 + k_7'xy_2 + k_8'y_2 + k_9'x^2 + k_{10}'x + k_{11}' = 0 \quad \text{.....(18)}$$

Comparing equations (12) and (18), it is obvious that they are identical except that in the latter one the constant coefficients are k_1' , k_2' .....etc., replacing k_1 , k_2 ....of the former one. Hence we get the same solution except for different coefficients.

$$y_2(x) = B_0\left[1 + m_1'x + n_1'x^2 + p_1'x^3 + q_1'x^4\right] + B_1\left[n_2'x^2 + p_2'x^3 + q_2'x^4\right] + B_2\left[p_3'x^3 + q_3'x^4\right] + B_3\left[q_4'x^4\right] + \quad (27)$$

Where B_0 , B_1 , B_2 and B_3 are constants of integration and m_1' , n_1' , n_2' .....etc., are coefficients as shown below:

$$m_1' = -\left[-\frac{k_4}{k_5}\right] \quad \text{.....(a)}$$

$$n_1' = -\left[-\frac{k_4}{k_6}\right]; \qquad n_2' = -\left[\frac{k_4}{k_5} + \frac{k_5}{k_6}\right] \quad \text{.....(b)}$$

$$p_1' = -\left[-\frac{k_4}{k_7}\right]; \qquad p_2' = -\left[\frac{k_4}{k_6} + \frac{k_5}{k_7}\right]; \qquad p_3' = -\left[\frac{k_4}{k_5} + \frac{k_5}{k_6} + \frac{k_6}{k_7}\right] \quad \text{.....(c)}$$

$$q_1' = -\left[\frac{k_4}{12k_2 - k_8}\right]; \qquad q_2' = -\left[\frac{k_5}{12k_3 - k_8}\right]; \qquad q_3' = -\left[\frac{k_6}{12k_2 - k_8}\right]; \qquad q_4' = -\left[\frac{k_7}{12k_2 - k_8}\right] \quad \text{.....(d)}$$

(28)

The constants of integration A_0 , A_1 , A_2 , A_3 , B_0 , B_1 , B_2 and B_3 are determined from the following boundary conditions:

@ $x = o$; $y_1 = o$ .....(i)

@ $x = o$; $\frac{dy_1}{dx} = o$ .....(ii)

@ $x = a$; $\frac{dy_1}{dx} = \phi_1$ .....(iii)

@ $x = a$; $\frac{dy_1}{dx} = \frac{dy_2}{dx}$ .....(iv)

@ $x = a$; $\frac{d^2y_1}{dx^2} = \frac{d^2y_2}{dx^2}$ .....(v)

@ $x = a+\frac{b}{2}$; $\frac{dy_2}{dx} = o$ .....(vi)

@ $x = (a+b)$; $\frac{dy_2}{dx} = \phi_2$ .....(vii)

@ $x = a+b$; $\frac{dy_1}{dx} = \frac{dy_2}{dx}$ .....(viii)

@ $x = 2a+b$; $\frac{dy_2}{dx} = o$ .....(ix)

(Refer to Fig. 10)

(29)

Applying the boundary conditions (29) to the basic equations (26) and (27) :

(i) $$o = A_o \left[1 + o \right] \qquad \underline{A_o = o} \quad \text{.....(a)}$$

(ii) $$\left[\frac{dy_1(x)}{dx} \right]_{x = o} = A_1 \left[2n_2 x + 3p_2 x^2 + 4q_2 x^3 \right] + A_2 \left[3p_3 x^2 + 4q_3 x^3 \right] + A_3 \left[4q_4 x^3 \right] = \phi_1 = o$$ gives us a trivial solution..(b)

which does not satisfy our requirements since the solution has to be non-trivial. With $A_o = o$ the expression for y_1 becomes as follows, while y_2 retains the same shape.

$$y_1(x) = A_1 \left[n_2 x^2 + p_2 x^3 + q_2 x^4 \right] + A_2 \left[p_3 x^3 + q_3 x^4 \right] + A_3 \left[q_4 x^4 \right] + \text{.....}$$

$$y_2(x) = B_0 \left[1 + m_1' x + n_1' x^2 + p_1' x^3 + q_1' x^4 \right] + B_1 \left[n_2' x^2 + p_2' x^3 + q_2' x^4 \right] + B_2 \left[p_3' x^3 + q_3' x^4 \right] + B_3 \left[q_4' x^4 \right]$$

Differentiating the above two expressions w.r.t. x, we get

$$\frac{dy_1(x)}{dx} = A_1 \left[2n_2 x + 3p_2 x^2 + 4q_2 x^3 \right] + A_2 \left[3p_3 x^2 + 4q_3 x^3 \right] + A_3 \left[4q_4 x^3 \right] + \text{.....}$$

$$\frac{dy_2(x)}{dx} = B_0 \left[m_1' + 2n_1' x + 3p_1' x^2 + 4q_1' x^3 \right] + B_1 \left[2n_2' x + 3p_2' x^2 + 4q_2' x^3 \right] + B_2 \left[3p_3' x^2 + 4q_3' x^3 \right] + B_3 \left[4q_4' x^3 \right]$$

(iii) $x = a$; $\dfrac{dy_1}{dx}$ = Finite $\quad A_1[2n_2 a + 3p_2 a^2 + 4q_2 a^3] + A_2[3p_3 a^2 + 4q_3 a^3] + A_3[4q_4 a^3] = \phi_1$

= Finite .....(c) where

$$\alpha_1 = [2n_2 a + 3p_2 a^2 + 4q_2 a^3]$$

$$\alpha_2 = [3p_3 a^2 + 4q_3 a^3]$$

$$\alpha_3 = [4q_4 a^3]$$

(iv) $x = a;\ \frac{dy_1}{dx} = \frac{dy_2}{dx}$

$$A_1\left[2n_2a+3p_2a^2+4q_2a^3\right]+A_2\left[3p_3a^2+4q_3a^3\right]+A_3\left[4q_4a^3\right]-B_0\left[m_1'+2n_1'a+3p_1'a^2+4q_1'a^3\right]-B_1\left[2n_2'a+3p_2'a^2+4q_2'a^3\right]$$
$$-B_2\left[3p_3'a^2+4q_3'a^3\right]-B_3\left[4q_4'a^3\right]=0.$$

$A_1\beta_1+A_2\beta_2+A_3\beta_3-B_0\beta_4-B_1\beta_5-B_2\beta_6-B_3\beta_7 = 0$ ..... (d) where

---

$\beta_1 = \left[2n_2a+3p_2a^2+4q_3a^3\right]$; $\beta_5 = \left[2n_2'a+3p_2'a^2+4q_4'a^3\right]$

$\beta_2 = \left[3p_3a^2+4q_3a^3\right]$; $\beta_6 = \left[3p_3'a^2+4q_3'a^3\right]$

$\beta_3 = \left[4q_4a^3\right]$ $\beta_7 = \left[4q_4'a^3\right]$

$\beta_4 = \left[m_1'+2n_1'a+3p_1'a^2+4q_1'a^3\right]$;

(v) $x = a;\ \frac{d^2y_1}{dx^2} = \frac{d^2y_2}{dx^2}$; $\frac{d^2y_1}{dx^2} = A_1\left[2n_2+6p_2x+12q_2x^2\right]+A_2\left[6p_3x+12q_3x^2\right]+A_3\left[12q_4x^2\right]$

$$\frac{d^2y_2(x)}{dx^2} = B_0\left[2n_1'+6p_1'x+12q_1'x^2\right]+B_1\left[2n_2'+6p_2'x+12q_2'x^2\right]+B_2\left[6p_3'x+12q_3'x^2\right]+B_3\left[12q_4'x^2\right]$$

$$\therefore\ A_1\left[2n_2+6p_2a+12q_2a^2\right]+A_2\left[6p_3a+12q_3a^2\right]+A_3\left[12q_4a^2\right]-B_0\left[2n_1'+6p_1'a+12q_1'a^2\right]-B_1\left[2n_2'+6p_2'a+12q_2'a^2\right]$$
$$-B_2\left[6p_3'a+12q_3'a^2\right]-B_3\left[12q_4'a^2\right] = 0.$$

$A_1\gamma_1+A_2\gamma_2+A_3\gamma_3-B_0\gamma_4-B_1\gamma_5-B_2\gamma_6-B_3\gamma_7 = 0$ ..... (e) where

---

$\gamma_1 = \left[2n_2+6p_2a+12q_2a^2\right]$; $\gamma_6 = \left[6p_3'a+12q_3'a^2\right]$

$\gamma_2 = \left[6p_3a+12q_3a^2\right]$; $\gamma_7 = \left[12q_4'a^2\right]$

$\gamma_3 = \left[12q_4a^2\right]$;

$\gamma_4 = \left[2n_1'+6p_1'a+12q_1'a^2\right]$;

$\gamma_5 = \left[2n_2'+6p_2'a+12q_2'a^2\right]$;

(vi) $\dfrac{dy_2(x)}{dx} = B_0\left[m_1'+2n_1'x+3p_1'x^2+4q_1'x^3\right] + B_1\left[2n_2'x+3p_2x^2+4q_2'x^3\right] + B_2\left[3p_3'x^2+4q_3'x^3\right] + B_3\left[4q_4'x^3\right]$

$x = \left[a+\dfrac{b}{2}\right]$; $\dfrac{dy_2(x)}{dx} = B_0\left[m_1'+2n_1'(a+b/2) + 3p_1'(a+b/2)^2 + 4q_1'(a+b/2)^3\right] + B_1\left[2n_2'(a+b/2) + 3p_2'(a+b/2)^2+4q_2'(a+b/2)^3\right]$

$+ B_2\left[3p_3'(a+\dfrac{b}{2})^2 + 4q_3'(a+\dfrac{b}{2})^3\right] + B_3\left[4q_4'(a+b/2)^3\right]$

$B_0\delta_1+B_1\delta_2+B_2\delta_3+B_3\delta_4 = 0$ .....(f) where

$\delta_1 = \left[m_1' + 2n_1'(a+b/2) + 3p_1'(a+b/2)^2 + 4q_1'(a+b/2)^3\right]$

$\delta_2 = \left[2n_2'(a+b/2) + 3p_2'(a+b/2)^2 + 4q_2'(a+b/2)^3\right]$

$\delta_3 = \left[3p_3'(a+\dfrac{b}{2})^2 + 4q_3'(a+\dfrac{b}{2})^3\right]$

$\delta_4 = \left[4q_4'(a+b/2)^3\right]$

(vii) $\left[\dfrac{dy_2(x)}{dx}\right]_{(a+b)} = B_0[m_1'+2n_1'(a+b)+3p_1'(a+b)^2+4q_1(a+b)^3] + B_1[2n_2'(a+b) + 3p_2'(a+b)^2 + 4q_2'(a+b)^3]+$

$+ B_2[3p_3'(a+b)^2+4q_3'(a+b)^3] + B_3[4q_4'(a+b)^3] = \phi_2$

where

$\lambda_4 = [m_1'+2n_1'(a+b) + 3p_1'(a+b)^2+4q_1'(a+b)^3]$;

$\lambda_5 = [2n_2'(a+b) + 3p_2'(a+b)^2+4q_2'(a+b)^3]$;

$\lambda_6 = [3p_3'(a+b)^2+4q_3'(a+b)^3]$; and

$\lambda_7 = [4q_4'(a+b)^3]$

(viii) $x = (a+b)$; $\dfrac{dy_1}{dx} = \dfrac{dy_2}{dx}$

$A_1\left[2n_2(a+b) + 3p_2(a+b)^2 + 4q_2(a+b)^3\right] + A_2\left[3p_3(a+b)^2 + 4q_3(a+b)^3\right] + A_3\left[4q_4(a+b)^3\right] - B_0\left[m_1'+2n_1'(a+b) + 3p_1(a+b)^2 + 4q_1(a+b)^3\right]$

$-B_1\left[2n_2'(a+b) + 3p_2'(a+b)^2 + 4q_2'(a+b)^3\right] - B_2\left[3p_3'(a+b)^2 + 4q_3'(a+b)^3\right] - B_3\left[4q_4'(a+b)^3\right] = 0$

$A_1\mu_1 + A_2\mu_2 + A_3\mu_3 - B_0\mu_4 - B_1\mu_5 - B_2\mu_6 - B_3\mu_7 = 0$.....(h)

where $\mu_1 = \left[2n_2(a+b) + 3P_2(a+b)^2 + 4q_2(a+b)^3\right]$ $\mu_5 = \left[2n'_2(a+b) + 3p'_2(a+b)^2 + 4q'_2(a+b)^3\right]$

$\mu_2 = \left[3p_3(a+b)^2 + 4q_3(a+b)^3\right]$ $\mu_6 = \left[3p'_3(a+b)^2 + 4q'_3(a+b)^3\right]$

$\mu_3 = \left[4q_4(a+b)^3\right]$ $\mu_7 = \left[4q'_4(a+b)^3\right]$

$\mu_4 = \left[m'_1 + 2n'_1(a+b) + 3p'_1(a+b)^2 + 4q'_1(a+b)^3\right]$

(ix) $x = (2a+b)$; $\frac{dy}{dx}^1 = o$

$$\left[2n_2(2a+b) + 3p_2(2a+b)^2 + 4q_2(2a+b)^3\right] A_1 + \left[3p_3(2a+b)^2 + 4q_3(2a+b)^3\right] A_2 + \left[4q_4(2a+b)^3\right] A_3 = \phi_2$$

or $\psi_1 A_1 + \psi_2 A_2 + \psi_3 A_3 = o$ .....(j) where:

$\psi_1 = \left[2n_2(2a+b) + 3p_2(2a+b)^2 + 4q_2(2a+b)^3\right]$

$\psi_2 = \left[3p_3(2a+b)^2 + 4q_3(2a+b)^3\right]$

$\psi_3 = \left[4q_4(2a+b)^3\right]$

Thence the complete set of equations for determining the constants of integration is:

$$\left.\begin{aligned}
A_1\alpha_1 + A_2\alpha_2 + A_3\alpha_3 \ldots\ldots\ldots\ldots\ldots\ldots &= \phi_1 \quad \ldots\ldots\ldots\ldots\ldots (c)\\
A_1\beta_1 + A_2\beta_2 + A_3\beta_3 - B_0\beta_4 - B_1\beta_5 - B_2\beta_6 - B_3\beta_7 &= o \quad \ldots\ldots\ldots\ldots\ldots (d)\\
A_1\gamma_1 + A_2\gamma_2 + A_3\gamma_3 - B_0\gamma_4 - B_1\gamma_5 - B_2\gamma_6 - B_3\gamma_7 &= o \quad \ldots\ldots\ldots\ldots\ldots (e)\\
B_0\delta_1 + B_1\delta_2 + B_2\delta_3 + B_3\delta_4 &= o \quad \ldots\ldots\ldots\ldots\ldots (f)\\
\ldots\ldots\ldots\ldots B_0\lambda_4 + B_1\lambda_5 + B_2\lambda_6 + B_3\lambda_7 &= \phi_2 \quad \ldots\ldots\ldots\ldots\ldots (g)\\
A_1\mu_1 + A_2\mu_2 + A_3\mu_3 - B_0\mu_4 - B_1\mu_5 - B_2\mu_6 - B_3\mu_7 &= o \quad \ldots\ldots\ldots\ldots\ldots (h)\\
A_1\psi_1 + A_2\psi_2 + A_3\psi_3 \ldots\ldots\ldots\ldots\ldots\ldots &= o \quad \ldots\ldots\ldots\ldots\ldots (j)
\end{aligned}\right\} \quad (30$$

Equation (30) can be written in the matrix form as shown in equation (31)

$$\begin{bmatrix} \alpha_1 & \alpha_2 & \alpha_3 & \alpha & 0 & 0 & 0 \\ \beta_1 & \beta_2 & \beta_3 & -\beta_4 & -\beta_5 & -\beta_6 & -\beta_7 \\ \gamma_1 & \gamma_2 & \gamma_3 & -\gamma_4 & -\gamma_5 & -\gamma_6 & -\gamma_7 \\ 0 & 0 & 0 & \delta_1 & \delta_2 & \delta_3 & \delta_4 \\ 0 & 0 & 0 & +\lambda_4 & +\lambda_5 & +\lambda_6 & +\lambda_7 \\ \mu_1 & \mu_2 & \mu_3 & -\mu_4 & -\mu_5 & -\mu_6 & -\mu_7 \\ \psi_1 & \psi_2 & \psi_3 & 0 & 0 & 0 & 0 \end{bmatrix} \begin{Bmatrix} A_1 \\ A_2 \\ A_3 \\ B_0 \\ B_1 \\ B_2 \\ B_3 \end{Bmatrix} = \begin{bmatrix} \phi_1 \\ 0 \\ 0 \\ 0 \\ \phi_2 \\ 0 \\ 0 \end{bmatrix}$$

.....(31) Which in short notation can be written as $[A]\{B\} = [\varphi]$

$$\begin{Bmatrix} A_1 \\ A_2 \\ A_3 \\ B_0 \\ B_1 \\ B_2 \\ B_3 \end{Bmatrix} = \begin{bmatrix} \phi_1 \\ 0 \\ 0 \\ 0 \\ \phi_2 \\ 0 \\ 0 \end{bmatrix} \begin{bmatrix} \alpha'_1 & \alpha'_2 & \alpha'_3 & 0 & 0 & 0 & 0 \\ \beta'_1 & \beta'_2 & \beta'_3 & \beta'_4 & -\beta'_5 & -\beta'_6 & -\beta'_7 \\ \gamma'_1 & \gamma'_2 & \gamma'_3 & -\gamma'_4 & -\gamma'_5 & -\gamma'_6 & -\gamma'_7 \\ 0 & 0 & 0 & \delta'_1 & \delta'_2 & \delta'_3 & \delta'_4 \\ 0 & 0 & 0 & +\lambda'_4 & +\lambda'_5 & \lambda'_6 & +\lambda'_7 \\ \mu'_1 & \mu'_2 & \mu'_3 & -\mu'_4 & -\mu'_5 & -\mu'_6 & -\mu'_7 \\ \psi'_1 & \psi'_2 & \psi'_3 & 0 & 0 & 0 & 0 \end{bmatrix} \quad (32)$$

where the prime (') indicates the elements in the inverted matrix. The matrix can be inverted using Cayley-Hamilton or Gauss-Jordan Method. The following are the coefficients of integration :

$$\left.\begin{aligned} A_1 &= \alpha'_1\phi_1 \\ A_2 &= \beta'_1\phi_1 - \beta'_5\phi_2 \\ A_3 &= \gamma'_1\phi_1 - \gamma'_5\phi_2 \\ B_0 &= \delta'_2\phi \\ B_1 &= \lambda'_5\phi_2 \\ B_2 &= \mu'_1\phi_1 - \mu'_5\phi_2 \\ B_3 &= \psi'_1\phi_1 \end{aligned}\right\} \quad (33)$$

Making use of the coefficients, the deflections Y_1 and y_2 can be written as follows:

$$y_1(x) = A_1x + A_2x^2 + A_3x^3 \quad ; \quad \frac{dy_1(x)}{dx} = A_1 + 2A_2x + 3A_3x^2 \quad ; \quad \frac{d^2y_1(x)}{dx^2} = 2A_2 + 6A_3x$$

$$y_2(x) = B_1x + B_2x^2 + B_3x^3$$

The bending moment $(M_2)_0$ at the bond edges is given by:

$$(M_2)_0 = (M_1)_{x=a} = -Df_1 \left[\frac{d^2y_1(x)}{dx^2}\right]_{x=a} = -Df_1\left[2A_2 + 6A_3a\right]$$

$$\therefore \boxed{(M_2)_0 = -Df_1\left[2A_2 + 6A_3a\right]} \quad \ldots\ldots\ldots\ldots\ldots\ldots (34).$$

NOTE:

(i) The expression for $(M_2)_0$ can be further refined by taking additional terms in the expression for $y_1(x)$ and then revising the whole derivation.

(ii) The term β has only been used to refine the term $(M_2)_0$. Its use in forming the equilibrium equations in subsequent sections has been dropped for simplicity in calculations.

5.3 EQUILIBRIUM AND STRAIN EQUATIONS FOR THE BONDED REGION

We now consider the bonded region. The ends of the lower sheets (Fig. 11) are acted upon by a tensile force resultant T_f and by a bending moment resultant $(M_2)_0$ given by Eq. (34). Because the bond is considered in its undeformed state, symmetry requires the shear to vanish at the ends. The x-axis has its origin, as shown in Fig. 11. Equations which must be satisfied by each of the bonded sheets and by the adhesive will now be formulated.

According to the theory of cylindrically-bent plates, an element of the upper sheet, (Fig. 12a) will be acted upon by T_u and Q_u, the axial and the shear force resultants and by M_u a bending moment resultant as shown in Fig. 12 (a). Counter-clockwise moments and downward forces are taken positive. Since the forces and the moments are in equilibrium with the adhesive stresses σ and τ, the following equations hold:

$$\left.\begin{aligned} \frac{dM_u}{dx} + Q_u + \frac{\xi f \tau}{2} &= 0 \\ \frac{dQ_u}{dx} + \sigma &= 0 \\ \frac{dT_u}{dx} + \tau &= 0 \end{aligned}\right\} \qquad (35)$$

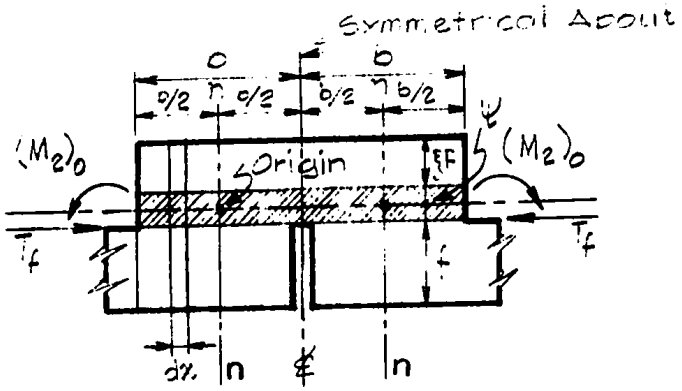

FIG. 11 BONDED REGION SHOWING APPLIED LOADS

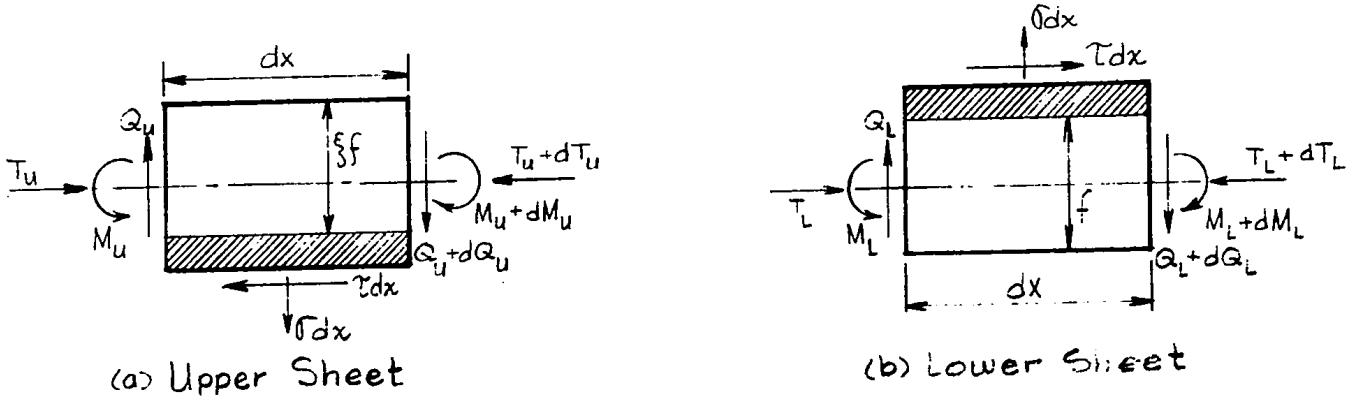

FIG. 12 STRESSES ON AN ELEMENT OF BONDED REGION

Similarly, if an element of the lower sheet (Fig.12(b)is considered, then for equilibrium, the following equations must be satisfied.

$$\left.\begin{aligned} \frac{dM_L}{dx} - Q_L + \frac{\xi f}{2} &= 0 \\ \frac{dQ_L}{dx} - \sigma &= 0 \\ \frac{dT_L}{dx} - \tau &= 0 \end{aligned}\right\} \qquad (36)$$

If the positive transverse deflections of the neutral planes of the upper and lower sheets are denoted by w_u and w_L respectively, then from the theory of elasticity:

$$\left.\begin{aligned} \frac{d^2w_u}{dx^2} &= -\frac{M_u}{\xi^3 D_{f_2}} \\ \frac{d^2w_L}{dx^2} &= -\frac{M_L}{D_{f_2}} \end{aligned}\right\} \qquad (37)$$

If u_U and u_L are the longitudinal displacement of the lowermost and the uppermost fibres of the upper and lower sheets respectively, then:

$$\left.\begin{aligned} \frac{du_U}{dx} &= \frac{1}{E}\left[\frac{T_u}{\xi f} + \frac{6M_u}{\xi^3 f^2}\right] \\ \frac{du_L}{dx} &= \frac{1}{E}\left[-\frac{T_L}{\xi} - \frac{6M_L}{f^2}\right] \end{aligned}\right\} \qquad (38)$$

Finally, from the stress-strain relations in the adhesive, we have:

$$\frac{\tau}{G_c} = \frac{u_L - u_U}{\psi} \quad \text{.....Horizontal strain} \qquad (39)$$

$$\frac{\sigma}{E_c} = \frac{w_L - w_U}{\psi} \quad \text{.....Vertical strain} \qquad (40)$$

where E_c and G_c are the Young's and shear moduli respectively for the adhesive.

5.4 FORMATION OF DIFFERENTIAL EQUATIONS FOR ADHESIVE STRESSES τ AND σ

Equations for the determination of the adhesive stresses σ and τ can now be formulated. Differentiating Eq. (39) and using Eq. (38) gives:

$$\frac{d\tau}{dx} = \frac{G_c}{\psi E f}\left[\left(T_L - \frac{6M_L}{f}\right) - \frac{1}{\xi}\left(T_u + \frac{6M_u}{\xi f}\right)\right] \tag{41}$$

Differentiating Eq. (41) twice and using Eqs. (35) and Eqs. (36), we obtain $\frac{d^3\tau}{dx^3} = \frac{G_c}{E\psi f}\left[\frac{4(1+\xi)}{\xi}\frac{d\tau}{dx} + \frac{6(1-\xi^2)}{\xi^2 f}\sigma\right]$ ... (42)

In a similar manner, differentiating Eq. (40) and using Eqs. (37), we obtain:

$$\frac{d^2\sigma}{dx^2} = \frac{E_c}{\psi D_{f_2}}\left[\frac{M_u}{\xi^3} - M_L\right] \tag{43}$$

Differentiating Eq. (43) twice and using Eqs. (35) and (36) gives:

$$\frac{d^4\sigma}{dx^4} = -\frac{E_c}{\psi D_{f_2}}\left[\frac{f(1-\xi^2)}{2\xi^2}\frac{d\tau}{dx} + \frac{(1+\xi^3)}{\xi^3}\sigma\right] \tag{44}$$

Eqs. (42) and (44) form a pair of simultaneous, ordinary differential equations with constant coefficients for determination of the stress distribution in the adhesive. Moreover, seven conditions are necessary with which to evaluate the seven arbitrary constants involved in the solution of Eqs. (42) and (44). The following physical conditions hold at the bond edges:

$$\left.\begin{aligned} &M_u = Q_u = T_u = 0 \\ &M_L = (M_2)_0 \;;\quad T_L = T_f \;;\quad Q_L = 0 \end{aligned}\right\} \quad @\ x = \pm b/2 \tag{45}$$

Equivalently, by the use of Eqs. (41) and (43), Eq. (45) may be written as

$$\frac{d\tau}{dx} = \frac{G_c}{\psi E f}\left[T_f - \frac{6(M_2)_0}{f}\right] \quad @\ x = \pm b/2 \tag{46}$$

$$\frac{d^2\sigma}{dx^2} = -\frac{E_c}{\psi D_{f_2}}(M_2)_0 \quad \ldots\ldots\ @\ x = \pm b/2 \tag{47}$$

To equations (46) and (47) the following equilibrium and symmetry conditions are added for $\xi = 1$

$$\int_{-b/2}^{b/2}\tau dx = T_f \;;\quad \int_{-b/2}^{b/2}\sigma dx = 0 \;;\quad \sigma\left(\frac{b}{2}\right) = \sigma\left(-\frac{b}{2}\right) \tag{48}$$

5.4.1 Solution of the Differential Equations (42) and (44) for $\xi = 1$

The solution of Eqs. (42) and (44) for the adhesive stresses subject to Eqs. (46) to (48) will now be considered. For the special case of $\xi = 1$, that is, when both sheets are of equal thickness, Eqs. (42) and (44) reduce to

$$\frac{d^3\tau}{dx^3} = \frac{8G_c}{E\psi f}\frac{d\tau}{dx} \tag{49}$$

$$\frac{d^4\sigma}{dx^4} = -\frac{2E_c}{\psi D_{f_2}}\sigma \tag{50}$$

which are independent of each other.
The solution of Eq. (49) with boundary conditions specified by Eqs. (46) to (48) is:

$$\tau = \left[\frac{3T_f + \frac{6(M_2)_0}{f}}{4b}\right] + \frac{\frac{\sqrt{2}}{4}\left(\frac{G_c}{E\psi f}\right)^{\frac{1}{2}}\left(T_f - \frac{6(M_2)_0}{f}\right)\cosh\left\{2\sqrt{2}\left(\frac{G_c}{E\psi f}\right)^{\frac{1}{2}}x\right\}}{\sinh\left\{2\sqrt{2}\left(\frac{G_c}{E\psi f}\right)^{\frac{1}{2}}\frac{b}{2}\right\}} \tag{51}$$

The solution of Eq. (50) under the conditions given by Eqs. (46) to (48) is:

$$\sigma = -2\left(\frac{E_c}{2\psi D_{f_2}}\right)^{\frac{1}{2}}(M_2)_0\left[\sinh\left\{\left(\frac{E_c}{2\psi D_{f_2}}\right)^{\frac{1}{4}}b\right\} + \sinh\left\{\left(\frac{E_c}{2\psi D_{f_2}}\right)^{\frac{1}{4}}b\right\}\right]^{-1}\times\left[<\cos\left\{\left(\frac{E_c}{2\psi D_{f_2}}\right)^{\frac{1}{4}}b/2\right\}\sinh\left\{\left(\frac{E_c}{2\psi D_{f_2}}\right)^{\frac{1}{4}}\frac{b}{2}\right\} - \right.$$

$$\sin\left\{\left(\frac{E_c}{2\psi D_{f_2}}\right)^{\frac{1}{4}}\frac{b}{2}\right\}\cosh\left\{\left(\frac{E_c}{2\psi D_{f_2}}\right)^{\frac{1}{4}}\frac{b}{2}\right\}>\cos\left\{\left(\frac{E_c}{2\psi D_{f_2}}\right)^{\frac{1}{4}}x\right\}\cosh\left\{\left(\frac{E_c}{2\psi D_{f_2}}\right)^{\frac{1}{4}}x\right\} + <\cos\left\{\left(\frac{E_c}{2\psi D_{f_2}}\right)^{\frac{1}{4}}\frac{b}{2}\right\}\sinh\left\{\left(\frac{E_c}{2\psi D_{f_2}}\right)^{\frac{1}{4}}\frac{b}{2}\right\}$$

$$\left. + \sin\left\{\left(\frac{E_c}{2\psi D_{f_2}}\right)^{\frac{1}{4}}\frac{b}{2}\right\}\cosh\left\{\left(\frac{E_c}{2\psi D_{f_2}}\right)^{\frac{1}{4}}\frac{b}{2}\right\}>\sin\left\{\left(\frac{E_c}{2\psi D_{f_2}}\right)^{\frac{1}{4}}x\right\}\sinh\left\{\left(\frac{E_c}{2\psi D_{f_2}}\right)^{\frac{1}{4}}x\right\}\right] \tag{52}$$

Both σ max and τ max occur at the bond edges and are given by:

$$\tau_{max} = \left[\frac{3T_f + \frac{6(M_2)_0}{f}}{4b}\right] + \frac{\sqrt{2}}{4}\left(\frac{G_c}{E\psi f}\right)^{\frac{1}{2}}\left(T_f - \frac{6(M_2)_0}{f}\right)\coth\left\{2\sqrt{2}\left(\frac{G_c}{E\psi f}\right)^{\frac{1}{2}}\frac{b}{2}\right\} \tag{53}$$

$$\sigma_{max} = \frac{-\left(\frac{E_c}{2\psi D_{f_2}}\right)^{\frac{1}{2}}(M_2)_0\left[\sinh\left\{\left(\frac{E_c}{2\psi D_{f_2}}\right)^{\frac{1}{4}}b\right\} - \sin\left\{\left(\frac{E_c}{2\psi D_{f_2}}\right)^{\frac{1}{4}}b\right\}\right]}{\left[\sinh\left\{\left(\frac{E_c}{2\psi D_{f_2}}\right)^{\frac{1}{4}}b\right\} + \sin\left\{\left(\frac{E_c}{2\psi D_{f_2}}\right)^{\frac{1}{4}}b\right\}\right]} \tag{54}$$

5.5 SOLUTION OF DIFFERENTIAL EQUATIONS (42) AND (44) FOR $0 < \xi < 1$
(For Plates of Different Thicknesses)

The two basic differential equations as derived in the previous pages combining τ and σ are :

$$\frac{d^3\tau}{dx^3} = \frac{G_c}{\psi Ef}\left[\frac{4(1+\xi)}{\xi}\frac{d\tau}{dx} + \frac{6(1-\xi^2)}{\xi^2 f}\sigma\right] \quad \ldots\ldots(42)$$

$$\frac{d^4\sigma}{dx^4} = -\frac{E_c}{\psi D_{f_2}}\left[\frac{f(1-\xi^2)}{2\xi^2}\frac{d\tau}{dx} + \frac{(1+\xi^3)}{\xi^3}\sigma\right] \quad \ldots\ldots(44)$$

Re-arranging (42) and (44), we get:

$$\frac{d^3\tau}{dx^3} - \left(\frac{G_c}{\psi Ef}\right)\left(\frac{4(1+\xi)}{\xi}\right)\frac{d\tau}{dx} - \left(\frac{G_c}{\psi Ef}\right)\left(\frac{6(1-\xi^2)}{\xi^2 f}\right)\sigma = 0 \quad \ldots\ldots(45)$$

$$\frac{d^4\sigma}{dx^4} + \left(\frac{E_c}{\psi D_{f_2}}\right)\left(\frac{f(1-\xi^2)}{2\xi^2}\right)\frac{d\tau}{dx} + \left(\frac{E_c}{\psi D_{f_2}}\right)\left(\frac{1+\xi^3}{\xi^3}\right)\sigma = 0 \quad \ldots\ldots(46)$$

For brevity in calculations, we substitute the following:

$$\left.\begin{aligned} &\left(\frac{G_c}{\psi Ef}\right)\left(\frac{4(1+\xi)}{\xi}\right) = x_1 \ldots(a); \quad \left(\frac{G_c}{\psi Ef}\right)\left(\frac{6(1-\xi^2)}{\xi^2 f}\right) = x_2 \ldots(b) \\ &\left(\frac{E_c}{\psi D_{f_2}}\right)\left(\frac{f(1-\xi^2)}{2\xi^2}\right) = x_3 \ldots(c); \quad \left(\frac{E_c}{\psi D}\right)\left(\frac{1+\xi^3}{\xi^3}\right) = x_4 \ldots..(d) \end{aligned}\right\} \quad \ldots\ldots(47)$$

Substituting Eqs. (47) into (45) and (46), the following is obtained:

$$\frac{d^3\tau}{dx^3} - x_1\frac{d\tau}{dx} - x_2\sigma = 0 \quad \ldots\ldots(48)$$

$$\frac{d^4\sigma}{dx^4} + x_3\frac{d\tau}{dx} + x_4\sigma = 0 \quad \ldots\ldots(49)$$

Using the D-operator notation,

$$D^3\tau - x_1 D\tau - x_2\sigma = 0 \quad \ldots\ldots\ldots\ldots\ldots\ldots (50)$$

$$D^4\sigma + x_3 D\tau - x_4\sigma = 0 \quad \ldots\ldots\ldots\ldots\ldots\ldots (51)$$

$$(D^3 - x_1 D)\tau - x_2\sigma = 0 \quad \ldots\ldots\ldots\ldots\ldots\ldots (52)$$

$$x_3 D\tau + (D^4 - x_4)\sigma = 0 \quad \ldots\ldots\ldots\ldots\ldots\ldots (53)$$

Eliminating σ from Eqs. (52) and (53)

$$(D^3 - x_1 D)(D^4 - x_4)\tau - x_2(D^4 - x_4)\sigma = 0$$

$$x_2 x_3 D\tau + x_2(D^4 - x_4)\sigma = 0$$

$$(D^3 - x_1 D)(D^4 - x_4)\tau + x_2 x_3 D\tau = 0$$

$$(D^7 - x_4 D^3 - x_1 D^5 - x_1 x_4 D)\tau + x_2 x_3 D\tau = 0 \quad \ldots\ldots\ldots (54)$$

$$\frac{d^7\tau}{dx^7} - x_1\frac{d^5\tau}{dx^5} - x_4\frac{d^3\tau}{dx^3} + (-x_1 x_4 + x_2 x_3)\frac{d\tau}{dx} = 0 \quad \ldots\ldots\ldots (55)$$

Similarly,

$$(D^3 - x_1 D)\tau - x_2\sigma = 0$$

$$x_3 D\tau + (D^4 - x_4)\sigma = 0 \qquad \text{Eliminating } \tau \text{ from Eqs. (52) and (53).}$$

$$x_3 D(D^3 - x_1 D)\tau - x_2 x_3 D\sigma = 0.$$

$$x_3 D(D^3 - x_1 D)\tau + (D^3 - x_1 D)(D^4 - x_4)\sigma = 0.$$

$$-x_2 x_3 D - (D^7 - x_4 D^3 - x_1 D^5 - x_1 x_4 D)\sigma = 0$$

$$\frac{d^7\sigma}{dx^7} - x_1\frac{d^5\sigma}{dx^5} - x_4\frac{d^3\sigma}{dx^3} + (-x_1 x_4 + x_2 x_3)\frac{d\tau}{dx} = 0 \quad \ldots\ldots\ldots (56)$$

$$\left[D^7 - x_1 D^5 - x_4 D^3 + (-x_1 x_4 + x_2 x_3) D\right] \frac{\tau}{\delta} \text{ or } = o \quad \ldots\ldots\ldots\ldots\ldots (57)$$

$$D\left[D^6 - x_1 D^4 - x_4 D^2 + (-x_1 x_4 + x_2 x_3) D\right] \frac{\tau}{\delta} \text{ or } = o \quad \ldots\ldots\ldots\ldots\ldots\ldots (58)$$

$$D^6 - \frac{4G_c}{\psi E f}\,\frac{(1+\xi)}{\xi} D^4 - \frac{E_c}{\psi D}\,\frac{1+\xi^3}{\xi^3} D^2 + \frac{E_c G_c}{\psi^2 E D f \xi^4}\left[\xi^4 + 4\xi^3 - 6\xi^2 + 4\xi + 1\right] D = o \quad \ldots\ldots\ldots (59)$$

Using the integrating function $\frac{d\sigma}{dx} = e^{mx}$ we get the following:

$$m^6 - \frac{4G_c}{\psi E f}\,\frac{(1+\xi)}{\xi} m^4 - \frac{E_c}{\psi D}\,\frac{(1+\xi^3)}{\xi^3} m^2 + \frac{E_c G_c}{\psi^2 E d f \xi^4}\left[\xi^4 + 4\xi^3 - 6\xi^2 + 4\xi + 1\right] = o \quad \ldots\ldots\ldots\ldots (60)$$

Equation (60) is a cubic in m^2. If we denote the roots of this equation by $z^2, Z^2, \bar{Z}^2$, then $\{m_N\}$ will be given by $\pm z, \pm Z$ and $\pm \bar{Z}$. Hence the following:

$$\tau = A_0 + \sum_{n=1}^{6} A_n e^{m_N x} \quad \ldots\ldots\ldots\ldots\ldots\ldots\ldots\ldots\ldots (61)$$

where A_0 and An are the constants of integration to be determined from the boundary conditions.

Substituting the value of τ from Eq. (61) into Eq. (42); we get

$$\sigma = \frac{E\psi f^2 \xi^2}{6G_c(1-\xi^2)} \sum_{n=1}^{6} m_N \left[m_N^2 - \frac{4G_c}{E\psi f}\,\frac{(1+\xi)}{\xi}\right] A_n e^{m_N x} \quad \ldots\ldots\ldots\ldots (62)$$

Hence the general expressions for the normal and shear stresses are :

$$\tau = A_0 + \sum_{n=1}^{6} A_n e^{m_N x} \quad \ldots\ldots\ldots\ldots\ldots\ldots\ldots\ldots\ldots (61)$$

$$\sigma = \frac{E\psi f^2 \xi^2}{6G_c(1-\xi^2)} \sum_{n=1}^{6} m_N \left[m_N^2 - \frac{4G_c}{E\psi f}\,\frac{(1+\xi)}{\xi}\right] A_n e^{m_N x} \quad \ldots\ldots\ldots\ldots\ldots (62)$$

Using matrix $\left\{m_N\right\}$, Eqs. (61) and (62) become

$$\tau = A_0 + A_1 \cosh zx + A_2 \sinh zx + A_3 \cosh Zx + A_4 \sinh Zx + A_5 \cosh \bar{Z}x + A_6 \sinh \bar{Z}x \quad \ldots\ldots(63)$$

$$\sigma = \frac{E\psi f^2\xi^2}{6G_c(1-\xi^2)} \left[z\left(z^2 - \frac{4G_c(1+\xi)}{E\psi f\xi}\right)\left\{A_1 \sinh zx + A_2 \cosh zx\right\} + Z\left(Z^2 - \frac{4G_c(1+\xi)}{E\psi f\xi}\right)\left\{A_3 \sinh Zx + A_4 \cosh Zx\right\} + \bar{z}\left(\bar{z}^2 - \frac{4G_c(1+\xi)}{E\psi f\xi}\right)\left\{A_5 \sinh \bar{Z}x + A_6 \cosh \bar{Z}x\right\}\right] \quad \ldots\ldots(64)$$

Now we apply the following boundary conditions to Eqs. (63) and (64):

$$\left.\begin{aligned}
&\frac{d\tau}{dx} = \frac{G_c}{\psi Ef}\left(T_f - \frac{6M_f}{f}\right) \text{ @ } x = \pm b/2 \quad \ldots\ldots(a)\\
&\frac{d^2\sigma}{dx^2}_{b/2} = -\frac{E_c}{\psi D_{f_2}} M_f \ldots \text{@ } x = \pm b/2 \quad \ldots\ldots(b)\\
&\int_{-b/2}^{+b/2} \tau dx = T_f \quad \ldots\ldots(c)\\
&\int_{-b/2}^{+b/2} \sigma dx = 0 \quad \ldots\ldots(d)\\
&\sigma(b/2) = \sigma(-b/2) \quad \ldots\ldots(e)
\end{aligned}\right\} \ldots\ldots(65)$$

$$\frac{d\tau}{dx} = A_1 z \sinh zx + A_2 z \cosh zx + A_3 Z \sinh Zx + A_4 Z \cosh x + A_5 \bar{Z} \sinh \bar{Z}x + A_6 \bar{Z} \cosh \bar{Z}x.$$

$$\frac{d\sigma}{dx} = \frac{E\psi f^2\xi^2}{6G_c(1-\xi^2)} \left[z(z^2 - \frac{4G_c(1+\xi)}{E\psi f\xi}) \left\{ A_1 z \cosh zx + A_2 z \sinh zx \right\} + Z(Z^2 - \frac{4G_c(1+\xi)}{E\psi f\xi}) \left\{ A_3 Z \cosh Zx + A_4 Z \sinh Zx \right\} \right.$$
$$\left. + \bar{Z} (\bar{Z}^2 - \frac{4G_c(1+\xi)}{E\psi f\xi}) \left\{ A_5 \bar{Z} \cosh \bar{Z}x + A_6 \bar{Z} \sinh \bar{Z}x \right\} \right]$$

$$\frac{d^2\sigma}{dx^2} = \frac{E\psi f^2\xi^2}{6G_c(1-\xi^2)} \left[z(z^2 - \frac{4G_c(1+\xi)}{E\psi f\xi}) \left\{ A_1 z^2 \sinh zx + A_2 z^2 \cosh zx \right\} + z(Z^2 - \frac{4G_c(1+\xi)}{E\psi f\xi}) \left\{ A_3 Z^2 \sinh Zx + A_4 Z^2 \cosh Zx \right\} \right.$$
$$\left. + \bar{Z} (\bar{Z}^2 - \frac{4G_c(1+\xi)}{E\psi f\xi}) \left\{ A_5 \bar{Z}^2 \sinh \bar{Z}x + A_6 \bar{Z}^2 \cosh \bar{Z}x \right\} \right]$$

$$\int \tau dx = A_0 x + A_1 /_z \sinh zx + A_2 /_z \cosh zx + A_3 /_Z \sinh Zx + A_4 /_Z \cosh Zx + A_5 /_{\bar{Z}} \sinh \bar{Z}x + A_6 /_{\bar{Z}} \cosh Zx.$$

$$\int \sigma dx = \frac{E\psi f^2\xi^2}{6G_c(1-\xi^2)} \left[z(z^2 - \frac{4G_c(1+\xi)}{E\psi f\xi}) \left\{ A_1 /_z \cosh zx + A_2 /_z \sinh zx \right\} + Z(Z^2 - \frac{4G_c(1+\xi)}{E\psi f\xi}) \left\{ A_3 /_Z \cosh Zx + A_4 /_Z \sinh Zx \right\} \right.$$
$$\left. + \bar{Z}(\bar{Z}^2 - \frac{4G_c(1+\xi)}{E\psi f\xi}) \left\{ A_5 /_{\bar{Z}} \cosh \bar{Z}x + A_6 /_{\bar{Z}} \sinh \bar{Z}x \right\} \right]$$

Now we form the Equations:

$$\left[z \sinh z\frac{b}{2} \right] A_1 + \left[z \cosh z\frac{b}{2} \right] A_2 + \left[Z \sinh Z\frac{b}{2} \right] A_3 + \left[Z \cosh Z\frac{b}{2} \right] A_4 + \left[\bar{Z} \sinh \bar{Z}\frac{b}{2} \right] A_5 + \left[\bar{Z} \cosh \bar{Z}\frac{b}{2} \right] A_6 = \frac{G_c}{\psi Ef} \left[T_f - \frac{6M_f}{f} \right] \ldots (i)$$

$$- \left[z \sinh z\frac{b}{2} \right] A_1 + \left[z \cosh z\frac{b}{2} \right] A_2 - \left[Z \sinh Z\frac{b}{2} \right] A_3 + \left[Z \cosh Z\frac{b}{2} \right] A_4 - \left[\bar{Z} \sinh \bar{Z}\frac{b}{2} \right] A_5 + \left[\bar{Z} \cosh \bar{Z}\frac{b}{2} \right] A_6 = \frac{G_c}{\psi Ef} \left[T_f - \frac{6M_f}{f} \right] \ldots (ii)$$

$$\left[\frac{E\psi f^2\xi^2 z^3}{6G_c(1-\xi^2)} (z^2 - \frac{4G_c(1+\xi)}{E\psi f\xi}) \sinh z\frac{b}{2} \right] A_1 + \left[\frac{E\psi f^2\xi^2 z^3}{6G_c(1-\xi^2)} (z^2 - \frac{4G_c(1+\xi)}{E\psi f\xi}) \cosh z\frac{b}{2} \right] A_2 + \left[\frac{E\psi f^2\xi^2 Z^3}{6G_c(1-\xi^2)} (Z^2 - \frac{4G_c(1+\xi)}{E\psi f\xi}) \sinh Z\frac{b}{2} \right] A_3$$
$$+ \left[\frac{E\psi f^2\xi^2 Z^3}{6G_c(1-\xi^2)} (Z^2 - \frac{4G_c(1+\xi)}{E\psi f\xi}) \cosh Z\frac{b}{2} \right] A_4 + \left[\frac{E\psi f^2\xi^2\bar{Z}^3}{6G_c(1-\xi^2)} (\bar{Z}^2 - \frac{4G_c(1+\xi)}{E\psi f\xi}) \sinh \bar{Z}\frac{b}{2} \right] A_5 + \left[\frac{E\psi f^2\xi^2\bar{Z}^3}{6G_c(1-\xi^2)} (\bar{Z}^2 - \frac{4G_c(1+\xi)}{E\psi f\xi}) \right] A_6 = -\frac{E_c}{\psi D} M_f \ldots (iii)$$

..(66)

$$-\left[\frac{E\psi f^2\xi^2 z^3}{6G_c(1-\xi^2)}\left(z^2 - \frac{4G_c(1+\xi)}{E\psi f\xi}\right)\sinh z\frac{b}{2}\right]A_1 + \left[\frac{E\psi f^2\xi^2 z^3}{6G_c(1-\xi^2)}\left(z^2 - \frac{4G_c(1+\xi)}{E\psi f\xi}\right)\cosh z\frac{b}{2}\right]A_2 - \left[\frac{E\psi f^2\xi^2 z^3}{6G_c(1-\xi^2)}\left(\bar{z}^2 - \frac{4G_c(1+\xi)}{E\psi f\xi}\right)\sinh z\frac{b}{2}\right]A_3$$

$$+\left[\frac{E\psi f^2\xi^2 z^3}{6G_c(1-\xi^2)}\left(z^2 - \frac{4G_c(1+\xi)}{E\psi f\xi}\right)\cosh z\frac{b}{2}\right]A_4 - \left[\frac{E\psi f^2\xi^2\bar{z}^3}{6G_c(1-\xi^2)}\left(\bar{z}^2 - \frac{4G_c(1+\xi)}{E\psi f\xi}\right)\sinh \bar{z}\frac{b}{2}\right]A_5 + \left[\frac{E\psi f^2\xi^2 z^3}{6G_c(1-\xi^2)}\left(\bar{z}^2 - \frac{4G_c(1+\xi)}{E\psi f\xi}\right)\right]A_6 = -\frac{E_c}{\psi D}M_f \quad \ldots(iv)$$

$$\left[A_0\left(\frac{b}{2}\right) + A_1/_z\sinh z\left(\frac{b}{2}\right) + A_2/_z\cosh z\left(\frac{b}{2}\right) + A_3/_z\sinh z\left(\frac{b}{2}\right) + A_4/_z\cosh z\left(\frac{b}{2}\right) + A_5/_{\bar{z}}\sinh \bar{z}\left(\frac{b}{2}\right) + A_6/_{\bar{z}}\cosh \bar{z}\left(\frac{b}{2}\right)\right] +$$

$$\left[A_0\left(\frac{b}{2}\right) + A_1/_z\sinh z\frac{b}{2} - A_2/_z\cosh z\frac{b}{2} + A_3/_z\sinh z\frac{b}{2} - A_4/_z\cosh z\frac{b}{2} + A_5/_{\bar{z}}\sinh \bar{z}\frac{b}{2} - A_6/_{\bar{z}}\cosh \bar{z}\frac{b}{2}\right]$$

$$= A_0 b + 2A_1/_z\sinh z\left(\frac{b}{2}\right) + 2A_3/_z\sinh z\left(\frac{b}{2}\right) + 2A_5/_{\bar{z}}\sinh \bar{z}\left(\frac{b}{2}\right) = T_f \quad \ldots(v)$$

$$\int_{-b/2}^{b/2}\sigma\,dx = \frac{E\psi f^2\xi^2}{6G_c(1-\xi^2)}\left[\lambda\left(z^2 - \frac{4G_c(1\ \ \xi)}{E\psi f\xi}\right)\left\{A_1/_\lambda\cosh z\left(\frac{b}{2}\right) + A_2/_\lambda\sinh z\left(\frac{b}{2}\right)\right\} + \lambda\left(z^2 - \frac{4G_c(1+\xi)}{E\psi f\xi}\right)\left\{A_3/_\lambda\cosh z\frac{b}{2} + A_4/_\lambda\sinh z\frac{b}{2}\right\}\right.$$

$$\left. + \bar{\lambda}\left(\bar{z}^2 - \frac{4G_c(1+\xi)}{E\psi f\xi}\right)\left\{A_5/_{\bar{\lambda}}\cosh \bar{z}\left(\frac{b}{2}\right) + A_6/_{\bar{\lambda}}\sinh \bar{z}\left(\frac{b}{2}\right)\right\}\right] - \frac{E\psi f^2\xi^2}{6G_c(1-\xi^2)}\left[\lambda\left(z^2 - \frac{4G_c(1+\xi)}{E\psi f\xi}\right)\left\{A_1/_\lambda\cosh z\left(\frac{b}{2}\right)\right.\right.$$

$$\left. - A_2/_\lambda\sinh z\left(\frac{b}{2}\right)\right\} + \lambda\left(z^2 - \frac{4G_c(1+\xi)}{E\psi f\xi}\right)\left\{A_3/_\lambda\cosh z\frac{b}{2} - A_4/_\lambda\sinh z\frac{b}{2}\right\} + \bar{\lambda}\left(z^2 - \frac{4G_c(1+\xi)}{E\psi f\xi}\right)\left\{A_5/_{\bar{\lambda}}\right.$$

$$\left.\left.\cosh \bar{z}\left(\frac{b}{2}\right) - A_6/_{\bar{\lambda}}\sinh \bar{z}\left(\frac{b}{2}\right)\right\}\right]$$

$$= \left[\frac{E\psi f^2\xi^2}{3G_c(1-\xi^2)}\left(z^2 - \frac{4G_c(1+\xi)}{E\psi f\xi}\right)\sinh z\frac{b}{2}\right]A_2 + \left[\frac{E\psi f^2\xi^2}{3G_c(1-\xi^2)}\left(z^2 - \frac{4G_c(1+\xi)}{E\psi f\xi}\right)\sinh z\frac{b}{2}\right]A_4 +$$

$$+\left[\frac{E\psi f^2\xi^2}{3G_c(1-\xi^2)}\left(z^2 - \frac{4G_c(1+\xi)}{E\psi f\xi}\right)\sinh \bar{z}\frac{b}{2}\right]A_6 = 0 \quad \ldots(vi)$$

(66)

$$\frac{E\rho\xi^2\zeta^2}{6G_c(1-\zeta^2)}\left[\alpha(\alpha^2-\frac{4G_c(1+\zeta)}{E\rho\xi\zeta})\left\{A_1\sinh\alpha(\frac{b}{2})+A_2\cosh\alpha(\frac{b}{2})\right\}+\alpha(\alpha^2-\frac{4G_c(1+\zeta)}{E\rho\xi\zeta})\left\{A_3\sinh\alpha(\frac{b}{2})+A_4\cosh\alpha(\frac{b}{2})\right\}+\right.$$
$$\bar{\alpha}(\bar{\alpha}^2-\frac{4G_c(1+\zeta)}{E\rho\xi\zeta})\left\{A_5\sinh\bar{\alpha}(\frac{b}{2})+A_6\cosh\bar{\alpha}(\frac{b}{2})\right\}\Big]+\frac{E\rho\xi^2\zeta^2}{6G_c(1-\zeta^2)}\left[\alpha(\alpha^2-\frac{4G_c(1+\zeta)}{E\rho\xi\zeta})\left\{-A_1\sinh\alpha\frac{b}{2}\right.\right.$$
$$\left.+A_2\cosh\alpha\frac{b}{2}\right\}+\alpha(\alpha^2-\frac{4G_c(1+\zeta)}{E\rho\xi\zeta})\left\{-A_3\sinh\alpha\frac{b}{2}+A_4\cosh\alpha\frac{b}{2}\right\}+\bar{\alpha}(\bar{\alpha}^2-\frac{4G_c(1+\zeta)}{E\rho\xi\zeta})\left\{A_5\sinh\bar{\alpha}(\frac{b}{2})\right.$$
$$\left.\left.+A_6\cosh\bar{\alpha}\frac{b}{2}\right\}\right]$$
$$-\left[2\alpha(\alpha^2-\frac{4G_c(1+\zeta)}{E\rho\xi\zeta})\sinh\alpha(\frac{b}{2})\right]A_1+\left[2\alpha(\alpha^2-\frac{4G_c(1+\zeta)}{E\rho\xi\zeta})\sinh\alpha(\frac{b}{2})\right]A_3+\left[2\bar{\alpha}(\bar{\alpha}^2-\frac{4G_c(1+\zeta)}{E\rho\xi\zeta})\sinh\bar{\alpha}(\frac{b}{2})\right]A_5=0 \quad \ldots(66)$$
$$\ldots\ldots(vii)$$

Equations (i), (ii).....(vii) in (66) form a set of simultaneous equations for the determination of the constants of integration $A_1, A_2, \ldots\ldots\ldots A_6$. Eqs.(66) can be written in the matrix form as follows:

$$\begin{bmatrix}
0 & \alpha\sinh\alpha\frac{b}{2} & \alpha\cosh\alpha\frac{b}{2} & \alpha\sinh\alpha(\frac{b}{2}) & \bar{\alpha}\sinh\bar{\alpha}(\frac{b}{2}) & \bar{\alpha}\cosh\bar{\alpha}(\frac{b}{2}) \\
0 & -\alpha\sinh\alpha\frac{b}{2} & \alpha\cosh\alpha\frac{b}{2} & -\alpha\sinh\alpha(\frac{b}{2}) & -\bar{\alpha}\sinh\bar{\alpha}\frac{b}{2} & \bar{\alpha}\cosh\bar{\alpha}(\frac{b}{2}) \\
0 & \frac{E\rho\xi^2\zeta^2\alpha^2}{6G_c(1-\zeta^2)}(\alpha^2-\frac{4G_c(1+\zeta)}{E\rho\xi\zeta})\sinh\alpha(\frac{b}{2}) & \frac{E\rho\xi^2\zeta^2\alpha^2}{6G_c(1-\zeta^2)}(\alpha^2-\frac{4G_c(1+\zeta)}{E\rho\xi\zeta})\cosh\alpha(\frac{b}{2}) & \frac{E\rho\xi^2\zeta^2\alpha^2}{6G_c(1-\zeta^2)}(\alpha^2-\frac{4G_c(1+\zeta)}{E\rho\xi\zeta})\sinh\alpha(\frac{b}{2}) & \frac{E\rho\xi^2\zeta^2\bar{\alpha}^2}{6G_c(1-\zeta^2)}(\bar{\alpha}^2-\frac{4G_c(1+\zeta)}{E\rho\xi\zeta})\sinh\bar{\alpha}(\frac{b}{2}) & \frac{E\rho\xi^2\zeta^2\bar{\alpha}^2}{6G_c(1-\zeta^2)}(\bar{\alpha}^2-\frac{4G_c(1+\zeta)}{E\rho\xi\zeta})\cosh\bar{\alpha}(\frac{b}{2}) \\
0 & -\frac{E\rho\xi^2\zeta^2\alpha^2}{6G_c(1-\zeta^2)}(\alpha^2-\frac{4G_c(1+\zeta)}{E\rho\xi\zeta})\sinh\alpha(\frac{b}{2}) & \frac{E\rho\xi^2\zeta^2\alpha^2}{6G_c(1-\zeta^2)}(\alpha^2-\frac{4G_c(1+\zeta)}{E\rho\xi\zeta})\cosh\alpha(\frac{b}{2}) & -\frac{E\rho\xi^2\zeta^2\alpha^2}{6G_c(1-\zeta^2)}(\alpha^2-\frac{4G_c(1+\zeta)}{E\rho\xi\zeta})\sinh\alpha(\frac{b}{2}) & -\frac{E\rho\xi^2\zeta^2\bar{\alpha}^2}{6G_c(1-\zeta^2)}(\bar{\alpha}^2-\frac{4G_c(1+\zeta)}{E\rho\xi\zeta})\sinh\bar{\alpha}(\frac{b}{2}) & \frac{E\rho\xi^2\zeta^2\bar{\alpha}^2}{6G_c(1-\zeta^2)}(\bar{\alpha}^2-\frac{4G_c(1+\zeta)}{E\rho\xi\zeta})\cosh\bar{\alpha}(\frac{b}{2}) \\
b & \frac{1}{\alpha}\sinh\alpha(\frac{b}{2}) & 0 & \frac{1}{\alpha}\sinh\alpha(\frac{b}{2}) & \frac{1}{\bar{\alpha}}\sinh\bar{\alpha}(\frac{b}{2}) & 0 \\
0 & 0 & \frac{E\rho\xi^2\zeta^2}{3G_c(1-\zeta^2)}(\alpha^2-\frac{4G_c(1+\zeta)}{E\rho\xi\zeta})\sinh\alpha(\frac{b}{2}) & 0 & 3\bar{\alpha}(\bar{\alpha}^2-\frac{4G_c(1+\zeta)}{E\rho\xi\zeta})\sinh\bar{\alpha}(\frac{b}{2}) & \frac{E\rho\xi^2\zeta^2}{3G_c(1-\zeta^2)}(\bar{\alpha}^2-\frac{4G_c(1+\zeta)}{E\rho\xi\zeta})\sinh\bar{\alpha}(\frac{b}{2}) \\
0 & 2\alpha(\alpha^2-\frac{4G_c(1+\zeta)}{E\rho\xi\zeta})\sinh\alpha(\frac{b}{2}) & 0 & 2\alpha(\alpha^2-\frac{4G_c(1+\zeta)}{E\rho\xi\zeta})\sinh\alpha(\frac{b}{2}) & 0 & 0
\end{bmatrix}
\begin{Bmatrix}A_1\\A_2\\A_3\\A_4\\A_5\\A_6\end{Bmatrix}=\begin{bmatrix}\frac{C_c}{\rho E\xi}(\tau_{\xi}-\frac{6R_{\xi}}{\xi})\\ \frac{G_c}{\rho E\xi}(\tau_{\xi}-\frac{6R_{\xi}}{\xi})\\ -\frac{R_{\xi}}{\rho D_{\xi}}\\ -\frac{R_c}{\rho D_{\xi}}\\ \tau_{\xi}\\ 0\\ 0\end{bmatrix} \quad (67)$$

$$\text{MATRIX}\left[K\right] \qquad \left\{A\right\} \qquad \left[B\right]$$

or in compact notation $\left[\ k\ \right]_{-1} = \left\{A\right\}\left[\ B\ \right]$ .....(68)

$\left\{A\right\} = \left[\ k\ \right]^{-1}\left[B\ \right]$ ....(69); Matrix $\left[\ k\ \right]^{-1}$ can be easily solved by using Cayley-Hamilton Inversion method.

Having calculated the values of the constants of integration, the values of τ and σ can be written as follows:

$$\tau = A_0 + A_1 \cosh zx + A_2 \sinh zx + A_3 \cosh Zx + A_4 \sinh Zx + A_5 \cosh Zx + A_6 \sinh \bar{Z}x \quad .....(70)$$

$$\sigma = \frac{E\psi f^2\xi^2}{6G_c(1-\xi^2)}\left[z(z^2 - \frac{4G_c(1+\xi)}{E\psi f\xi})\left\{A_1 \sinh zx + A_2 \cosh zx\right\} + Z(Z^2 - \frac{4G_c(1+\xi)}{E\psi f\xi})\left\{A_3 \sinh Zx + A_4 \cosh Zx\right\} + \bar{Z}(\bar{Z}^2 - \frac{4G_c(1+\xi)}{E\psi f\xi})\left\{A_5 \sinh \bar{Z}x + A_6 \cosh \bar{Z}x\right\}\right] .....(71)$$

5.6 ILLUSTRATIVE EXAMPLE

Calculations of stresses in the adhesive are made for actual values of the parameters in a stiffened plate in this Chapter. Specimens of joints used for experimental verification were fabricated using the same values of parameters for comparison. (For specimen designations, their types, modes of testing, etc., refer to Chapter VII). For the plates, the values chosen are $E_{A\ell} = 10.25 \times 10^6$ psi; $\nu = 0.33$; $a = 2.0$ in.; $b = 4.0$ in.; $f = 0.030$ in.; $\psi = 0.0128$ in. For the bond, the material constants are $E_c = 516 \times 10^3$ psi and $G_c = 184 \times 10^3$ psi, which are representative values for Waldex W-105 adhesive.

Values of $(M_2)_o$ - the stress couple resultant acting on the facings of the bond edges are calculated for three different values of T_f corresponding to 500, 750 and 100 lbs. of applied load using Eq. (34). This is accomplished by first calculating the elements of the coefficient matrix in Eq. (31). Then, making use of Eqs. (32) and (33), the constants of integration A_2 and A_3 are calculated. The value of β was determined experimentally for each loading.

Coefficient matrices $[A]_s$ and their inverses $[A]_s^{-1}$ calculated for 500, 750 and 1,000 lbs. of loads are shown on pages 94, 95 and 96.

Now making use of Eqs. (51), (52), (53) and (54) values of τ, δ, τ_{max} and δ_{max} have been calculated and plotted against the bond length b. The graphs are shown on pages 97, 98 and 99.

5.7 CONCLUSIONS

The study of graphs in Figs. 13, 14 and 15 shows 15-18% higher values of stresses as compared to those calculated in Chapter IV, using the Small Deflection Theory. This is explained by the inclusion of the term β- the component of the axial force induced in the aluminum facings due to external loading - which increases the stress couple $(M_2)_o$. σ_{max} appears to be the stress which produces yielding as compared to τ_{max} because Waldex W-105 adhesive has a yield stress of 1250 psi in tension, as compared to 2485 psi in shear. Furthermore, it is seen from Fig. 15 that the maximum stress is independent of bond length except when the bond length is very small. Hence, the bond will yield by tearing off at its edges. This tear travels in towards the centre of the bond and will probably stop when the remaining overlap becomes small.

0.1183E+01	0.9830E+01	0.2080E+02	0.0000E+00	0.0000E+00	0.0000E+00	0.0000E+00
0.4640E+01	0.9830E+01	-0.2080E+02	-0.6800E-01	0.2079E+02	0.1760E+01	-0.2200E+02
-0.1690E+01	0.1123E+02	-0.3120E+02	-0.1350E+00	0.4940E+00	-0.7760E+01	-0.3300E+02
0.0000E+00	0.0000E+00	0.0000E+00	-0.1829E+01	-0.1736E+02	0.1346E+03	-0.5930E+03
0.0000E+00	0.0000E+00	0.0000E+00	-0.7800E+01	0.3125E+02	-0.6169E+03	-0.2740E+04
-0.1088E+04	0.7260E+03	-0.2600E+04	-0.7800E+01	-0.9554E+02	0.5911E+03	-0.2744E+04
-0.2094E+03	0.1217E+04	-0.4490E+04	0.0000E+00	0.0000E+00	0.0000E+00	0.0000E+00

MATRIX [A] OF EQUATION (31) CORRESPONDING TO LOAD : 500 LBS.

0.5897E-02	-0.8160E-03	-0.1618E-01	0.4662E-02	0.2790E-03	-0.1034E-02	0.7410E-03
0.3207E-01	0.1200E-04	0.2230E-03	-0.6400E-04	-0.3000E-05	0.1400E-04	0.2890E-03
0.1724E-01	0.4100E-04	0.8150E-03	-0.2350E-03	-0.1100E-04	0.5200E-04	0.1790E-03
0.5848E+01	0.1077E+00	-0.2414E+02	-0.6765E-01	0.2966E+00	0.7774E-02	0.1898E+00
-0.1375E-01	0.4752E-01	0.2143E-02	-0.2415E-02	-0.1570E-03	0.2720E-03	-0.4560E-03
0.1836E-02	0.4329E-02	-0.1249E-01	0.3477E-02	0.6650E-03	0.2800E-04	0.5800E-04
-0.1722E-01	-0.7400E-03	-0.7154E-01	-0.6180E-03	-0.1061E-02	-0.2500E-04	-0.5580E-03

INVERSE OF MATRIX [A]

-0.8770E+00	0.1240E+02	-0.2950E+02	0.0000E+00	0.0000E+00	0.0000E+00	0.0000E+00
0.7100E+01	0.1240E+02	-0.2950E+02	0.1068E+00	-0.2442E+02	0.1078E+02	-0.2480E+02
-0.1978E+01	0.1578E+02	-0.4430E+02	0.3870E-01	-0.1610E+01	0.1341E+02	-0.3710E+02
0.0000E+00	0.0000E+00	0.0000E+00	-0.1120E+01	-0.2916E+02	0.1920E+03	-0.6690E+03
0.0000E+00	0.0000E+00	0.0000E+00	0.6760E+01	-0.1337E+03	0.7944E+03	-0.3100E+04
-0.1638E+03	0.9860E+03	-0.3684E+04	0.6756E+01	-0.3106E+04	0.7946E+03	-0.3100E+04
-0.2809E+03	0.1664E+04	-0.6360E+04	0.0000E+00	0.0000E+00	0.0000E+00	0.0000E+00

MATRIX [A] OF EQUATION (31) CORRESPONDING TO LOAD : 750 LBS.

0.2955E-01	0.1170E+00	-0.1589E+00	0.4993E-02	0.8070E-03	-0.9180E-03	0.9590E-03
0.2109E+00	0.1064E-01	0.1446E-01	-0.4540E-03	-0.7300E-04	0.8400E-04	-0.1078E-02
-0.2578E-01	-0.7953E-02	0.1080E-01	-0.3390E-03	-0.5800E-04	0.6200E-04	-0.4820E-03
-0.1974E+01	0.1053E+00	0.2093E+01	-0.4199E+00	0.6551E-01	-0.7900E-03	-0.5404E-02
0.1545E-02	-0.1220E-03	0.1820E-03	-0.5000E-05	0.3350E-03	-0.3350E-03	0.1860E-03
-0.2476E+00	0.1320E-01	0.2625E+00	-0.4025E-02	-0.2274E-02	-0.1040E-03	-0.6810E-03
-0.6782E-01	0.3618E-02	0.7182E-01	-0.1947E-02	-0.7770E-03	-0.1400E-04	-0.1940E-03

INVERSE OF MATRIX [A]

0.8440E+01	0.2318E+02	-0.2540E+02	0.0000E+00	0.0000E+00	0.0000E+00	0.0000E+00
0.7460E+01	0.2318E+02	0.2580E+02	-0.2700E-02	-0.1700E+02	0.1282E+02	-0.1710E+02
0.4700E+01	0.2347E+02	-0.3820E+02	-0.7530E-01	-0.1981E+01	0.1573E+02	-0.1700E+02
0.0000E+00	0.0000E+00	0.0000E+00	-0.1440E+01	-0.3367E+02	0.2200E+03	-0.4610E+03
0.0000E+00	0.0000E+00	0.0000E+00	-0.7246E+01	-0.1499E+03	0.9032E+03	-0.2136E+04
0.1537E+03	0.6368E+03	-0.3180E+04	-0.7247E+01	-0.1499E+03	0.9032E+03	-0.2136E+04
0.2410E+03	0.9366E+03	-0.5490E+04	0.0000E+00	0.0000E+00	0.0000E+00	0.0000E+00

MATRIX [A] OF EQUATION (31) CORRESPONDING TO LOAD : 1,000 LBS.

0.2219E+00	-0.1600E-04	0.7350E-03	-0.2470E-03	0.4452E-01	-0.4448E-01	0.2473E-01
-0.8012E-02	0.6000E-05	-0.2860E-03	0.9600E-04	-0.1730E-01	0.1729E-01	-0.9857E-02
0.4080E-02	0.0000E+00	-0.1600E-04	0.5000E-05	-0.9900E-03	0.9900E-03	-0.7800E-03
0.1435E+01	0.3617E-01	-0.1666E+02	0.5572E+01	-0.3664E+01	0.2590E+01	-0.1390E+01
0.6651E-01	-0.6385E-01	-0.2973E-01	0.2436E-01	-0.1523E-01	-0.1073E-01	-0.6610E-02
-0.3580E-02	-0.5150E-02	0.8039E-01	0.1364E-01	0.8680E-02	-0.1223E-01	0.6520E-02
-0.1105E-01	0.1070E-02	0.9236E-01	-0.1484E-01	0.1670E-01	-0.1471E-01	0.7940E-02

INVERSE OF MATRIX [A]

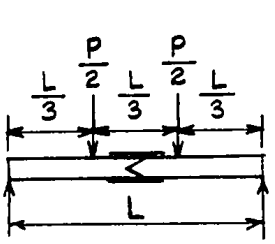

SET-UP FOR FLEXURAL TESTING

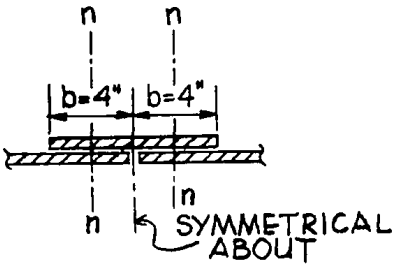

SKETCH SHOWING COVER PLATE BONDED TO ALUMINUM FACINGS

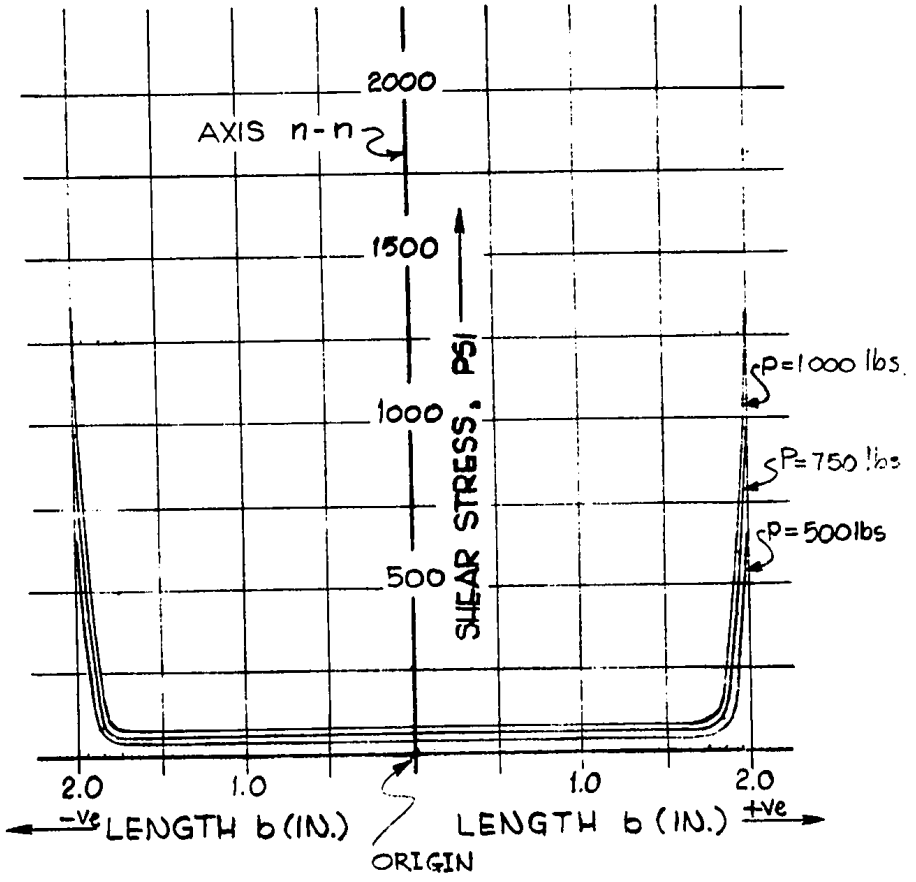

FIG. 13 THEORETICAL DISTRIBUTION OF SHEAR STRESS IN ADHESIVE ON THE COMPRESSION SIDE OF SPECIMEN A$_1$ IN FLEXURAL TESTING (LARGE DEFLECTION THEORY).

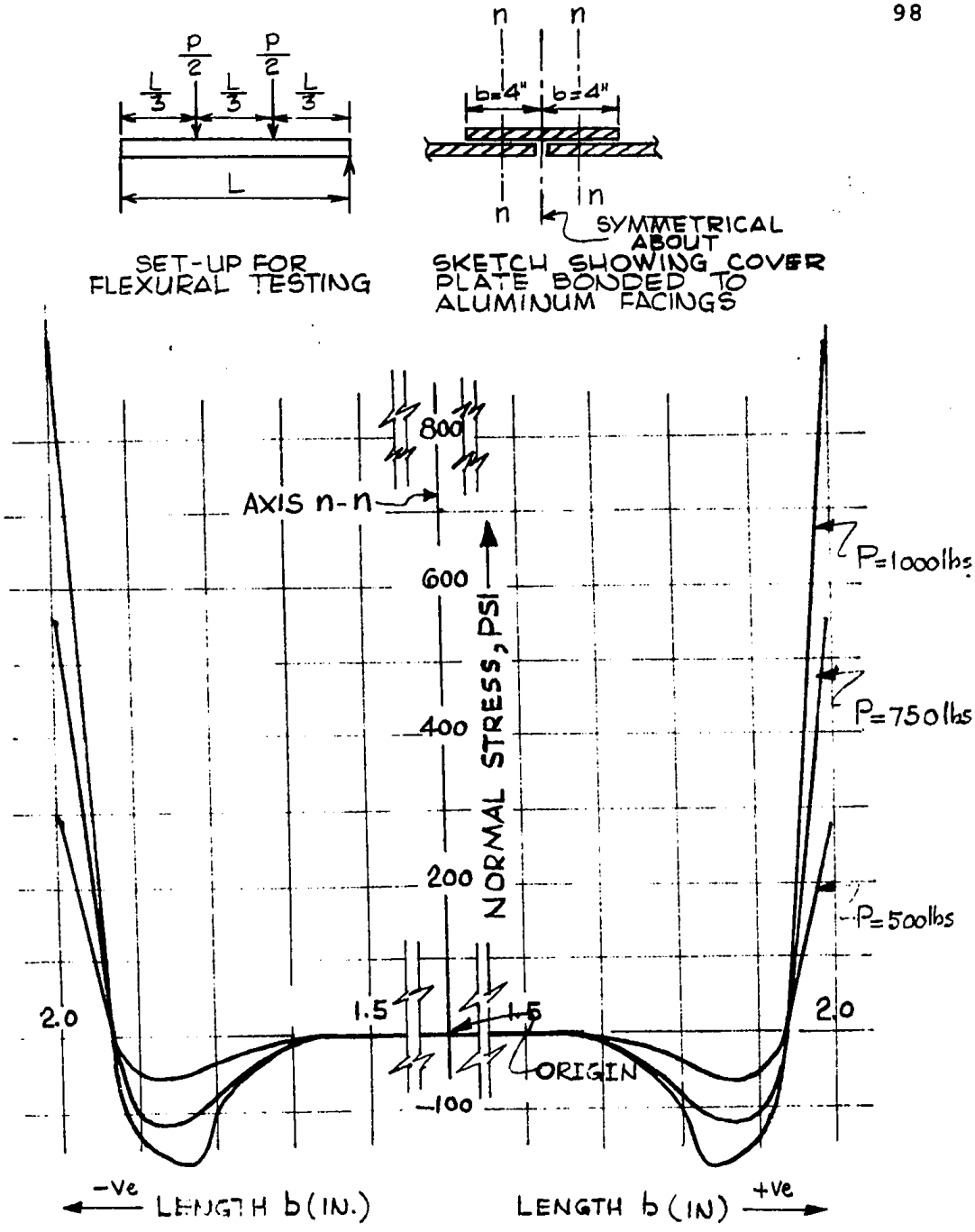

FIG. 14 THEORETICAL DISTRIBUTION OF NORMAL STRESS IN ADHESIVE ON THE COMPRESSION SIDE OF SPECIMEN A_1 IN FLEXURAL TESTING (LARGE DEFLECTION THEORY)

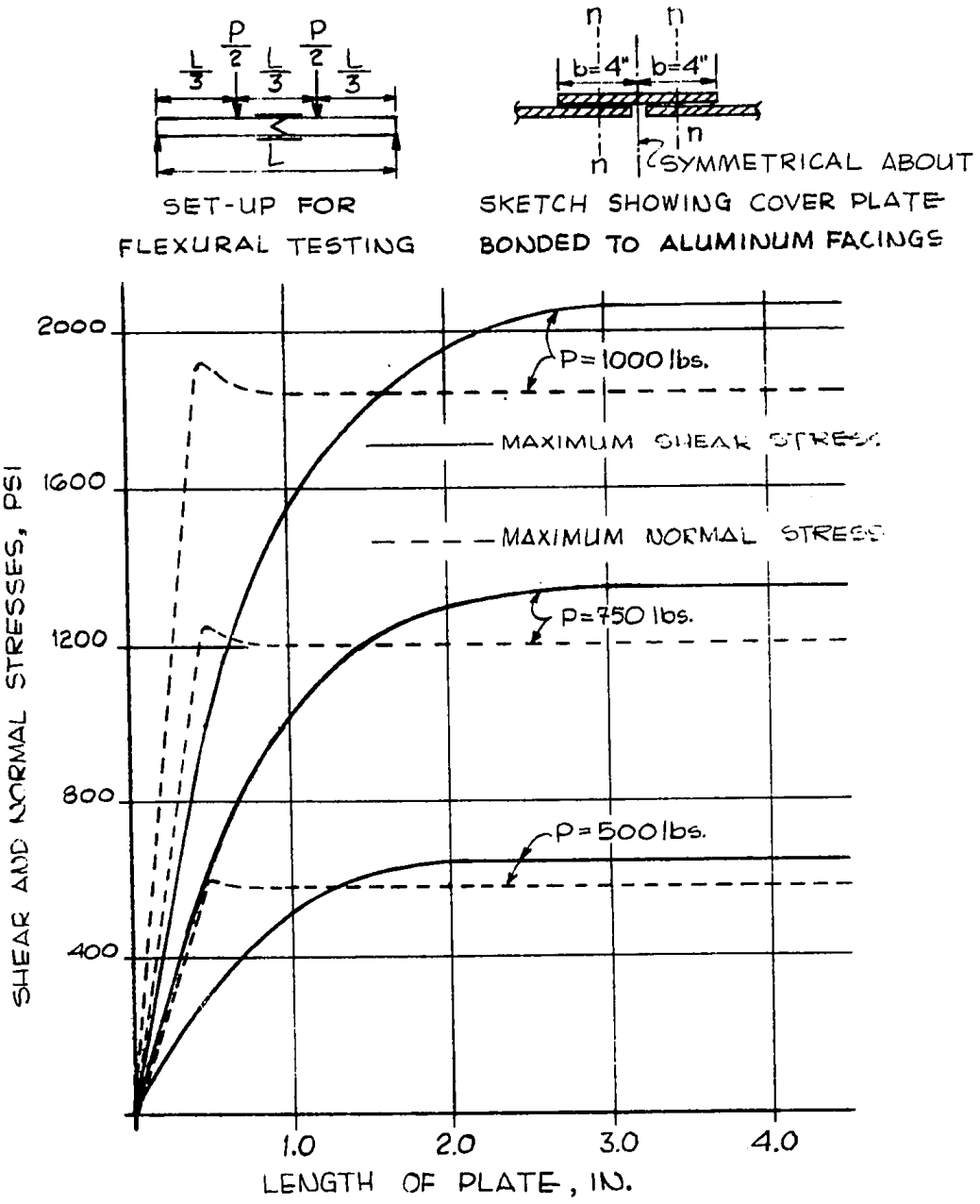

FIG. 15 MAXIMUM SHEAR AND NORMAL STRESSES IN ADHESIVE AS FUNCTIONS OF BOND LENGTH ON THE COMPRESSION SIDE OF SPECIMEN A_1 IN FLEXURAL TESTING (LARGE DEFLECTION THEORY).

CHAPTER VI

THEORETICAL ANALYSIS OF ADHESIVE BONDED MID-PANEL JOINTS CONNECTING SANDWICH PANELS

LARGE DEFLECTION THEORY: TENSION SIDE OF SPECIMENS

The joint to be analysed is the same as used in Chapter IV.

This type of joint, as shown in Fig. 3, is primarily dependent on adhesives for its strength. The most critical area from the strength point of view, is the adhesive between the cover plate and the aluminum facings. This connection is to be used in joining sandwich panels in which all bending moment is taken by the aluminum facings and the shear by the core.

As shown in Fig. 16, we are considering two rectangular sheets of the same material of unit width and of lengths $(2a + b)$ and b. The faces of the longer and shorter sheets of thickness f and ξf, respectively, $(0 < \xi < 1)$, are cemented by an adhesive layer of thickness ψ, where ψ is small compared to f. The force T_f induced in the faces due to bending of the sandwich beam is considered per unit width. The stiffened structure is considered as a homogrneous thin plate with finite discontinuities in its thickness and in its neutral plane. Bending of the neutral plane will occur under the applied loads; hence, a bending moment and a compressive force act on the longer sheet at the bond edges.

6.1 STRESS RESULTANTS AT THE BOND EDGES

Because of the variable thickness of the structure shown in Fig. 16, bending will occur under the loading T_f and M_f and will produce a stress couple resultant $(M_2)_o$ acting on the facings at the bond edges. To determine this bending moment, the structure will be considered as a homogeneous cylindrically bent plate with a discontinuous thickness and neutral plane. For this calculation, since $\psi << f$, the effect of adhesive will be neglected.

We know that

$$\frac{d^2y}{dx^2} = -\frac{M}{D} \qquad (1)$$

which is the general expression relating curvature and bending moment, where D, the flexural rigidity of the plate, is given by

$$D = \frac{E_f \cdot f^3}{12(1 - \nu^2)}$$

In this analysis, two values of D, i.e., D_{f_1} and D_{f_2} have been used corresponding to Section I and Section II of the composite plate, respectively (Fig. 16).

E_f is Young's modulus for facings, and ν is Poisson's ratio for them.

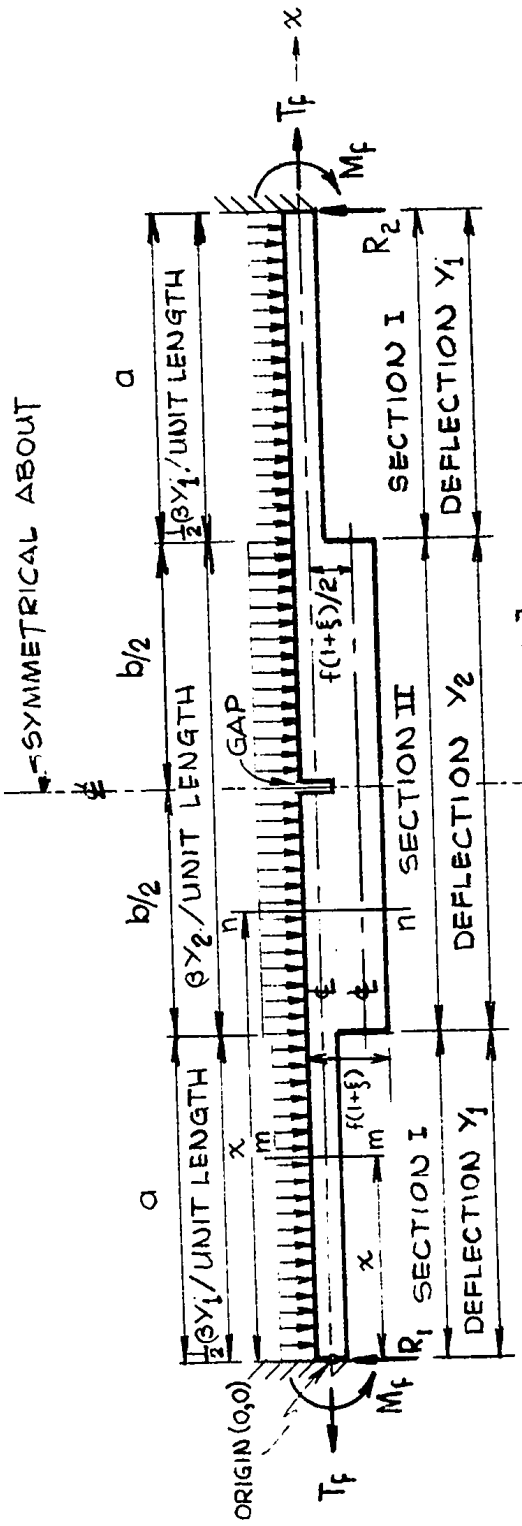

FIG. 16 ALUMINUM FACING AND COVER PLATE SHOWN AS A COMPOSITE PLATE WITH FINITE DISCONTINUITIES IN ITS THICKNESS (Thickness of Adhesive Being Neglected).

The deformation of the structure may be conveniently studied by separating it into Sections 1 and 2 with coordinates (x,y_1) and (x,y_2), respectively, where both coordinate systems are as shown in Fig. 16. The bending moments acting at the general sections m-m and n-n of regions 1 and 2, respectively, are given by

$$M_1 = M_f - [\beta y_1 a + \tfrac{1}{2}\beta y_2 b]x + T_f y_1 + \beta y_1 \frac{x^2}{2} \quad \ldots \quad 0 \leq x \leq a \tag{2}$$

$$M_2 = M_f - [\beta y_1 a + \tfrac{1}{2}\beta y_2 b]x + T_f[y_2 + \frac{f}{2}(1 + \xi) + \beta y_2 \frac{(x - a)^2}{2}$$

$$+ \beta y_1 a(x - \frac{a}{2}) \quad \ldots \quad a \leq x \leq b \tag{3}$$

Eqs. (2) and (3) are simplified working along the same lines as shown in Chapter V. As a result, the following differential equation is obtained containing y_1

$$\frac{d^4y_1}{dx^4} + K_1x^2\frac{d^2y_1}{dx^2} + K_2x\frac{d^2y_1}{dx^2} + K_3\frac{d^2y_1}{dx^2} + K_4x^4y_1 +$$

$$+ K_5x^3y_1 + K_6x^2y_1 + K_7xy_1 + K_8y_1 + K_9x^2 +$$

$$+ K_{10}x + K_{11} = 0 \tag{12}$$

where $K_1, K_2 \ldots\ldots\ldots K_{11}$ are the coefficients, as shown below

$$k_1 = +\left[\frac{T_f}{D_{f_2}} + \frac{\beta a^2}{2D_{f_2}} + \frac{T_f}{D_{f_1}}\right] \quad \text{(a)}$$

$$k_2 = +\left[\frac{\beta}{2D_{f_2}} + \frac{\beta}{4D_{f_1}}\right] \quad \text{(b)}$$

$$k_3 = -\left[\frac{\beta a}{2D_{f_1}} + \frac{\beta a}{D_{f_2}} + \frac{\beta b}{2D_{f_2}}\right] \quad \text{(c)}$$

$$k_4 = \left[\frac{\beta^2}{8D_{f_1}D_{f_2}}\right] \quad \text{(d)}$$

$$k_5 = -\left[\frac{\beta^2 a}{2D_{f_1}D_{f_2}} + \frac{\beta^2 b}{8D_{f_1}D_{f_2}}\right] \quad \text{(e)}$$

$$k_6 = \left[\frac{3\beta T_f}{4D_{f_1}D_{f_2}} + \frac{5\beta^2 a^2}{8D_{f_1}D_{f_2}} + \frac{\beta^2 ab}{4D_{f_1}D_{f_2}}\right] \quad \text{(f)} \quad (13)$$

$$k_7 = -\left[\frac{3T_f\beta a}{2D_{f_1}D_{f_2}} + \frac{T_f\beta b}{2D_{f_1}D_{f_2}} + \frac{\beta^2 a^3}{4D_{f_1}D_{f_2}} + \frac{\beta^2 a^2 b}{8D_{f_1}D_{f_2}}\right] \quad \text{(g)}$$

$$k_8 = \left[\frac{T_f^2}{D_{f_1}D_{f_2}} + \frac{T_f\beta a^2}{2D_{f_1}D_{f_2}}\right] \quad \text{(h)}$$

$$k_9 = \left[\frac{M_f\beta}{2D_{f_1}D_{f_2}}\right] \quad \text{(i)}$$

$$k_{10} = +\left[\frac{M_f\beta a}{D_{f_1}D_{f_2}} + \frac{T_f\beta b.f}{4D_{f_1}D_{f_2}} - \frac{T_f\beta b\xi f}{4D_{f_1}D_{f_2}}\right] \quad \text{(j)}$$

$$k_{11} = \left[\frac{M_f T_f}{D_{f_1}D_{f_2}} + \frac{M_f\beta a^2}{2D_{f_1}D_{f_2}}\right] \quad \text{(k)}$$

(NOTE: For convenience in reading, equations in this Chapter have been numbered in the same sequence as in Chapter V, which should be referred to for the missing equations in this derivation).

Similarly, the differential equation containing y_2 is as follows:

$$\frac{d^4y_2}{dx^4} + K_1'x^2\frac{d^2y_2}{dx^2} + K_2'x\frac{d^2y_2}{dx^2} + K'_3\frac{d^2y_2}{dx^2} + K_4'x^4y_2$$

$$+ K_5'x^3y_2 + K_6'x^2y_2 + K_7'xy_2 + K_8'y_2 + K_9'x + K_{10}'x + K_{11}' = 0 \qquad (18)$$

where K_1', K_2' .....K_{11}' are the coefficients, as shown below:

$$k_1' = +\left[\frac{T_f}{D_{f_2}} + \frac{\beta a^2}{2D_{f_2}} + \frac{T_f}{D_{f_1}}\right] \qquad (a)$$

$$k_2' = +\left[\frac{\beta}{2D_{f_2}} + \frac{\beta}{4D_{f_1}}\right] \qquad (b)$$

$$k_3' = -\left[\frac{\beta a}{2D_{f_1}} + \frac{\beta a}{D_{f_2}} + \frac{\beta b}{2D_{f_2}}\right] \qquad (c)$$

$$k_4' = \left[\frac{\beta^2}{8D_{f_1}D_{f_2}}\right] \qquad (d) \qquad (19)$$

$$k_5' = -\left[\frac{\beta^2 a}{2D_{f_1}D_{f_2}} + \frac{\beta^2 b}{8D_{f_1}D_{f_2}}\right] \qquad (e)$$

$$k_6' = \left[\frac{3\beta T_f}{4D_{f_1}D_{f_2}} + \frac{5\beta^2a^2}{8D_{f_1}D_{f_2}} + \frac{\beta^2 ab}{4D_{f_1}D_{f_2}}\right] \qquad (f)$$

$$k_7' = -\left[\frac{3T_f\beta a}{2D_{f_1}D_{f_2}} + \frac{T_f\beta b}{2D_{f_1}D_{f_2}} + \frac{\beta^2a^3}{2D_{f_1}D_{f_2}} + \frac{\beta^2a^2b}{8D_{f_1}D_{f_2}}\right] \qquad (g)$$

$$k'_8 = \left[\frac{T_f^2}{D_{f_1}D_{f_2}} + \frac{T_f\beta a^2}{2D_{f_1}D_{f_2}}\right] \quad (h)$$

$$k'_9 = \left[-\frac{M_f\beta}{4D_{f_1}D_{f_2}} + \frac{T_f.f\beta}{8D_{f_1}D_{f_2}} + \frac{T_f.\xi f\beta}{8D_{f_1}D_{f_2}}\right] \quad (i)$$

$$k'_{10} = -\left[\frac{M_f\beta a}{2D_{f_1}D_{f_2}} + \frac{T_f\beta af}{4D_{f_1}D_{f_2}} + \frac{T_f.\xi f\beta a}{4D_{f_1}D_{f_2}}\right] \quad (j) \qquad (19)$$

$$k'_{11} = \left[\frac{T_f^2.f}{2D_{f_1}D_{f_2}} + \frac{T_fM_f}{D_{f_1}D_{f_2}} + \frac{T_f^2.\xi f}{2D_{f_1}D_{f_2}} + \frac{M_f\beta a^2}{2D_{f_1}D_{f_2}}\right] \quad (k)$$

6.1.1 Solution of the Differential Equations for Deflections y_1 and y_2

The differential equations (12) and (18) are linear, non-homogeneous with variable coefficients.

The integration of the two equations will be obtained by assuming y to be an unknown function expandable into an infinite series (converging for all values of x), i.e., - $y(x) = A_o + A_1x + A_2x^2 + A_3x^3 \quad \ldots\ldots + A_nx^n$ where the A_n's are undetermined coefficients. From here onward, we proceed along the same lines as described in Chapter V, until Eq. (31), where we get the same coefficient matrix [A] except that some of the elements have their signs reversed.

$$\begin{bmatrix} \alpha_1 & \alpha_2 & \alpha_3 & 0 & 0 & 0 & 0 \\ \beta_1 & \beta_2 & \beta_3 & \beta_4 & \beta_5 & \beta_6 & \beta_7 \\ \gamma_1 & \gamma_2 & \gamma_3 & -\gamma_4 & -\gamma_5 & -\gamma_6 & -\gamma_7 \\ 0 & 0 & 0 & \delta_1 & \delta_2 & \delta_3 & \delta_4 \\ 0 & 0 & 0 & +\lambda_4 & +\lambda_5 & +\lambda_6 & +\lambda_7 \\ \mu_1 & \mu_2 & \mu_3 & \mu_4 & \mu_5 & \mu_6 & \mu_7 \\ \psi_1 & \psi_2 & \psi_3 & 0 & 0 & 0 & 0 \end{bmatrix} \begin{Bmatrix} A_1 \\ A_2 \\ A_3 \\ B_o \\ B_1 \\ B_2 \\ B_3 \end{Bmatrix} = \begin{bmatrix} \phi_1 \\ 0 \\ 0 \\ 0 \\ \phi_2 \\ 0 \\ 0 \end{bmatrix} \tag{31}$$

The bending moment $(M_2)_o$ at the bond edge and at the compression side is given by

$$(M_2)_o = -D_{f_1}[2A_2 + 6A_3 a] \tag{34}$$

6.2 EQUATIONS FOR BONDED REGIONS: EQUATIONS FOR THE ADHESIVE STRESS τ AND σ : SOLUTION OF THE DIFFERENTIAL EQUATIONS FOR $\xi = 1$

We now consider the bonded region. The ends of the lower sheets (Fig. 17) are acted upon by a tensile force resultant T_f and by a bending moment resultant $(M_2)_o$ given by Eq. (34). Because the bond is considered in its undeformed state, symmetry requires the shear to vanish at the ends. The x-axis has its origin as shown in Fig. 17. Equations which must be satisfied by each of the bonded sheets and by the adhesive will now be formulated.

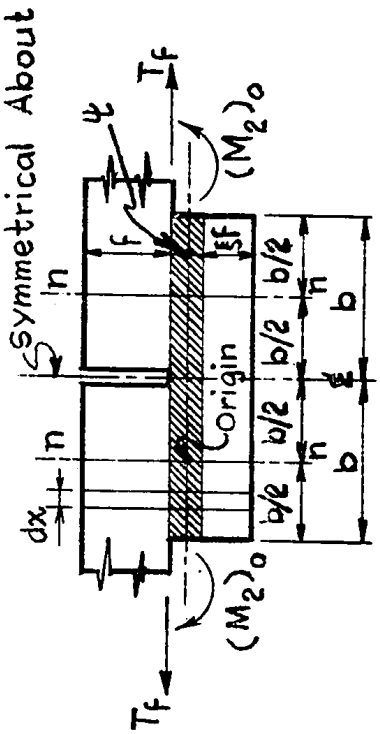

FIG. 17 BONDED REGION SHOWING APPLIED LOADS

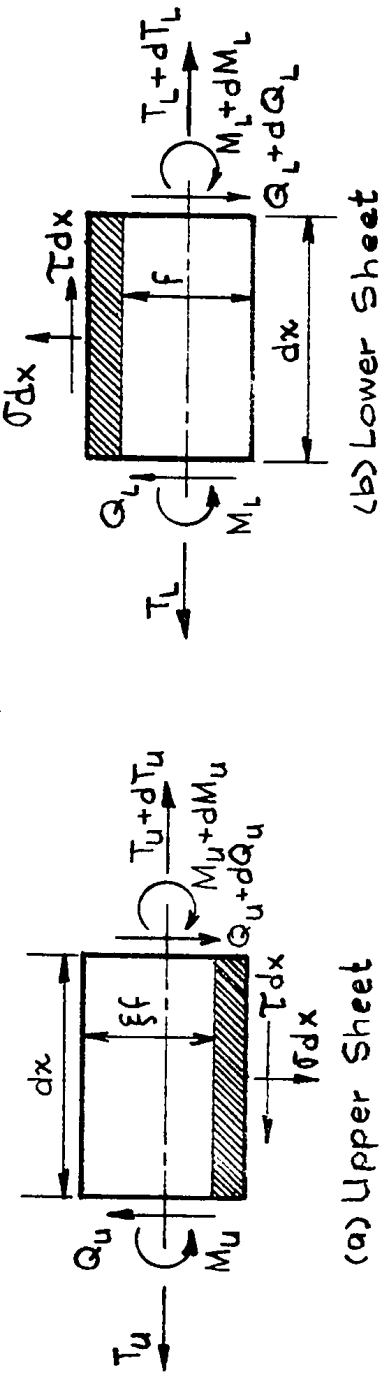

FIG. 18 STRESSES ON AN ELEMENT OF BONDED REGION

According to the theory of cylindrically-bent plates, an element of the upper sheet (Fig. 18a) will be acted upon by T_u and Q_u, the axial and the shear force resultants, and by M_u, a bending moment resultant. Counter-clockwise moments and downward forces are taken positive. Since the forces and the moments are in equilibrium with the adhesive stresses σ and τ, the following equations hold:

$$\left.\begin{aligned} \frac{dM_u}{dx} + Q_u + \frac{\xi f \tau}{2} &= 0 \\ \frac{dQ_u}{dx} + \sigma &= 0 \\ \frac{dT_u}{dx} - \tau &= 0 \end{aligned}\right\} \qquad (35)$$

Similarly, if an element of the lower sheet (Fig. 18b) is considered, then for equilibrium the following equations must be satisfied.

$$\left.\begin{aligned} \frac{dM_L}{dx} + Q_L + \frac{\xi f}{2} &= 0 \\ \frac{dQ_L}{dx} - \sigma &= 0 \\ \frac{dT_L}{dx} + \tau &= 0 \end{aligned}\right\} \qquad (36)$$

Solving the sets of equations (35) and (36) for the same boundary conditions as shown in Chapter IX, the following values of τ are obtained:

$$\tau = \left[\frac{3T_f + \frac{6(M_2)_0}{f}}{4b}\right] + \frac{\frac{\sqrt{2}}{4}\left(\frac{G_c}{E\psi f}\right)^{\frac{1}{2}}\left(T_f - \frac{6(M_2)_0}{f}\right)\cosh\left\{2\sqrt{2}\left(\frac{G_c}{E\psi f}\right)^{\frac{1}{2}}x\right\}}{\sinh\left\{2\sqrt{2}\left(\frac{G_c}{E\psi f}\right)^{\frac{1}{2}}\frac{b}{2}\right\}} \tag{51}$$

The solution of Eq. (50) under the conditions given by Eqs. (46) to (48) is:

$$\sigma = -2\left(\frac{E_c}{2\psi D_{f_2}}\right)^{\frac{1}{2}}(M_2)_0\left[\sinh\left\{\left(\frac{E_c}{2\psi D_{f_2}}\right)^{\frac{1}{4}}b\right\} + \sinh\left\{\left(\frac{E_c}{2\psi D_{f_2}}\right)^{\frac{1}{4}}b\right\}\right]^{-1}\times\left[<\cos\left\{\left(\frac{E_c}{2\psi D_{f_2}}\right)^{\frac{1}{4}}b/2\right\}\sinh\left\{\left(\frac{E_c}{2\psi D_{f_2}}\right)^{\frac{1}{4}}\frac{b}{2}\right\} -\right.$$

$$\sin\left\{\left(\frac{E_c}{2\psi D_{f_2}}\right)^{\frac{1}{4}}\frac{b}{2}\right\}\cosh\left\{\left(\frac{E_c}{2\psi D_{f_2}}\right)^{\frac{1}{4}}\frac{b}{2}\right\}>\cos\left\{\left(\frac{E_c}{2\psi D_{f_2}}\right)^{\frac{1}{4}}x\right\}\cosh\left\{\left(\frac{E_c}{2\psi D_{f_2}}\right)^{\frac{1}{4}}x\right\} + <\cos\left\{\left(\frac{E_c}{2\psi D_{f_2}}\right)^{\frac{1}{4}}\frac{b}{2}\right\}\sinh\left\{\left(\frac{E_c}{2\psi D_{f_2}}\right)^{\frac{1}{4}}\frac{b}{2}\right\}$$

$$\left. + \sin\left\{\left(\frac{E_c}{2\psi D_{f_2}}\right)^{\frac{1}{4}}\frac{b}{2}\right\}\cosh\left\{\left(\frac{E_c}{2\psi D_{f_2}}\right)^{\frac{1}{4}}\frac{b}{2}\right\}>\sin\left\{\left(\frac{E_c}{2\psi D_{f_2}}\right)^{\frac{1}{4}}x\right\}\sinh\left\{\left(\frac{E_c}{2\psi D_{f_2}}\right)^{\frac{1}{4}}x\right\}\right] \tag{52}$$

Both σ max and τ max occur at the bond edges and are given by:

$$\tau_{max} = \left[\frac{3T_f + \frac{6(M_2)_0}{f}}{4b}\right] + \frac{\sqrt{2}}{4}\left(\frac{G_c}{E\psi f}\right)^{\frac{1}{2}}\left(T_f - \frac{6(M_2)_0}{f}\right)\coth\left\{2\sqrt{2}\left(\frac{G_c}{E\psi f}\right)^{\frac{1}{2}}\frac{b}{2}\right\} \tag{53}$$

$$\sigma\ max = \frac{-\left(\frac{E_c}{2\psi D_{f_2}}\right)^{\frac{1}{2}}(M_2)_0\left[\sinh\left\{\left(\frac{E_c}{2\psi D_{f_2}}\right)^{\frac{1}{4}}b\right\} - \sin\left\{\left(\frac{E_c}{2\psi D_{f_2}}\right)^{\frac{1}{4}}b\right\}\right]}{\left[\sinh\left\{\left(\frac{E_c}{2\psi D_{f_2}}\right)^{\frac{1}{4}}b\right\} + \sin\left\{\left(\frac{E_c}{2\psi D_{f_2}}\right)^{\frac{1}{4}}b\right\}\right]} \tag{54}$$

6.3 ILLUSTRATIVE EXAMPLE

Calculations of stresses in the adhesive are made for actual values of the parameters in a stiffened plate in this Chapter. Specimens of joints used for experimental verification were fabricated using the same values of parameters for comparison. For specimen designations, their types, modes of testing, etc., refer to Chapter VII. For the plates, the values chosen are $E_{A\ell} = 10.25 \times 10^6$ psi; $\nu = 0.33$; a = 2.0 in.; b = 4.0 in.; f = 0.030 in.; $\psi = 0.0128$ in. For the adhesive, the material constants are $E_c = 516 \times 10^3$ psi and $G_c = 184 \times 10^3$ psi, which are representative values for Waldex W-105 adhesive.

Values of $(M_2)_o$ - the stress couple resultant acting on the facings of the bond edges are calculated for three different values of T_f corresponding to 500, 750 and 1,000 lbs. of applied load using Eq. (34). The value of β was determined experimentally for each loading.Coefficient matrices $[A]_s$ and their inverses $[A]_s^{-1}$ calculated for 500, 750 and 1,000 lbs. of loads are shown on pages 112, 113 and 114.

Now making use of Eqs. (51), (52), (53) and (54), values of τ, σ, τ_{max} and σ_{max} have been calculated and plotted against the bond length b. The graphs are shown on pages 115,116 and 117.

6.4 CONCLUSIONS

The study of graphs in Figs. (19), (20) and (21), shows 16-19% higher values of stresses, as compared to those calculated in Chapter IV, using the Small Deflection Theory. This is explained by the inclusion of the term β- the component of the axial force T_f in the aluminum facings - which increases the stress couple $(M_2)_o$. σ_{max} on the tension side appears to be the stress which produces yielding as compared to τ_{max} because Waldex W-105 adhesive has a yield stress of 1250 psi in tension as compared to 2485 psi in shear. Furthermore, it is seen from Fig. (21) that the maximum stress is independent of bond length except when the bond length is very small. Hence, the bond will yield by tearing off at its edges. This tear travels in towards the centre of the bond and will probably stop when the remaining overlap becomes small.

Chapter VII will cover the experimental work carried out on various test specimens to substantiate the theory presented in Chapters V and VI. It is hoped that this would complete a major phase of study of the joints for sandwich panels.

0,1171E+01	0,9720E+01	0,2017E+02	0,0000E+00	0,0000E+00	0,0000E+00	0,0000E+00
0,4520E+01	0,9170E+01	-0,1998E+02	-0,6200E-01	0,2067E+02	0,1670E+01	-0,2123E+02
-0,1630E+01	0,1225E+02	-0,3115E+02	-0,1670E+00	0,4920E+00	-0,7750E+01	-0,3267E+02
0,0000E+00	0,0000E+00	0,0000E+00	-0,1827E+01	-0,1725E+02	0,1345E+03	-0,5927E+03
0,0000E+00	0,2000E+00	0,0000E+00	-0,7680E+01	0,3125E+02	-0,6167E+03	-0,2741E+04
-0,1388E+04	0,7260E+03	-0,2600E+04	-0,8700E+01	-0,9556E+02	0,5911E+03	-0,2744E+04
-0,2484E+03	0,1217E+04	-0,4490E+04	0,0000E+00	0,0000E+00	0,0000E+00	0,0000E+00

MATRIX [A] OF EQUATION (31) CORRESPONDING TO LOAD : 500 LBS.

0,5679E-02	-0,6183E-03	-0,1618E-01	0,4661E-02	0,2790E-03	-0,1134E-02	0,7210E-03
0,3232E-01	0,2100E-04	0,3220E-03	-0,4600E-04	-0,3000E-05	0,1300E-04	0,2890E-03
0,5210E-03	0,4200E-04	0,8140E-03	-0,2340E-03	-0,1100E-04	0,5200E-04	0,1780E-03
0,5847E+01	0,1376E+00	-0,2314E+02	-0,6765E-01	0,2966E+00	0,7674E-02	0,1889E+00
-0,1457E-01	0,4652E-01	0,2144E-02	-0,2451E-02	-0,1570E-03	0,2680E-03	-0,4660E-03
0,1853E-02	0,4392E-02	-0,1285E-01	0,3476E-02	0,6560E-03	0,2700E-04	0,5700E-04
-0,1722E-01	-0,7410E-03	-0,7153E-01	-0,6170E-03	-0,1057E-02	-0,5200E-04	-0,5670E-03

INVERSE OF MATRIX [A]

-0.8670E+00	0.1238E+02	-0.2943E+02	0.0000E+00	0.0000E+00	0.0000E+00	0.0000E+00
0.7390E+01	0.1235E+02	-0.2963E+02	0.1168E+00	-0.2439E+02	0.1068E+02	-0.2478E+02
-0.1965E+01	0.1572E+02	-0.4428E+02	0.3780E-01	-0.1620E+01	0.1339E+02	-0.3708E+02
0.0000E+00	0.0000E+00	0.0000E+00	-0.1210E+01	-0.2961E+02	0.1920E+03	-0.6690E+03
0.0000E+00	0.0000E+00	0.0000E+00	0.6750E+01	-0.1339E+03	0.7949E+03	-0.3210E+04
-0.1625E+03	0.9863E+03	-0.3648E+04	0.6752E+01	-0.3206E+04	0.7936E+03	-0.3104E+04
-0.2814E+03	0.1663E+04	-0.6463E+04	0.0000E+00	0.0000E+00	0.0000E+00	0.0000E+00

MATRIX [A] OF EQUATION (31) CORRESPONDING TO LOAD : 750 LBS.

0.2956E-01	0.1196E+00	-0.1689E+00	0.4992E-02	0.8050E-03	-0.9180E-03	0.9690E-03
0.2109E+00	0.1064E-01	0.1449E-01	-0.5440E-03	-0.7200E-04	0.8300E-04	-0.1078E-02
-0.2577E-01	-0.7859E-02	0.1081E-01	-0.3370E-03	-0.5300E-04	0.6300E-04	-0.4830E-03
-0.1964E+01	0.1053E+00	0.2093E+01	-0.4197E+00	0.6532E-01	-0.7900E-03	-0.5404E-02
0.1554E-02	-0.1220E-03	0.1820E-03	-0.5000E-05	0.3360E-03	-0.3370E-03	0.1680E-03
-0.2476E+00	0.1321E-01	0.2625E+00	-0.4052E-02	-0.2275E-02	-0.1050E-03	-0.6790E-03
-0.6782E-01	0.3681E-02	0.7282E-01	-0.1947E-02	-0.7670E-03	-0.1940E-03	0.0000E+00

INVERSE OF MATRIX [A]

0,8460E+01	0,2317E+02	-0,2642E+02	0,0000E+00	0,0000E+00	0,0000E+00	0,0000E+00
0,7440E+01	0,2382E+02	0,2581E+02	-0,2600E-02	-0,1700E+02	0,1282E+02	-0,1710E+02
0,4700E+01	0,2347E+02	-0,3826E+02	-0,7420E-01	-0,1981E+01	0,1536E+02	-0,1698E+02
0,0000E+00	0,0000E+00	0,0000E+00	-0,1340E+01	-0,3376E+02	0,2202E+03	-0,4610E+03
0,0000E+00	0,0000E+00	0,0000E+00	-0,6246E+01	-0,1498E+03	0,9032E+03	-0,2136E+04
0,1537E+03	0,6368E+03	-0,3181E+04	-0,7257E+01	-0,1497E+03	0,9032E+03	-0,2137E+04
0,2410E+03	0,9370E+03	-0,5491E+04	0,0000E+00	0,0000E+00	0,0000E+00	0,0000E+00

MATRIX [A] OF EQUATION (31) CORRESPONDING TO LOAD : 1,000 LBS.

0,2219E+00	-0,1503E-04	0,6370E-03	-0,2460E-03	0,4452E-01	-0,4448E-01	0,2473E-01
-0,8013E-02	0,5000E-05	-0,2850E-03	0,9600E-04	-0,1731E-01	0,1729E-01	-0,9856E-02
0,4080E-02	0,0000E+00	-0,1600E-04	0,5000E-05	-0,9900E-03	0,9900E-03	-0,7700E-03
0,1435E+01	0,3616E-01	-0,1666E+02	0,5572E+01	-0,3674E+01	0,2590E+01	-0,1390E+01
0,6651E-01	-0,6375E-01	-0,2793E-01	0,2463E-01	-0,1523E-01	-0,1073E-01	-0,6610E-02
-0,3570E-02	-0,5160E-02	0,8038E-01	0,1346E-01	0,8670E-02	-0,1223E-01	0,6520E-02
-0,1126E-01	0,1072E-02	0,9236E-01	-0,1484E-01	0,1671E-01	-0,1472E-01	0,7950E-02

INVERSE OF MATRIX [A]

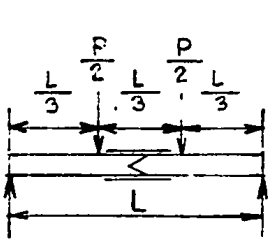

SET-UP FOR FLEXURAL TESTING

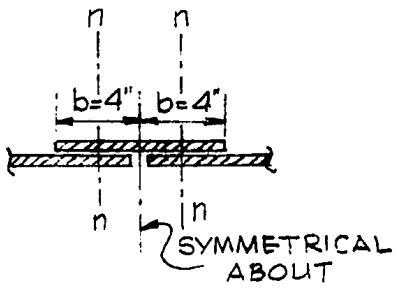

SKETCH SHOWING COVER PLATE BONDED TO ALUMINUM FACINGS

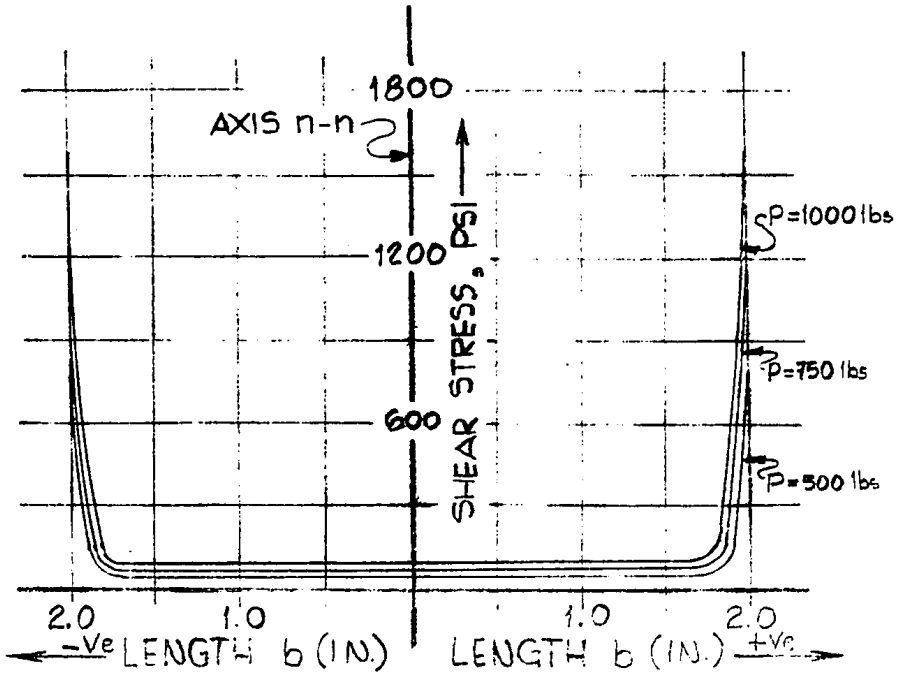

FIG. 19 THEORETICAL DISTRIBUTION OF SHEAR STRESS IN ADHESIVE ON THE TENSION SIDE OF SPECIMEN A_1 IN FLEXURAL TESTING (LARGE DEFLECTION THEORY)

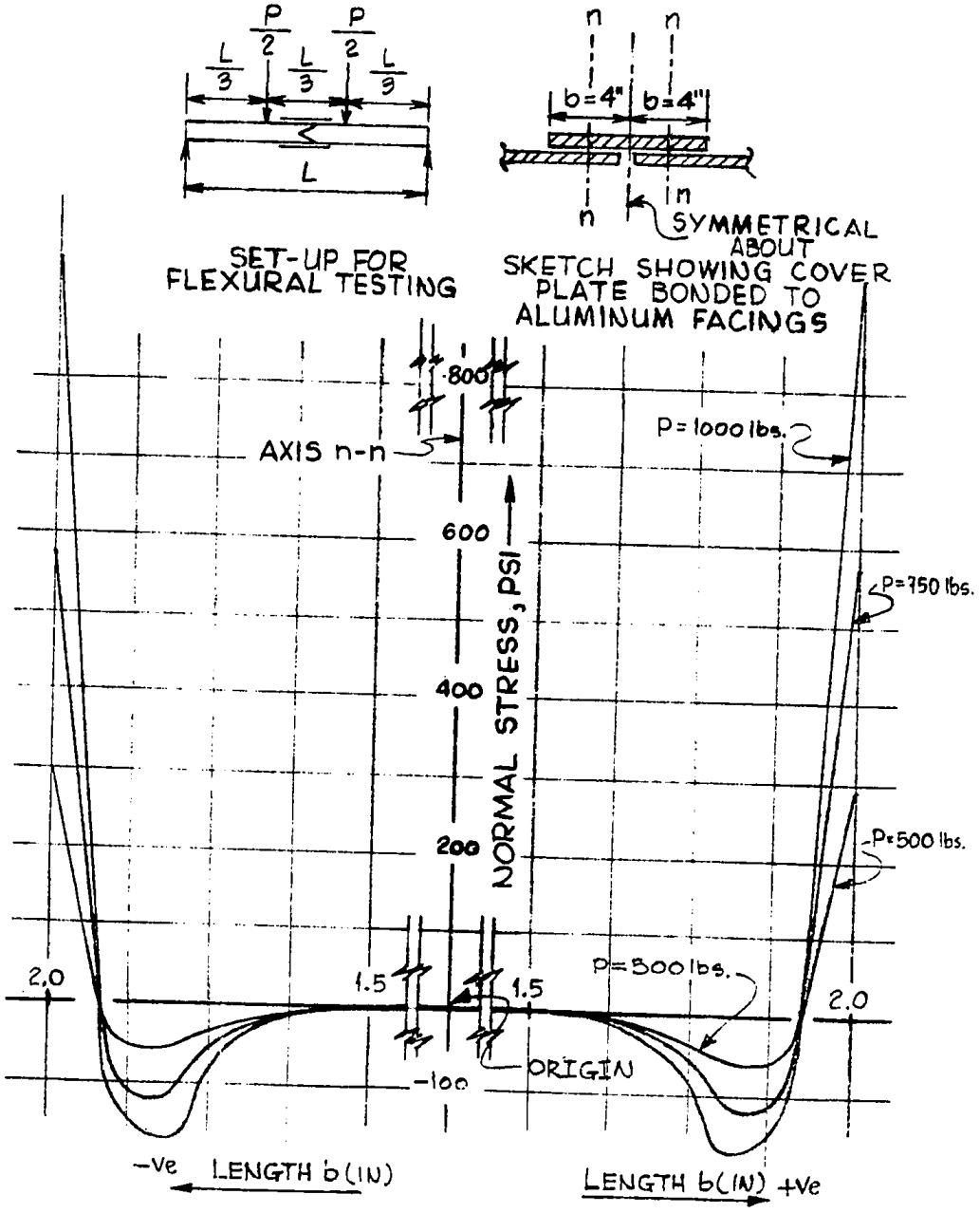

FIG. 20 THEORETICAL DISTRIBUTION OF NORMAL STRESS IN ADHESIVE ON THE TENSION SIDE OF SPECIMEN A, IN FLEXURAL TESTING (LARGE DEFLECTION THEORY)

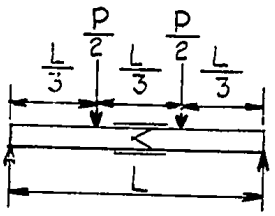

SET-UP FOR FLEXURAL TESTING

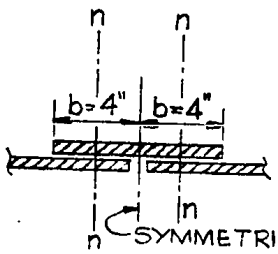

SKETCH SHOWING COVER PLATE BONDED TO ALUMINUM FACINGS

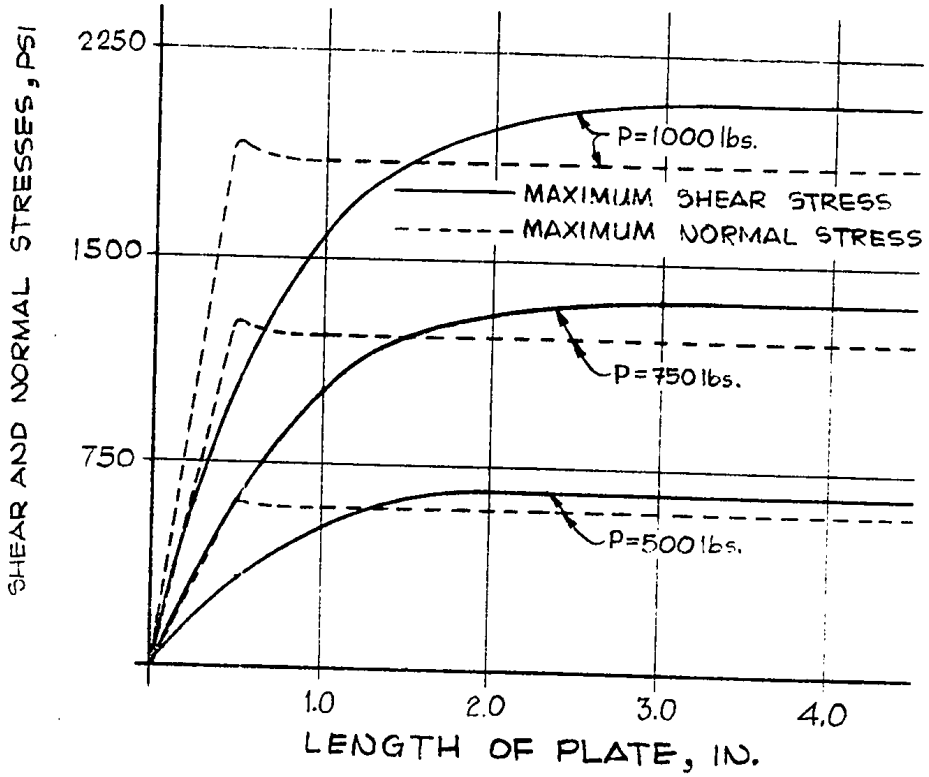

FIG. 21 THEORETICAL MAXIMUM SHEAR AND NORMAL STRESS IN ADHESIVE AS FUNCTIONS OF BOND LENGTH ON THE TENSION SIDE OF SPECIMEN A_1 IN FLEXURAL TESTING (LARGE DEFLECTION THEORY)

CHAPTER VII

EXPERIMENTAL STUDY OF ADHESIVE CONNECTIONS

7.1 INTRODUCTION

The reflective photoelastic technique has been used to study the stresses in the adhesive-bonded connections. Fundamentals of this theory are presented in this Chapter. Three different types of adhesive connections are tested for four different loading conditions (Figs. 22 to 26), with each test being performed for at least three different applied loads. The shear and normal stresses (τ,σ) in the adhesive layer are calculated by making use of the photoelastic test data in combination with the shear difference method of stress analysis.

7.2 BASIC PRINCIPLES OF REFLECTIVE PHOTOELASTICITY

Certain materials when strained become doubly-refracting. If a beam of white polarized light is passed through a strained model which is made of such a material, a coloured fringe pattern is observed. Analysing this colour pattern, the stress or strain distribution can be found in the model. This technique is called photoelasticity.

The photostress technique is a method of stress analysis in which the actual structure to be stress-analysed is coated with a photoelastic plastic. When the structure is loaded, the strains set up in it are transmitted to the

plastic coating, which then becomes birefringent. There exists a direct proportionality between this birefringence and the intensity of strains. If a reflective surface is provided at the interface between the structure and the plastic bonded to it, birefringence can be observed and measured by using a reflection polariscope. When observed with the polariscope's plane polarised white light, the distribution of strains in the actual structure is revealed by black and coloured fringe patterns. Unless otherwise specified, it is to be understood that the polarised light path is normal to the surface of the plastic. This type of illumination is called normal incidence.

The black fringes, or isoclinics, are the loci of points along which the principal strains have parallel directions. These directions are established by recording the angular position of a reference axis on the polariscope. The reflective-type polariscope is so designed that the directions of principal strains of any isoclinic are always paralell to the reference axis. Thus by rotation of the reference axis of the polariscope (from 0° to 90°), it is possible to detect an isoclinic at any point on the surface of the subject under investigation. The isoclinics, thus determined make it possible to define the direction of principal strains over the entire structure. From these isoclinic fringes the two families of isostatics (stress trajectories) can be plotted.

Inserting two additional optical components (quarter

wave plates) in the light path of the reflection polariscope, the isoclinics can be suppressed such that only coloured fringes remain visible in the photostress plastic.

The coloured fringes, or the isochromatics, observed with polarized light falling on the plastic coating under normal incidence, are the loci of points where the principal strain difference $(\varepsilon_1 - \varepsilon_2)$ is constant.

Areas showing black fringes with quarter wave plates in the field of observation, indicate areas where the principal strain difference is zero, whereas, an area of uniform colour denotes an area of uniform shear strain. Colour gradients correspond to shear strain gradients and colour concentrations correspond to shear strain concentrations. Since the birefringence is directly proportional to $(\varepsilon_1 - \varepsilon_2)$, it is possible to determine the quantitative values of $(\varepsilon_1 - \varepsilon_2)$ by measuring the degree of birefringence present in the photoelastic plastic.

The measurement of the strain difference is accomplished by optical compensation (which implies addition or subtraction of birefringence). A reflective polariscope is used to accomplish optical compensation. By shifting one of instrument's components, the isoclinics are eliminated from the field and a precise amount of birefringence can be subtracted from the unknown birefringence in the photostress plastic. When compensation is achieved at a given point or area of the photostress plastic, the plastic appears black. The amount of subtracted birefringence is indicated in the polariscope

and is proportional to $(\varepsilon_1 - \varepsilon_2)$ present in the structure. The coefficient of proportionality is either given by the manufacturer of the plastic or can be obtained by calibration. The accuracy of results can be considerably increased when the birefringence in the photostress plastic is brought by compensation to a reference colour (other than black), generally purple red, which is called the "tint of passage". This sensitive tint of passage corresponds to a very precisely defined and known birefringence value. The birefringence in the coating is then obtained as follows:

$$\delta_n = \text{(birefringence in coating)}$$

$$= \begin{pmatrix}\text{(Always-known birefringence}\\ \text{corresponding to the tint}\\ \text{of passage)}\end{pmatrix} - \begin{pmatrix}\text{Artificial birefring-}\\ \text{ence introduced by}\\ \text{photostress meter)}\end{pmatrix}$$

The birefringence (δ_n) measured under normal incidence and the principal strains in the plastic are related by the following formula:

$$(\varepsilon_1 - \varepsilon_2) = \frac{\delta n}{2tK} \qquad [29]$$

where

t: thickness of the coating and

K: the strain optical constant of the photoelastic plastic.

Using the relationship of the theory of elasticity, the difference of the principal stresses in the structure is given by:

$$(\sigma_1 - \sigma_2) = (\varepsilon_1 - \varepsilon_2) \frac{E}{1 + \mu} \quad \text{where}$$

E: Modulus of elasticity of the structure.

μ: Poisson's ratio of the structure.

σ_1: Major principal stress and

σ_2: Minor principal stress

Also τ_{max} (maximum shear stress) in the structure is given by $\frac{1}{2}(\sigma_1 - \sigma_2)$.

The value of $(\sigma_1 - \sigma_2)$ and the directions of σ_1 and σ_2 being known, it is possible to determine the individual values of principal stresses σ_1 and σ_2. Along any free boundary, where most failures occur, the stress normal to the boundary is zero; therefore, the tangential stress is given directly by the instrument reading. However, in a general case of experimental stress analysis where individual principal stresses should be determined only empirically, a photoelastic analysis made with oblique incidence will provide σ_1 and σ_2 in magnitude and sign. The procedure for recording oblique incidence readings is identical to the one used for normal incidence readings.

Another important factor to record is the thickness of the plastic because the birefringence in it is a function of its thickness, as well as of strain in it. However, the directions of the principal strain difference (isoclinic) are independent of the thickness of the plastic.

7.3 EXPERIMENTAL SET-UP AND FABRICATION OF SPECIMENS

In order to proceed with the analysis of adhesive bonded joints in sandwich material, 15 joint specimens were fabricated - all having the same type of tapered shear key as shown in Fig. 22. In order to transfer forces from the facings across the joint, aluminum cover plates were bonded to the facings by three different methods.

(a) Using Waldex W-105 Adhesive only....designated as Specimen As.

(b) Using nails only....designated as Specimen Bs.

(c) Using both adhesive and nails....designated as Specimen Cs.

A mathematical analysis has been developed for the bonded joints using adhesive only. A comparison of experimental and theoretical results is made in Chapter VIII.

All the joint specimens were subjected to the following loading conditions.

(i) Flexural Loading....Henceforth designated as loading condition 1. (Fig. 23)

(ii) Direct Shear Loading....Henceforth designated as loading condition 2. (Fig. 24)

(iii) Direct Compression....Henceforth designated as loading condition 3. (Fig. 25)

(iv) Direct Tension.....Henceforth designated as loading condition 4. (Fig. 26)

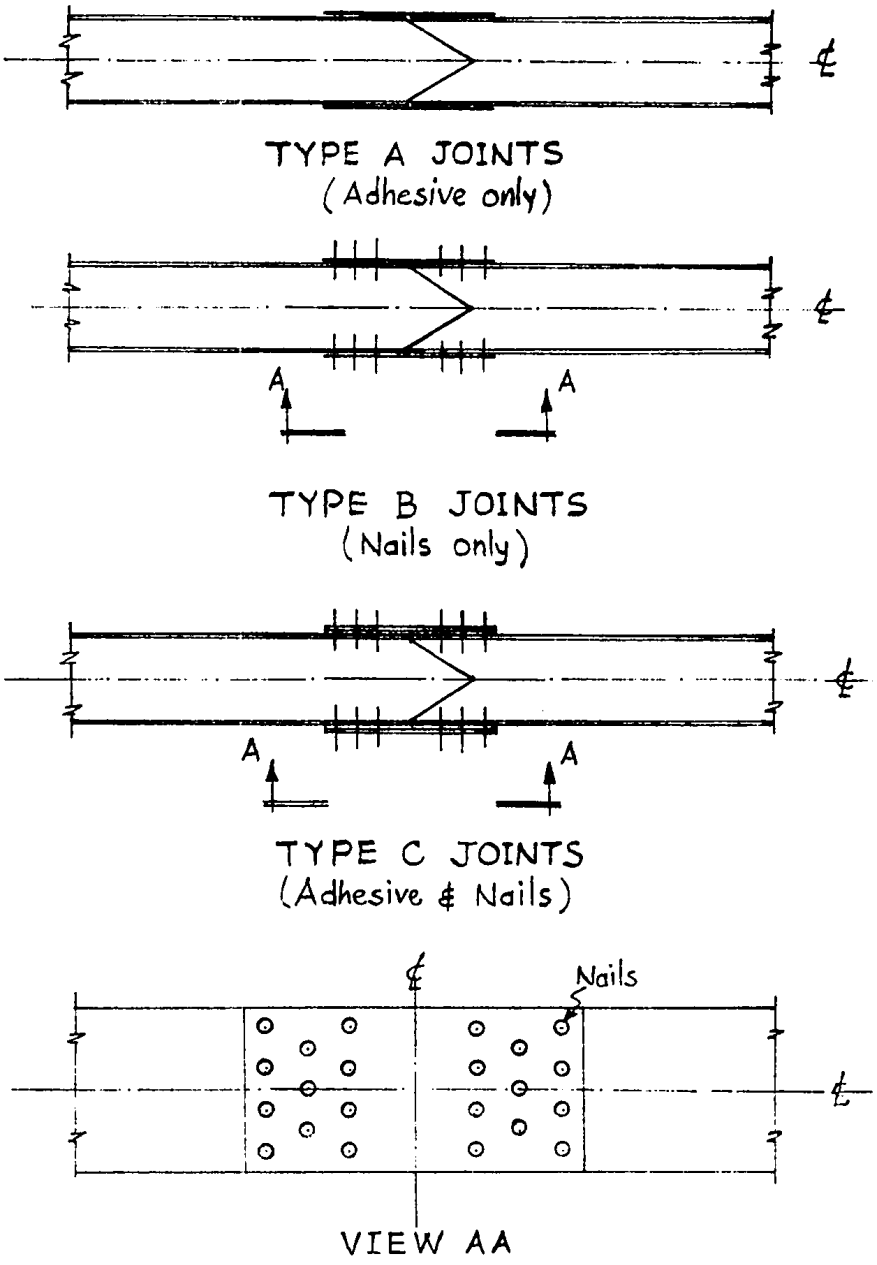

FIG. 22 THREE TYPES OF JOINTS TESTED

The above system of nomenclature has been adopted for easy identification of the various test specimens. For example: B3 is a specimen of the connections made with nails only and tested in direct compression (Fig. 25). C4 is a specimen of the connections made with both nails and adhesive and tested in direct tension (Fig. 26).

Load magnitudes were varied for each test in order to establish relationship between external loads and internal stresses.

Standard photoelastic method of analysis was used to analyse the joint specimens. Photostress plastic sheets were bonded to the cover plates using reflective adhesive and cured at room temperature. Photographs of isoclinics were taken for angle settings of 0°, 30°, 45°, 60° and 90° on the polariscope dial whereas, isochlormatics were shot for half and integral order fringes. This data was used to determine σ(the normal stress) and τ(the shear stress) in the adhesive using Shear Difference Method, as described in the following pages.

7.4 EXPERIMENTAL DETERMINATION OF SHEAR STRESS (τ) AND NORMAL STRESS (σ) IN THE ADHESIVE LAYER

As mentioned in the beginning of this Chapter, it is possible to determine the difference of principal stresses $(\sigma_1 - \sigma_2)$ from the isochromatic patterns and that the maximum shear stress could also be determined provided the two principal stresses are of opposite sign. Also, at free

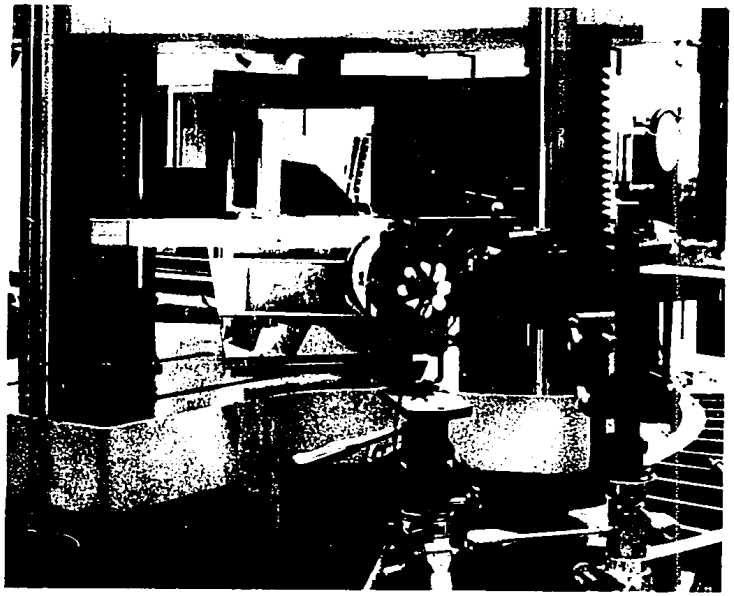

FIG. 23 A GENERAL VIEW OF THE EXPERIMENTAL SET-UP, TINUS OLSON TESTING MACHINE WITH FOUR-POINT LOADING SYSTEM FOR FLEXURAL TESTING OF SPECIMENS.

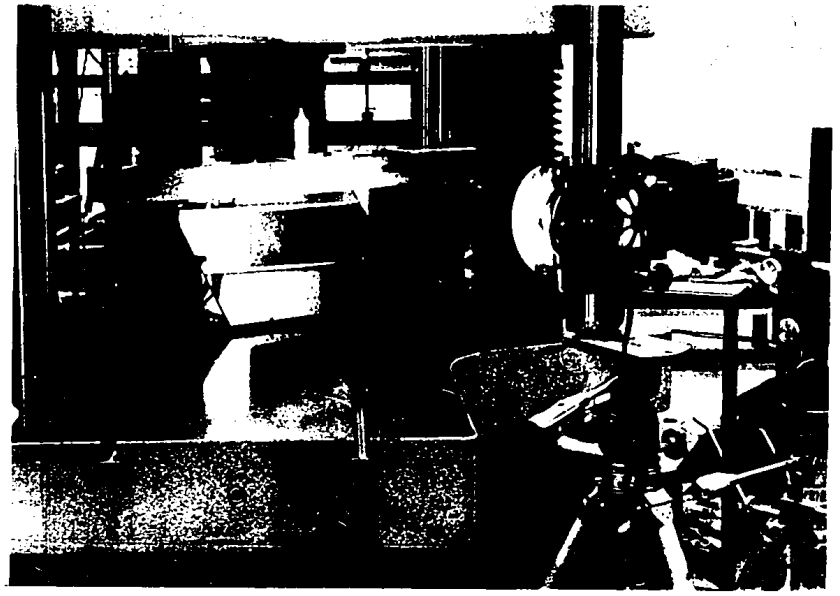

FIG. 24 A VIEW OF THE THREE-POINT LOADING SYSTEM FOR SHEAR TESTING OF THE SPECIMENS.

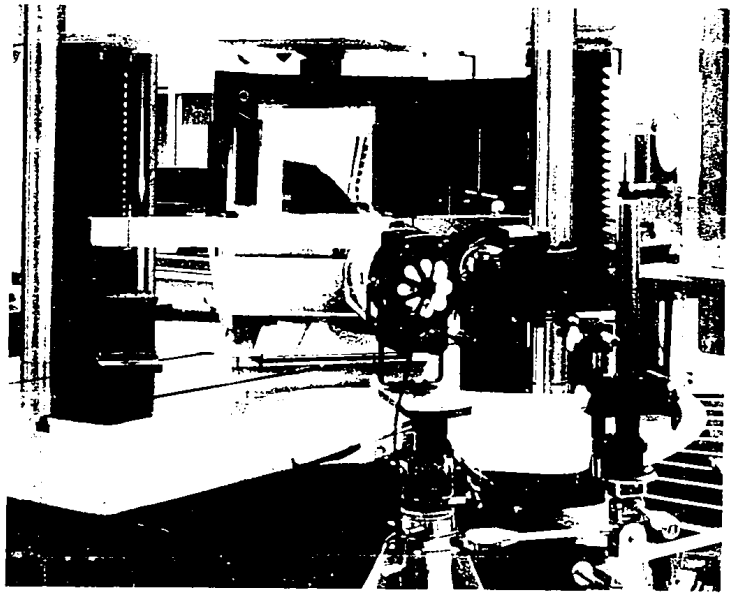

FIG. 23 A GENERAL VIEW OF THE EXPERIMENTAL SET-UP, TINUS OLSON TESTING MACHINE WITH FOUR-POINT LOADING SYSTEM FOR FLEXURAL TESTING OF SPECIMENS.

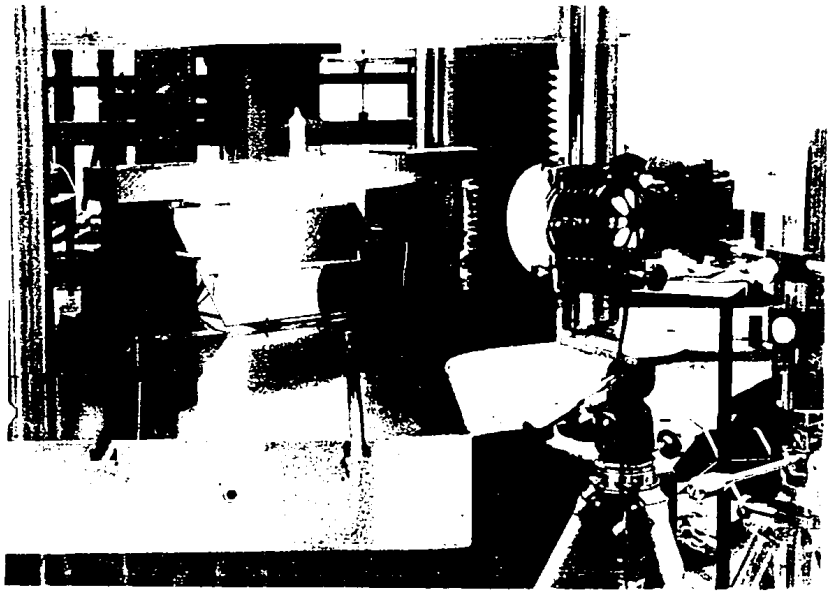

FIG. 24 A VIEW OF THE THREE-POINT LOADING SYSTEM FOR SHEAR TESTING OF THE SPECIMENS.

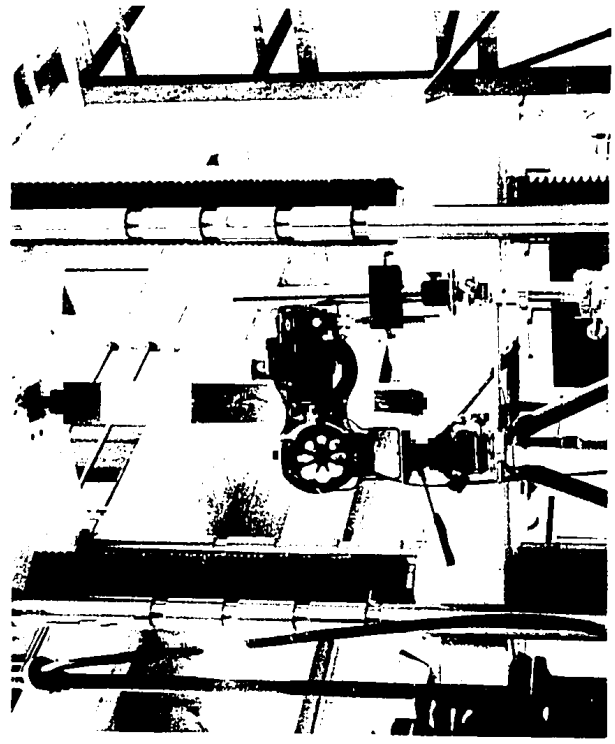

FIG. 26 A VIEW OF THE LOADING SYSTEM FOR DIRECT TENSION TEST OF THE SPECIMENS.

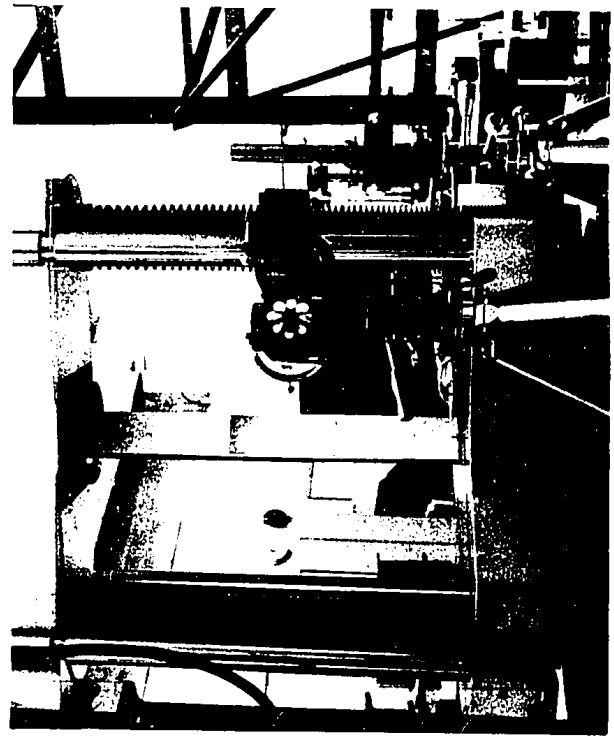

FIG. 25 A VIEW OF THE LOADING SYSTEM FOR DIRECT COMPRESSION TEST OF THE SPECIMENS.

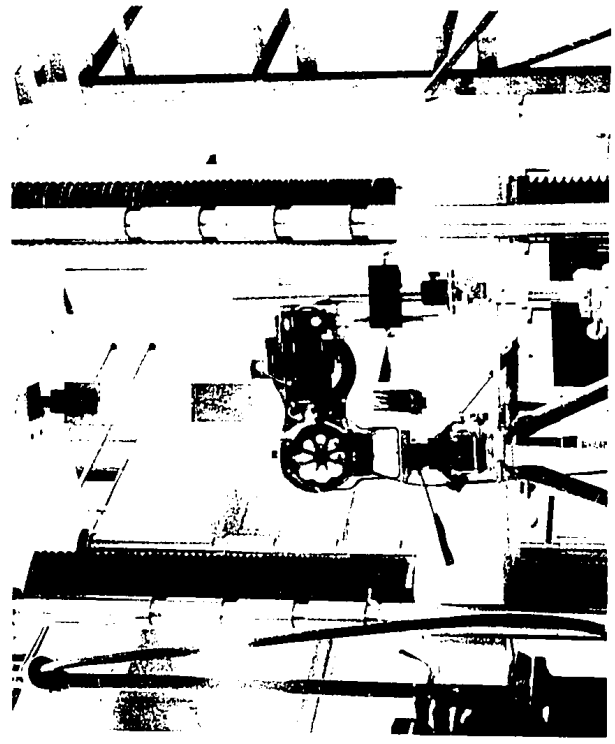

FIG. 26 A VIEW OF THE LOADING SYSTEM FOR DIRECT TENSION TEST OF THE SPECIMENS.

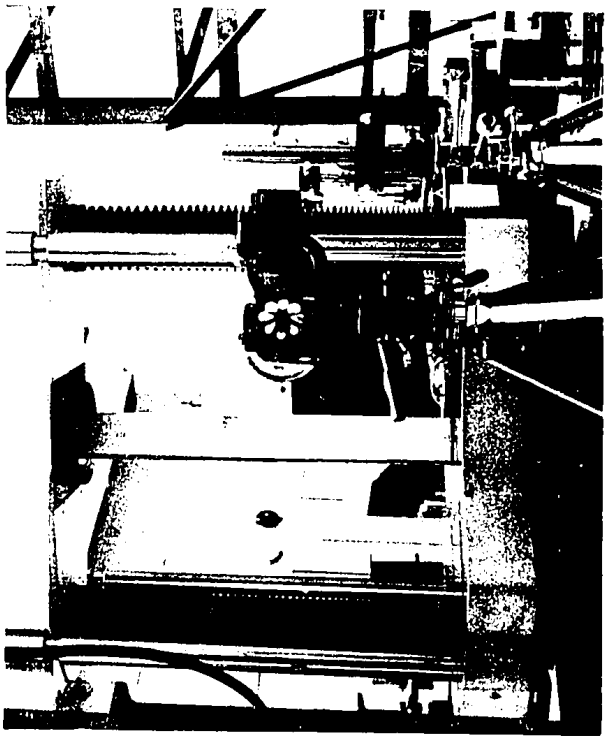

FIG. 25 A VIEW OF THE LOADING SYSTEM FOR DIRECT COMPRESSION TEST OF THE SPECIMENS.

boundaries, the principal stress normal to the boundary is zero, and the isochromatic data yield directly the value of the other principal stress. However, it is frequently necessary or desirable to obtain the individual values of the principal stresses throughout the interior regions of the plastic specimen. This separation of the principal stresses requires the usage of supplementary data or the employment of numerical methods. A very commonly used method is the shear-difference method.

7.4.1 The Shear Difference Method

It is a convenient method that may be used to determine the principal stresses at interior points in the model which is based upon the equations of equilibrium. These equations, when applied to the plane-stress problem in the absence of body forces, reduce to

$$\left.\begin{aligned} \frac{\partial \sigma_{xx}}{\partial x} + \frac{\partial \tau_{xy}}{\partial y} &= 0 \\ \frac{\partial \tau_{xy}}{\partial x} + \frac{\partial \sigma_{yy}}{\partial y} &= 0 \end{aligned}\right] \qquad (1)$$

The first of Eqs. (1) can be integrated along x as

$$\int_{x_o}^{x_1} \frac{\partial \sigma_{xx}}{\partial x}\, \partial x = -\int_{x_o}^{x_1} \frac{\partial \tau_{xy}}{\partial y}\, \partial x$$

This equation can be evaluated numerically by employing finite-difference methods, where the partial differentials are replaced by differences, as shown below:

$$\int_{x_o}^{x_1} \frac{\partial \sigma xx}{\partial x}\, \partial x = \sigma xx]_{x_1} - \sigma xx]_{x_o} = -\frac{\Delta \tau xy}{\Delta y}]_{\left(\frac{x_o+x_1}{2}\right)} \Delta x \qquad (2)$$

where x_o, x_1, etc., represent positions along x. Δ_x and Δ_y represent finite intervals along x or y, as defined in Fig. 28. If, in particular, Δ_x is selected equal to Δ_y, Eq. (2) reduces to

$$\sigma xx]_{x_1} = \sigma xx]_{x_o} - \Delta \tau xy]_{\left(\frac{x_o+x_1}{2}\right)} \qquad (3a)$$

The value of $\sigma xx]_{x_o}$ can be obtained directly from isochromatic data since the point x_o is on a free boundary. The value of $\Delta \tau xy$ can be computed from isochromatic and isoclinic data. Hence, it is possible to determine σ_{xx} at the interior point x_1. If the procedure is continued stepwise, the value of σ_{xx} can be determined across the entire length of the line segment OP. (Fig. 28).

$$\begin{aligned} \sigma xx]_{x_2} &= \sigma xx]_{x_1} - \Delta \tau xy]_{\left(\frac{x_1+x_2}{2}\right)} \\ \sigma xx]_{x_3} &= \sigma xx]_{x_2} - \Delta \tau xy]_{\left(\frac{x_2+x_3}{2}\right)} \\ \sigma xx]_{x_4} &= \sigma xx]_{x_3} - \Delta \tau xy]_{\left(\frac{x_3+x_4}{2}\right)} \end{aligned} \qquad (3b)$$

where τxy is given by the equation

$$\tau xy = -\tfrac{1}{2}[\sigma_1 - \sigma_2]\sin 2\theta = -\frac{Nf_\sigma}{2h} \sin 2\theta \qquad (4)$$

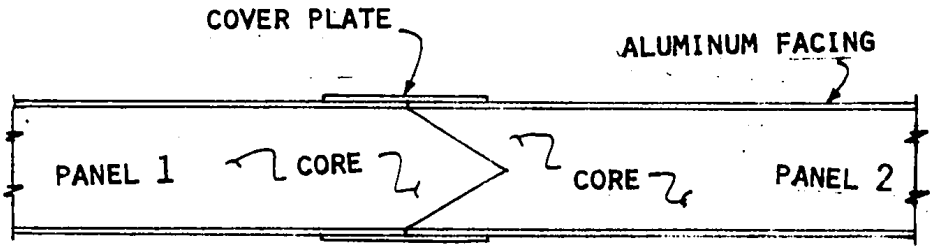

FIG. 27 ADHESIVE-BONDED TAPERED JOINT OF TWO SANDWICH PANELS

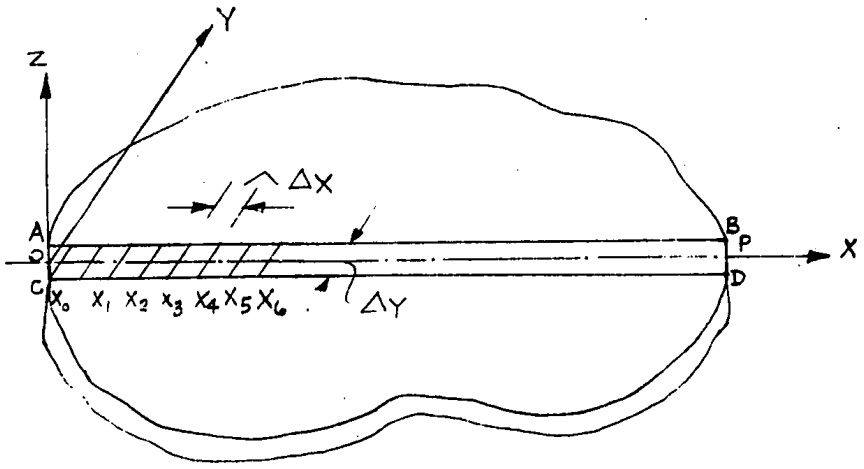

FIG. 28 GRID SYSTEM EMPLOYED IN THE APPLICATION OF THE SHEAR DIFFERENCE METHOD

where

N: Fringe order

f_σ: The material fringe value, psi-in.

h: Thickness of model, in.

The shear-difference method, which employs only isochromatic and isoclinic data, can be used to separate the stresses along any arbitrary line OP. (Fig. 28).

It should be noted that the normal stresses (σ) in the adhesive layer given by the experimental method are normal to the y z plane, whereas, the normal stresses given by the theories developed are normal to the x y plane.

When the two were compared, however, there was a strong agreement between them. As a result, comparisons between experimental normal stresses σ_x and theoretical normal stresses σ_y have been made in this work without distinction in subscript. The subscript y has been adopted.

The agreement between the two normal stresses in different plane may be explained as follows: only normal stresses (σ_y) may be induced in an element of adhesive. Since the Poisson's ratio of the adhesive used is approximately equal to 1, the strains in the x direction (ε_x) would be equal and opposite to ε_y. However, the strain ε_x is not allowed to occur due to the relatively high rigidity of the aluminum facings and the relative thinness of the adhesive layer, thus introducing normal stresses in the x

direction of the same magnitude as there are in the y direction.

7.5 TRANSFERENCE OF STRESSES FROM THE COVER PLATES TO THE ADHESIVE

The photoelastic test data obtained from the experiments shows the strains in the cover plate and not in the adhesive. In order to transfer stresses from the cover plate to the adhesive a linear stress distribution is assumed for the entire specimen, as shown in Fig. 39. The modulus of elasticity for aluminum and adhesive are respectively E_{Al} and E_{Ad}. Strains ε_2 and ε_1 are related by the equation

$$\left(\frac{\varepsilon_2}{\varepsilon_1}\right) = \left(\frac{c}{2} + f + \psi\right) / \left(\frac{c}{2} + 2f + \psi\right) \quad \text{or}$$

$$\varepsilon_2 = \varepsilon_1 \frac{\left(\frac{c}{2} + f + \psi\right)}{\left(\frac{c}{2} + 2f + \psi\right)} \quad \text{where}$$

ε_1 : Strain in the aluminum facing

ε_2 : Strain in the adhesive

$\frac{c}{2}$: Half the thickness of the core

f : Thickness of the facing

ψ : Thickness of adhesive

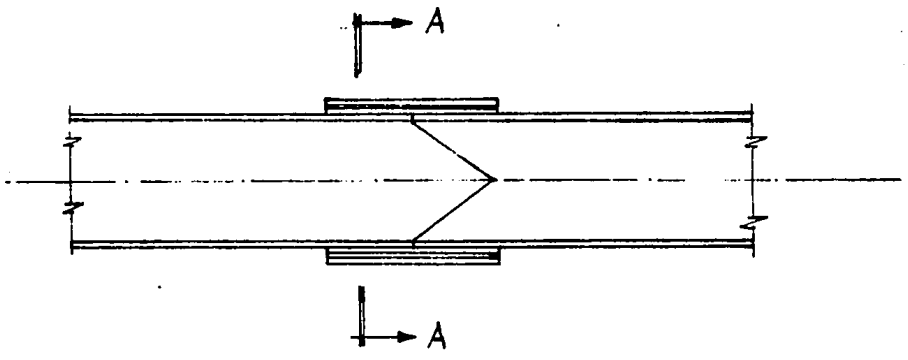

FIG. 29 A SANDWICH BEAM SHOWING COVER PLATE, ADHESIVE AND THE PHOTOELASTIC PLASTIC

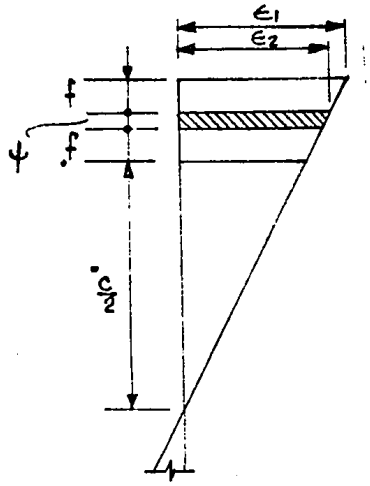

FIG. 30 STRAIN DIAGRAM ACROSS THE BEAM AT SECTION AA

Now defining $\frac{E_{A\ell}}{E_{Ad}} = n;$

$$\text{stress}_{Ad} = \varepsilon_1 \left[\frac{(\frac{c}{2} + f + \psi)}{(\frac{c}{2} + 2f + \psi)}\right] \frac{E_{A\ell}}{n}$$

7.6 A BRIEF DESCRIPTION OF THE ADHESIVE USED

The adhesive used in bonding aluminum cover plates to the facings of the beam-specimens used in the experimental part of this investigation is Waldex W-105. This is a two-component, expoxy resin/hardener system, formulated to provide reliable adhesive bonds to a large variety of materials. The most useful feature of this particular formulation is the flexibility range of the cured adhesive which can be controlled by varying the proportion of hardener. If a very flexible bond is required, e.g., soft rubber to soft rubber, 200 parts of W-105 hardener to 100 parts of W-105 resin should be used. Conversely, if a more rigid bond is desired, as in this case for bonding metals, 50 parts of W-105 Hardener to 100 parts of W-105 resin are used.

After the addition of hardener, W-105 cures at room temperature without the application of heat or pressure, although heating may be used to accelerate the curing process. The fully cured adhesive exhibits good mechanical strength, good insulating properties, resistance to moisture and it will not corrode any surface to which it is applied.

At room temperature, W-105 becomes sufficiently

hard after 8 to 12 hours for bonded parts to be handled, clamps removed, etc. To achieve optimum properties, however, the minimum curing time at 72^{o}F. is 3 days.

7.7 PRESENTATION OF THE EXPERIMENTAL VALUES OF τ AND σ IN THE ADHESIVE LAYER : SPECIMEN A_1: FLEXURAL TESTING

Making use of the theory outlined under "The Shear Difference Method" and "Transference of Stresses from the Cover Plate to the Adhesive", the shear stress (τ) and the normal stress (σ) in the adhesive layer of the bonded joint were calculated for three different values of applied loads on the specimen, vis. 500 lbs., 750 lbs., and 1,000 lbs. (Table 1) The photoelastic test data is presented in Tables 2 to 7, along with the calculated values of τ and σ.

In Figs. 31 and 33 are plotted the variations of τ (the shear stress) for the compression and tension sides of the specimens, respectively, whereas Figs. 32 and 34 show the plot of σ (the normal stress) for the same.

TABLE 1

SUMMARY OF EXPERIMENTAL TEST DATA (TESTS ON PANEL CONNECTIONS)

Specimen Designation	Type of Test	Side of Specimen	Load Applied (P) lbs.	Page on Which Results Appear	Experimental Set-Up
A_1	Flexural	Compression	500, 750, 1,000	136-138; 139-140	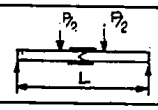
		Tension	500, 750, 1,000	141-143; 144-145	
A_2	Shear	Compression	1,250	147; 148-149	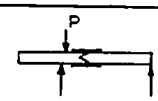
		Tension	1,250	150; 151-152	
A_3	Compression	One	2,500	153; 154-155	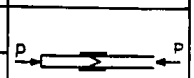
		Two	2,500	156; 157-158	
A_4	Tension	One	1,500	159; 160-161	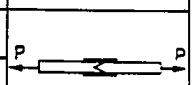
		Two	1,500	159; 160-161	
B_1	Flexural	Compression	2,000	165	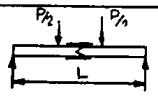
		Tension	1,000	166	
B_2	Shear	Compression	700	167	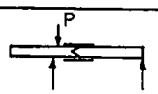
		Tension	700	168	
B_3	Compression	One	2,500	169	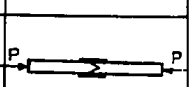
		Two	2,500	170	
B_4	Tension	One	The specimen broke, test could not be completed	-	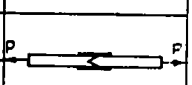
		Two		-	
C_1	Flexural	Compression	1,000	170	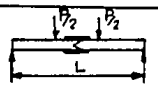
		Tension	1,750	171	
C_2	Shear	Compression	2,700	172	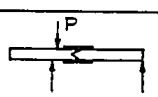
		Tension	2,700	173	
C_3	Compression	One	7,500	174	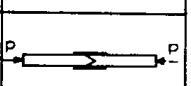
		Two	7,500	175	
C_4	Tension	One	1,750	176	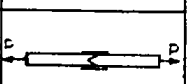
		Two	2,250	177	

TABLE 2

EXPERIMENTAL PHOTOELASTIC DATA AND THE CALCULATED VALUES OF SHEAR STRESS (τ) AND NORMAL STRESS (σ) IN ADHESIVE CORRESPONDING TO THE COMPRESSION SIDE OF SPECIMEN A_1 FOR 500 LBS. OF LOAD IN FLEXURAL TESTING. (FOR PLOT SEE FIGS. 31 AND 32).

Point*	Isochromatics (N)		Isoclinics (θ°)		τ psi	σ psi
	Line AB	Line CD	Line AB	Line CD		
-2.00	2.18	2.18	60	60	620.00	270.00
-1.9375	2.16	2.16	59	59	265.00	107.00
-1.90	2.13	2.13	58	58	150.67	0.0
-1.875	2.09	2.09	58	58	61.50	- 51.70
-1.8125	2.05	2.05	57	57	47.82	- 52.50
-1.75	2.00	2.00	57	57	33.75	- 26.60
-1.625	1.79	1.79	56	56	31.62	- 10.00
-1.50	1.85	1.85	55	55	28.37	- 9.67
-1.25	1.65	1.65	50	50	26.52	- 9.67
-1.00	1.35	1.35	48	48	16.10	- 9.67
-0.75	1.00	1.00	43	43	12.13	- 9.67
-0.50	0.75	0.75	40	40	10.27	- 9.67
-0.25	0.45	0.45	38	38	10.27	- 9.67
origin	0.15	0.15	35	35	10.27	- 9.67
0.25	0.45	0.45	38	38	10.27	- 9.67
0.50	0.75	0.75	40	40	10.27	- 9.67
0.75	1.00	1.00	43	43	12.13	- 9.67
1.00	1.35	1.35	48	48	16.10	- 9.67
1.25	1.65	1.65	50	50	26.52	- 9.67
1.50	1.85	1.85	55	55	28.37	- 9.67
1.625	1.79	1.79	56	56	31.62	-10.00
1.75	2.00	2.00	57	57	33.75	-26.60
1.8125	2.05	2.05	57	57	47.82	-52.50
1.875	2.09	2.09	58	58	61.50	-51.70
1.90	2.13	2.13	58	58	150.67	0.0
1.9375	2.16	2.16	59	59	265.00	107.00
2.00	2.18	2.18	60	60	620.00	270.00

* The points marked are shown on the abscissa starting from the left-hand side of Figs. 31 and 32.

TABLE 3

EXPERIMENTAL PHOTOELASTIC DATA AND THE CALCULATED VALUES OF SHEAR STRESS (τ) AND NORMAL STRESS (σ) IN ADHESIVE CORRESPONDING TO THE COMPRESSION SIDE OF SPECIMEN A_1 FOR 750 LBS. OF LOAD IN FLEXURAL TESTING (FOR PLOT SEE FIGS. 31 AND 32)

Point* (in)	Isochromatics (N)		Isoclinics (θ°)		τ psi	σ psi
	Line AB	Line CD	Line AB	Line CD		
-2.00	2.50	2.50	65	65	934.00	522.29
-1.9375	2.45	2.45	65	65	398.00	188.21
-1.90	2.40	2.40	65	65	145.67	0.0
-1.875	2.25	2.25	64	64	92.50	-104.29
-1.8125	2.10	2.10	64	64	68.29	-106.31
-1.75	2.00	2.00	63	63	51.00	- 55.11
-1.625	1.85	1.85	61	61	41.27	- 14.20
-1.50	1.75	1.75	60	60	31.23	- 14.20
-1.25	1.50	1.50	57	57	27.29	- 14.20
-1.00	1.25	1.25	53	53	19.61	- 14.20
-0.75	0.85	0.85	49	49	18.37	- 14.20
-0.50	0.35	0.35	45	45	15.27	- 14.20
-0.25	0.16	0.16	42	42	15.27	- 14.20
origin	0.10	0.10	40	40	15.27	- 12.67
0.25	0.16	0.16	42	42	15.27	- 14.20
0.50	0.35	0.35	45	45	15.27	- 14.20
0.75	0.85	0.85	49	49	18.37	- 14.20
1.00	1.25	1.25	53	53	19.61	- 14.20
1.25	1.50	1.50	57	57	27.29	- 14.20
1.50	1.75	1.75	60	60	31.23	- 14.20
1.625	1.85	1.85	61	61	41.27	- 14.20
1.75	2.00	2.00	63	63	51.00	- 55.11
1.8125	2.10	2.10	64	64	68.29	-106.31
1.875	2.25	2.25	64	64	92.50	-104.29
1.90	2.40	2.40	65	65	145.67	0.0
1.9375	2.45	2.45	65	65	398.00	188.21
2.00	2.50	2.50	65	65	934.00	522.29

* The points marked are shown on the abscissa starting from the left-hand side of Figs. 31 and 32.

TABLE 4

EXPERIMENTAL PHOTOELASTIC DATA AND THE CALCULATED VALUES OF SHEAR STRESS (τ) AND NORMAL STRESS (σ) IN ADHESIVE CORRESPONDING TO THE COMPRESSION SIDE OF SPECIMEN A_1 FOR 1,000 LBS. OF LOAD IN FLEXURAL TESTING (FOR PLOT SEE FIGS. 31 AND 32)

Point* (in)	Isochromatics (N)		Isoclinics (θ°)		τ psi	σ psi
	Line AB	Line CD	Line AB	Line CD		
-2.00	2.75	2.75	74	74	1250.00	870.00
-1.9375	2.75	2.75	74	74	534.00	384.00
-1.90	2.75	2.75	73	73	327.67	0.0
-1.875	2.67	2.67	72	72	123.50	-134.50
-1.8125	2.66	2.66	71	71	98.25	-163.00
-1.75	2.65	2.65	70	70	67.80	- 79.80
-1.625	2.55	2.55	67	67	65.27	- 17.91
-1.50	2.40	2.40	65	65	45.62	- 17.91
-1.25	2.15	2.15	63	63	39.43	- 17.91
-1.00	1.85	1.85	60	60	30.21	- 17.91
-0.75	1.65	1.65	57	57	25.67	- 17.91
-0.50	0.75	0.75	50	50	19.67	- 17.91
-0.25	0.45	0.45	48	48	19.67	- 17.91
origin	0.21	0.21	44	44	19.67	- 15.65
0.25	0.45	0.45	48	48	19.67	- 17.91
0.50	0.75	0.75	50	50	19.67	- 17.91
0.75	1.65	1.65	57	57	25.67	-17.91
1.00	1.85	1.85	60	60	30.21	-17.91
1.25	2.15	2.15	63	63	39.43	-17.91
1.50	2.40	2.40	65	65	45.62	-17.91
1.625	2.55	2.55	67	67	65.27	-17.91
1.75	2.65	2.65	70	70	67.80	-79.80
1.8125	2.66	2.66	71	71	98.25	-163.00
1.875	2.67	2.67	72	72	123.50	-134.50
1.90	2.75	2.75	73	73	327.67	0.0
1.9375	2.75	2.75	74	74	534.00	384.0
2.00	2.75	2.75	74	74	1250.00	870.0

* The points marked as shown on the abscissa starting from the left-hand side of Figs. 31 and 32.

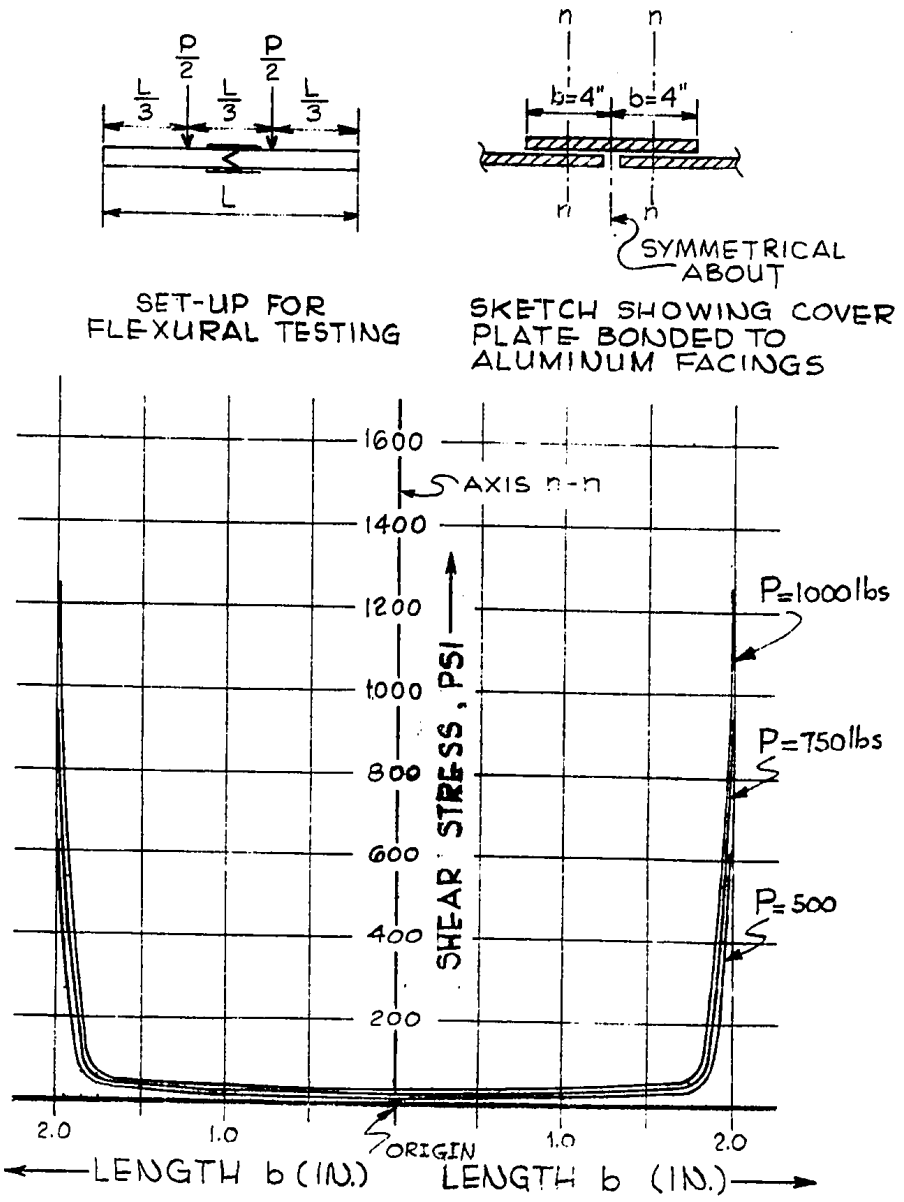

FIG. 31 EXPERIMENTAL DISTRIBUTION OF SHEAR STRESS IN ADHESIVE ON THE COMPRESSION SIDE OF SPECIMEN A, FOR 500, 750 AND 1,000 LBS. OF LOADS IN FLEXURAL TESTING. (TABLES 2, 3 and 4)

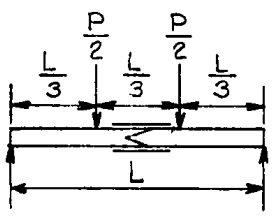

SET-UP FOR FLEXURAL TESTING

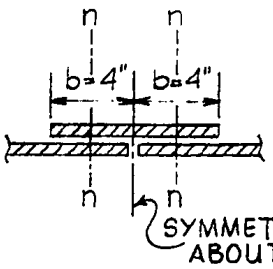

SKETCH SHOWING COVER PLATE BONDED TO ALUMINUM FACINGS

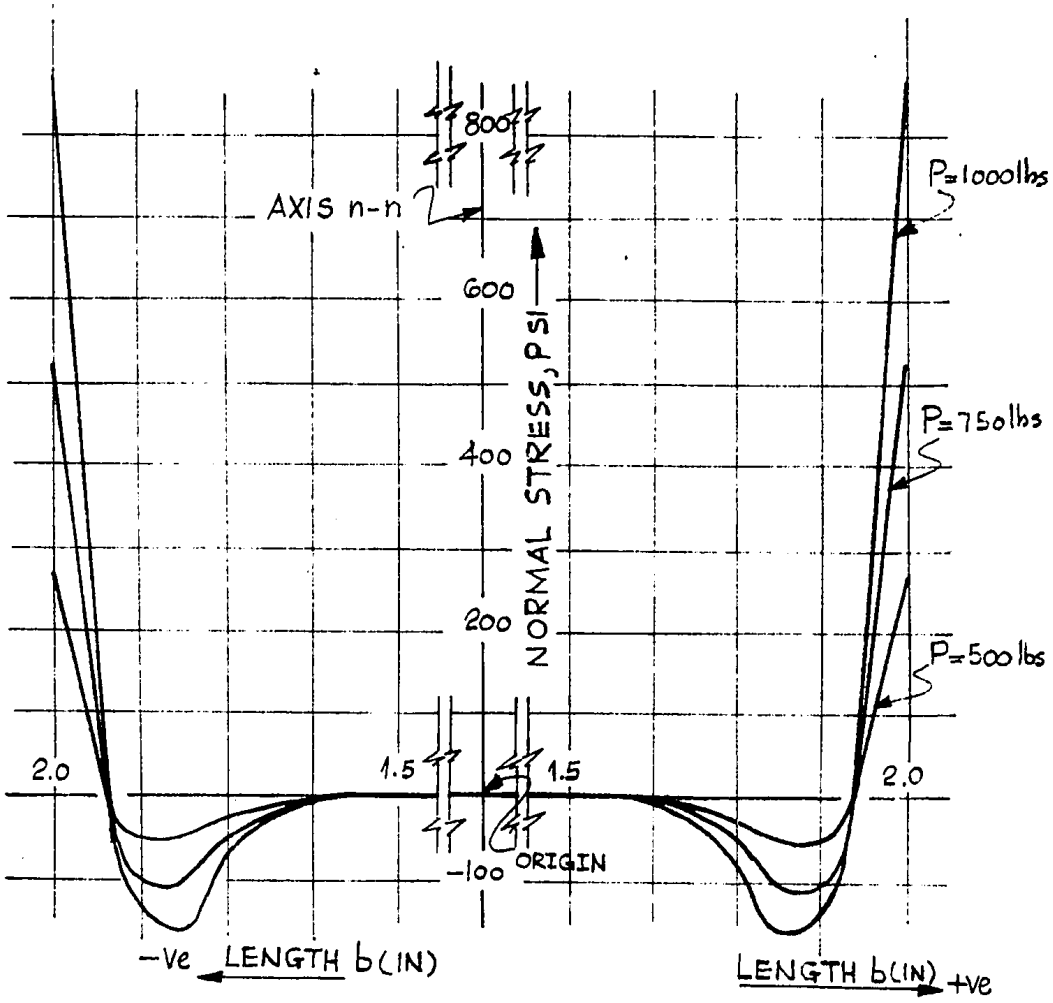

FIG. 32 EXPERIMENTAL DISTRIBUTION OF NORMAL STRESS IN ADHESIVE ON THE COMPRESSION SIDE OF SPECIMEN A1- FOR 500, 750 AND 1,000 LBS. OF LOAD IN FLEXURAL TESTING (TABLES 2, 3 and 4)

TABLE 5

EXPERIMENTAL PHOTOELASTIC DATA AND THE CALCULATED VALUES OF SHEAR STRESS (τ) AND NORMAL STRESS (σ) IN ADHESIVE CORRESPONDING TO THE TENSION SIDE OF SPECIMEN A_1 FOR 500 LBS. OF LOAD IN FLEXURAL TESTING (FOR PLOT SEE FIGS. 33 AND 34)

Point* (in)	Isochromatics (N)		Isoclinics ($\theta°$)		τ psi	σ psi
	Line AB	Line CD	Line AB	Line CD		
-2.00	2.25	2.25	60	60	621.00	271.00
-1.9375	2.20	2.20	59	59	265.00	109.63
-1.90	2.15	2.15	58	58	119.23	0.00
-1.875	2.10	2.10	57	57	61.60	- 52.10
-1.8125	2.05	2.05	56	56	51.50	- 53.00
-1.75	2.00	2.00	56	56	34.00	- 27.20
-1.625	1.96	1.96	55	55	31.23	- 10.00
-1.50	1.95	1.95	55	55	29.61	- 10.00
-1.25	1.50	1.50	53	53	25.83	- 10.00
-1.00	1.25	1.25	49	49	21.27	- 10.00
-0.75	0.98	0.98	45	45	16.81	- 10.00
-0.50	0.75	0.75	40	40	10.87	- 10.00
-0.25	0.26	0.26	35	35	10.87	- 10.00
origin	0.15	0.15	30	30	10.87	- 10.00
0.25	0.26	0.26	35	35	10.87	- 10.00
0.50	0.75	0.75	40	40	10.87	- 10.00
0.75	0.98	0.98	45	45	16.81	-10.00
1.00	1.25	1.25	49	49	21.27	-10.00
1.25	1.50	1.50	53	53	25.83	-10.00
1.50	1.95	1.95	55	55	29.61	-10.00
1.625	1.96	1.96	55	55	31.23	-10.00
1.75	2.00	2.00	56	56	34.00	-27.20
1.8125	2.05	2.05	56	56	51.50	-53.00
1.875	2.10	2.10	57	57	61.60	-52.10
1.90	2.15	2.15	58	58	119.23	0.00
1.9375	2.20	2.20	59	59	265.00	109.63
2.00	2.25	2.25	60	60	621.00	271.00

* The points marked are shown on the abscissa starting from the left-hand side of Figs. 33 and 34.

TABLE 6

EXPERIMENTAL PHOTOELASTIC DATA AND THE CALCULATED VALUES OF SHEAR STRESS (τ) AND NORMAL STRESS (σ) IN ADHESIVE CORRESPONDING TO THE TENSION SIDE OF SPECIMEN A_1 FOR 750 LBS. OF LOAD IN FLEXURAL TESTING (FOR PLOT SEE FIGS.33 AND 34)

Point* (in)	Isochromatics (N)		Isoclinics (θ°)		τ psi	σ psi
	Line AB	Line CD	Line AB	Line CD		
-2.00	2.50	2.50	65	65	934.00	532.21
-1.9375	2.45	2.45	65	65	398.00	190.26
-1.90	2.35	2.35	63	63	211.75	0.0
-1.875	2.25	2.25	63	63	92.60	-105.26
-1.8125	2.20	2.20	62	62	67.83	-107.21
-1.75	2.15	2.15	62	62	51.20	- 55.40
-1.625	2.10	2.10	59	59	45.29	- 14.35
-1.50	2.00	2.00	58	58	35.47	- 14.35
-1.25	1.75	1.75	55	55	29.33	- 14.35
-1.00	1.50	1.50	50	50	25.73	- 14.35
-0.75	1.25	1.25	47	47	21.63	- 14.35
-0.50	1.00	1.00	45	45	14.97	- 13.97
-0.25	0.65	0.65	42	42	14.97	- 13.97
origin	0.20	0.20	40	40	14.97	- 13.97
0.25	0.65	0.65	42	42	14.97	- 13.97
0.50	1.00	1.00	45	45	14.97	- 13.97
0.75	1.25	1.25	47	47	21.63	-14.35
1.00	1.50	1.50	50	50	25.73	-14.35
1.25	1.75	1.75	55	55	29.33	-14.35
1.50	2.00	2.00	58	58	35.47	-14.35
1.625	2.10	2.10	59	59	45.29	-14.35
1.75	2.15	2.15	62	62	51.20	-55.40
1.8125	2.20	2.20	62	62	67.83	-107.21
1.875	2.25	2.25	63	63	92.60	-105.26
1.90	2.35	2.35	63	63	211.75	0.0
1.9375	2.45	2.45	65	65	398.00	190.26
2.00	2.50	2.50	65	65	934.00	532.21

* The points marked are shown on the abscissa starting from the left-hand side of Figs. 33 and 34.

TABLE 7

EXPERIMENTAL PHOTOELASTIC DATA AND THE CALCULATED VALUES OF SHEAR STRESS (τ) AND NORMAL STRESS (σ) IN ADHESIVE CORRESPONDING TO THE TENSION SIDE OF SPECIMEN A_1 FOR 1,000 LBS. OF LOAD IN FLEXURAL TESTING (FOR PLOT SEE FIGS. 33 AND 34)

Point* (in)	Isochromatics (N)		Isoclinics (θ°)		τ psi	σ psi
	Line AB	Line CD	Line AB	Line CD		
-2.00	2.75	2.75	75	75	1255.00	875.00
-1.9375	2.75	2.75	75	75	534.00	387.29
-1.90	2.70	2.70	73	73	329.67	0.00
-1.875	2.65	2.65	72	72	124.00	-135.11
-1.8125	2.60	2.60	72	72	110.23	-164.00
-1.75	2.56	2.56	72	72	67.80	- 80.50
-1.625	2.40	2.40	71	71	51.23	- 18.00
-1.50	2.13	2.13	70	70	47.67	- 18.00
-1.25	2.00	2.00	65	65	41.23	- 18.00
-1.00	1.50	1.50	57	57	37.25	- 18.00
-0.75	1.25	1.25	51	51	27.83	- 18.00
-0.50	0.95	0.95	49	49	18.87	- 18.00
-0.25	0.75	0.75	47	47	18.87	- 13.71
origin	0.21	0.21	46	46	18.87	- 13.71
0.25	0.75	0.75	47	47	18.87	- 13.71
0.50	0.95	0.95	49	49	18.87	- 18.00
0.75	1.25	1.25	51	51	27.83	- 18.00
1.00	1.50	1.50	57	57	37.25	- 18.00
1.25	2.00	2.00	65	65	41.23	- 18.00
1.50	2.13	2.13	70	70	47.67	- 18.00
1.625	2.40	2.40	71	71	51.23	- 18.00
1.75	2.56	2.56	72	72	67.80	- 80.60
1.8125	2.60	2.60	72	72	110.23	-164.00
1.875	2.65	2.65	72	72	124.00	-135.11
1.90	2.70	2.70	73	73	329.67	0.00
1.9375	2.75	2.75	75	75	534.00	387.29
2.00	2.75	2.75	75	75	1255.00	875.00

* The points marked are shown on the abscissa starting from the left-hand side of Figs. 33 and 34.

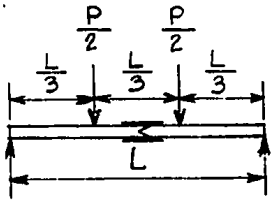

SET-UP FOR FLEXURAL TESTING

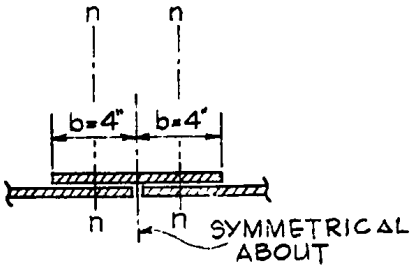

SKETCH SHOWING COVER PLATE BONDED TO ALUMINUM FACINGS

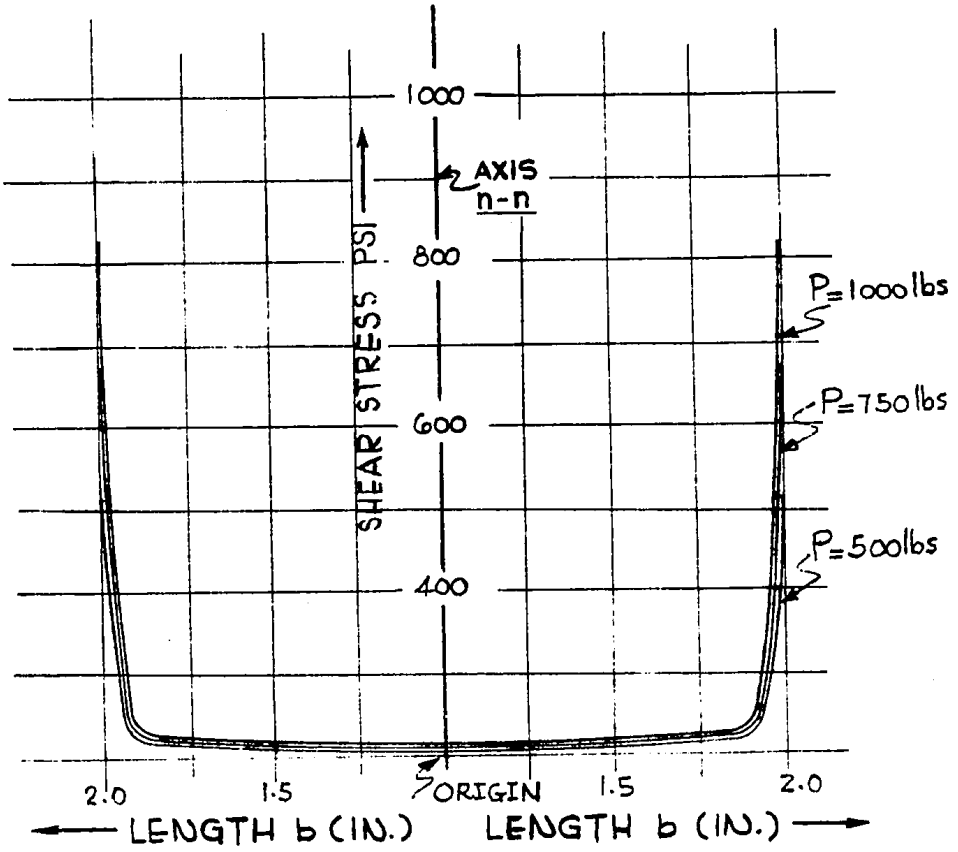

FIG. 33 EXPERIMENTAL DISTRIBUTION OF SHEAR STRESS IN ADHESIVE ON THE TENSION SIDE OF SPECIMEN A$_1$ FOR 500, 750 AND 1,000 LBS. OF LOAD IN FLEXURAL TESTING (TABLES 5, 6 and 7)

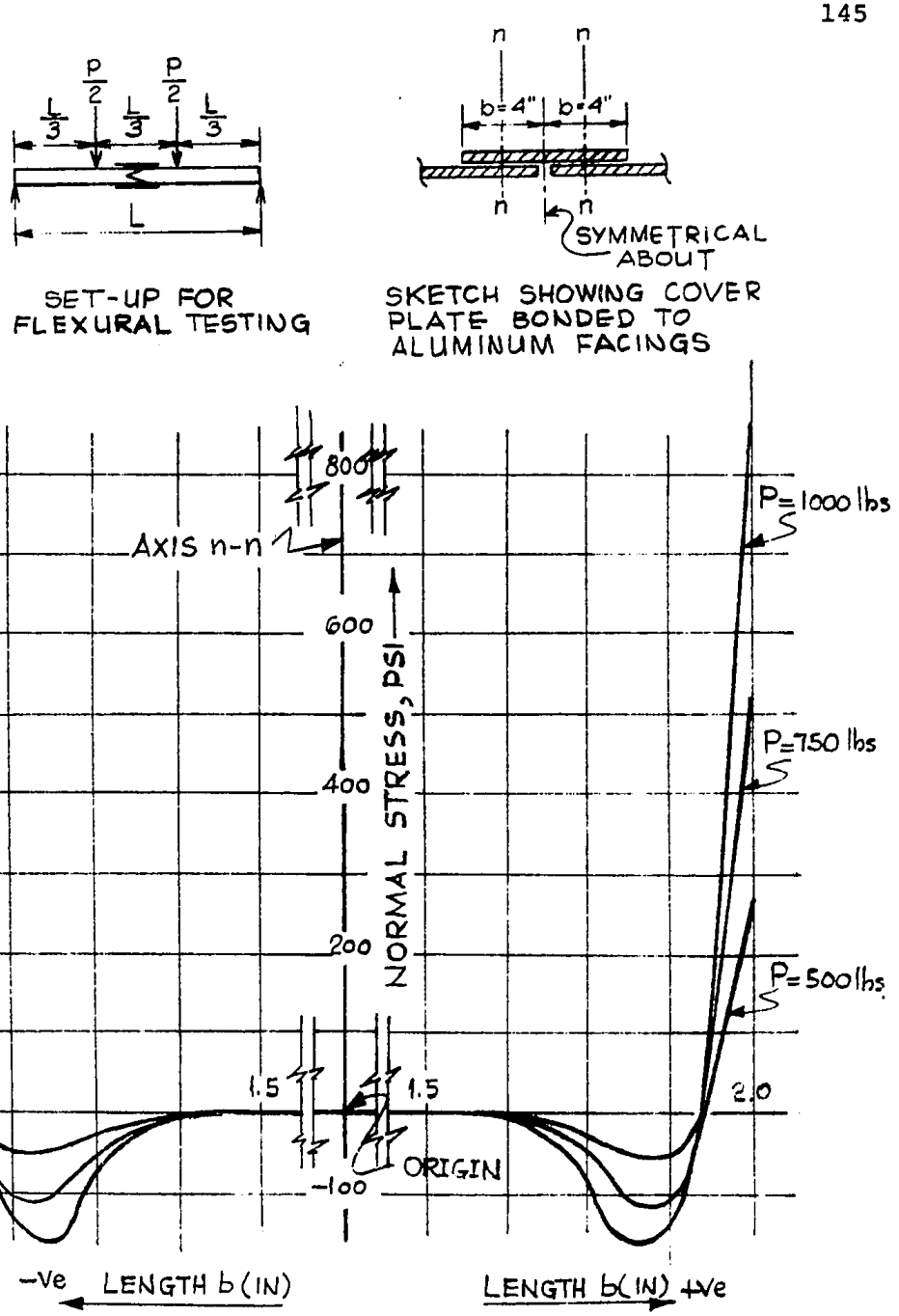

FIG. 34 EXPERIMENTAL DISTRIBUTION OF NORMAL STRESS IN ADHESIVE ON THE TENSION SIDE OF SPECIMEN A, FOR 500, 750 AND 1,000 LBS. OF LOAD IN FLEXURAL TESTING (TABLES 5, 6 and 7).

7.8 PRESENTATION OF EXPERIMENTAL VALUES OF τ AND σ IN THE ADHESIVE LAYER : SPECIMENS A_2, A_3 AND A_4 : FLEXURAL TESTING

Making use of the theory outlined under "The Shear Difference Method" and "Transference of Stresses from the Cover Plates to the Adhesive", the shear stress (τ) and the normal stress (σ) in the adhesive layer of the bonded joint were calculated for several different values of applied loads on the specimen (Table 1). The photoelastic test data is presented in Tables 8 to 12, along with the calculated values of τ and σ.

Here is a summary of the results presented:

Test Type	Specimen	Table of Photo-elastic Data	Figures
Shear	A_2	8,9	35,36 & 37,38
Compression	A_3	10,11	39,40 & 41,42
Tension	A_4	12	43 & 44

TABLE 8

EXPERIMENTAL PHOTOELASTIC DATA AND THE CALCULATED VALUES OF SHEAR STRESS (τ) AND NORMAL STRESS (σ) IN ADHESIVE CORRESPONDING TO THE COMPRESSION SIDE OF SPECIMEN A$_2$ FOR 1,250 LBS. OF LOAD IN SHEAR TESTING (FOR PLOT SEE FIGS. 35 AND 36)

Point* (in)	Isochromatics (N)		Isoclinics (θ°)		τ psi	σ psi
	Line AB	Line CD	Line AB	Line CD		
-2.00	1.50	1.50	75	75	321.25	275.39
-1.75	1.35	1.35	70	70	151.23	- 61.23
-1.50	1.15	1.15	65	65	62.21	- 37.61
-1.25	1.00	1.00	60	60	38.97	- 8.21
-1.00	0.85	0.85	55	55	25.11	- 8.21
-0.75	0.75	0.75	45	45	15.23	- 8.21
-0.50	0.50	0.50	35	35	15.23	- 8.21
-0.25	0.35	0.35	20	20	15.23	- 8.21
origin	0.25	0.25	15	15	15.23	- 8.21
0.25	0.35	0.35	20	20	15.23	- 8.21
0.50	0.50	0.50	35	35	15.23	- 8.21
0.75	0.75	0.75	45	45	15.23	- 8.21
1.00	0.85	0.85	55	55	25.11	- 8.21
1.25	1.00	1.00	60	60	38.97	- 8.21
1.50	1.15	1.15	65	65	62.21	- 37.61
1.75	1.35	1.35	70	70	151.23	- 61.23
2.00	1.50	1.50	75	75	321.25	275.39

* The points marked are shown on the abscissa starting from the left-hand side of Figs. 35 and 36.

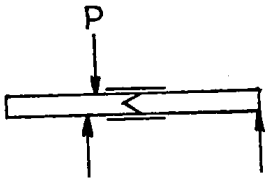

SET-UP FOR SHEAR TESTING

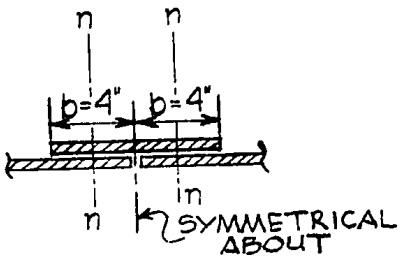

SKETCH SHOWING COVER PLATE BONDED TO ALUMINUM FACINGS

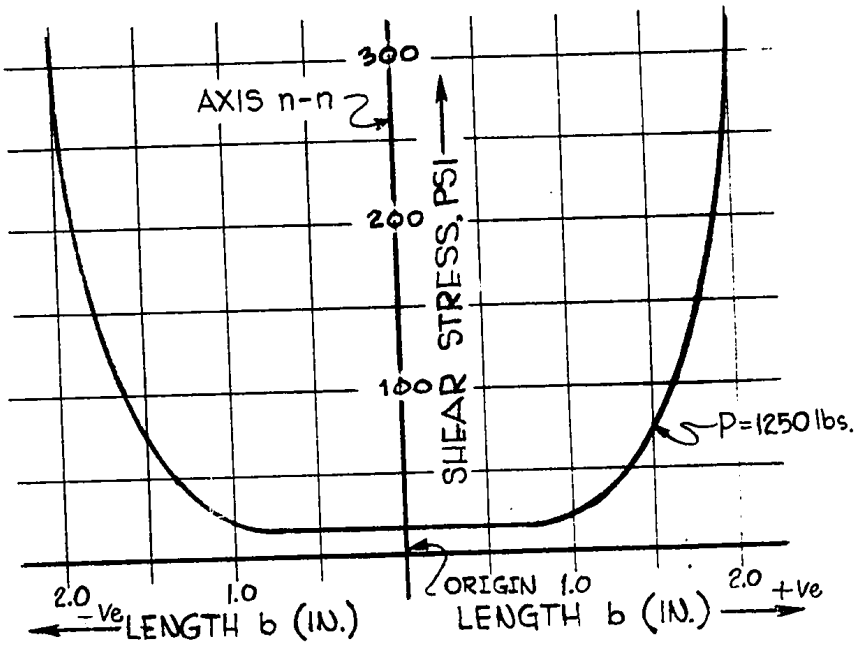

FIG. 35 EXPERIMENTAL DISTRIBUTION OF SHEAR STRESS IN ADHESIVE ON THE COMPRESSION SIDE OF SPECIMEN A_2 FOR 1,250 LBS. OF LOAD IN SHEAR TESTING. (TABLE 8)

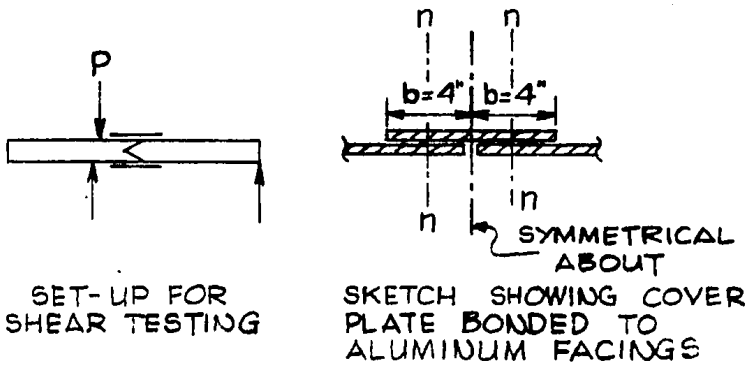

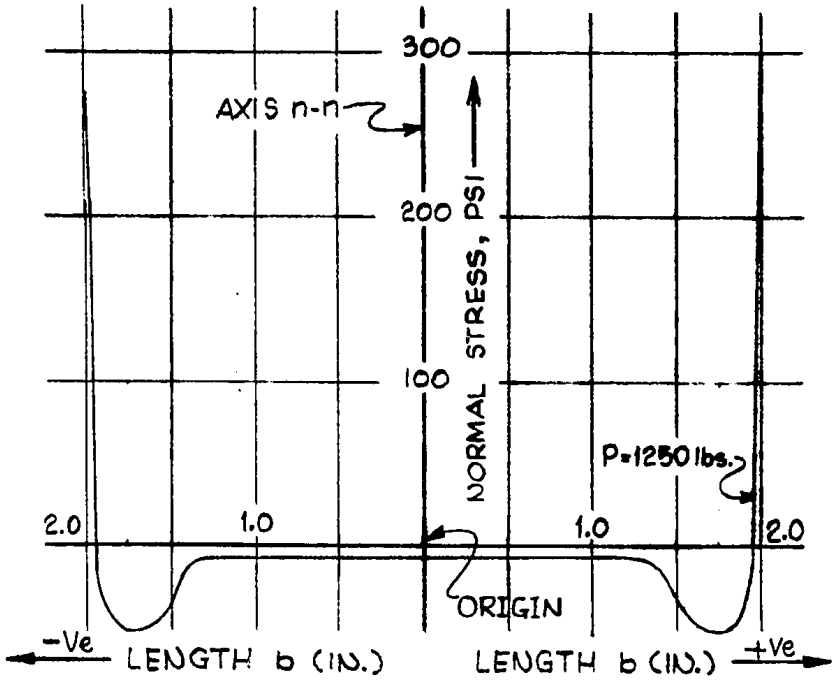

FIG. 36 EXPERIMENTAL DISTRIBUTION OF NORMAL STRESS IN ADHESIVE ON THE COMPRESSION SIDE OF SPECIMEN A_2 FOR 1,250 LBS. OF LOAD IN SHEAR TESTING (TABLE 8)

TABLE 9

EXPERIMENTAL PHOTOELASTIC DATA AND THE CALCULATED VALUES OF SHEAR STRESS (τ) AND NORMAL STRESS (σ) IN ADHESIVE CORRESPONDING TO THE TENSION SIDE OF SPECIMEN A_2 FOR 1,250 LBS. OF LOAD IN SHEAR TESTING (FOR PLOT SEE FIGS. 37 AND 38)

Point* (in)	Isochromatics (N)		Isoclinics (θ°)		τ psi	σ psi
	Line AB	Line CD	Line AB	Line CD		
-2.00	1.50	1.50	75	75	320.67	273.61
-1.75	1.35	1.35	70	70	150.11	- 60.23
-1.50	1.15	1.15	65	65	62.00	- 37.29
-1.25	1.00	1.00	60	60	37.81	- 8.11
-1.00	0.85	0.85	55	55	24.11	- 8.11
-0.75	0.75	0.75	45	45	15.61	- 8.11
-0.50	0.50	0.50	35	35	15.61	- 8.11
-0.25	0.35	0.35	20	20	15.61	- 8.11
origin	0.25	0.25	15	15	15.61	- 8.11
0.25	0.35	0.35	20	20	15.61	- 8.11
0.50	0.50	0.50	35	35	15.61	- 8.11
0.75	0.75	0.75	45	45	15.61	- 8.11
1.00	0.85	0.85	55	55	24.11	- 8.11
1.25	1.00	1.00	60	60	37.81	- 8.11
1.50	1.15	1.15	65	65	62.00	- 37.29
1.75	1.35	1.35	70	70	150.11	- 60.23
2.00	1.50	1.50	75	75	320.67	273.61

* The points marked are shown on the abscissa starting from the left-hand side of Figs. 37 and 38.

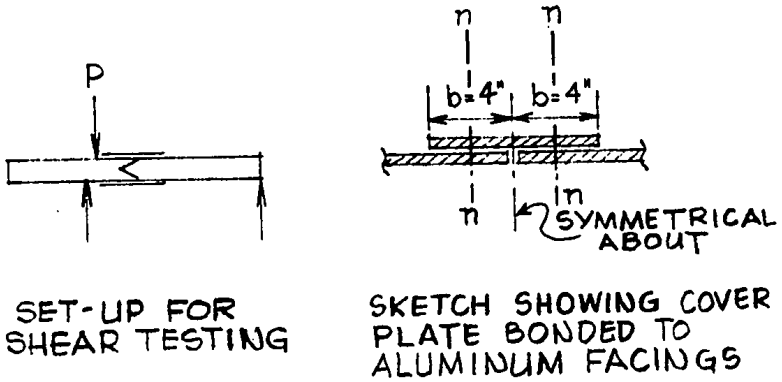

SET-UP FOR SHEAR TESTING

SKETCH SHOWING COVER PLATE BONDED TO ALUMINUM FACINGS

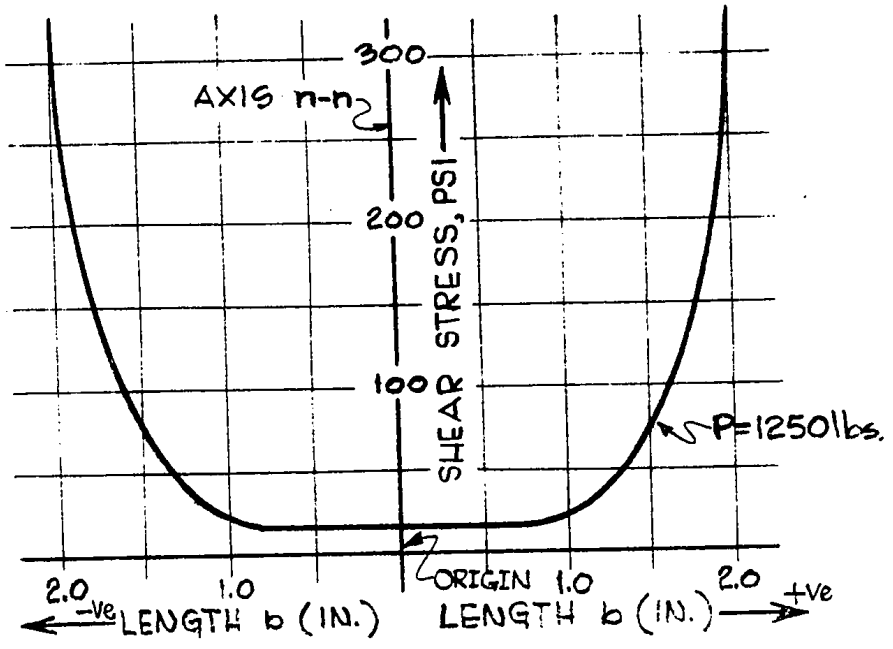

FIG. 37 EXPERIMENTAL DISTRIBUTION OF SHEAR STRESS IN ADHESIVE ON THE TENSION SIDE OF SPECIMEN A, FOR 1,250 LBS. OF LOAD IN SHEAR TESTING. (TABLE 9)

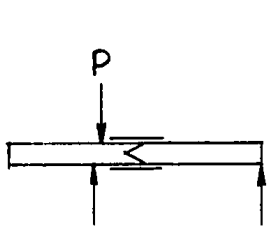

SET-UP FOR SHEAR TESTING

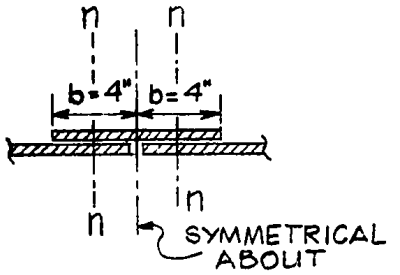

SKETCH SHOWING COVER PLATE BONDED TO ALUMINUM FACINGS

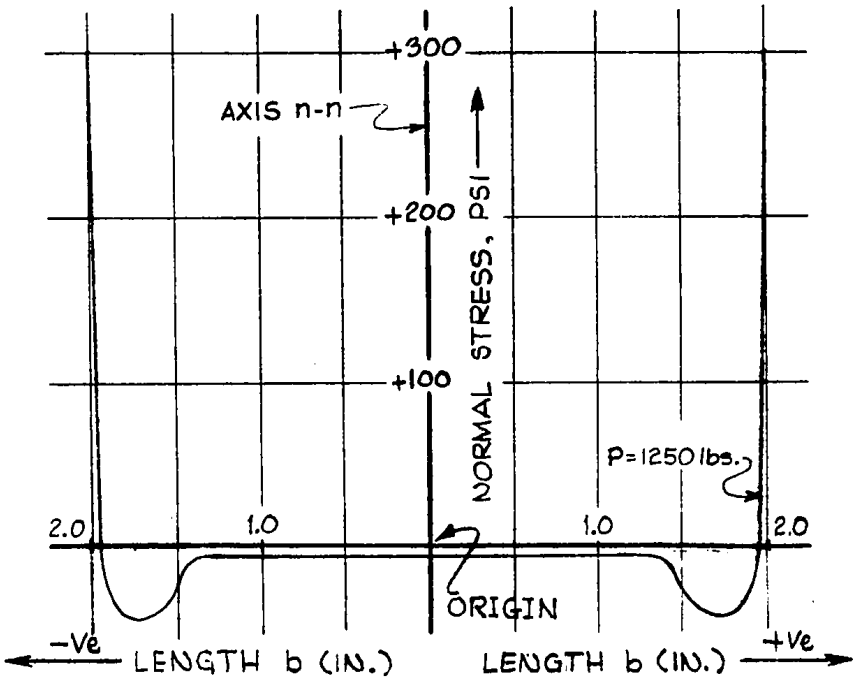

FIG. 38 EXPERIMENTAL DISTRIBUTION OF NORMAL STRESS IN ADHESIVE ON THE TENSION SIDE OF SPECIMEN A_2 FOR 1,250 LBS. OF LOAD IN SHEAR TESTING. (TABLE 9)

TABLE 10

EXPERIMENTAL PHOTOELASTIC DATA AND THE CALCULATED VALUES OF SHEAR STRESS (τ) AND NORMAL STRESS (σ) IN ADHESIVE CORRESPONDING TO SIDE ONE OF SPECIMEN A_3 FOR 2,500 LBS. OF LOAD IN COMPRESSION TESTING (FOR PLOT SEE FIGS. 39 AND 40*)

Point* (in)	Isochromatics (N)		Isoclinics (θ°)		τ psi	σ psi
	Line AB	Line CD	Line AB	Line CD		
-2.00	3.00	3.00	85	85	602.23	298.23
-1.75	2.65	2.65	75	75	250.61	- 45.71
-1.50	2.35	2.35	70	70	131.31	- 23.61
-1.25	1.85	1.85	60	60	80.11	- 9.37
-1.00	1.45	1.45	50	50	45.62	- 9.37
-0.75	1.00	1.00	40	40	29.11	- 9.37
-0.50	0.75	0.75	30	30	15.23	- 9.37
-0.25	0.50	0.50	25	25	15.23	- 9.37
origin	0.25	0.25	15	15	13.11	- 9.37
0.25	0.50	0.50	25	25	15.23	- 9.37
0.50	0.75	0.75	30	30	15.23	- 9.37
0.75	1.00	1.00	40	40	29.11	- 9.37
1.00	1.45	1.45	50	50	45.62	- 9.37
1.25	1.85	1.85	60	60	80.11	- 9.37
1.50	2.35	2.35	70	70	131.31	- 23.61
1.75	2.65	2.65	75	75	250.61	- 45.71
2.00	3.00	3.00	85	85	602.23	298.23

* The points marked are shown on the abscissa starting from the left-hand side of Figs. 39 and 40.

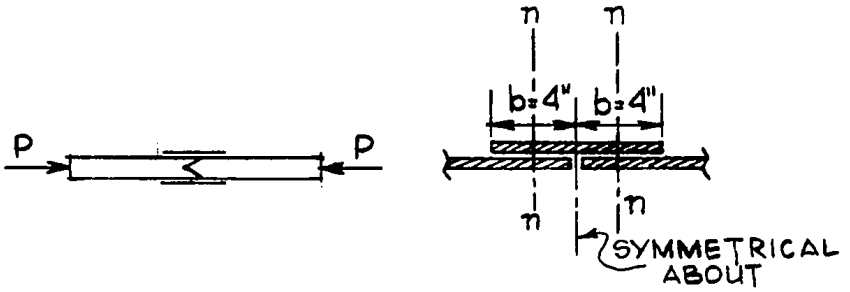

SET-UP FOR COMPRESSION TESTING

SKETCH SHOWING COVER PLATE BONDED TO ALUMINUM FACINGS

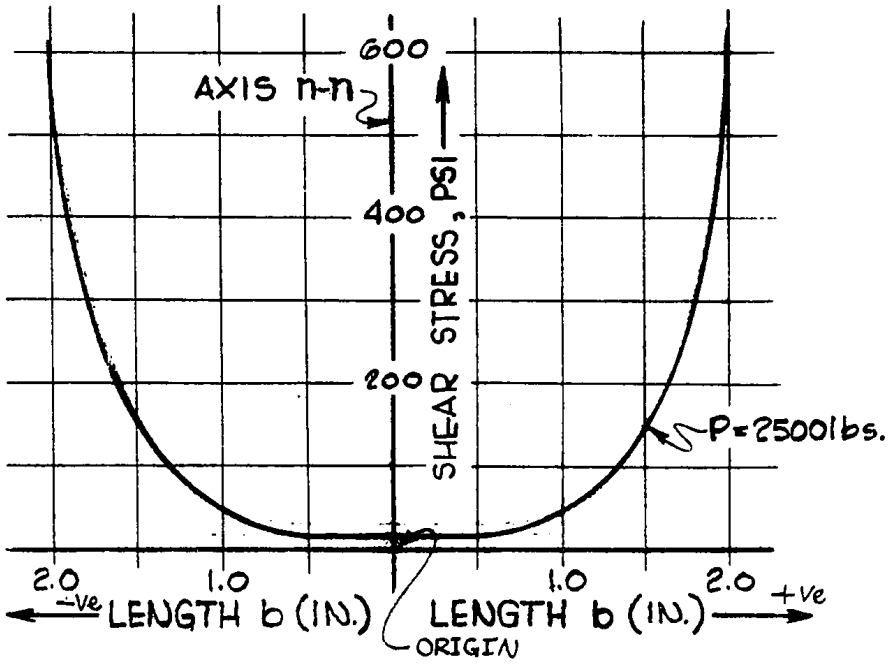

FIG. 39 EXPERIMENTAL DISTRIBUTION OF SHEAR STRESS IN ADHESIVE ON SIDE ONE OF THE SPECIMEN A$_3$ FOR 2,500 LBS. OF LOAD IN COMPRESSION TESTING (TABLE 10)

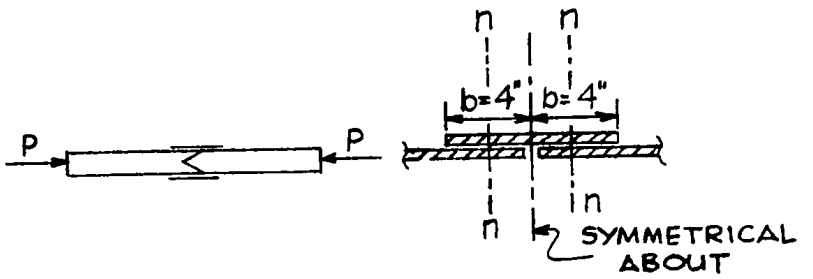

SET-UP FOR COMPRESSION TESTING

SKETCH SHOWING COVER PLATE BONDED TO ALUMINUM FACINGS

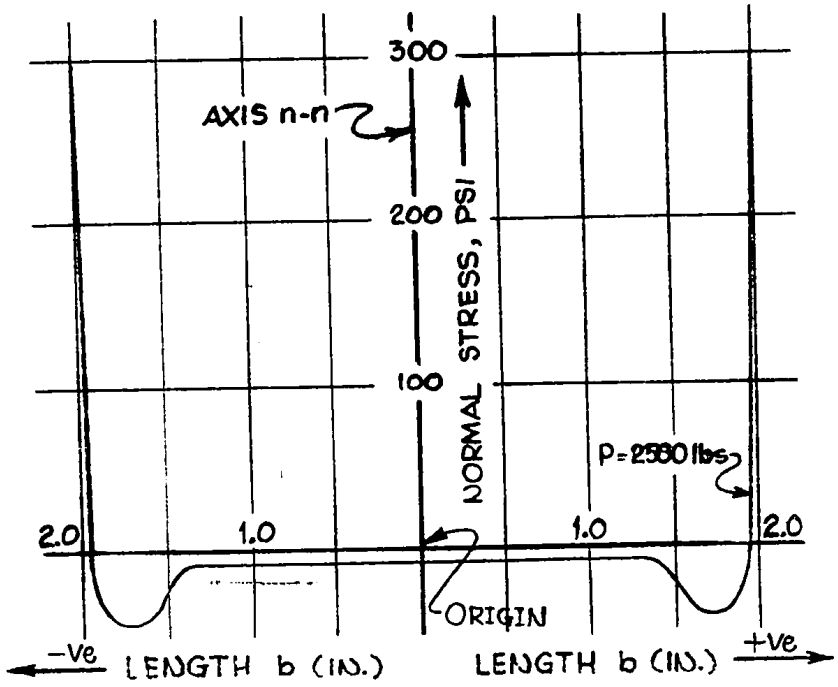

FIG. 40 EXPERIMENTAL DISTRIBUTION OF NORMAL STRESS IN ADHESIVE ON SIDE ONE OF THE SPECIMEN A_2 FOR 2,500 LBS. OF LOAD IN COMPRESSION TESTING. (TABLE 10)

TABLE 11

EXPERIMENTAL PHOTOELASTIC DATA AND THE CALCULATED VALUES OF SHEAR STRESS (τ) AND NORMAL STRESS (σ) IN ADHESIVE CORRESPONDING TO SIDE TWO OF SPECIMEN A_3 FOR 2,500 LBS. OF LOAD IN COMPRESSION TESTING. (FOR PLOT SEE FIGS. 41 AND 42)

Point* (in)	Isochromatics (N)		Isoclinics ($\theta°$)		τ psi	σ psi
	Line AB	Line CD	Line AB	Line CD		
-2.00	3.00	3.00	85	85	600.71	296.37
-1.75	2.65	2.65	75	75	250.27	- 44.61
-1.50	2.35	2.35	70	70	131.41	- 23.71
-1.25	1.85	1.85	60	60	80.71	- 8.71
-1.00	1.45	1.45	50	50	44.23	- 8.71
-0.75	1.00	1.00	40	40	28.11	- 8.71
-0.50	0.75	0.75	30	30	14.41	- 8.71
-0.25	0.50	0.50	25	25	14.41	- 8.71
origin	0.25	0.25	15	15	13.11	- 8.71
0.25	0.50	0.50	25	25	14.41	- 8.71
0.50	0.75	0.75	30	30	14.41	- 8.71
0.75	1.00	1.00	40	40	28.11	- 8.71
1.00	1.45	1.45	50	50	44.23	- 8.71
1.25	1.85	1.85	60	60	80.71	- 8.71
1.50	2.35	2.35	70	70	131.41	- 23.71
1.75	2.65	2.65	75	75	250.27	- 44.61
2.00	3.00	3.00	85	85	600.71	296.37

* The points marked are shown on the abscissa starting from the left-hand side of Figs. 41 and 42.

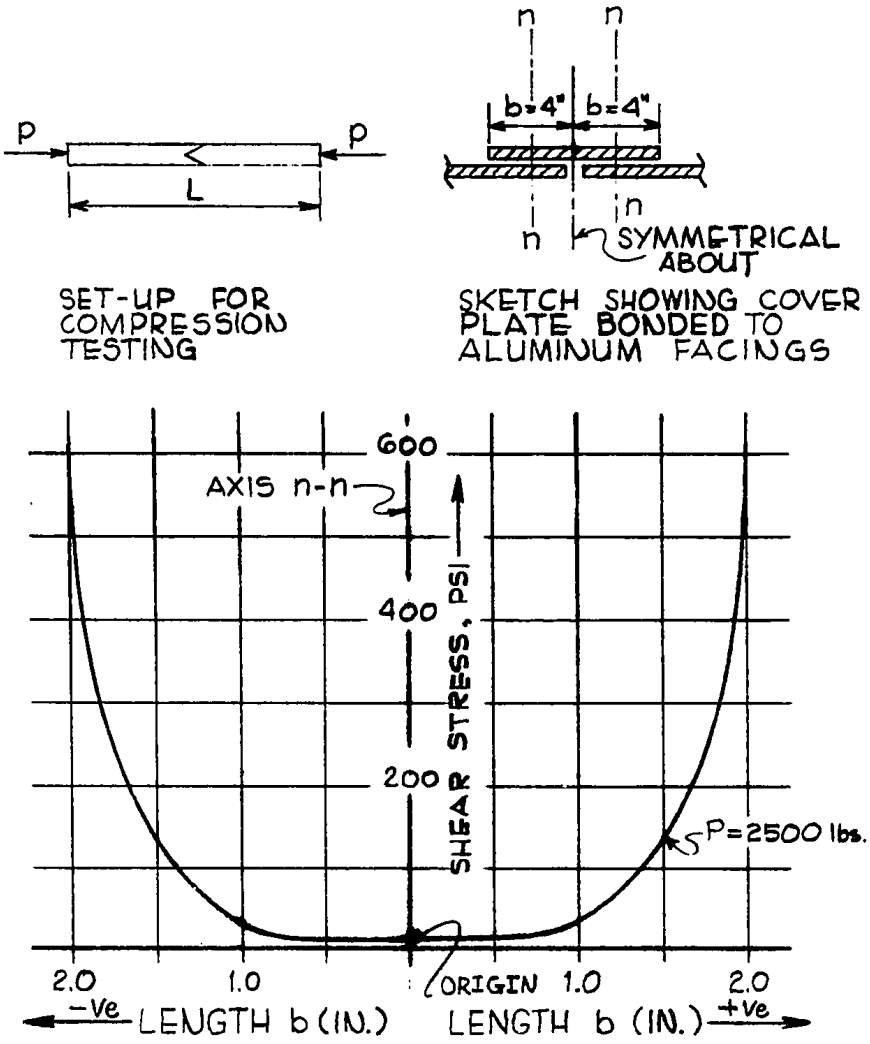

FIG. 41 EXPERIMENTAL DISTRIBUTION OF SHEAR STRESS IN ADHESIVE ON SIDE TWO OF THE SPECIMEN A_3 FOR 2,500 LBS. OF LOAD IN COMPRESSION TESTING (TABLE 11).

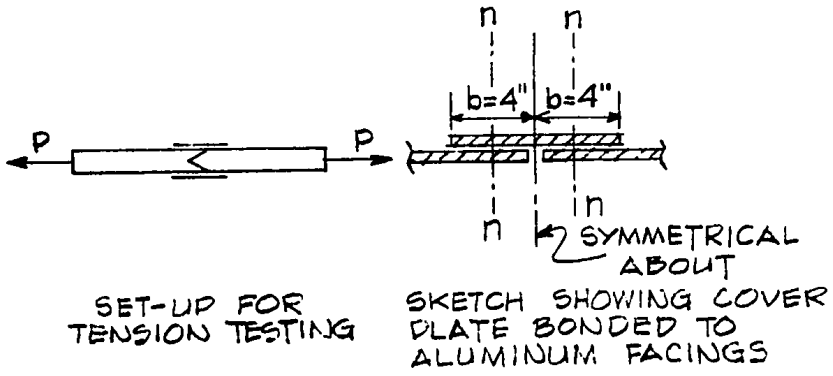

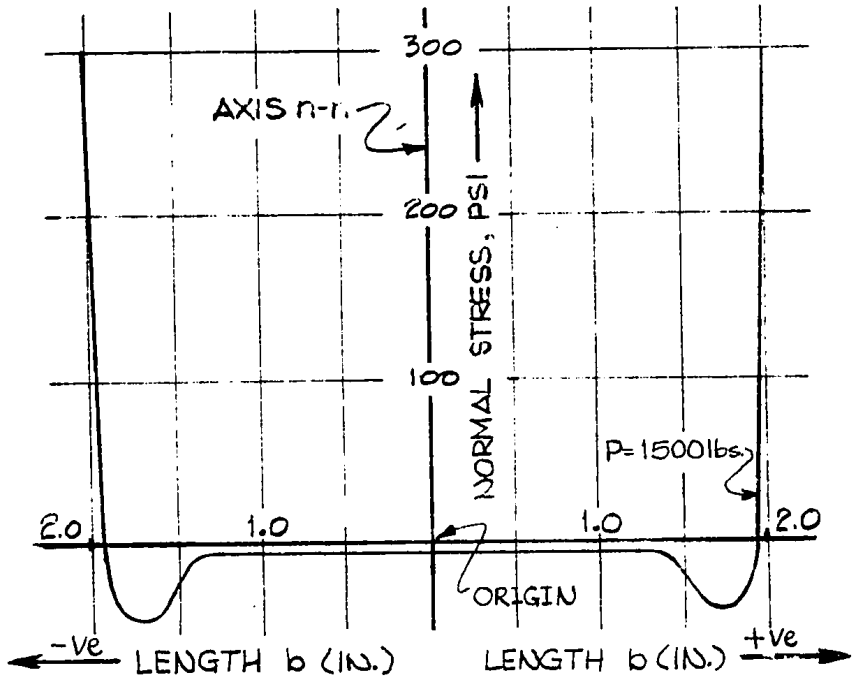

FIG. 42 EXPERIMENTAL DISTRIBUTION OF NORMAL STRESS IN ADHESIVE ON SIDE TWO OF THE SPECIMEN A_3 FOR 2,500 LBS. OF LOAD IN COMPRESSION TESTING. (TABLE 11)

TABLE 12

EXPERIMENTAL PHOTOELASTIC DATA AND THE CALCULATED VALUES OF SHEAR STRESS (τ) AND NORMAL STRESS (σ) IN ADHESIVE CORRESPONDING TO SIDE TWO OF SPECIMEN A_4 FOR 1,500 LBS. OF LOAD IN TENSION TESTING. (FOR PLOT SEE FIGS. 43 AND 44)

Point* (in)	Isochromatics (N)		Isoclinics (θ°)		τ psi	σ psi
	Line AB	Line CD	Line AB	Line CD		
-2.00	1.75	1.75	75	75	298.67	250.33
-1.75	1.65	1.65	65	65	141.97	- 45.67
-1.50	1.25	1.25	55	55	71.67	- 12.37
-1.25	1.00	1.00	45	45	48.23	- 8.61
-1.00	0.85	0.85	35	35	25.67	- 8.61
-0.75	0.75	0.75	30	30	22.11	- 8.61
-0.50	0.55	0.55	25	25	20.67	- 8.61
-0.25	0.35	0.35	20	20	19.87	- 8.61
origin	0.25	0.25	15	15	19.87	- 8.61
0.25	0.35	0.35	20	20	19.87	- 8.61
0.50	0.55	0.55	25	25	20.67	- 8.61
0.75	0.75	0.75	30	30	22.11	- 8.61
1.00	0.85	0.85	35	35	25.67	- 8.61
1.25	1.00	1.00	45	45	48.23	- 8.61
1.50	1.25	1.25	55	55	71.67	- 12.37
1.75	1.65	1.65	65	65	141.97	- 45.67
2.00	1.75	1.75	75	75	298.67	250.00

* The points marked are shown on the abscissa starting from the left-hand side of Figs. 43 and 44.

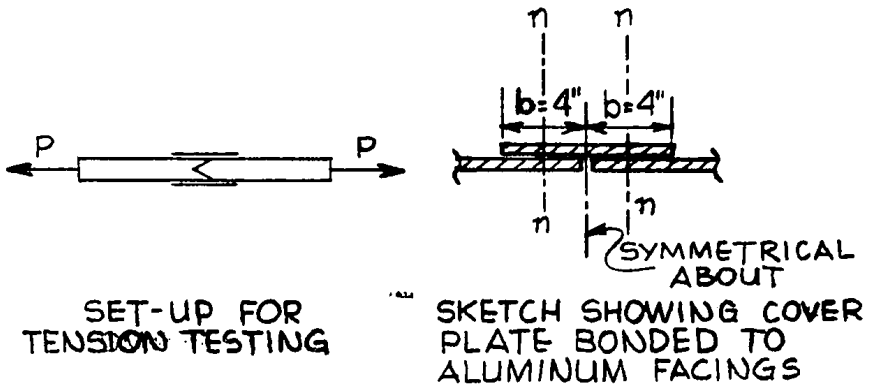

SET-UP FOR TENSION TESTING

SKETCH SHOWING COVER PLATE BONDED TO ALUMINUM FACINGS

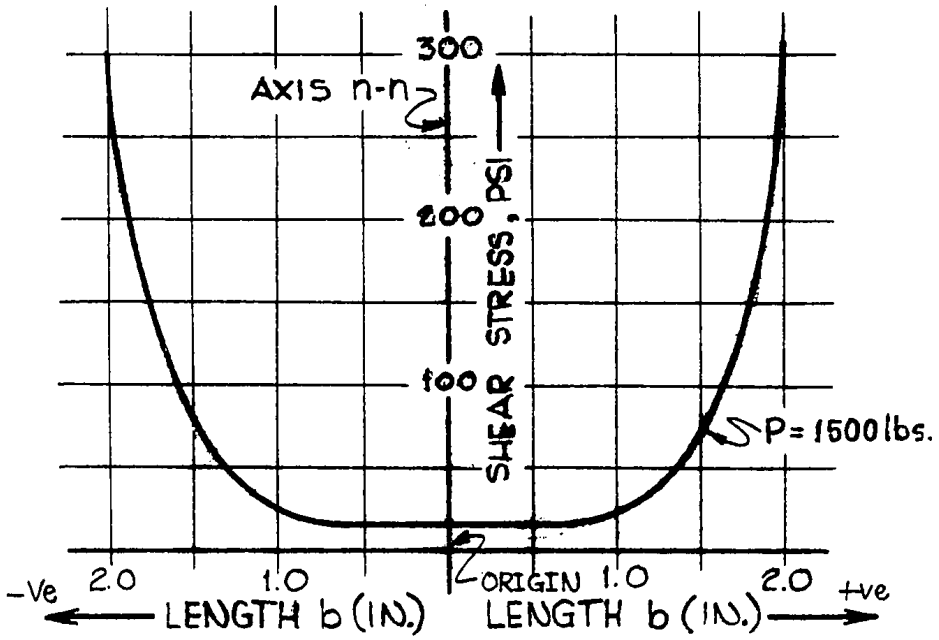

FIG. 43 EXPERIMENTAL DISTRIBUTION OF SHEAR STRESS IN ADHESIVE ON SIDE TWO OF THE SPECIMEN A_4 FOR 1,500 LBS. OF LOAD IN TENSION TESTING. (TABLE 12)

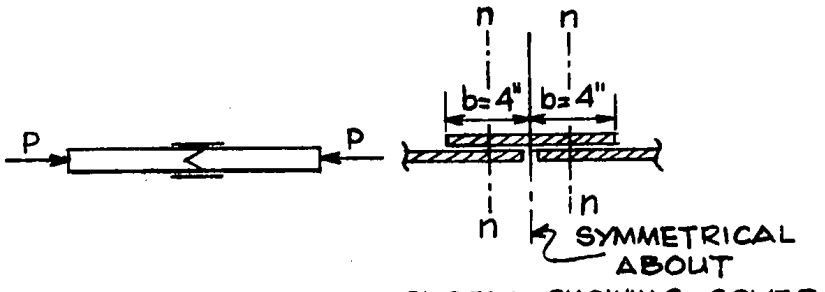

SET-UP FOR COMPRESSION TESTING

SKETCH SHOWING COVER PLATE BONDED TO ALUMINUM FACINGS

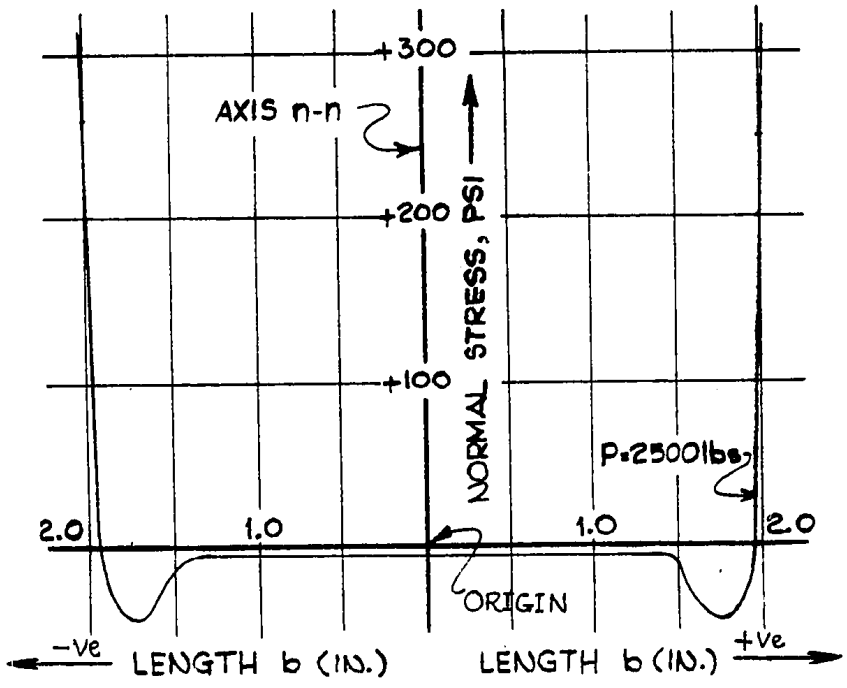

FIG. 44 EXPERIMENTAL DISTRIBUTION OF NORMAL STRESS IN ADHESIVE ON SIDE TWO OF SPECIMEN A4 FOR 1,500 LBS. OF LOAD IN TENSION TESTING. (TABLE 12)

CHAPTER VIII

GRAPHICAL PRESENTATION OF EXPERIMENTAL DATA OF NAILED (B) AND NAILED-ADHESIVE (C) CONNECTIONS

Presented in Figs. 45 to 58 is the distribution of principal stresses in the adhesive layer of specimens Bs and Cs tested with different loads under the following loading conditions:

(i) Flexural

(ii) Direct Shear

(iii) Direct Compression

(iv) Direct Tension.

A brief description of the method of calculating the stresses using photoelastic method of analysis is also included. Each figure carries a detailed title, which fully identifies it.

8.1 RESOLUTION OF PHOTOELASTIC DATA ON NAILED (B) AND NAILED-ADHESIVE (C) CONNECTIONS

In resolving the experimental data on nailed and nailed-adhesive connections, the composite data consisting of isochromatics and isoclinics was used. Since the photoelastic method of stress analysis was used, the difference in strain at any given point A is

$$\varepsilon_1 - \varepsilon_2 = [1 + \frac{\alpha}{180}] \text{ micro in/}_{\text{in}}$$

α being the indication of meter on analyser scale. As is

obvious, the plotting required stress calculations point by point, using the above relationship repetitiously. In order to convert strain into stress, the following formula was used

$$\sigma_1 - \sigma_2 = (\varepsilon_1 - \varepsilon_2) \frac{E}{1+\mu}$$

where E and μ are respectively the modulus of elasticity and Poisson's ratio of aluminum. The maximum principal shear stress is given by $\frac{1}{2}(\sigma_1 - \sigma_2)$ which has been plotted on the respective figures.

8.2 OBSERVATIONS DURING FAILING OF THE SPECIMENS

Joints of each specimen type (A,B and C) were failed to destruction in identical four-point flexural loading set up. The following points were observed during this experiment:

(i) The minimum failure load was recorded in nailed joint specimens (B) only.

(ii) Adhesive-bonded specimens (A), in all cases, could take more load as compared to specimen Bs before failing.

(iii) Nailed-adhesive connections (C) proved to be the strongest of the three since they could take the highest load before cracking up.

(iv) In loading nailed-adhesive connections (C), it was noticed that the adhesive layer cracked first,

before any strain was noticed on the nails. Of course, with the continuation of loading, the nails were eventually pulled out of the specimens.

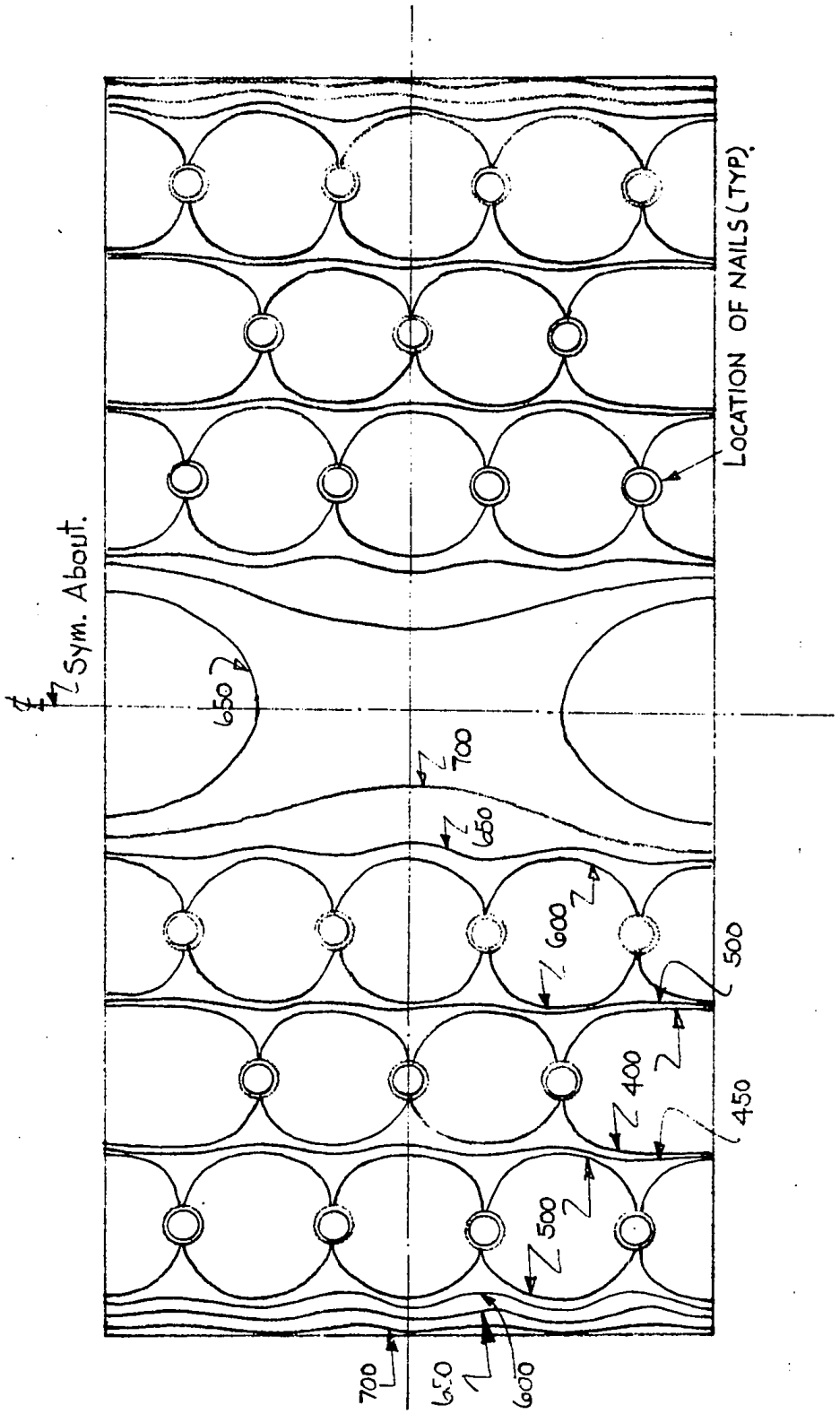

FIG. 45 PRINCIPAL STRESS DISTRIBUTION IN THE ADHESIVE LAYER FLEXURAL TEST LOAD 2,000 LBS : COMPRESSION SIDE : SPECIMEN B_1
(Figures Represent Stresses in psi)
(EXPERIMENTAL)

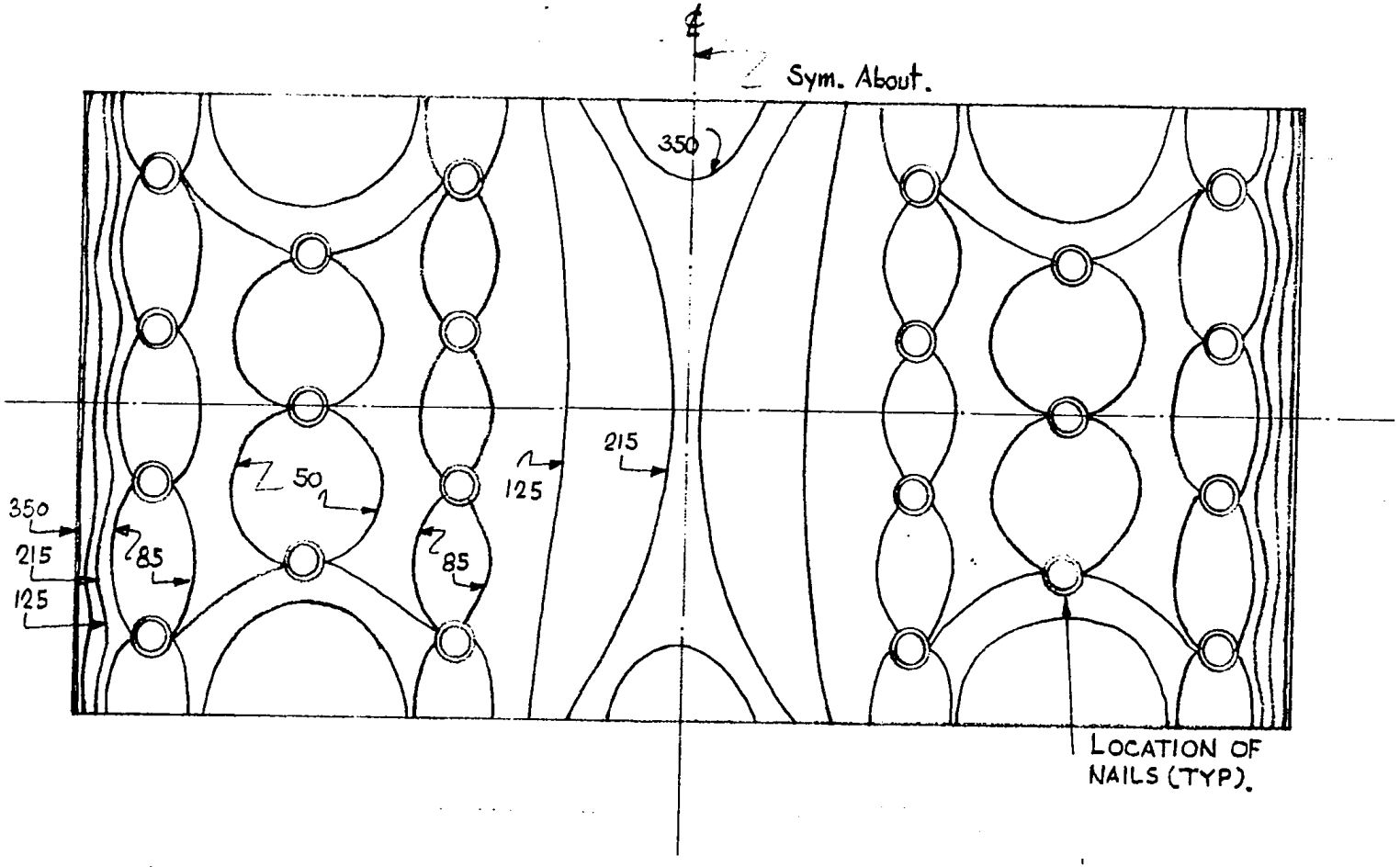

FIG. 46 PRINCIPAL STRESS DISTRIBUTION IN THE ADHESIVE LAYER FLEXURAL TEST: LOAD 1,000 LBS : TENSION SIDE : SPECIMEN B_1

(Figures Represent Stresses in psi)

(EXPERIMENTAL)

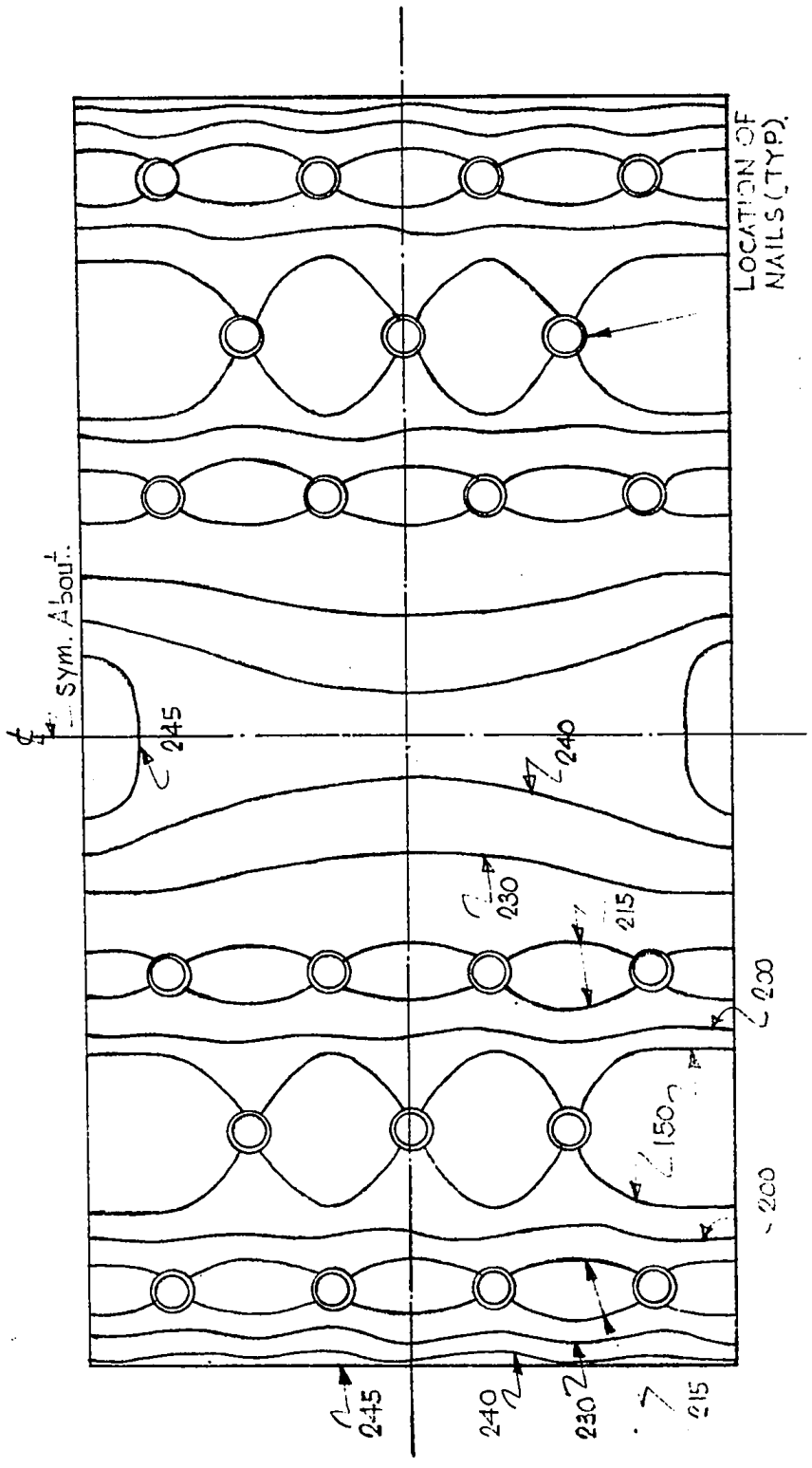

FIG. 47 PRINCIPAL STRESS DISTRIBUTION IN THE ADHESIVE LAYER
SHEAR TEST : LOAD 700 LBS : COMPRESSION SIDE : SPECIMEN B_2

(Figures Represent Stresses in psi)

(EXPERIMENTAL)

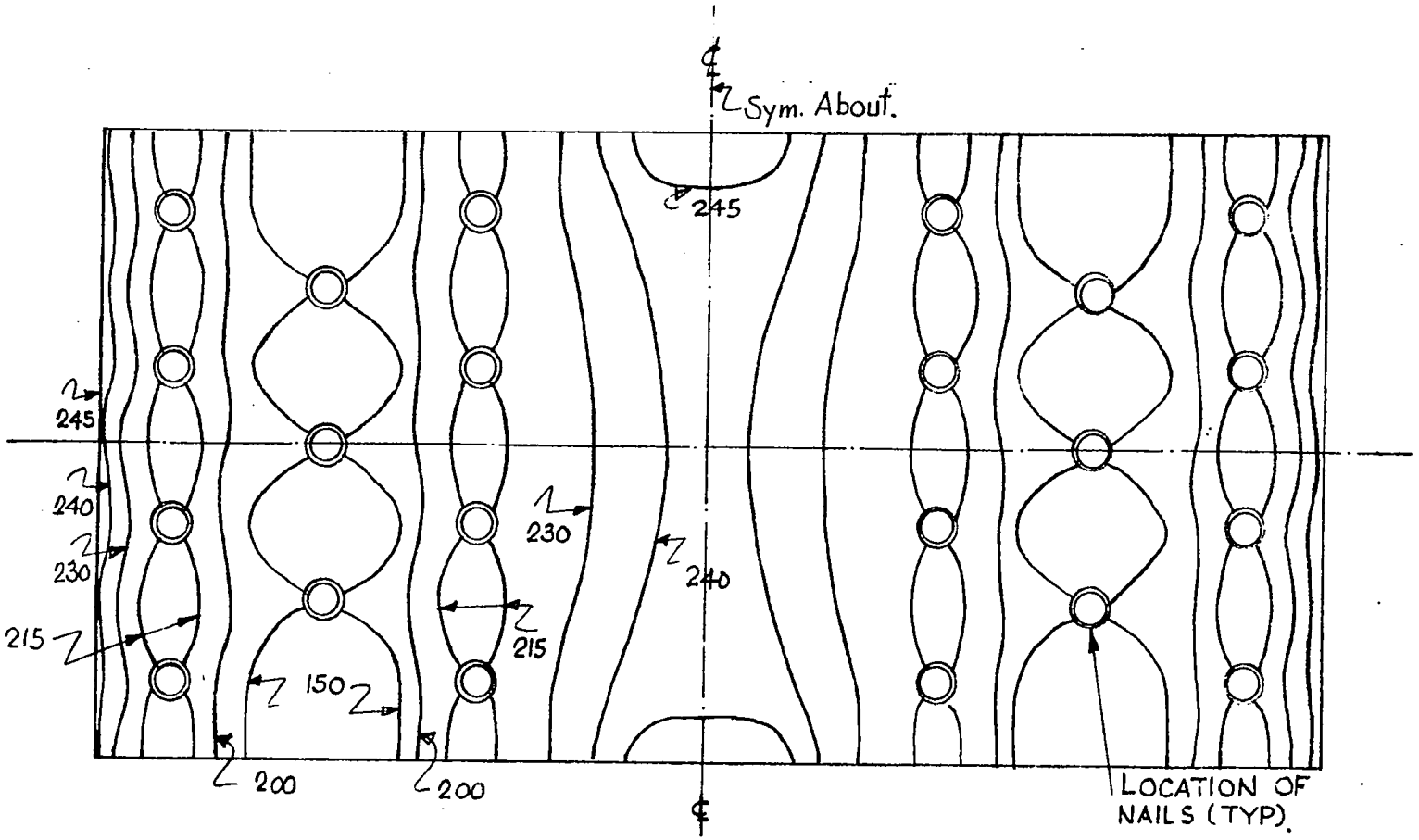

FIG. 48 PRINCIPAL STRESS DISTRIBUTION IN THE ADHESIVE SHEAR TEST : LOAD 700 LBS : TENSION SIDE : SPECIMEN B_2

(Figures Represent Stresses in psi)

(EXPERIMENTAL)

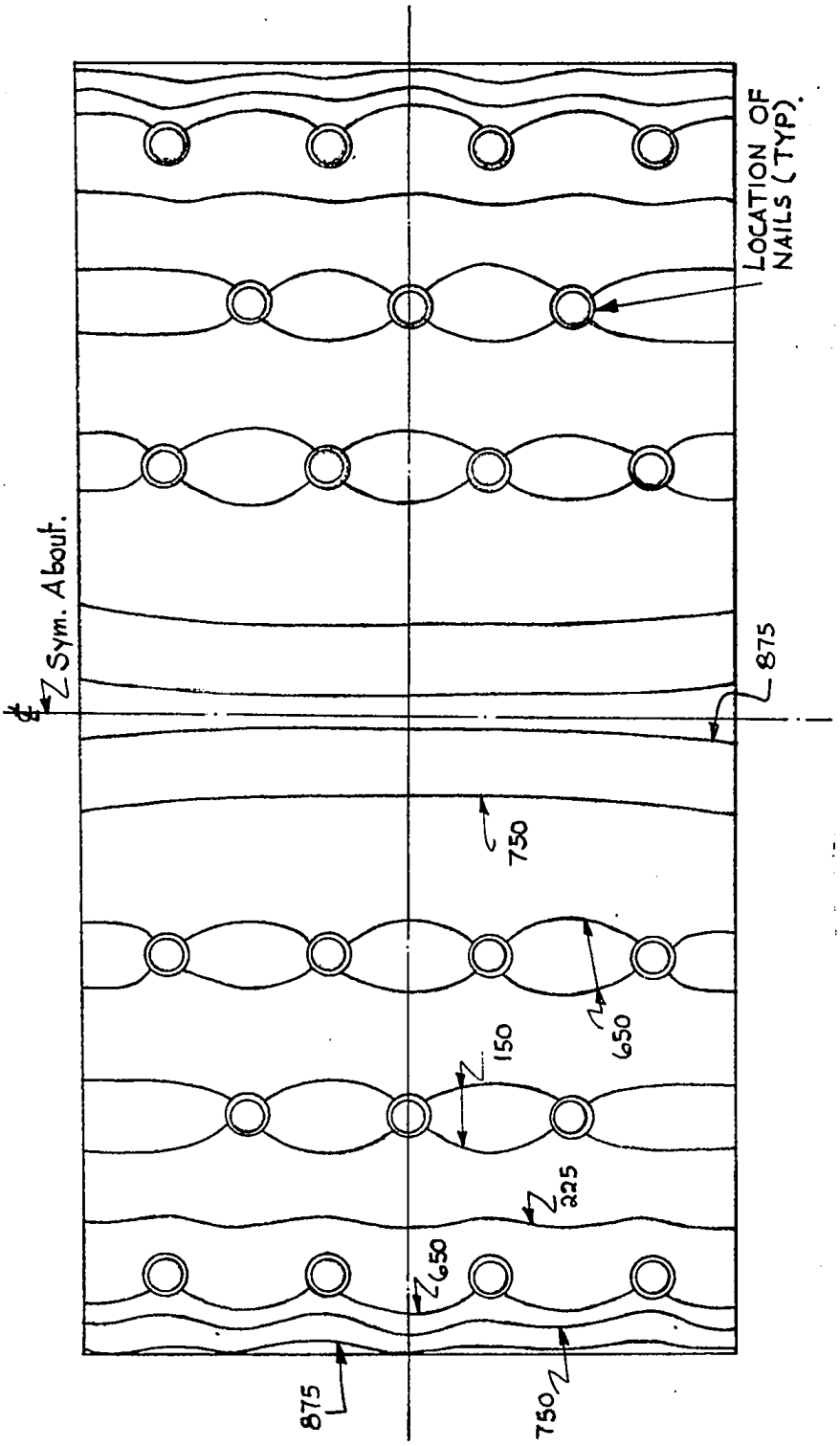

FIG. 49 PRINCIPAL STRESS DISTRIBUTION IN THE ADHESIVE LAYER
COMPRESSION TEST : LOAD 2,500 LBS : SIDE ONE : SPECIMEN B_3
(Figures Represent Stresses in psi)
(EXPERIMENTAL)

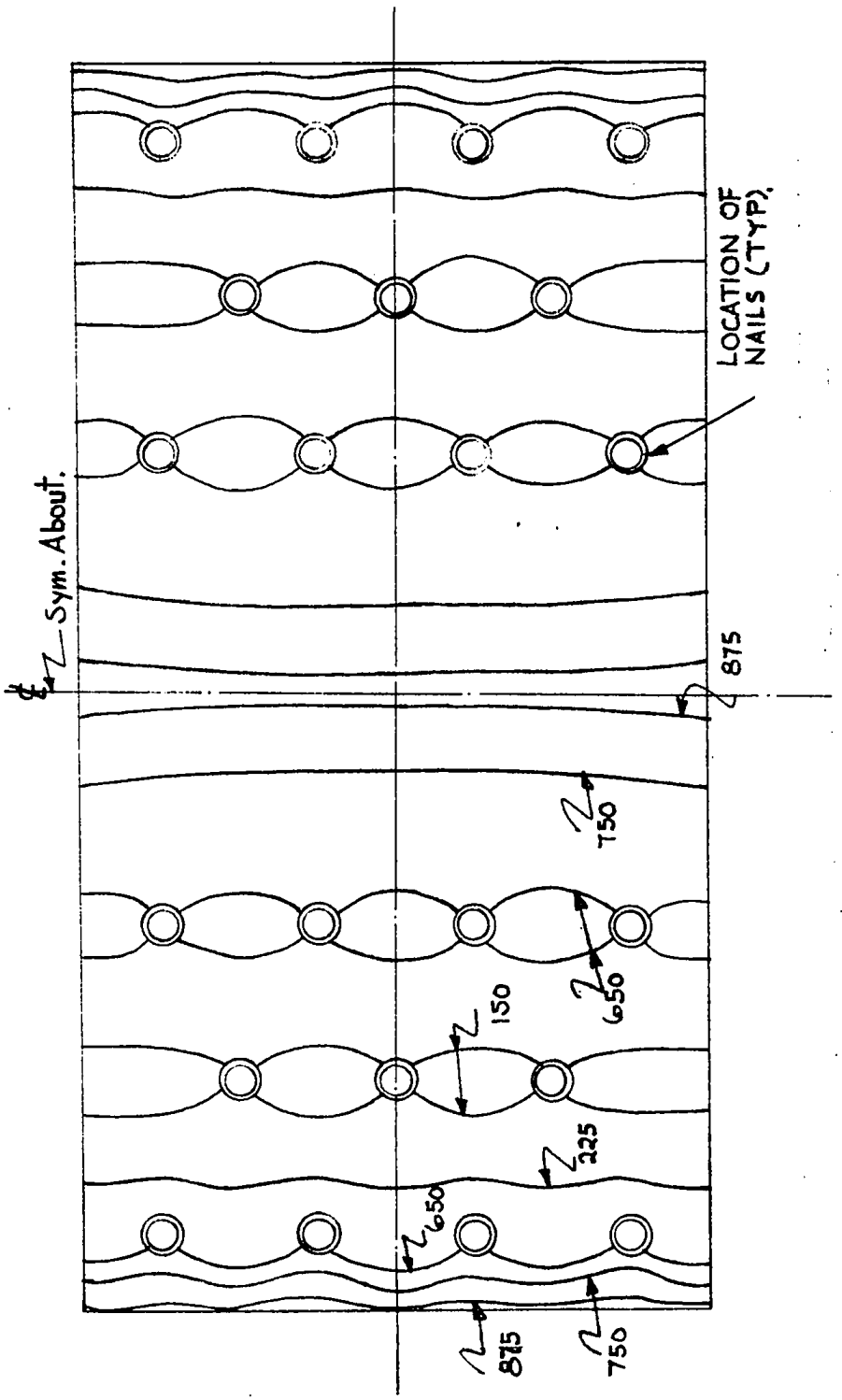

FIG. 50 PRINCIPAL STRESS DISTRIBUTION IN THE ADHESIVE LAYER
COMPRESSION TEST : LOAD 2,500 LBS : SIDE TWO : SPECIMEN B_3
(Figures Represent Stresses in psi)
(EXPERIMENTAL)

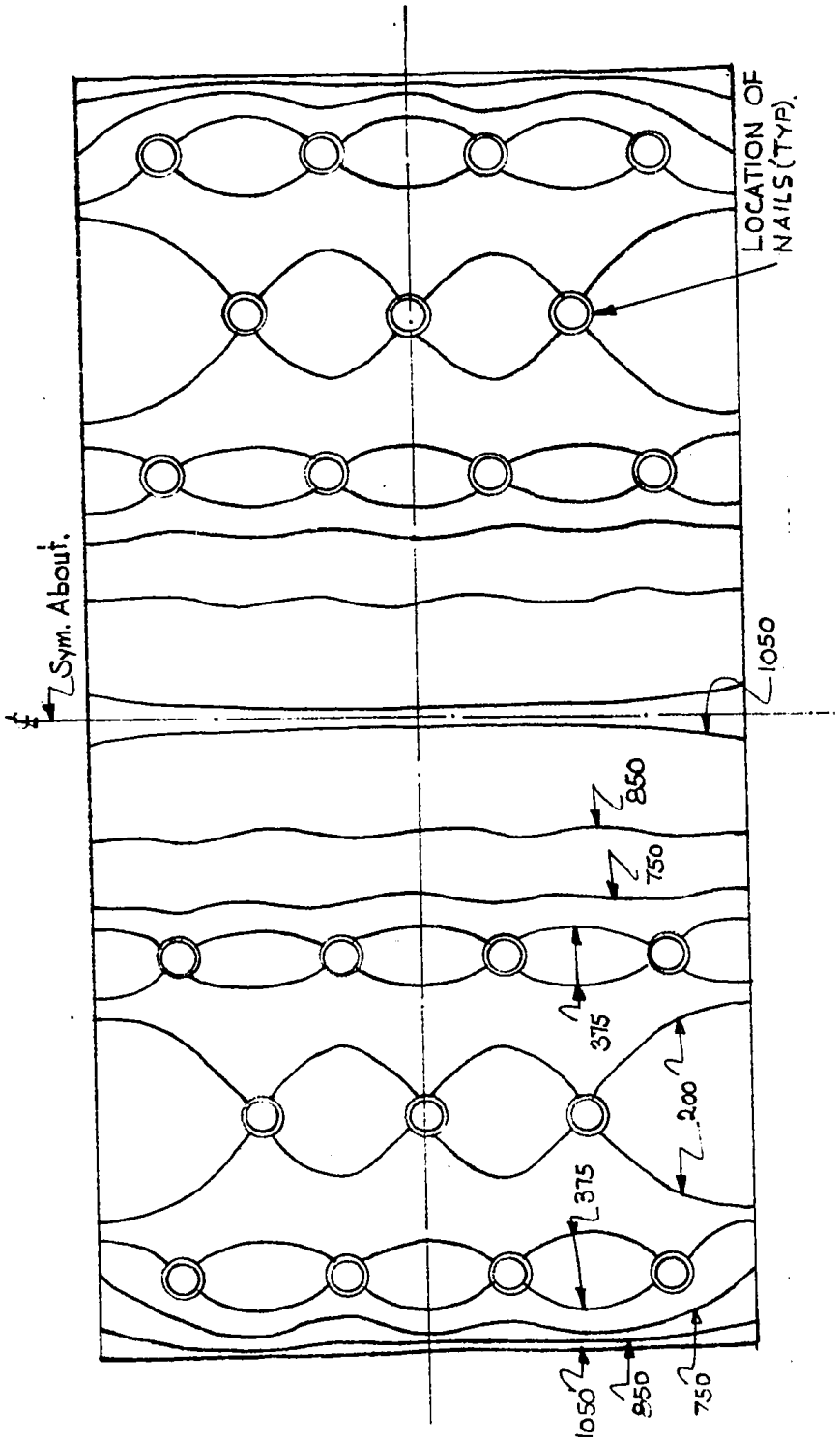

FIG. 51 PRINCIPAL STRESS DISTRIBUTION IN THE ADHESIVE LAYER FLEXURAL TEST : LOAD 1,000 LBS : COMPRESSION SIDE : SPECIMEN C_1

(Figures Represent Stresses in psi)

(EXPERIMENTAL)

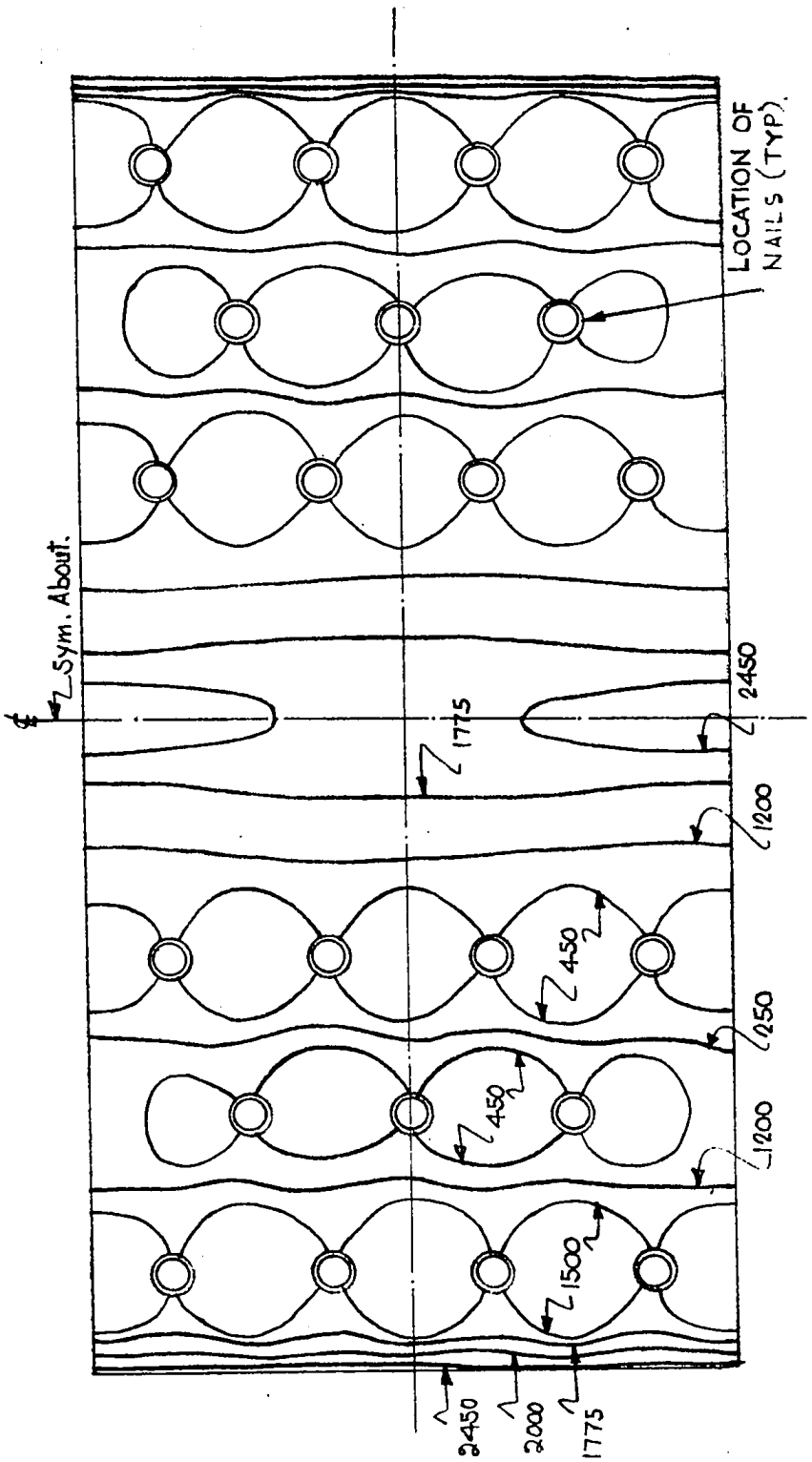

FIG. 52 PRINCIPAL STRESS DISTRIBUTION IN THE ADHESIVE LAYER FLEXURAL TEST : LOAD 1,750 LBS : TENSION SIDE : SPECIMEN C_1

(Figures Represent Stresses in psi)

(EXPERIMENTAL)

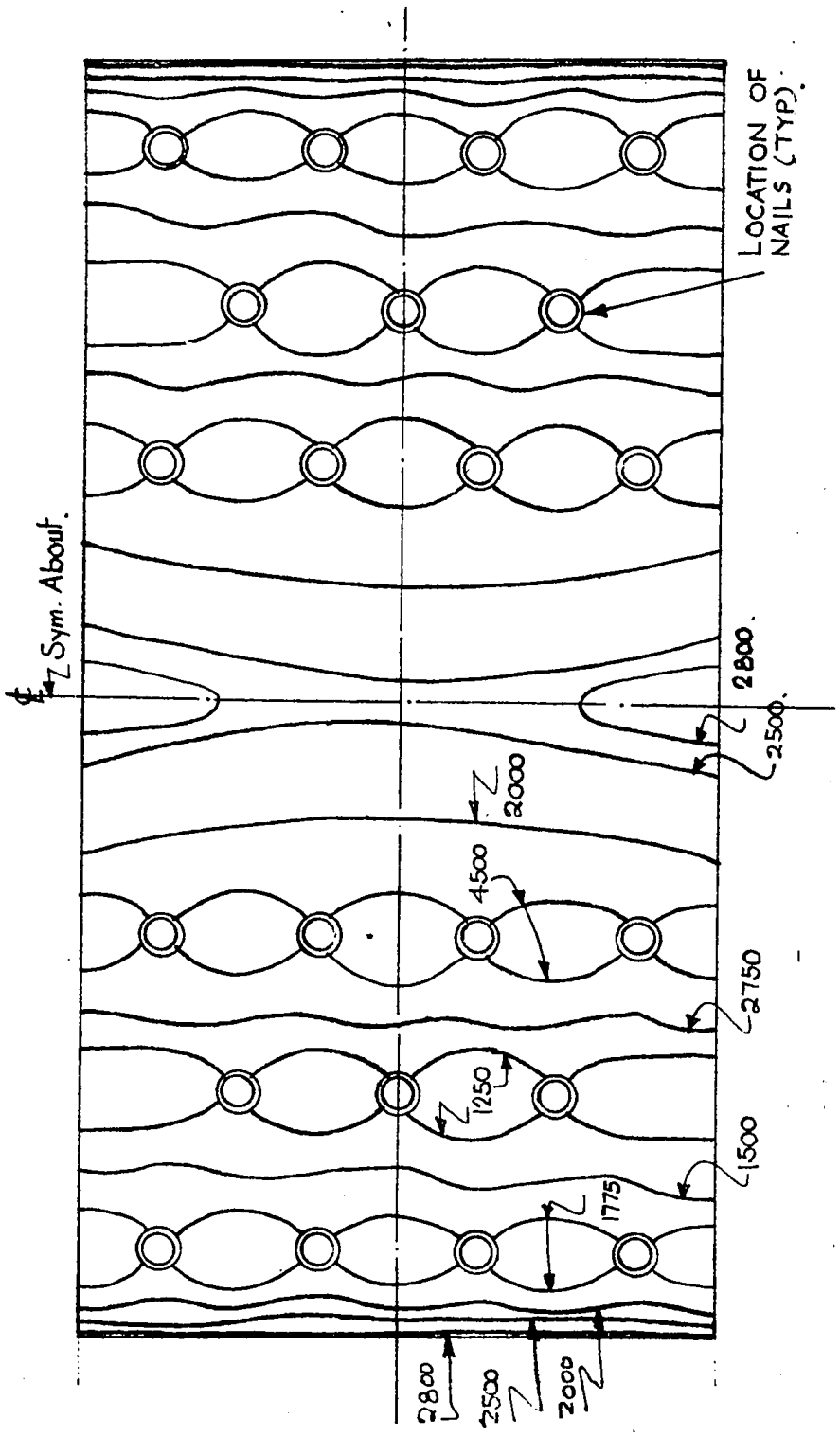

Fig. 53 PRINCIPAL STRESS DISTRIBUTION IN THE ADHESIVE LAYER SHEAR TEST:
LOAD 700 LBS : COMPRESSION SIDE : SPECIMEN C_2
(Figures Represent Stresses in psi)

(EXPERIMENTAL)

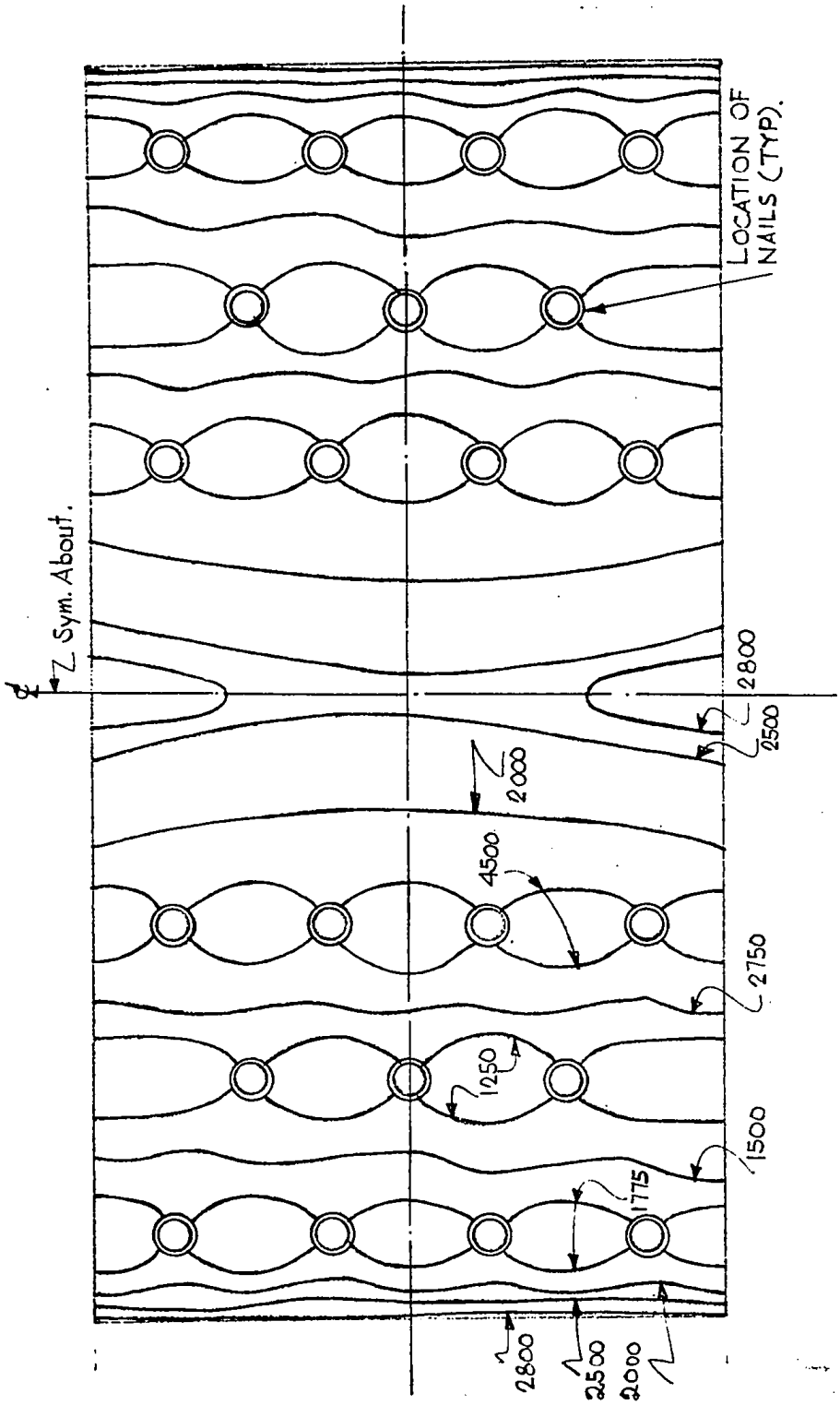

FIG. 54 PRINCIPAL STRESS DISTRIBUTION IN THE ADHESIVE LAYER SHEAR TEST:
LOAD 700 LBS : TENSION SIDE : SPECIMEN C_2
(Figures Represent Stresses in psi)
(EXPERIMENTAL)

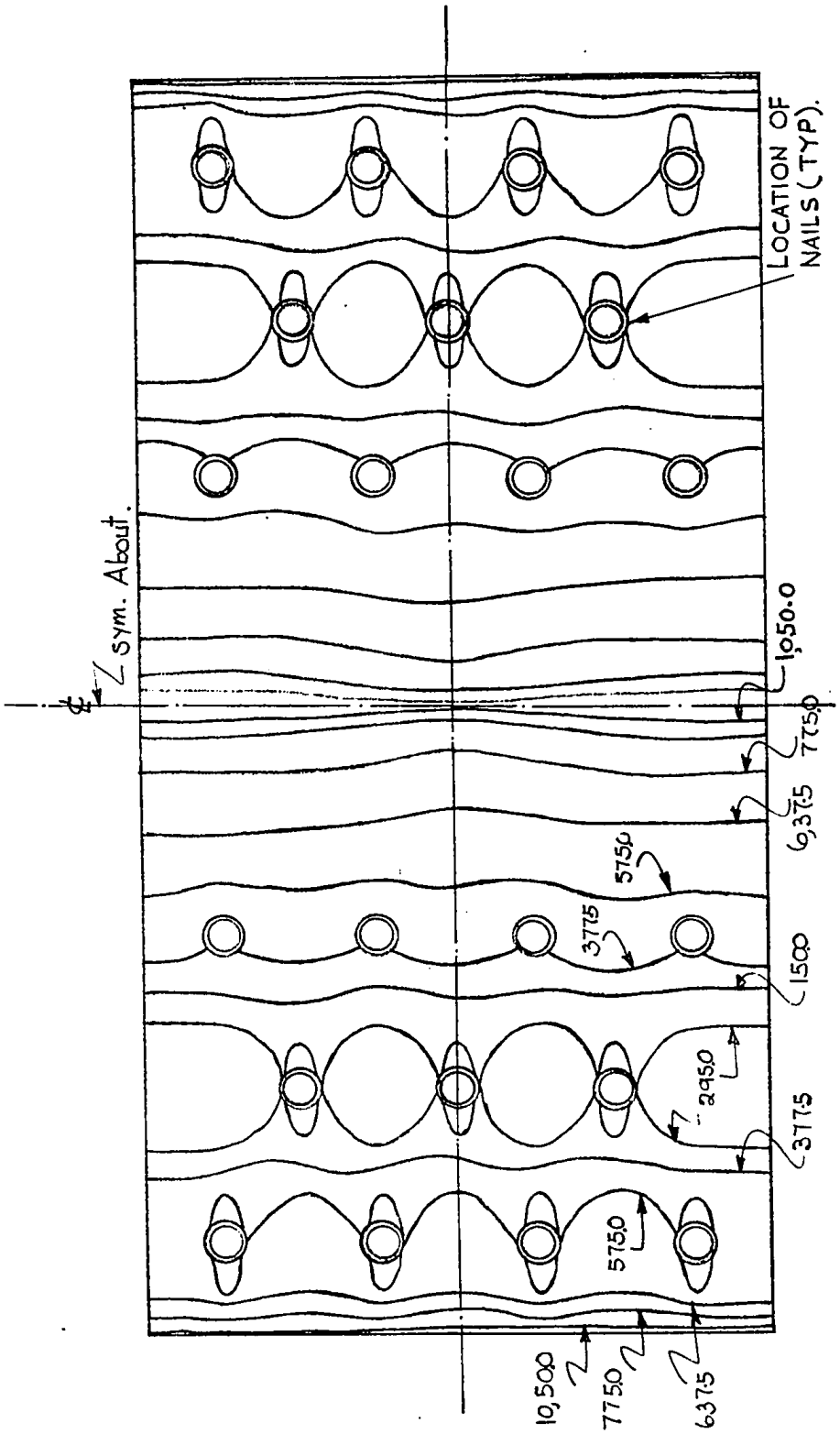

FIG. 55 PRINCIPAL STRESS DISTRIBUTION IN THE ADHESIVE LAYER COMPRESSION TEST : 7,500 LBS : SIDE ONE SPECIMEN C_3

(Figures Represent Stresses in psi)

(EXPERIMENTAL)

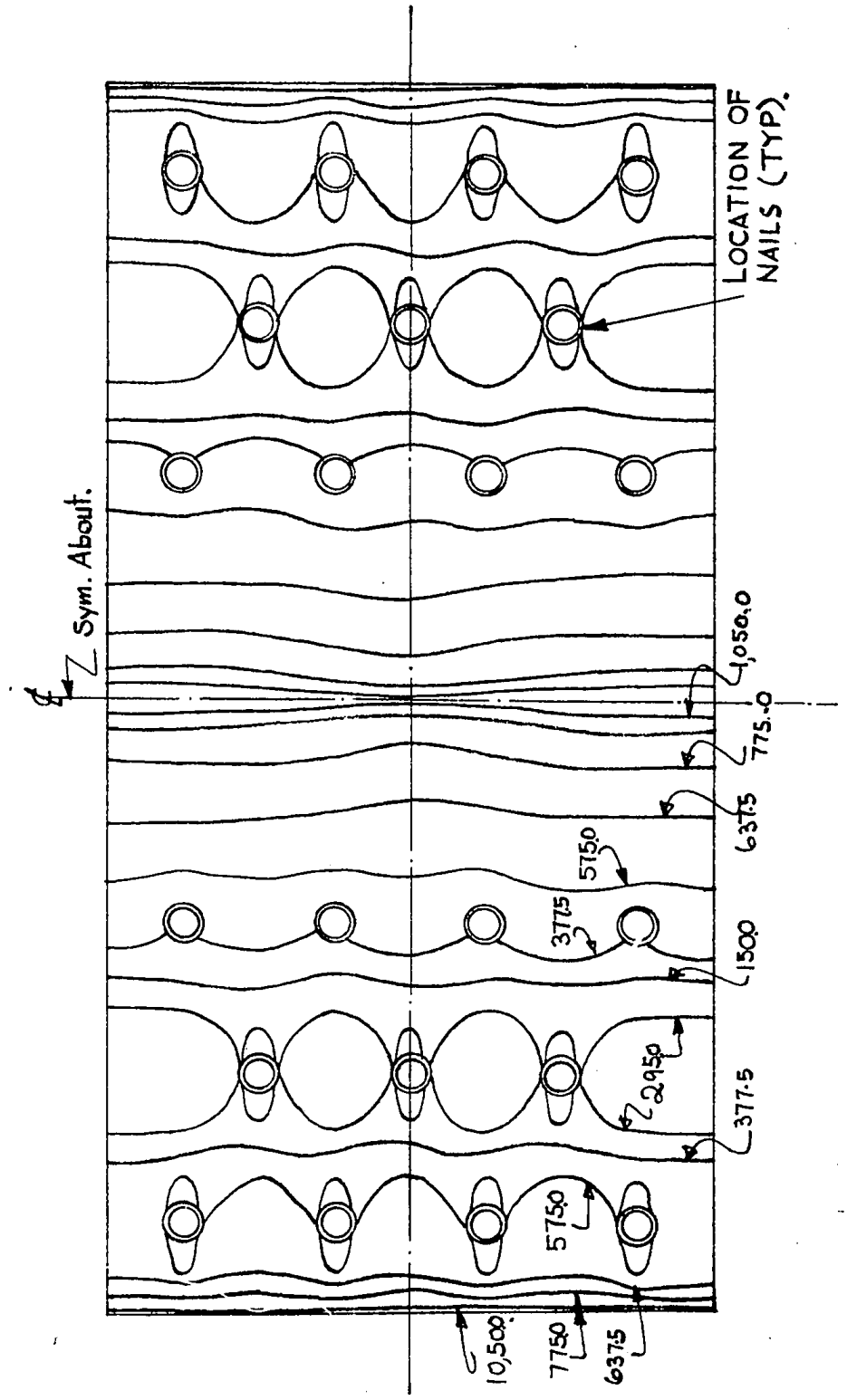

FIG. 56 PRINCIPAL STRESS DISTRIBUTION IN THE ADHESIVE LAYER COMPRESSION TEST : LOAD 7,500 LBS : SIDE TWO : SPECIMEN C_3

(Figures Represent Stresses in psi)

(EXPERIMENTAL)

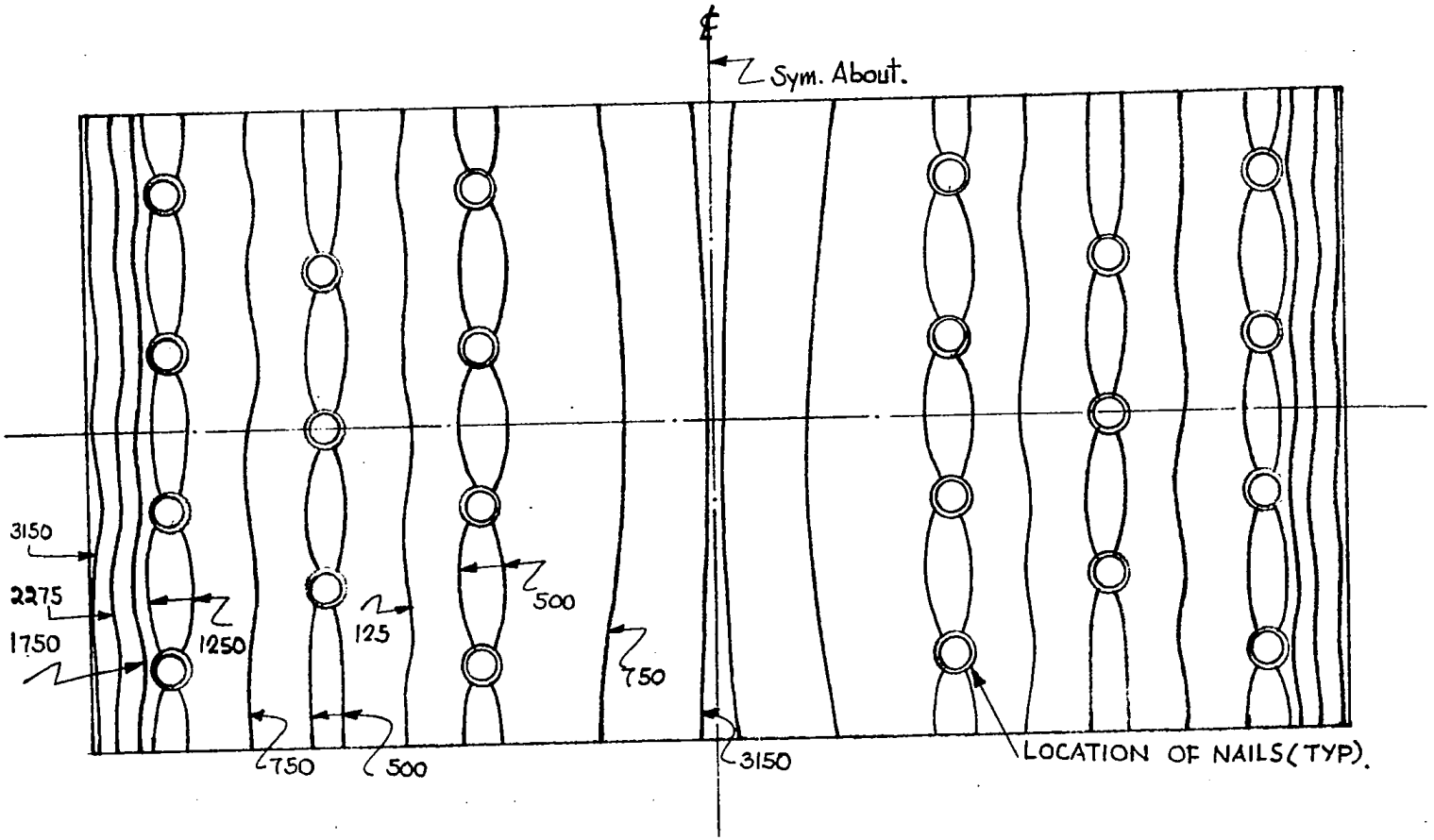

FIG. 57 PRINCIPAL STRESS DISTRIBUTION IN THE ADHESIVE LAYER TENSION TEST : LOAD 1,750 LBS : SIDE ONE : SPECIMEN C_4

(Figures Represent Stresses in psi)

(EXPERIMENTAL)

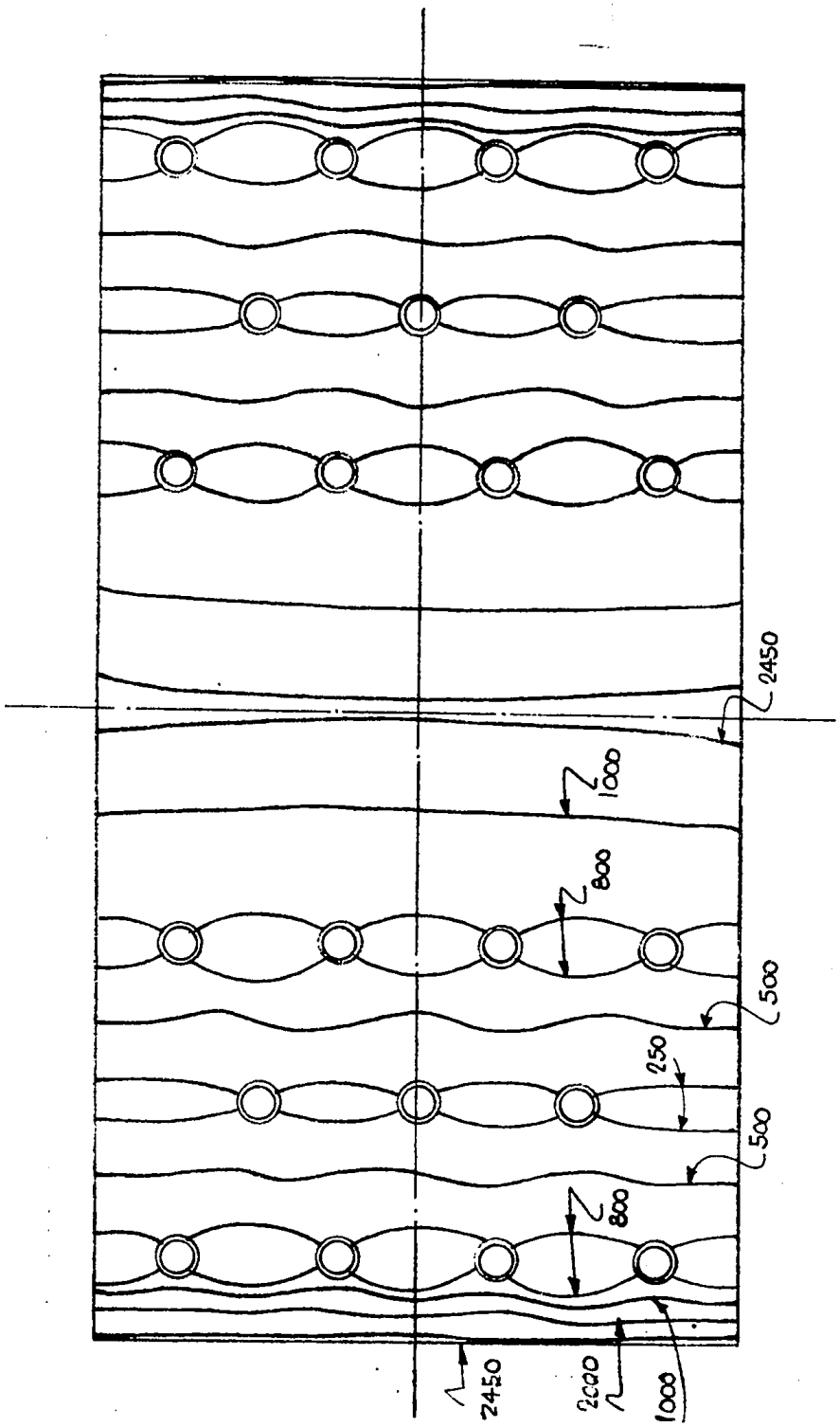

FIG. 58 PRINCIPAL STRESS DISTRIBUTION IN THE ADHESIVE LAYER TENSION TEST : LOAD 2,250 LBS. SIDE TWO : SPECIMEN C_4
(Figures Represent Stresses in psi)
(EXPERIMENTAL)

CHAPTER IX

COMPARISON AND DISCUSSION OF THEORETICAL AND EXPERIMENTAL RESULTS

9.1 COMPARISON OF THE THEORETICAL VALUES OF SHEAR AND NORMAL STRESSES IN THE ADHESIVE CONSIDERING THEORIES OF SMALL AND LARGE DEFLECTION (CHAPTERS IV AND V) : SPECIMEN A_1

Figure 59 shows graphs of the values of shear stress, τ obtained using theory of small deflection and theory of large deflection, whereas Fig. 60 presents graphs of the values of normal stress σ, using the same two theories of deflection.

The large deflection theory gives higher values of stress τ and σ. Their increase fluctuates between 15% and 18%, as compared to the values obtained in the small deflection theory. The loom in the stress values is due to the increased $(M_2)_o$ which, in turn, results by the inclusion of β (vertical component of T_f) in the moment-equations (2) and (3) of Chapter V.

Both theories give the maximum values of τ and σ at the edge of the bonded region. σ_{max} appears to be the stress which produces yielding, as compared to τ_{max} because Waldex W-105 has a yield stress of 1250 psi in tension as compared to 2485 psi in shear.

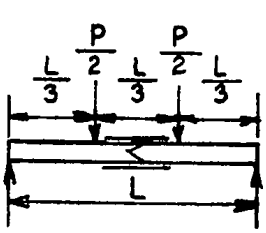

SET-UP FOR FLEXURAL TESTING

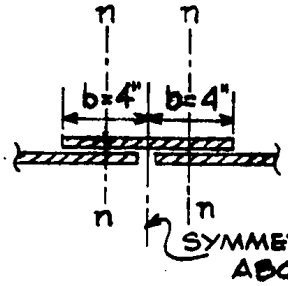

SKETCH SHOWING COVER PLATE BONDED TO ALUMINUM FACINGS

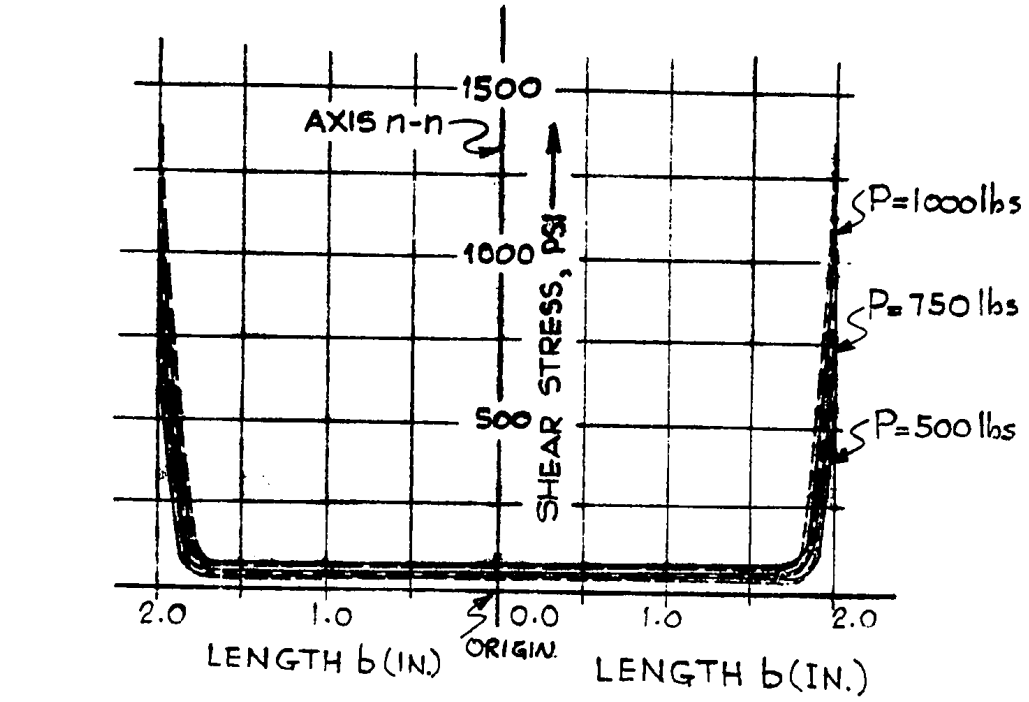

FIG. 59 COMPARISON OF THE THEORETICAL VALUES OF SHEAR STRESS IN THE ADHESIVE ON THE COMPRESSION SIDE OF SPECIMEN A, CONSIDERING THEORIES OF SMALL AND LARGE DEFLECTION.

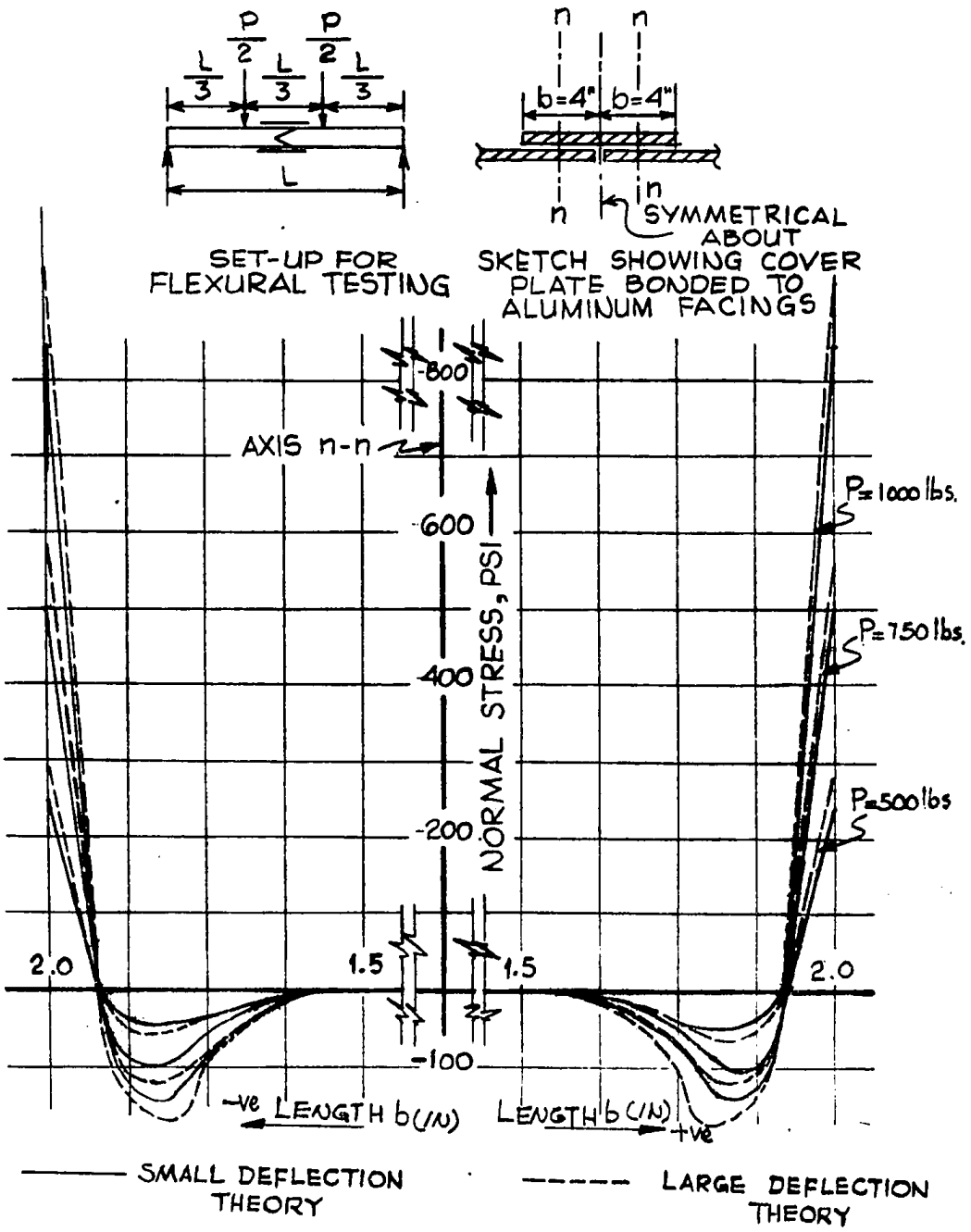

FIG. 60 COMPARISON OF THE THEORETICAL VALUES OF NORMAL STRESS IN THE ADHESIVE ON THE COMPRESSION SIDE OF SPECIMEN A, CONSIDERING THEORIES OF SMALL AND LARGE DEFLECTION.

9.2 COMPARISON OF THE THEORETICAL (LARGE DEFLECTION THEORY) AND EXPERIMENTAL VALUES OF THE SHEAR STRESS, τ AND THE NORMAL STRESS, σ IN ADHESIVE (CHAPTERS V AND VII) : SPECIMEN A_1

The graphs of the shear stress, τ and the normal stress σ (Fig. 61 and 62) obtained from the Experimental Study of Adhesive (Chapter VII) and their counterparts in the Theoretical Study (Chapters V, VI and VII) reveal a good general agreement as to the variational trend of the stress values, their maximum and minimum magnitudes and the points at which they occur.

Stress values obtained from experimental study are in general, lower than the theoretical ones. Their average deviations are within 7%. However, the plot of the theoretical and experimental values of τ (Fig.61) shows a considerable difference in their values in the middle of the bonded area, whereas its ends still show good agreement between the two.

The discrepancy arises from the photographs of isochromatics acquired in the experimental study. The light-source from the Reflection Polariscope falling directly in the middle of the bonded region on the photoelastic plastic bonded to the test specimens distorted the colour-pattern of the fringes. This reflection from the light source has shown itself up in the photographs of the Isochromatics thus making it difficult to decipher the correct fringe order in that area which appears predominantly black

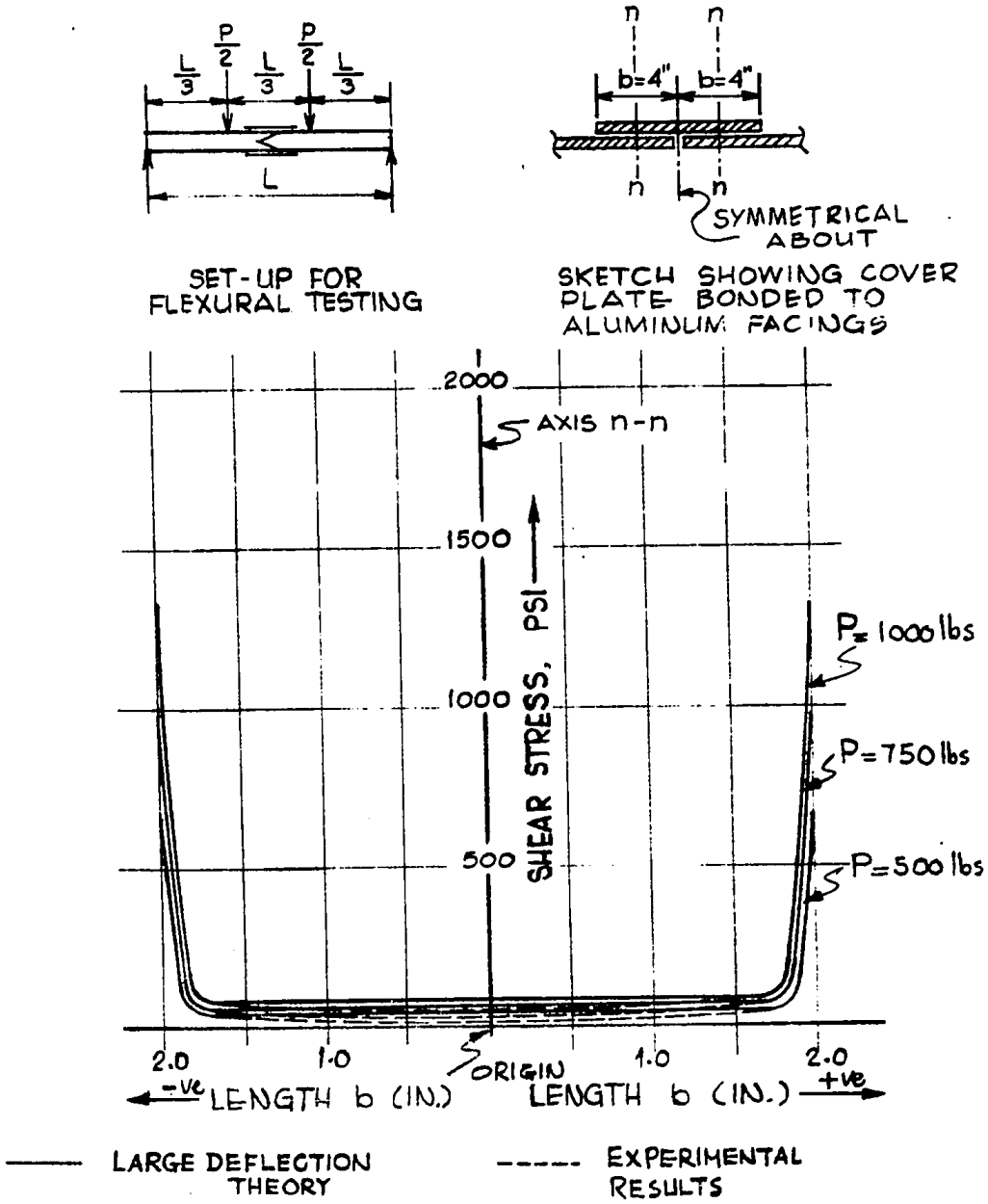

FIG. 61 COMPARISON OF THE THEORETICAL (LARGE DEFLECTION THEORY) AND EXPERIMENTAL VALUES OF SHEAR STRESS IN THE ADHESIVE ON THE COMPRESSION SIDE OF SPECIMEN A_1 FOR 500, 750 AND 1,000 LBS OF LOAD IN FLEXURAL TESTING .

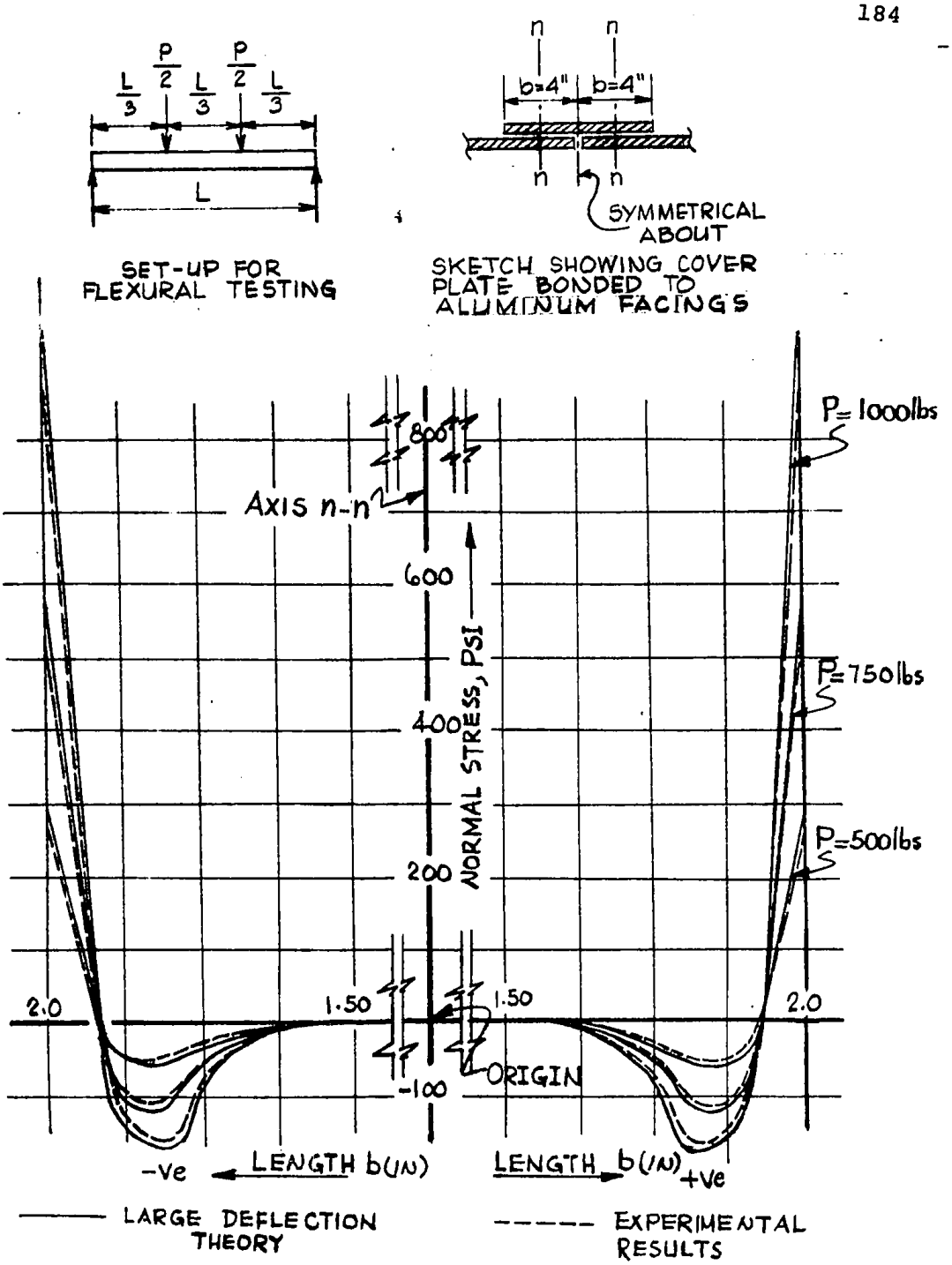

FIG. 62 COMPARISON OF THE THEORETICAL (LARGE DEFLECTION THEORY) AND EXPERIMENTAL VALUES OF NORMAL STRESS IN THE ADHESIVE ON THE COMPRESSION SIDE OF SPECIMEN A, IN 500, 750 AND 1,000 LBS. OF LOAD IN FLEXURAL TESTING.

corresponding to fringe order zero. That is why the experimental plot of τ (Fig. 61) shows little stress in that area, whereas the theoretical one gives a finite value. The ends of the bonded region, however, were not affected by this light-reflection and recorded easily-decipherable fringe patterns.

Since there is a good agreement between the theoretical and experimental values at the ends of the bonded region where the maximum values of stresses occur, a joint design based on the theoretical values of stresses will be on the conservative side.

CHAPTER X

CONCLUSIONS

10.1 INTRODUCTION

Theoretical and experimental analyses of the stress distribution in the adhesive layers of mid-panel joints between two sandwich panels have been carried out.

In the theoretical study two approaches have been used : (a) the small deflection theory and (b) the large deflection theory. In the experimental study fifteen bonded and nailed connections were tested in bending, shear, direct compression, and direct tension.

Comparisons have been made between the results of the two theories developed and between the results of the large deflection theory and experimental results obtained from the bonded connections.

10.2 CONCLUDING REMARKS

Theoretical and experimental results obtained in previous chapters are reviewed in the following sections.

10.2.1 Adhesive-Bonded Connections (Specimens A) in Flexural Testing

The study of the behaviour of the adhesive involved developing mathematical relationships for determining τ (the shear stress) and σ (the normal stress) in it; their maximum values and the points at which they occur.

To verify the theory, specimens A were tested in flexural loading and the experimental results plotted for τ and σ. As the plots of the theoretical and experimental values of τ (Figs. 13, 19,31 and 33) and that of σ (Figs. 14, 20,32 and 34) show that the yielding of the adhesive will occur at the bond edges where the maximum stresses develop. Notwithstanding the fact that σ_{max} is less than τ_{max}, the the former appears to be the stress which produces yielding because Waldex W-105 has a yield stress of about 2,485 psi in shear as compared to 1,250 psi in normal stress.

Furthermore, it is observed that the maximum values of stresses (both shear and normal) are independent of bond length except when the bond length is very small. (2 in.) (See Figs. 15 and 21). Hence, the bond will yield by tearing off at the edges giving rise to a stress-wave that travels in towards the center of the bond and will probably stop when the remaining overlap becomes small.

The theoretical study of the adhesive-bonded joints presents a comprehensive approach to determine the value of τ and σ in an adhesive layer for the combined effect of several parameters such as direct loads, bending moments, various boundary conditions, different elastic properties of materials bonded together and the equal or unequal thicknesses of the cover plates and the facings of the sandwich material. The simpler cases can, of course, be readily deduced from them. Especially reliable seems to be the large deflection theory approach which by eliminating the simplifying

assumptions of the small deflection theory has given better results as evidenced by their closer agreement with the experimental results (Fig. 61 and 62).

10.2.2 Adhesive-Bonded Connections (Specimens A) in Shear, Direct Compression and Direct Tension Testing

The plot of the experimental values, of τ and σ in the adhesive layers of joint specimens A tested under the above loading conditions appears in Figs. 35 to 44 (inclusive). The shear and normal stresses determined in these loading conditions follow the same pattern as in flexural testing. Both τ_{max} and σ_{max} occur at the bond edges and normal stress is once again the critical stress from the strength point of view of the joint.

10.2.3 Nailed Connections (Specimens B) in Flexural, Shear, Direct Compression and Direct Tension Testing

The plot of the principal stress distribution in the cover plate of nailed joints (specimen B) appears in Figs. 45 to 50 (inclusive). Stress concentrations appear around nails as shown on the plots. The highest values of principal stresses appear at the bond edges whereas the stresses in the middle of the nailed region are the lowest.

10.2.4 Nailed-Adhesive Connections (Specimen C) in Flexural, Shear, Direct Compression and Direct Tension Testing

Figs. 51 to 58 (inclusive) show the principal stress distribution in the adhesive layer of nailed-adhesive connec-

tions (Specimen C) for four different loading conditions, as mentioned above. Once again, the edges of the nailed-bonded area develop the maximum values of principal stresses depending on the magnitude of the applied loads. The middle part of the bonded area has relatively lower values of principal stresses, whereas nails have stress-envelopes around them.

10.3 RECOMMENDATIONS

Following from this investigation are a few salient points recommended for use in practice:

(i) Strength of a particular adhesive in terms of τ and σ can be safely ascertained by making use of Eqs. (70) and (71) (Chapter V). These two equations can be easily programmed for computer work, if hand calculations become laborious and time-consuming.

(ii) Nailed-only connections (B) do not offer a great promise as far as resisting external loads is concerned, no matter what the loading set-up is, i.e., flexural, shear, etc.

(iii) Notwithstanding the fact that the inclusion of nails in adhesive connections (Specimen C) introduces stress concentrations around them, thus making the adhesive more susceptible to failure, yet they strengthen the joint by providing additional cross-sectional area of metal in the adhesive layer for shearing resistance.

Wherever additional strength is demanded in joining two sandwich panels, the use of nails is recommended in addition to using adhesive provided nailing the specimen is acceptable and not too costly.

(iv) The theoretical analysis of adhesive joints presented in Chapters IV, V and VI pertains to the joints made with adhesives only. However, for future research, it can be extended further to take into account the effect of nails, as well.

SELECTED BIBLIOGRAPHY

1. Adams, C.M., Jr., "Cooling Rates and Peak Temperatures in Fusion Welding", The Welding Journal, pp. 210S-215S, May, 1958.

2. Addison, H. Jr., Fogg, W.E., Betz, I.G., and Hussey, F. W., "Explosive Welding of Aluminum Alloys", The Welding Journal, pp. 359S-364S, August, 1963.

3. Anderson, J.E., and Jackson, J.E., "Theory and Application of Pulsed Laser Welding", Welding Journal, pp. 1018-1026, December, 1965.

4. Bahrani, A.S., and Crossland, B., "Explosive Welding and Cladding: An Introductory Survey and Preliminary Results", Vol. 179, Part I, No.7, Proceedings of the Institution of Mechanical Engineers, 1964-1965.

5. Baird, B.L., "Biaxial Stress-Strain Properties of Welds in High Strength Alloys", The Welding Journal, pp.571S-576S, December, 1963.

6. Baldanza, Nicholas, T., "Survey of Plastics Sandwich Construction, AD 673-713, Plastics Technical Evaluation Center, Dover, New Jersey, May, 1968.

7. Ball, E.F., and Higgins, J.J., "Installation and Tightening of High-Strength Bolts", Proc. Amer. Soc. Civil Engrs., ST3 (J. Struct. Div.), pp.117-131, March, 1959.

8. Beedle, L.S., and Christopher, R., "Testings of Steel Moment Connections", AISC Engineering Journal, October, 1964.

9. Bratkovich, N.F., Roth, R.E., and Purdy, R.E., "Electron Beam Welding - Applications and Design Considerations for Aircraft Turbine Engine Gears", The Welding Journal, pp. 631-640, August, 1965.

10. Brungraber, R.J., and Clark, J.W., "Strength of Welded Aluminum Columns", Proc. Amer. Soc. Civil Engrs., ST8, (J. Struct. Div.) pp. 33-57, August, 1960.

11. Bryant, R.W., and Dukes, W.A., The Effect of Joint Design and Dimensions on Adhesive Strength", Applied Polymer Symposia, No. 3, pp.81-98, 1966.

12. Catchpole, E.J., "Some Recent European Developments in the Structural-Adhesive Field", Applied Polymer Symposia N3(1966), pp. 203-217, Aircraft Manufacture, pp. 11, December, 1967.

13. Chesson, E., Jr., and Munse, W.H.,"Riveted and Bolted Joints: Truss-Type Tensile Connections",Proc. Amer.Soc. Civil Engrs. ST1 (J. Struct. Div.), pp.67-106, February, 1963.

14. Clutterbuck, M.,"The Dependence of Stress Distribution on Elastic Constants",Brit. J. Appl.Phys. Vol. 9, pp. 323-329, 1958.

15. Coker, E.G., and L.N.G. Filon,"A Treatise on Photoelasticity",Cambridge University Press, New York, 1931.

16. Chesson, E., Jr., Faustino, N.L., and Munse, W.H., "High Strength Bolts Subjected To Tension and Shear",Proc. Amer. Soc. Civil Engrs., ST5 (J. Struct. Div.) pp.115-180, October, 1965.

17. Dean, R.B., "Waterproof Adhesives for Cellulose", J.Colloid, Sci. 6,4, pp.348-353, August, 1951.

18. Delollis, N.J., Rucker, N., and Wier, J.E., "Comparative Strength of Some Adhesive - Adherend Systems", Transactions of ASME, pp. 183-193, February, 1951.

19. Dietz, G.H., Albert, "Future Potential of Building Systems", ASCE Annual Meeting and National Meeting on Structural Engineering, Pittsburgh, Pa., September 30-October 4, 1968.

20. DiMaggio, F.L., "Principle of Virtual Work in Structural Analysis", Proc. ASCE, Journal of Structural Division, pp. 65-78, November, 1960.

21. Douty, R.T., and McGuire, W., "High Strength Bolted Moment Connections", Proc. Amer. Soc. Civil Engrs., ST2, (J. Struct. Div.), pp. 101-128, April, 1965.

22. Dudas, J.H., "Joining New High Strength Aluminum Alloy X7005", The Welding Journal, pp. 358S-364S, August, 1965.

23. Earvolino, L.P., and Kennedy, J.R., "Laser Welding of Aerospace Structural Alloys", Welding Journal, pp. 127S-134S, March, 1966.

24. Fairbanks, R.H., Sr., and Adams, C.M., Jr., "Laser Beam Fusion Welding", Welding Journal, pp. 97S-102S, March, 1964.

25. Fazio, P.P., and Kennedy, J.B., "Experimental and Theoretical Study of Aluminum Sandwich Elements and in Particular Aluminum Folded-Sandwich Plate Structures", A Report submitted to the Aluminum Company of Canada, by the University of Windsor, Windsor, Ontario, June, 1968.

26. Fefferman, R.L., and Langhaar, H.L., "Investigations of 24S-T Riveted Tension Joints", Journal of the Aeronautical Sciences, Vol. 14, No. 3, March, 1947.

27. Fisher, J.W., and Rumpf, J.L., "Analysis of Bolted Butt Joints", Proc. Amer. Soc. Civil Engrs., ST5 (J. Struct. Div.), pp.181-203, October, 1965.

28. Frey, K., "The Strength of Metal Joints Made With Synthetic Resin", Aircraft Engineering, 25, 296, pp.317-320, October, 1953.

29. Frocht, M.M., "Photoelasticity", John Wiley & Sons, Inc., New York, Vol. I, 1941, Vol.II, 1948.

30. Frocht, M.M., "A Rapid Method for the Determination of Principal Stresses Across Sections of Symmetry from Photoelastic Data",J. Appl. Mech. Vol. 5, pp.24-28, 1938.

31. Frocht, M.M., R. Guernsey, Jr., and D. Landsberg, "Photoelasticity - A Precision Instrument of Stress Analysis, Proc. SEAA, Vol. XI, No. 1, pp.105-112, 1953.

32. Gere, J.M., and Weaver, W.Jr., "Matrix Algebra for Engineers", D. Van Nostrand Co., Inc., Princeton, N.J., 1965.

33. Gere and Weaver, "Analysis of Framed Structures", Appendix A, pp. 322-451, D. Van Nostrand Co. Inc., 1968.

34. Goodwin, J.F., "Strength of Spot-and-Seam-Welded Aluminum Alloy Joints", The Welding Journal, pp.322S-328S, July, 1962.

35. Hansen, N.G., "Fatigue Tests of Joints of High-Strength Steels", Proc. Amer. Soc. Civil Engrs., ST3 (J. Struct. Div.) pp.51-69, March, 1959.

36. Heuschkel, J., "Composition Controlled, High Strength, Ductile Tough, Steel Weld Metals", The Welding Journal, pp.361S-384S, August, 1964.

37. Hewitt, D.F., "A Survey of Established Processes for the Jointing of Metals...Plastic Bonding", Sheet Metal Industries, pp.1399-1400, July, 1948.

38. Hewitt, D.F., "A Survey of Established Processes For The Jointing of Metals", Sheet Metal Industries, pp.363-372, February, 1948.

39. Hewitt, D.F., "A Survey of the Established Processes For the Jointing of Metals - Automatic and Semi-Automatic Processes", Sheet Metal Industries, pp.771-782, April, 1948.

40. Hewitt, D.F., "A Survey of the Established Processes for the Jointing of Metals - Fusion Welding", May, 1948, Sheet Metal Industries, pp.991-1004, May, 1948.

41. Hewitt, D.F., "A Survey of the Established Processes for the Jointing of Metals - Atomic Hydrogen Welding, pp.1205-1212, June, 1948.

42. Hewitt, D.F., "A Survey of Established Processes for the Jointing of Metals. Riveting", Sheet Metal Industries, pp.1813-1821, September, 1948.

43. Hughes, E.J., "Study of Micromechanical Properties of Adhesive Bonded Joints", AD 673 745, General Precision Systems, Inc., Little Falls, New Jersey, August, 1968.

44. Humke, R.K., "Selection Guide for Sandwich Panel Adhesives", Product Engineering,pp. 56-61, May 26, 1958.

45. Ito, K., "Note on Adhesive Strength Test by Lap Joint", Scient. Pap. Inst. Phys. Chem.Res., Tokyo 54, 3, pp.295-306, September, 1960.

46. Jessop, H.T., and F. C. Harris, "Photoelasticity: Principles and Methods", Dover Publications, Inc., New York, 1950.

47. Jones, J., "Effect of Bearing Ratio on Static Strength of Riveted Joints", Proc. Amer. Soc. Civil Engrs. ST6(J. Struct. Div.) pp.1108-1 to 1108-10, November, 1956.

48. Jones, J.B., Maropis, N., Thomas, J.G., and Bancroft, D., "Phenomenological Considerations in Ultrasonic Welding", The Welding Journal, pp.289S-305S, July, 1961.

49. Jones, J.B., and Meyer, F.R., "Ultrasonic Welding of Structural Aluminum Alloys", The Welding Journal, pp.81S-92S, March, 1958.

50. Kaehler, W.A., Jr., Bank, S., and Trabold, A.F., "Arc-Image Welding", The Welding Journal, pp.497S-503S, November, 1965.

51. Kinney, J.W., "Experience With High-Strength Bolts in The Mackinac Bridge", ST3 (J. Struct. Div.) pp.133-144, March, 1959.

52. Kneeland, A.Godfrey, Jr., "New Technology in Low Income Housing", Civil Engineering, Amer. Soc. of Civil Engrs., January, 1968.

53. Kobotake, Y., and Inoue, Y., "Mechanics of Adhesive Joints", I. Residual Stresses, Appl. Sci. Res. (a) 7, 1, pp.53-64, 1958.

54. Kobatake, Y., and Inoue, Y., "Mechanics of Adhesive Joints", II, "Stress Distribution in Adhesive Layer Under Tensile Loading", Appl. Sci. Res. (a) 7, 2/3, pp.100-108, 1958.

55. Kobatake, Y., and Inoue, Y., "Mechanics of Adhesive Joints", III, "Evaluation of Residual Stresses", Appl. Sci.Res.(a) 7, pp.314-324, 1958.

56. Koopman, K.H., "Elements of Joint Design for Welding", The Welding Journal, pp.579-588, June, 1958.

57. Kuenzi, E.W., "Determination of Mechanical Properties of Adhesives for Use in the Design of Bonded Joints", Forest Products Laboratory, Report No. 1851, January, 1956.

58. Lewitt, C.W., Chesson, E., Jr., and Munse, W.H., "Riveted and Bolted Joints: Fatigue of Bolted Structural Connections", Proc. Amer. Soc. Civil Engrs., ST1 (J. Struct. Div.), pp. 49-65, February, 1963.

59. Lohr, R.T., and Watkins, G.E., "Gas Metal-Arc Welding of Low-Alloy Steel Pipe", The Welding Journal, pp.379-386, May, 1965.

60. Lokshin, V.E., and Puzrin, L.G., "Some Data on the Formation of the Weld Seam in Electron Beam Welding", Soviet Physics - Doklady, Vol. 8, No. 12, pp.1227-1228, June,1964.

61. Long, J.V., and Cremer, G.D., "High-Temperature Corrosion-Resistance Brazing", Astronautics, pp.28-29, August, 1958.

62. Love, A.E.H., "A Treatise on the Mathematical Theory of Elasticity", Fourth Edition, The MacMillan Company, New York, N.Y., pp.465-467, 1927.

63. Lunsford, L.R., "Stress Analysis of Bonded Joints", Applied Polymer Symposia, No. 3, pp.57-73, 1966.

64. Masubuchi, Koichi, "Analytical Investigation of Residual Stresses and Distortions Due to Welding", The Welding Journal, pp.525S-537S, December, 1960.

65. McCampbell, W.M. Cook., G.E., Norholt, L.E., and Merrick, G.J., "The Development of A Weld Intelligence System", The Welding Journal, pp.139S-144S, March, 1966.

66. McCutcheon, J.O., So, W.C., Gersovitz, B., "Applied Mechanics Series", No. 2, 1963, McGill University, Department of Civil Engineering and Applied Mechanics, Montreal.

67. Meier, J.W., "Production Applications of Electron Beam Welding", Transactions of ASME, pp.280-286, August, 1964.

68. Miller, K.J., and Ninnikhoven, J.D., "Laser Welding" Machine Design, pp.120-125, August 5, 1965.

69. Monroe, G.M., "Analysis of Eccentrically Loaded Riveted or Bolted Joints", Journal of the Aeronautical Sciences, Vol. 16, pp.120-122, February, 1949.

70. Munse, W.H., and Chesson, E., Jr., "Riveted and Bolted Joints: Net Section Design", Proc. Amer. Soc. Civil Engrs., ST1 (J. Struct. Div.), pp.107-126, February, 1963.

71. Munse, W.H., Petersen, K.S., and Chesson, E.Jr., "Strengths of Rivets and Bolts in Tension", Proc. Amer. Soc. Civil Engrs., ST3, (J. Struct. Div.) pp.7-28, March, 1959.

72. Mylonas, C., and DeBruyne, "Theoretical Investigation of the Stresses in Joints", Part I; "Experimental Investigation of the Stresses in Joints", Part II; Aero Research Limited, Duxford, England.

73. Nelson, F.G., Kaufman, J.G., and Holt, M., "Fracture Characteristics of Welds in Aluminum Alloys", The Welding Journal, pp.321S-329S, July, 1966.

74. Perry, H.A., "How to Calculate Stresses in Adhesive Joints", Prod. Engng., 29, 27, pp.64-67, July, 1968.

75. Plantema, F.J., "Sandwich Construction; The Bending and Buckling of Sandwich Beams, Plates and Shells", John Wiley and Sons, Inc., New York, 1966.

76. Post, D. :"Photoelastic Evaluation of Individual Principal Stresses by Large Field Absolute Retardation Measurements", Proc. SESA, Vol. XIII, No. 2, pp.119-132, 1956.

77. Prynne, P., "Fundamentals of the Use of High Tensile Bolts in Structural Connections", Civil Engineering and Public Works Review, pp.375-383, March, 1965.

78. Przemieniecki, J.S., "Theory of Matrix Structural Analysis", McGraw-Hill Co., 1968.

79. Reissner, E., "The Effect of Transverse Shear Deformation on the Bending of Elastic Plates". J. Appl.Mech. Vol.12, pp. A-69-A-77.

80. Reissner, E., Goland, M., "The Stresses in Cemented Joints", Journal of Applied Mechanics, 11, 1, pp.A-17-A-27, March, 1944.

81. Ripling, E.J., Mostovoy, S., and Patrick, R.L., "Measuring Fracture Toughness of Adhesive Joints", Materials Research and Standards, pp.129-134, March, 1964.

82. Salvadori, M.G., and Schwarz, R.J., "Differential Equations in Engineering Problems", 4th Edition, Prentice-Hall, Inc., Englewood Cliffs, NewJersey, June, 1961.

83. Schmidt, A.O., Ham, I., and Hoshi, T., "An Evaluation of Laser Performance in Microwelding", Welding Journal, pp. 481S-488S, November, 1965.

84. Segerlind, L.J., "On the Shear Stress in Bonded Joints", Journal of Applied Mechanics, Transactions of the ASME Series, E. 35, 1, pp.177-178, March, 1968.

85. Shaffer, Bernard, W., "A Realistic Evaluation of the Factor of Safety of a Bolted Bracket", Int. J. Mech. Sci. 1, 1, pp.135-143, January, 1960.

86. Slaughter, G.M., Patriarca, P., and Manly, W.D., "Bonding of Cermet-Valve Components to Metals", The Welding Journal, pp.249S-254S, June, 1958.

87. Spraragen, W., "Pre-heating - Residual Stresses - Stress-Relieving", The Welding Journal, p.21S, January, 1958.

88. Sterling, G.H., and Fisher, J.W., "A440 Steel Joints Connected by A490 Bolts", Proc. Amer. Soc. Civil Engrs., ST3 (J. Struct. Div.) pp.101-118, June, 1966.

89. Sutherland, R.A., "Symposium on Welded Spiral Cases From the Consulting Engineers and Users Viewpoint", Transactions of the ASME 80, 5, pp.1143-1145, July, 1958.

90. Timoshenko, S.P., and Woinowsky-Krieger, S., "Theory of Plates and Shells", Second Edition, McGraw-Hill Book Company, 1959.

91. Timoshenko, S.P., and Goodier, J.N., "Theory of Elasticity", Second Edition, McGraw-Hill Book Company, 1951.

92. Tocher, J.L., "Analysis of Plate Bending Using Triangular Elements", University of California, Berkeley, Ph.D., 1963 Thesis.

93. Van Houten, G.R., "A Survey of the Bonding of Cermets to Metals", The Welding Journal, pp.558S-569S, December, 1958.

94. Vasarhelyi, D.D., Beano, S.Y., Madison, R.B., Lu, Zung-Au, and Vasishth, U.C., "Effect of Fabrication Techniques in Bolted Joints", Proc. Amer. Soc. Civil Engrs., ST3 (J. Struct. Div.) pp.71-116, March, 1959.

95. Vasarhelyi, D.D., and Chang, W.N., "Misalinement in Bolted Joints", Proc. Amer. Soc. Civil Engrs. ST4 (J.Struct. Div.)pp.1-15, August, 1965.

96. Volkarsen, O., "Die Nietkraftverteilung in Zugbeanspruchten Nietverbindungen mit Konstanten Laschenguerschnitten", Luftfahrt-Forschung, Bd., 15, 41, 1938.

97. Winter, G., "Tests on Bolted Connections in Light Gage Steel", Proc. Amer. Soc. Civil Engrs., ST2 (J. Struct. Div.), pp.920-1, 920-25, March, 1956.

98. Yamada, Y., Yoshimura, N., and Sakurai, T., "Plastic Stress Strain Matrix and Its Application for the Solution of Elastic Plastic Problems by the Finite Element Method", International Journal of Mechanical Science, Vol. 10, pp.343-354, 1968.

99. Yienger, J.A., and Walker, J.W., "Bolted Point Reactions", Machine Design, pp.181-182, June 24, 1965.

100. Zienkiewicz, O.C., and Cheung, Y.K., "The Finite Element Method in Structural and Continuum Mechanics", McGraw-Hill Co., 1967.

APPENDIX I

APPENDIX I

In addition to the mid-panel joint with double-tapered shear key between two sandwich panels (Fig.3), a few more joints have also been proposed in the following pages,as possible means of connecting them. Besides using adhesive, they also make use of nails for joining purposes.

Joint No. 1

1) The transversal shear resistance of this joint is considerable due to the inclined interface.

2) This connection is dependent on the strength of the adhesive between the cover-plates and the facings.

Joint No. 2

The bending resistance is increased in this joint by carrying the facings of one panel over the core of the other and by connecting the cover-plate with both adhesive and nails.

Joint Nos.3 and 4

Tongue and groove are used in joint 3 to increase the transversal shear capacity. The remaining features are the same as those of joint 1. Joint 4 is the same as 3, but makes use of both adhesive and nails to connect the cover-plates.

Joint Nos. 5 and 6

Joints 5 and 6 are similar to 3 and 4, respectively. A different type of shear groove is used, however.

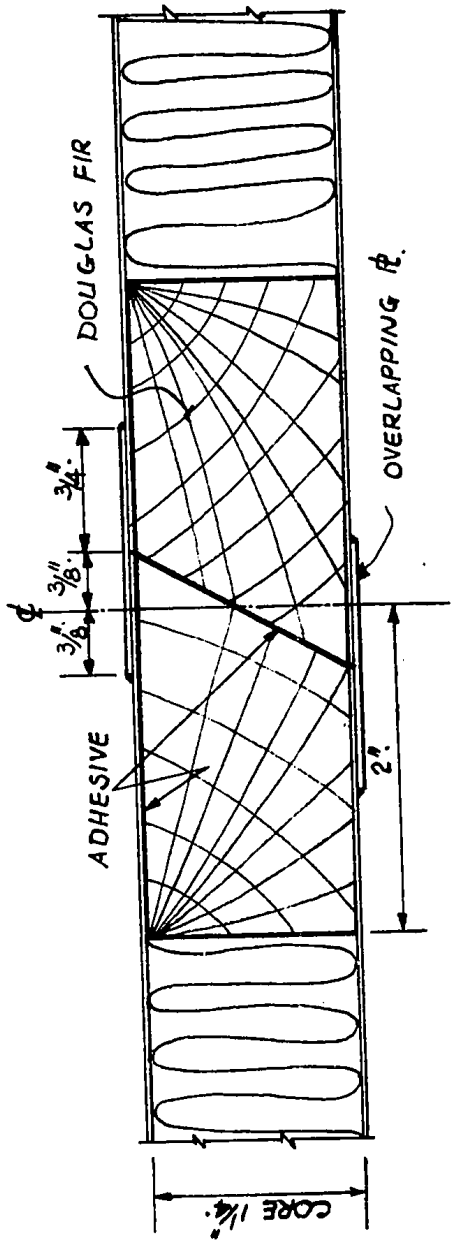

FIG. 63 PROPOSED JOINT NO: 1

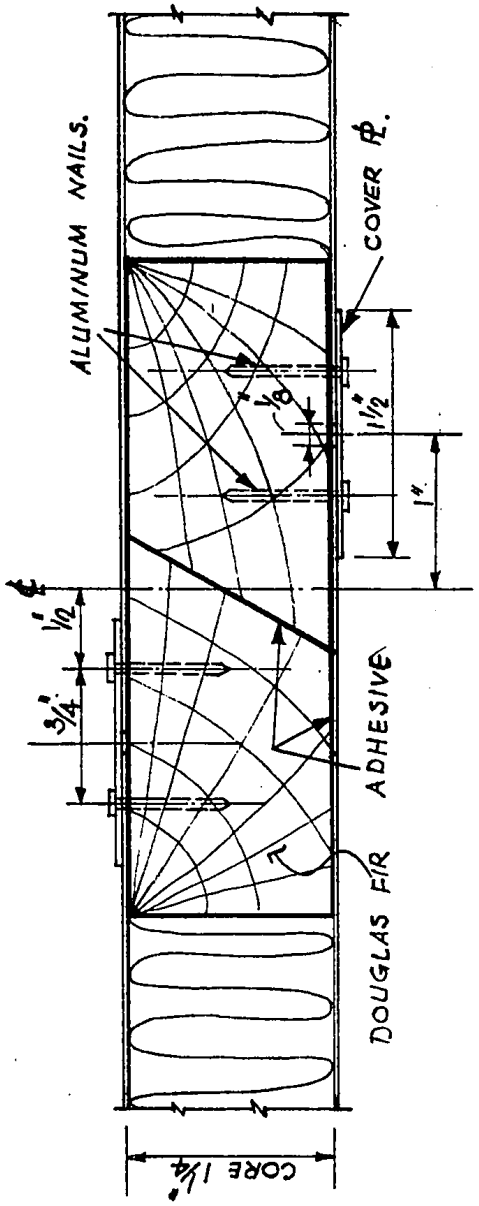

FIG. 64 PROPOSED JOINT NO: 2

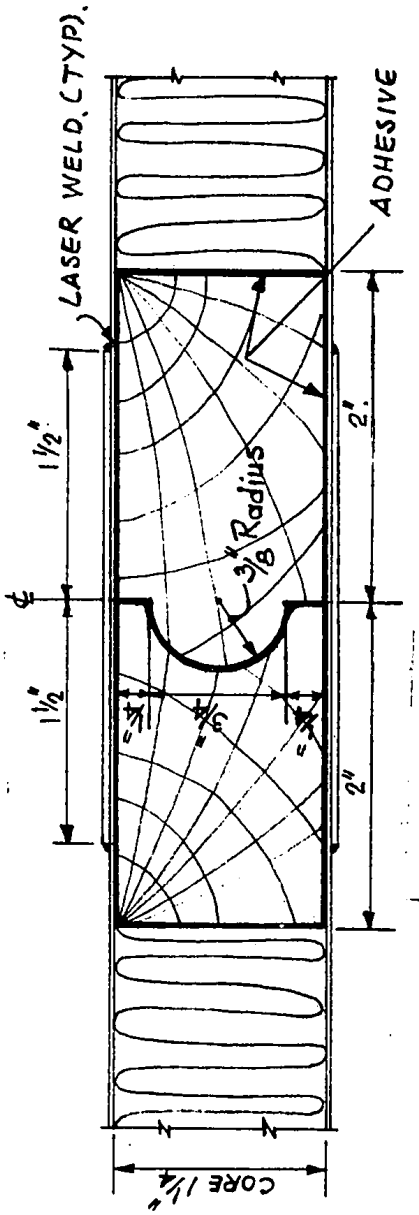

FIG. 65 PROPOSED JOINT NO: 3

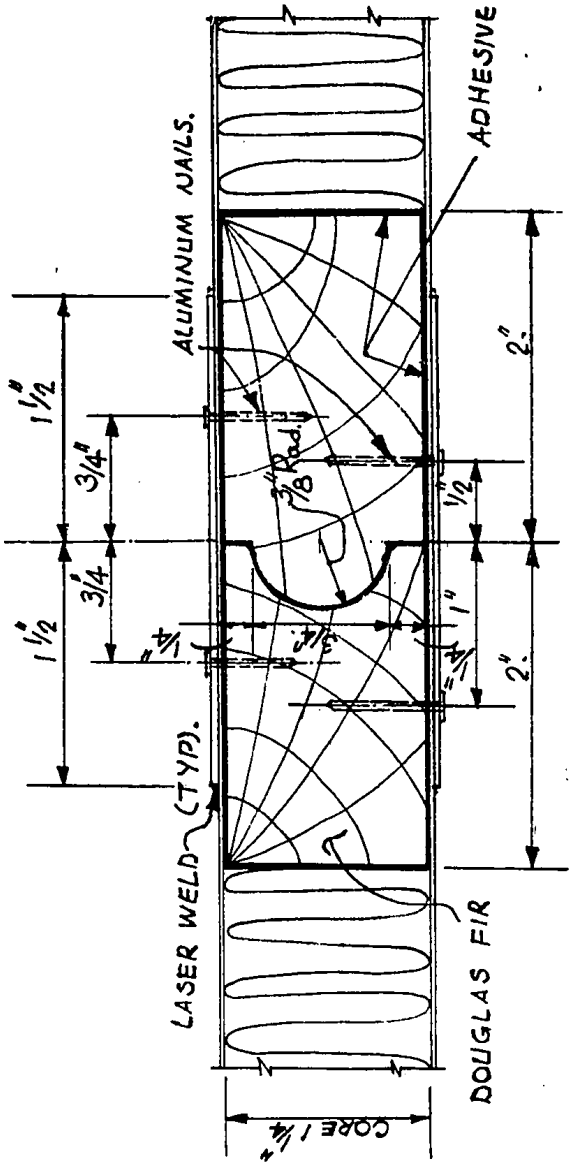

FIG. 66 PROPOSED JOINT NO: 4

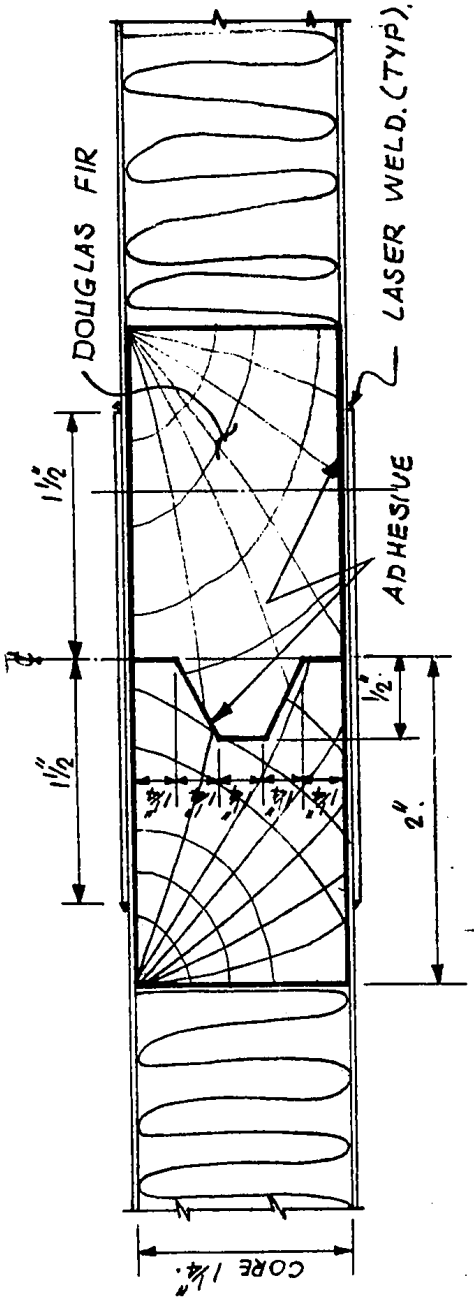

FIG. 67 PROPOSED JOINT NO: 5

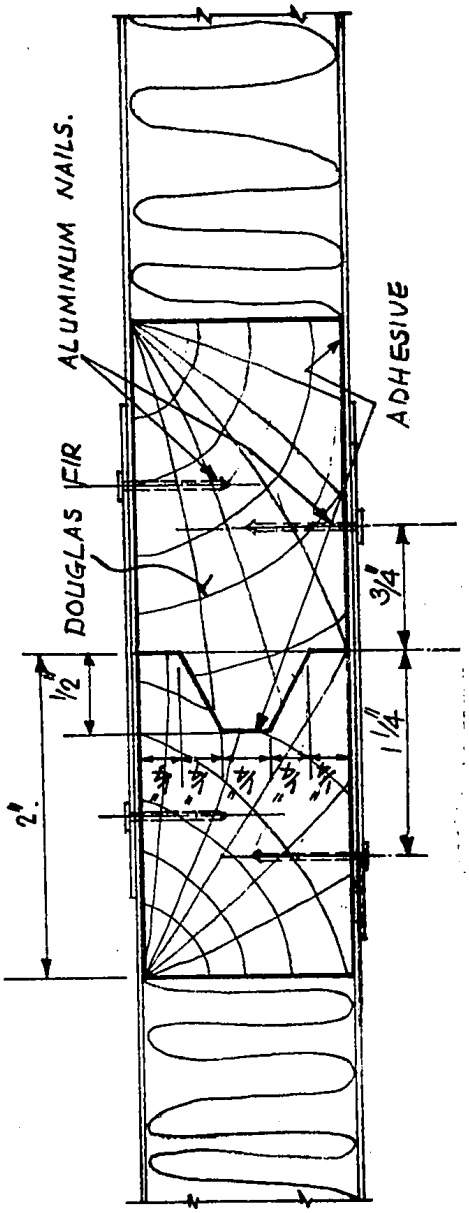

FIG. 68 PROPOSED JOINT NO: 6

APPENDIX II

SAMPLE PHOTOELASTIC PICTURES

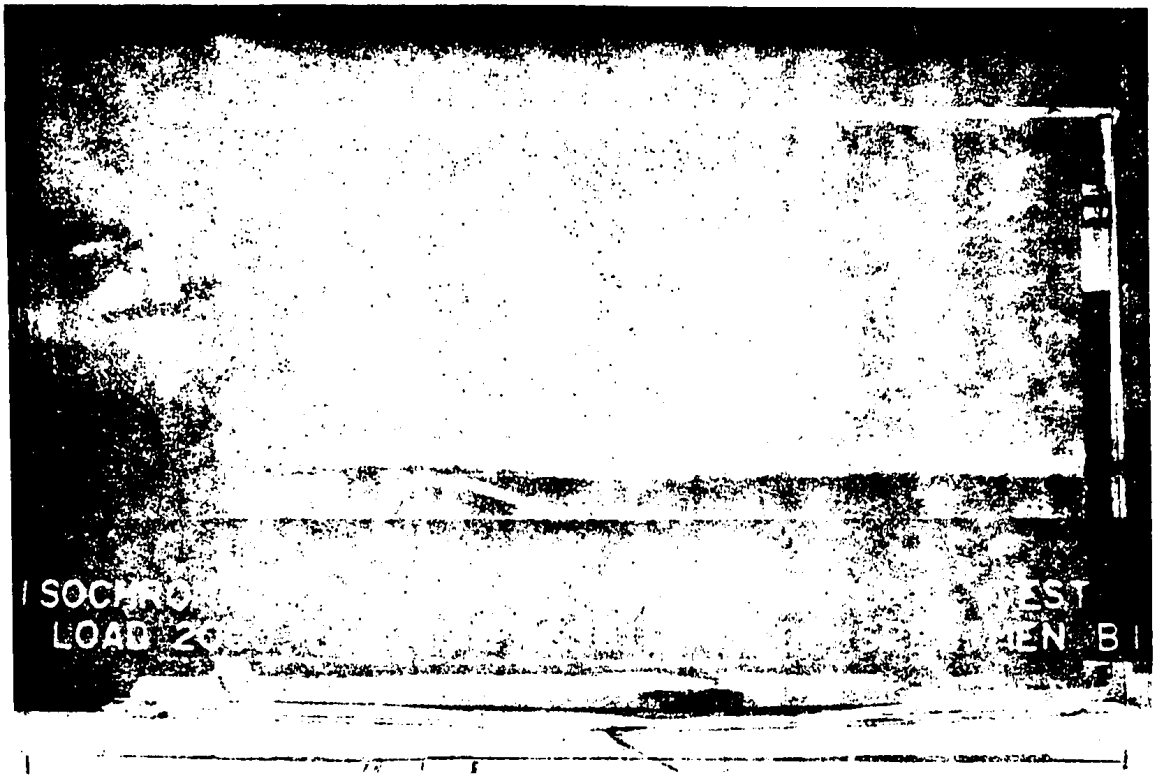
LOAD 2

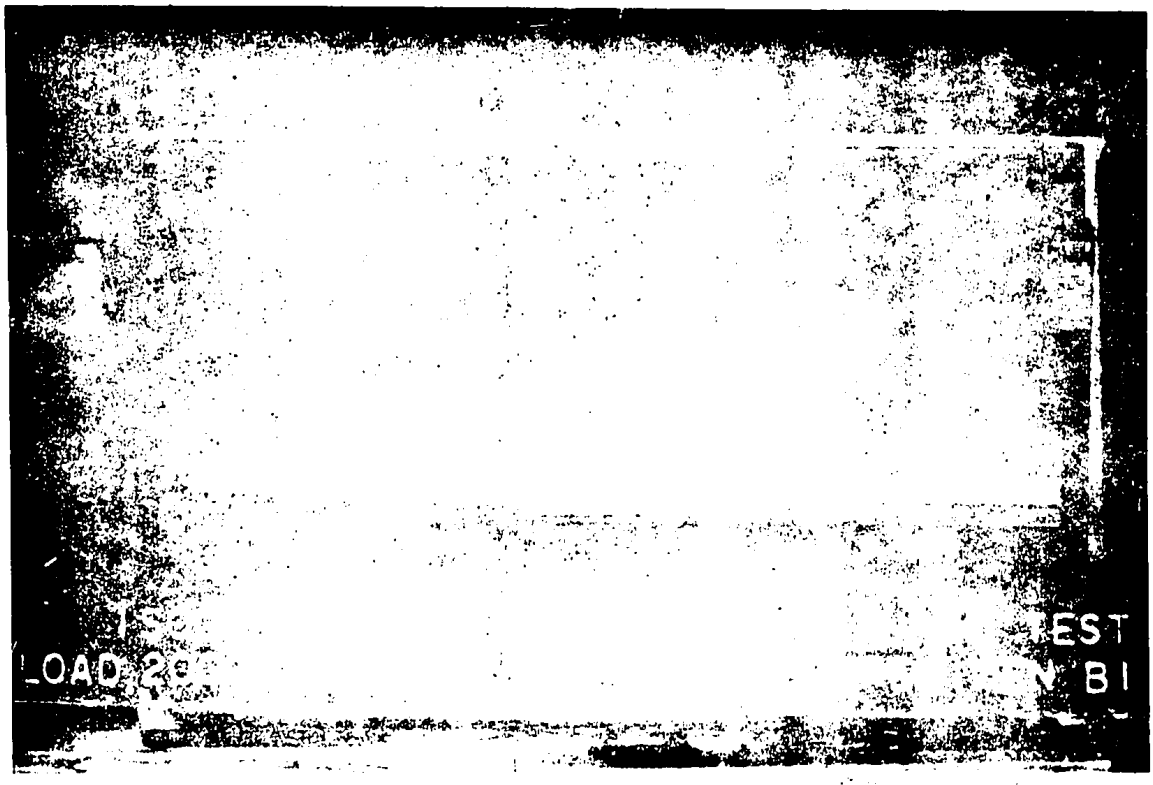
LOAD 2